

SULFATE ATTACK AND THE ROLE OF INTERNAL CARBONATE ON THE FORMATION OF THAUMASITE

THÈSE N° 3853 (2007)

PRÉSENTÉE LE 20 JUILLET 2007

À LA FACULTÉ DES SCIENCES ET TECHNIQUES DE L'INGÉNIEUR

Institut des matériaux

PROGRAMME DOCTORAL EN SCIENCE ET GÉNIE DES MATÉRIAUX

ÉCOLE POLYTECHNIQUE FÉDÉRALE DE LAUSANNE

POUR L'OBTENTION DU GRADE DE DOCTEUR ÈS SCIENCES

PAR

Thomas SCHMIDT

Dipl.-Ing. in Bauingenieurwesen, Bauhaus-Universität Weimar, Thüringen, Allemagne
et de nationalité allemande

acceptée sur proposition du jury:

Prof. H. J. Mathieu, président du jury

Prof. K. Scrivener, directrice de thèse

Prof. E. Brühwiler, rapporteur

Prof. D. E. Macphee, rapporteur

Dr B. Lothenbach, rapporteur



ÉCOLE POLYTECHNIQUE
FÉDÉRALE DE LAUSANNE

Suisse
2007

Acknowledgements

The present work was carried out with the financial support from cemsuisse (Association of the Swiss Cement Industry) under guidance of Dr. Gerhard Rytz and Dr. Jean-Gabriel Hammerschlag, who I would like to thank for their helpful discussions. The thesis was made possible due to the support at the Swiss Federal Laboratories for Materials testing and Research (Empa) in Dübendorf and the guidance of the Swiss Federal Institute of Technology Lausanne (EPFL) at the Laboratory of Construction Materials (LMC).

With Dr. Barbara Lothenbach and Dr. Michael Romer I had experienced scientists in my working environment who I would like to acknowledge for their guidance, suggestions and helpful discussions and for spending time with me for all the reviews of reports, manuscripts and papers. Thanks to Barbara, who guided me on the way of understanding the world of modelling approaches. I thank Michael, who initiated the PhD project and took his time in providing his expertise in the field of sulfate attack.

I would like to thank my thesis director, Prof. Karen Scrivener, who guided me and the project. Thanks for her interest, for the support, encouragement, helpful comments and advices during this study.

Thanks also to Dr. Emmanuel Gallucci, Dr. Lorenz Holzer and Phillip Gasser for their helpful guidance and support in the field of microscopy and microanalysis during this research work. Thanks to Dr. Frank Winnefeld, Dr. Joseph Kaufmann, Dr. Andreas Leemann for their helpful discussions. Thanks to Dr. Daniel Rentsch and Renato Figi and his team for their analytical support. Special thanks to Dr. Jürg Neuenschwander for his kind support in the field of nondestructive testing.

I would like to thank the members of the jury: Prof. H.-J. Mathieu, Prof. E. Brühwiler, Prof. D. E. Macphee for spending their time evaluating this thesis and providing comments.

Special appreciation goes to all my colleagues from Empa in the laboratory for concrete and construction chemistry in Dübendorf for their friendship and dynamic atmosphere that made these three years to pass so quickly. I also would like to thank all the people from the laboratory of construction materials LMC in Lausanne for creating a pleasant and dynamic atmosphere.

Last but not least, I would like to thank my parents Dr. Klaus-Dieter and Barbara Schmidt, my sister Anne-Kathrin Schmidt and my grandmother Christa Matzke for their support and encouragement during the time of my thesis.

Abstract

The sulfate attack is known to influence the durability of concrete. In general, significant damage due to sulfate interaction results in the structural breakdown of the concrete structure. However, the precipitation of thaumasite due to sulfate concentration, leaching and the role of internal carbonate in case of limestone filler in cement is still not understood in detail.

This work has adopted a combination of experimental and modeled data to investigate the formation of thaumasite under different exposure conditions. Experiments were carried out by using the progressive equilibrium approach (PEA). Further microstructural properties such as porosity, sulfate uptake, phase composition and phase transformation reactions during sulfate attack were investigated.

The results show that thaumasite formation is favoured at lower temperatures (8 °C) independently of the type of cement clinker (high and low C₃A content) used. Thaumasite was found to form only in cement systems which contained a source of carbonate and at high sulfate contents in the cement paste, i.e. the molar SO₃/Al₂O₃ ratio exceeded 3. Leaching, the reduction of alkalis and portlandite, had no significant influence on the stability of thaumasite. It slightly reduced the amounts of thaumasite formed. Thaumasite formation was found not to be a form of the initial sulfate attack. The phenomenon occurs at the late (last) stage of sulfate attack. The initial sulfate induced deterioration is caused by ettringite formation.

The thermodynamic approach used to investigate the chemical aspects of sulfate attack turned out to be a good tool for simulating external sulfate attack. However, in the experiments, the predicted equilibrium conditions have not been reached after 9 months.

Limestone addition of a few percent in Portland cement increased the compressive strength and reduced the porosity, especially the capillary porosity. Thereby, also the resistance of Portland cement systems against sulfate attack was increased. Furthermore, the hydration of Portland cement was influenced by limestone addition and monocarbonate was formed instead of monosulfate as stable AFm phase.

Keywords: sulfate attack; thaumasite formation; limestone filler; temperature

Zusammenfassung

Sulfatangriff beeinflusst die Dauerhaftigkeit von Beton. Die Sulfatinteraktion kann dabei bis zur völligen Zerstörung des Betonbauteils führen. Speziell die Ausfällung von Thaumasit infolge einer bestimmten Sulfatkonzentration, dem Auswaschen des Betons und die Rolle des internen Karbonats für den Einsatz von Kalksteinmehl im Zement sind bislang noch nicht im Detail verstanden.

In dieser Arbeit wird eine Kombination von experimentellen und modellierten Daten verwendet, um die Bildung von Thaumasit unter verschiedenen Expositionsbedingungen zu untersuchen. Die Experimente wurden mittels eines progressiven Gleichgewichts Ansatz (PEA) durchgeführt. In weiterführenden Untersuchungen wurden die mikrostrukturellen Eigenschaften wie Porosität, Sulfataufnahme, Phasenzusammensetzung und Phasenumwandlung während des Sulfatangriffs untersucht.

Die Resultate zeigen, dass die Thaumasitbildung bevorzugt bei tiefen Temperaturen (8 °C) stattfindet, unabhängig vom verwendeten Zementklinkertyp (hoher und niedriger C_3A Gehalt). Thaumasit bildet sich ausschliesslich in carbonathaltigen Zementsystemen bei entsprechend hohen Sulfatgehalten im Zementstein, das heisst bei einem molaren SO_3/Al_2O_3 Verhältnis von mehr als 3. Gewaschene Zementsysteme (Reduktion von Alkalien und Portlandit) haben keinen signifikanten Einfluss auf die Stabilität von Thaumasit. Lediglich die Menge an Thaumasit wurde leicht reduziert. Die Thaumasitbildung ist keine Form des anfänglichen Sulfatangriffs. Der Schaden tritt als letzte Stufe des Sulfatangriffs auf. Die ursprüngliche, sulfatinduzierte Schädigung wird durch die Ettringitbildung verursacht.

Der thermodynamische Ansatz, der zur Untersuchung der chemischen Aspekte des Sulfatangriffs benutzt wurde, erwies sich als nützliches Instrument, um den Sulfatangriff zu simulieren. Allerdings konnten in den Experimenten die vorausgesagten Gleichgewichtsbedingungen nach 9 Monaten nicht erreicht werden.

Die Kalksteinzugabe von wenigen Prozent im Portlandzement führte zu einer Erhöhung der Druckfestigkeit und einer Reduktion der Porosität, insbesondere der Kapillarporosität. Dadurch konnte der Widerstand von Portlandzementen gegenüber einem Sulfatangriff verbessert werden. Des Weiteren wird durch die Kalksteinzugabe die Hydratation von Portlandzement beeinflusst und Monocarbonat entsteht als stabile AFm Phase anstelle von Monosulfat.

Stichworte: Sulfatangriff; Thaumasitbildung; Kalksteinfüller; Temperatur

Nomenclature and notation

Cement shorthand notation

C = CaO

S = SiO₂

H = H₂O

A = Al₂O₃

F = Fe₂O₃

\bar{S} = SO₃

\bar{C} = CO₃

| | |
|---------|--|
| AFm | aluminate-ferrite-mono hydrate phase |
| AFt | aluminate-ferrite-tri hydrate phase |
| BSE | backscattered electron |
| EDS | energy dispersive spectroscopy |
| GEMS | Gibbs free energy minimization program |
| HS | sulfate resistant cement |
| ICP-OES | inductively coupled plasma optical emission spectroscopy |
| LF | limestone filler |
| MIP | mercury intrusion porosimetry |
| NMR | nuclear magnetic resonance |
| OPC | ordinary Portland cement |
| PEA | progressive equilibrium approach |

| | |
|-----|---|
| SE | secondary electron |
| SEM | scanning electron microscopy |
| TGA | thermogravimetric analysis |
| TIC | Total inorganic carbon |
| TSA | thaumasite form of sulfate attack |
| w/c | water to cement ratio |
| wt% | weight percent |
| XRD | X-ray diffraction |
| XRF | X-ray fluorescence |
| ZAF | correction factor; atomic number, X-ray absorption and fluorescence |

Table of contents

| | |
|--|------------|
| ACKNOWLEDGEMENTS | I |
| ABSTRACT | III |
| ZUSAMMENFASSUNG | V |
| NOMENCLATURE AND NOTATION | VII |
| TABLE OF CONTENTS | IX |
| 1 INTRODUCTION | 1 |
| 1.1 INITIAL SITUATION..... | 1 |
| 1.2 THESIS OBJECTIVES | 2 |
| 1.3 OUTLINE OF THE THESIS | 2 |
| 2 STATE OF RESEARCH..... | 5 |
| 2.1 PORTLAND CEMENT SYSTEMS | 5 |
| 2.1.1 <i>Hydration mechanisms</i> | 5 |
| 2.1.2 <i>Influence of limestone addition</i> | 6 |
| 2.2 EXTERNAL SULFATE ATTACK | 8 |
| 2.2.1 <i>Ettringite formation</i> | 8 |
| 2.2.2 <i>Gypsum formation</i> | 11 |
| 2.2.3 <i>Thaumasite form of sulfate attack</i> | 13 |
| 2.2.4 <i>Parameters influencing sulfate attack</i> | 19 |
| 2.3 SUMMARY..... | 22 |
| 2.4 REFERENCES..... | 23 |
| 3 MATERIALS AND METHODS..... | 29 |
| 3.1 LABORATORY CEMENTS..... | 30 |
| 3.2 CEMENT PASTE SAMPLES | 32 |
| 3.2.1 <i>Experimental set up</i> | 32 |
| 3.2.2 <i>Progressive equilibrium approach PEA</i> | 33 |
| 3.2.3 <i>Analytical methods</i> | 35 |
| 3.3 MORTAR SAMPLES | 38 |
| 3.3.1 <i>Experimental set up</i> | 38 |
| 3.3.2 <i>Ultrasonic measurements</i> | 39 |
| 3.3.3 <i>Analytical methods</i> | 41 |
| 3.4 MICROSCOPY AND MICROANALYSIS | 42 |
| 3.5 THERMODYNAMIC MODELLING APPROACH..... | 44 |
| 3.6 REFERENCES..... | 46 |

| | | |
|----------|--|------------|
| 4 | BINDER SYSTEMS BEFORE SULFATE EXPOSURE..... | 47 |
| 4.1 | CHARACTERISATION OF THE BINDER SYSTEMS..... | 47 |
| 4.1.1 | <i>Influence of limestone addition on physical properties.....</i> | <i>47</i> |
| 4.1.2 | <i>Chemical influence of limestone addition</i> | <i>50</i> |
| 4.1.3 | <i>Influence of leaching.....</i> | <i>54</i> |
| 4.1.4 | <i>Microstructural aspects.....</i> | <i>55</i> |
| 4.2 | SUMMARY AND CONCLUSIONS..... | 58 |
| 4.3 | REFERENCES..... | 59 |
| 5 | CEMENT PASTE EXPERIMENTS | 61 |
| 5.1 | THERMODYNAMIC MODELLING AND THAUMASITE FORMATION | 61 |
| 5.1.1 | <i>Model of initial hydrate phases.....</i> | <i>61</i> |
| 5.1.2 | <i>Effect of sulfate interaction</i> | <i>62</i> |
| 5.1.3 | <i>Effect of temperature</i> | <i>68</i> |
| 5.1.4 | <i>Effect of leaching</i> | <i>71</i> |
| 5.1.5 | <i>Aspects of reaction solution.....</i> | <i>75</i> |
| 5.1.6 | <i>Microstructural aspects.....</i> | <i>78</i> |
| 5.2 | SUMMARY AND CONCLUSIONS..... | 83 |
| 5.3 | REFERENCES..... | 85 |
| 6 | MORTAR EXPERIMENTS..... | 87 |
| 6.1 | PHYSICAL AND MICROSTRUCTURAL ASPECTS OF SULFATE ATTACK..... | 87 |
| 6.1.1 | <i>Expansion and mass change</i> | <i>87</i> |
| 6.1.2 | <i>Ultrasonic surface velocity.....</i> | <i>92</i> |
| 6.1.3 | <i>Visual appearance.....</i> | <i>95</i> |
| 6.1.4 | <i>Sulfate uptake and relevant phases.....</i> | <i>97</i> |
| 6.1.5 | <i>Microstructure and microanalysis</i> | <i>99</i> |
| 6.2 | DISCUSSION | 110 |
| 6.3 | SUMMARY AND CONCLUSIONS..... | 114 |
| 6.4 | REFERENCES..... | 115 |
| 7 | GENERAL DISCUSSION AND CONCLUSIONS..... | 117 |
| | REFERENCES | 122 |
| | APPENDIX | 123 |

1 Introduction

1.1 Initial situation

Resistance against sulfate attack is an important factor influencing concrete durability and serviceability. The thaumasite form of sulfate attack (TSA) is characterised by significant damage of concrete and other cement based materials due to swelling, cracking and loss of cohesion. Cases of structural deterioration due to TSA have already been reported from a number of countries.

Some factors leading to the formation of thaumasite like high levels of sulfate and temperatures below 15 °C are known in the meantime. However, the formation of thaumasite was also observed at temperatures above 20 °C. Up to now, only a few cases of thaumasite formation were reported in the presence of low sulfate concentrations.

The fact that sulfate resistant cement is not effective in preventing thaumasite formation is generally accepted. However, it is not clear if the thaumasite form of sulfate attack is a cause or an effect of the damage due to sulfate attack. The occurrence of thaumasite related damage might be underestimated as most of the affected structures, e.g. tunnel structures are difficult to access.

Different theories about the formation mechanisms of thaumasite have been published. It is widely discussed whether it forms at the expense of C-S-H or by nucleation from ettringite. However, the exact mechanism and the role of carbonate are still unclear. Especially, the importance of leaching and the cement composition is not understood in detail.

Due to ecological and economical aspects cement clinker in Portland cements is replaced more and more by limestone filler. So far, limestone filler was regarded as an inert constituent in cementitious building materials. Further sources of carbonate are present in ground water. Some indication that calcium carbonate from aggregate or filler can act as a supplier of carbonate ions for thaumasite formation are documented in the literature.

This poses the question how additional limestone filler in Portland cement is affecting the durability of cementitious building materials in contact with sulfate. Furthermore the work aims to investigate how leaching as observed in real conditions affects sulfate interaction and especially thaumasite formation.

1.2 Thesis objectives

The main focus of this thesis is to investigate the influence of internal carbonate of a binder system on the formation of thaumasite under external sulfate attack.

The project aims to elaborate the driving force of thaumasite formation. Therefore it is important to investigate which conditions promote thaumasite formation.

Therefore the work seeks to address the following questions regarding sulfate attack:

- What is the influence of the limestone filler in the binder system?
- What effect has the sulfate concentration?
- How important are storage temperature and the time?
- What is the effect of leaching due to real conditions?
- What is the influence of aluminium and the C_3A content of the clinker?

Additionally, the physical consequences of a sulfate attack are studied. All results are discussed in relation to other projects and to the predicted results using thermodynamic modelling.

1.3 Outline of the thesis

The thesis composes of seven chapters and the appendix. The following paragraphs give a short outline of each chapter as part of the overall content.

Chapter 2 gives a short overview on Portland cement systems and a comprehensive state of research in the field of sulfate attack with special focus on thaumasite formation. The chapter summarizes the key questions of this study.

Chapter 3 describes the strategy, the materials and the various techniques used to characterize and understand the specific phenomena of sulfate attack. The progressive equilibrium approach (PEA) is used to investigate the chemical aspects of sulfate attack in combination with thermodynamic modelling. The physical aspects of sulfate attack are illustrated with the use of a surface sensitive ultrasonic method using Rayleigh waves.

Chapter 4 is a brief chapter for the characterization of the binder systems involving the influence of limestone addition. The initial hydrate phase composition as well as physical and chemical properties are described and compared to predicted data.

Chapter 5 presents the results of the investigations on the conditions of thaumasite formation on the cement paste. The study involves the thermodynamically modeled data and the experimental results obtained from the progressive equilibrium approach (PEA) in order to understand the precipitation reactions for thaumasite during sulfate attack. Additionally, SEM microscopy and microanalysis are used to clarify the impact of sulfate interaction and leaching.

Chapter 6 describes the investigations on the physical consequences of sulfate attack on mortar samples. The results evaluate the influence of various boundary conditions, e.g. temperature and sulfate concentration in solution during sulfate interaction. The new developed, surface sensitive ultrasonic method as well as macroscopic and microstructural findings are discussed and compared.

Chapter 7 concludes the thesis with a summary of the results obtained in the phenomena of sulfate attack, in particular the influence of limestone and the conditions of thaumasite formation in laboratory cements.

2 State of research

2.1 Portland cement systems

Portland cement is polyphase and the principal constituents are impure forms of calcium silicate (C_3S , C_2S), calcium aluminate (C_3A) and ferrite (C_4AF) in relative amounts given in table 2.1:

Table 2.1: Portland cement clinker phases and mineral composition [1]

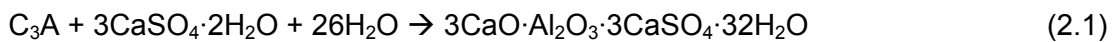
| Phase | Formula | percentage |
|-----------|-----------|------------|
| Alite | C_3S : | 40 – 80 |
| Belite | C_2S : | 5 – 35 |
| Aluminate | C_3A : | 0 – 15 |
| Ferrite | C_4AF : | 0 – 20 |

Minor phases, such as gypsum ($C\bar{S}H_2$) are added during grinding

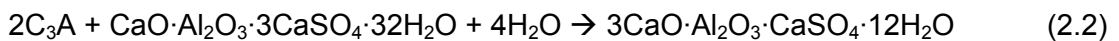
During the hydration of ordinary Portland cement the main constituents may react with water and ionic species of calcium sulfates (hemihydrate, gypsum, anhydrite), calcite, calcium oxide, magnesium oxide and alkalis (Na, K) to form various hydration products [1, 2, 3, 4].

2.1.1 Hydration mechanisms

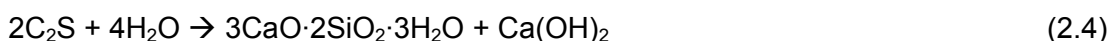
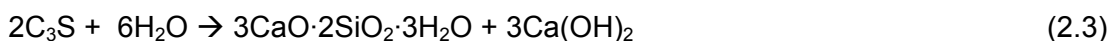
An overview of the development of the microstructure of Portland cement during hydration is given in Fig. 2.1. A part of C_3A reacts with calcium sulfate to form ettringite (AFt):



When the added sulfate is exhausted in the absence of limestone, monosulfate (an AFm Phase) starts to form from the ettringite and C_3A available:



In parallel the calcium silicates (C_3S , C_2S) react to form the C-S-H phases and portlandite, with C_3S forming more portlandite:



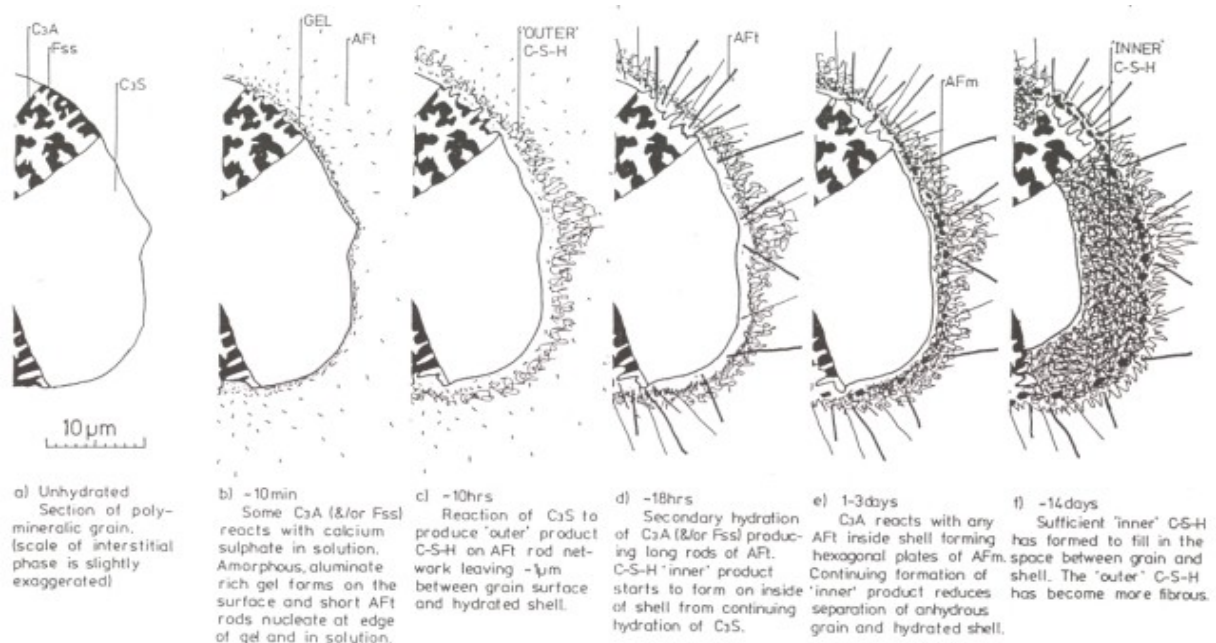


Fig. 2.1: Hydration of Portland cement reproduced from Scrivener [3]:

As described by Scrivener [3], first the outer $C-S-H$ is formed in free pore space at the surface of the polymineralic grains and later the inner $C-S-H$ forms within the boundaries of the grains. Generally, the hydration mechanisms of C_2S are similar to C_3S but its hydration is slower [1].

The alumino-ferrite phase (C_4AF) of unhydrated cement was found to be less reactive in comparison to calcium aluminate phase (C_3A) in alkaline conditions of cementitious systems [1, 5].

The formation of the microstructure during the hydration of Portland cement is very complex and the calcium silicates and calcium aluminates reaction mechanisms are not separated or independent from each other.

2.1.2 Influence of limestone addition

In many cases limestone additions have been regarded as an inert component in the cement. In the last years, however, it has been recognized that limestone filler influences and affects the physical and chemical properties of cement.

The physical influence of limestone addition was concluded to be its filler effect. It was found by Tsivilis et al. [6] that small amounts of limestone filler added to the cement reduced porosity and permeability at a constant w/c ratio, this was confirmed by Stark [7]. A refinement in pore structure during cement hydration was observed earlier by Uchikawa et al. [8] for very fine limestone fillers. Higher amounts of limestone filler added to the cement

system resulted in higher permeability of the investigated cements and faster degradation during sulfate attack according to Irassar et al. [9]. These observations were confirmed by Torres et al. [10] for mortars made with Portland-limestone cements.

Limestone addition also influences the chemistry of the cement system. The presence of carbonate in the cement system leads to the formation of monocarbonate as the stable AFm phase [11, 12, 13]. Furthermore the additional calcite was found to act as a source of Ca buffering the cement system, e.g. in the case of leaching [14].

Thermodynamic calculations (e.g. [12, 13]) indicate that depending on the amount of calcite present hemihydrate and monosulfate can form as stable phases beside monocarbonate during the hydration of ordinary Portland cements. Fig. 2.2 illustrates the hydration of a Portland cement and the resulting changes in volume.

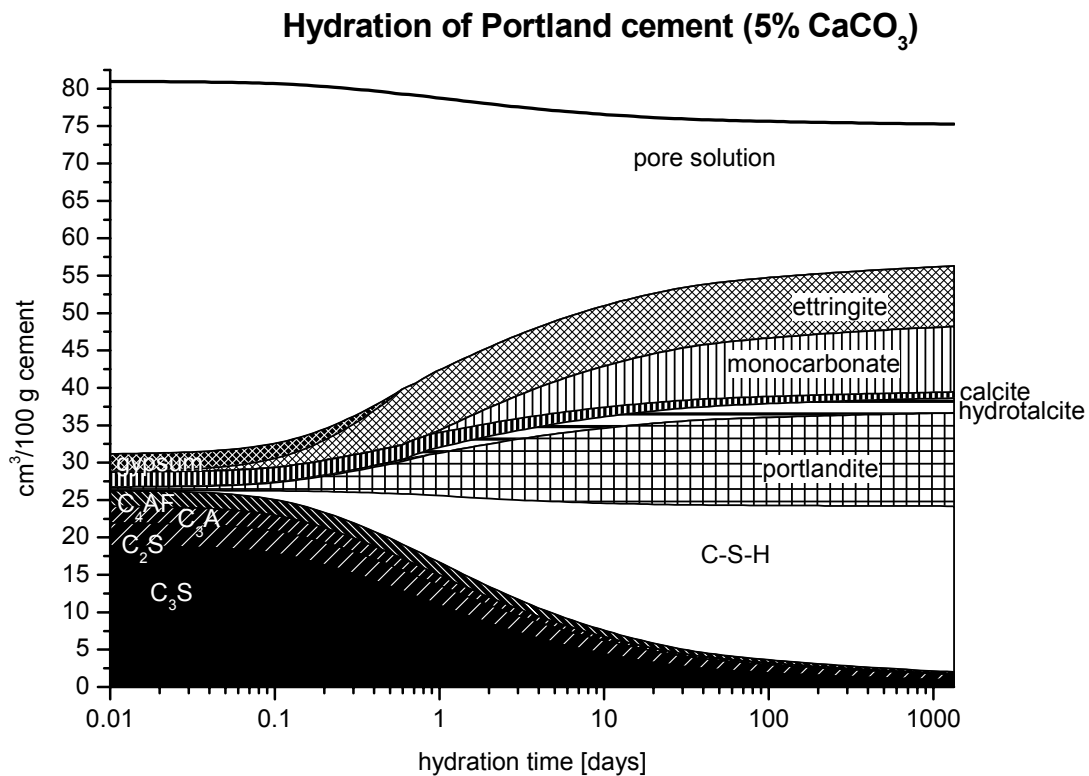


Fig. 2.2: Calculated volume changes during the hydration of ordinary Portland cement containing 5 wt% CaCO_3 ; w/c = 0.5

2.2 External sulfate attack

External sulfate attack on mortars and concretes usually results in the formation of phases like ettringite ($3\text{CaO}\cdot\text{Al}_2\text{O}_3\cdot3\text{CaSO}_4\cdot32\text{H}_2\text{O}$) and gypsum ($\text{CaSO}_4\cdot2\text{H}_2\text{O}$). However, in cements and concretes containing a source of carbonate, in addition the formation of thaumasite ($\text{CaSiO}_3\cdot\text{CaCO}_3\cdot\text{CaSO}_4\cdot15\text{H}_2\text{O}$) can be observed.

The interaction of sulfates with hardened cement paste is often described and associated with expansion. The formation of sulfate phases due to sulfate supersaturation leads to crystallisation pressure through dissolution and precipitation processes as described by Taylor et al. [15]. According to Scherer [16], the precipitation of secondary sulfate phases, forming large crystals, in hardened cement paste matrix leads to expansion caused by a confinement in the microstructure which is most likely for sulfate alteration.

Beside that in over sulfated cement systems at early ages, interparticular forces can generate swelling pressure as described by Metha [17]. This is unlikely in hardened cement systems since ettringite is not colloidal but a fine dispersed phase.

2.2.1 Ettringite formation

Secondary ettringite formation due to external sulfate attack has been investigated for many years now. Systematic studies and reviews were done to evaluate the deterioration processes of secondary ettringite formation due to external sulfate attack on hydrated cement paste, mortar and concrete [18, 19].

The mineral ettringite is characterised by its hexagonal, prismatic needlelike morphology as shown in Fig. 2.3.

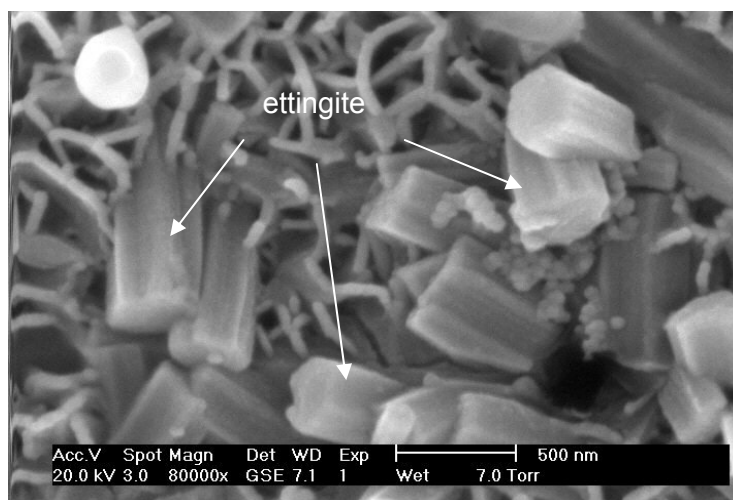
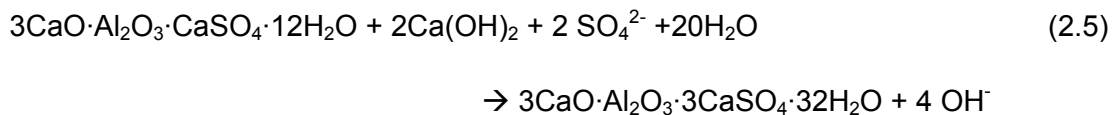


Fig. 2.3: ESEM image of ettringite needles in cement paste, 56 days, Empa

Ettringite formation leads to an increase in solid volume. The theoretical volume increase varies depending on the source of aluminium available [20]. Ettringite has a relative low density (1.75 g/cm^3) in comparison to e.g. C-S-H phase (2.0 g/cm^3). Thus the formation of secondary ettringite provides potential stress in hardened cement paste. However, ettringite formation does not necessarily lead to primary expansion since pores and voids in the microstructure provide space for ettringite precipitation especially in the beginning of sulfate exposure [21].

It was found by Skalný et al. [19] that reactive aluminium in hydrated cement paste provides a potential risk for the formation of secondary ettringite during the migration of sulfate ions SO_4^{2-} into the concrete structure during sulfate attack. The sources of reactive aluminium are (i) AFm phases (monosulfate, monocarbonate) and (ii) calcium aluminate originating from the clinker phases (C_3A , C_4AF). The following equation shows one possible way of ettringite formation from monosulfate with participation of portlandite during sulfate attack.



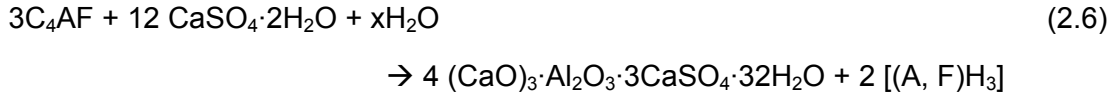
Thermodynamic calculations [13] indicate that hemihydrate and hydrotalcite could be sources of reactive aluminium.

Ettringite formation can be reduced by lowering the C_3A content of the cement. According to the standards EN 196, 197 cements with high sulfate resistance are limited in the C_3A content $< 3\%$ and the Al_2O_3 content $< 5\%$, whereas the ASTM C1157-03 limits the C_3A content $\leq 5\%$ and $2\text{C}_3\text{A} + \text{C}_4\text{AF} < 25\%$ for Type V cements.

However, the results of Monteiro and Kurtis [22] show that the amounts of C_3A (0-8%) in the cement systems do not necessarily protect from sulfate deterioration. In contrast the w/c ratio of the investigated samples had a major impact on the failure time of the samples during 40 years of exposure under real conditions. They concluded that the permeability (porosity) of the concrete samples investigated has a major influence on the deterioration of the samples. These observations were confirmed by Khatari and Sirivivatnanon [23].

It is generally agreed that the aluminoferrite phase (C_4AF) seems to be less important with regard to secondary ettringite formation during sulfate attack due to its lower reaction kinetics [24, 1]. The " C_4AF " phase is very inhomogeneous with respect to the Al and Fe content [1]. Certain amounts of the Al could dissolve and react with sulfate ions to form secondary ettringite. Studies of the pure C_4AF phase by Neubauer and Götz-Neunhoffer [25] showed that with increasing Al/Fe-ratio the reactivity of the alumina-ferrite phase increases. The Fate

of the iron originating from the dissolution of C_4AF is not clear. Iron could precipitate as iron hydroxide $Fe(OH)_3$ or as mixed Al-Fe-ettringite or AFm. Furthermore investigations from Möschner et al. [26] show that iron-rich ettringite (Aft) is thermodynamically less stable with increasing pH. The formation of secondary ettringite from C_4AF in the presence of gypsum (sulfate) and the formation of aluminium- (AlH_3) and iron hydroxide (FeH_3) is given in eq. 2.6:



It has been observed that in the presence of portlandite, the concentration of aluminium in the pore solution decreases. In the absence of portlandite the mobility of aluminium somewhat increases as reported by Damidot and Glasser [4]. Thus, in the presence of portlandite secondary ettringite would be more likely to form in regions close to the initial aluminium source, causing expansion. In the absence of portlandite, as in the case of leached samples, ettringite could be more likely to form in regions of higher porosity, causing less expansion as proposed by Taylor and Gollop [15].

Moreover, it was observed by NMR data that aluminium can substitute to some extent for silicate in the C-S-H [27, 28]. It was not investigated if the aluminium substituted in C-S-H can contribute to ettringite formation due to external sulfate attack. Beside that, the C-S-H phase was found to adsorb certain amounts of sulfate in its structure [19]. It was found that the adsorbed sulfate can act as a source of sulfate for secondary ettringite formation especially under wet and moist conditions [19].

Ettringite was found to be stable at pH levels between 10.5-13.0 in pure systems and stable up to pH of 14 in cement systems but starting to decompose with decreasing pH (≤ 10.5) [4, 29]. However, as already outlined, the formation of ettringite is an important factor for the deterioration of concrete undergoing sulfate attack but it is not the only one.

2.2.2 Gypsum formation

Beside ettringite, gypsum can also form during sulfate attack as shown in Fig. 2.4, especially in highly concentrated sulfate solutions, e.g. sodium sulfate ($\geq 24\text{g SO}_4^{2-}/\text{l}$) according to Gollop and Taylor [30, 31].

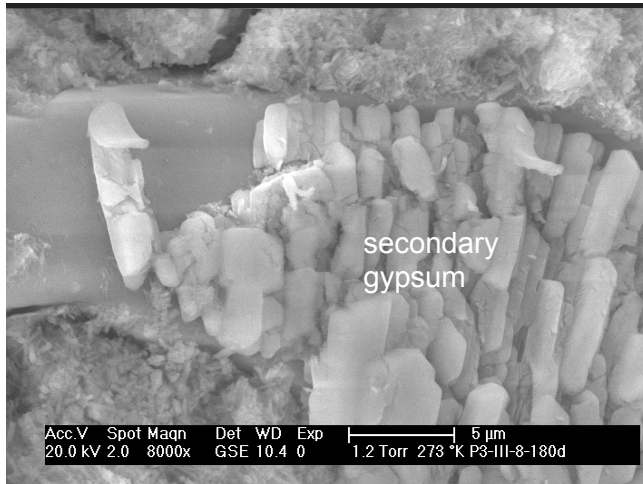
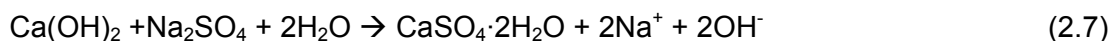


Fig. 2.4: SE image of gypsum crystals formed in deteriorated mortar sample, 180 days, Empa

The influence of gypsum formation on the performance of cement pastes, mortars and concrete has been studied by various authors [9, 32, 22, 33]. It has been suggested that secondary gypsum formation is related to the amount of alite (C_3S) in the cement system as a potential risk factor due to the possibility of portlandite formation.

Metha [29] and Monteiro and Kurtis [22] state that cements containing little or no portlandite (Ca(OH)_2) performed much better when exposed to sulfate attack than cements with high alite contents. The transformation of portlandite into gypsum (eq. 2.7) seems to be an important factor for the durability of concrete exposed to sulfate attack.



Kollmann and Kollmann et al. [34, 21, 35] report that the reaction above can cause expansion, usually later during sulfate exposure. Similar results were given by Metha [29], Irassar et al. [9] and Santhanam et al. [33] who reported that beside the observed expansion also softening of the near surface regions due to gypsum formation was observed. The softening has been attributed to the decalcification of the C-S-H phase.

The above mentioned studies suggest that the formation of gypsum is a significant factor during sulfate resistance experiments performed in the laboratory according to Koch and Steinegger [36], Wittekindt [37] or ASTM C 1157-03. All these methods use high sulfate concentrations to accelerate sulfate attack. However, these high sulfate concentrations are not representative of real conditions of sulfate exposure in the field.

Marchand et al. [32] showed that the formation of gypsum is rarely observed under field conditions where moderate or low sulfate concentrations (5-10 g $\text{SO}_4^{2-}/\text{l}$) are present. Investigations from Bellmann et al. [38] on a mixture of portlandite and gypsum showed that gypsum can precipitate at a sulfate concentration of 3g $\text{SO}_4^{2-}/\text{l}$. They further calculated and showed experimentally that at reduced pH values (12.5 to 12.9) gypsum precipitated in the presence of sulfate concentrations between 3.5 and 18.3g $\text{SO}_4^{2-}/\text{l}$.

It was generally concluded that minimizing the amount of portlandite in the hydrated cement paste increases the resistance of gypsum formation. The investigations indicate that some expansive deterioration of the concrete can be attributed to the formation of gypsum due to the high sulfate concentrations in the attacking solution. In addition, gypsum may acts as a source of sulfate for the formation of AFt phases (ettringite, thaumasite) as mentioned in section 2.2.1 and 2.2.3.

2.2.3 Thaumasite form of sulfate attack

Thaumasite in cementitious materials was reported by Erlin and Stark [39]. In recent years the formation of thaumasite during sulfate attack has been collected systematically on concrete structures by the Thaumasite Expert Group [40].

Crystal structure and morphology of thaumasite

The natural mineral thaumasite ($\text{CaSiO}_3 \cdot \text{CaSO}_4 \cdot \text{CaCO}_3 \cdot 15\text{H}_2\text{O}$) was investigated in 1880 by Nordenskiöld [41]. The structure of thaumasite remained unclear for quite some time. In recent years the mineral thaumasite has been studied by various authors using different analytical methods, e.g. XRD, IR, SEM/EDS or ^{29}Si -NMR [42-47].

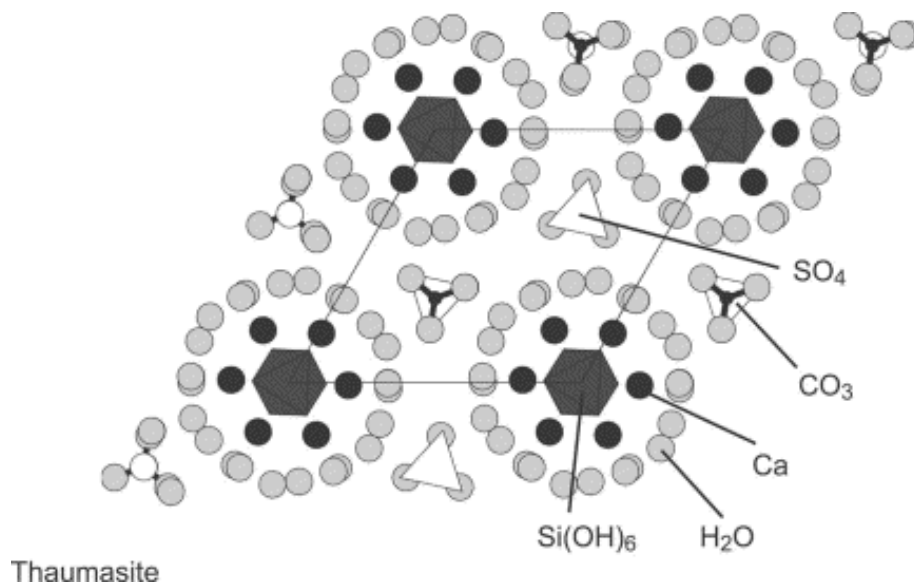


Fig. 2.5: Crystal structure of thaumasite—projection on *a-b* plane, reproduced from [48]

Thaumasite is structurally very similar to ettringite. It was recognized that in the structure of thaumasite the silicon has an octahedral coordination. Compared to ettringite the alumina is replaced by silicon and the carbonate partly substitutes the sulfate in the structure of thaumasite [48] (Fig. 2.5).

The morphology of thaumasite can be described as thin prismatic needles which form as bunches naturally as well as in affected concrete structures as shown in Fig. 2.6.

The length of these needles was found to be in the range of 50 – 200 μm and the thickness was measured to be 0.5 – 2 μm .

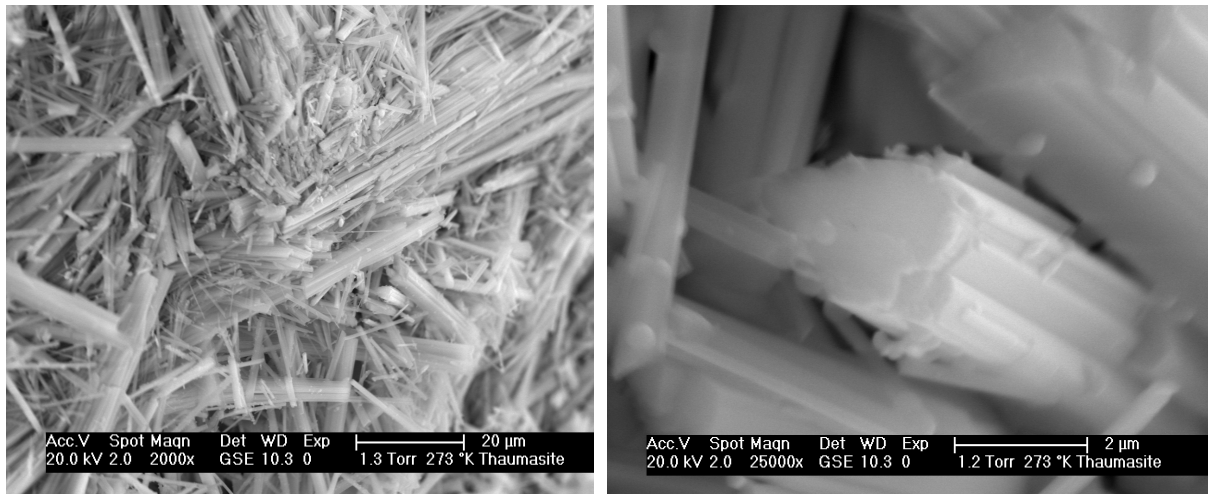


Fig. 2.6: SE image of natural mineral thaumasite, Ettringer Bellerberg, Laacher See (Germany), Empa

Conditions of thaumasite formation

The formation of thaumasite requires a source of calcium silicate, i.e. C-S-H; sulfate, carbonate and humidity [49, 43, 44, 50, 40]. Furthermore it has been suggested by Bensted [49, 43] that thaumasite is more stable at lower temperatures since silicon tends to adopt the octahedral co-ordination found in thaumasite more easily at lower temperatures. However, thaumasite is formed also at temperatures around 20 °C and above as reported for buildings in Southern California [51] and Italy [52]. Once thaumasite has formed, it remains stable up to 30 °C according to Macphee and Barnett [69].

Thaumasite has been observed to form both in the presence and in the absence of portlandite. However it has been suggested that thaumasite formation tends to occur in leached, surface near regions of the concrete [53]. It was observed that alkaline conditions ($\text{pH} \geq 12.5$) enhance thaumasite formation [54], while during strong leaching at low pH levels ($\text{pH} \leq 8.0$) gypsum becomes the dominant sulfate phase and the amount of thaumasite decreases [55]. However, findings from Gaze and Crammond [56] and Jallad et al. [57] show that once thaumasite forms it remains stable also at low pH levels between 6-8.

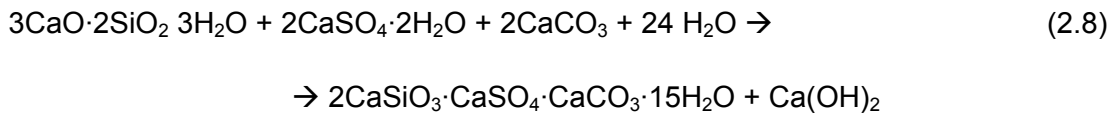
The formation of thaumasite always needs a source of carbonate which can be supplied from the limestone contained in the cement itself [58, 45] as minor component up to 5 wt% (CEM I) or as major component with up to 35 wt% (CEM II/A B-LL).

Furthermore, carbonate containing aggregate, or limestone fillers used in self compacting concretes SCC could favour thaumasite formation as reported by Kalinowski and Trägårdh [58]. Hartshorn et al. [59] found that increasing amounts of limestone filler in cement increased the amount of thaumasite formed in mortars. Other sources of carbonate were found to be carbonate in ground waters [60], soils [50] or atmospheric carbon dioxide CO₂ [61]. The latter generates calcite by transformation of portlandite which could also lead to thaumasite formation. However, only very small amounts of thaumasite have been observed in the carbonated zone of the affected concrete structures in tunnels [62] and bridges [40].

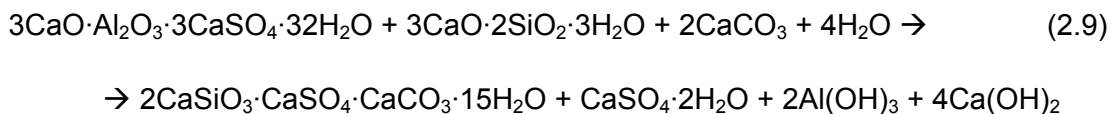
Thaumasite has been found in cement systems with both high and low C₃A contents [63-65]. Although thaumasite itself contains no aluminium, aluminium has been proposed to play a catalytic role and to promote thaumasite formation [66]. In contrast Juel et al. [67] shows that in cements with small amounts of aluminium, the amounts of sulfate which are consumed by secondary ettringite formation are small and therefore more sulfate is available for thaumasite and gypsum formation. Cement systems with high C₃A content could theoretically reduce the amount of thaumasite formed as more sulfate is needed to form secondary ettringite during sulfate interaction as suggested by Blanco-Varela et al. [63].

Because of the similarities between ettringite and thaumasite the solid solution between the two has been studied [68, 69, 48]. Barnett et al. [70] showed that ettringite and thaumasite can both adopt variable amounts of aluminium, sulfate and carbonate but a distinct miscibility gap was observed. Glasser [71] proposed a generalised stability diagram for ettringite, carbonate ettringite and thaumasite which also shows a miscibility gap. However, Pajares et al. [72] found that ettringite starts to decompose as it incorporates increasing amounts of carbonate in its structure.

Thaumasite formation is often described to occur directly from C–S–H [73, 74] reacting with appropriate carbonate, sulfate, Ca²⁺ ions and excess water eq. 2.8:



The other possible reaction for thaumasite formation was described to be from ettringite called the “Woodfordite-route” where ettringite is reacting with C–S–H, carbonate, Ca²⁺ ions and water, in which thaumasite arises directly from ettringite (eq. 2.9):



Köhler et al. [75] suggested that ettringite can act as a template for the nucleation of thaumasite. Their results further indicated that the reactions for thaumasite formation seemed to be rather slow and irregular. Bensted [73] claimed that the “Woodfordite-Route” of thaumasite formation might be possible but only at very low temperatures ($\leq 2\text{ }^{\circ}\text{C}$) during rather long periods of time.

Systematic investigations on the stability and formation of thaumasite assuming equilibrium conditions have been made by Juel et al. [67]. It was found that thaumasite only forms in cements systems where enough sulfate has been added to transform all available aluminium into ettringite. Thaumasite was observed to form at rather high sulfate contents (7-10 wt% SO_3) by weight of anhydrous cement.

Furthermore Bellmann et al. [76, 77] reported that thaumasite is not stable in the presence of ettringite and C-S-H together with calcite. The investigations from Bellmann [76, 77] show that thaumasite can be formed from gypsum, calcite, portlandite, C-S-H and water. The precipitation of thaumasite was calculated to be possible at low sulfate concentrations of 1,5g $\text{SO}_4^{2-}/\text{l}$ in solution which is in agreement with the observations of Mulenga et al. [78] who showed that even at low sulfate concentrations ($\leq 3\text{g SO}_4^{2-}$) in solution thaumasite formation is possible.

Other investigations on field samples in South Africa [79] showed that thaumasite formation is enabled at low sulfate content (4.3 wt% SO_3) by weight of cement but during rather long periods of exposure time. It was believed that the oxidation of pyrites from aggregates forms gypsum which later reacts with calcite and C-S-H and external sulfate to form thaumasite. However, the actual amount of sulfate necessary for thaumasite formation is not well known. Generally, it has been concluded that both the presence of gypsum [80] or sulfate rich solution [59, 67] can lead to thaumasite formation in carbonate containing cements.

Thaumasite deterioration of concrete

The damage due to thaumasite formation has been investigated by various authors [81-85, 60]. Thaumasite deterioration has been reported in the USA for pavements, sewer pipes which were severely damaged after 11 years. In Canada a case of thaumasite sulfate attack (TSA) on concrete foundations was reported in the Canadian arctic which caused significant degradation after only 2-4 years by Bickley et al. [81]. Cases of TSA in South Africa have been reported by Oberholster [79] and in Italy by Collepardi [52] in concrete linings and historic brickwork made of limestone after almost 40 years possibly indicating that thaumasite deterioration takes much longer at higher temperatures.

In the UK many investigations have been made of concrete foundations of domestic houses and motorway bridges [86, 87, 40, 54]. The majority of cases, thaumasite was found in deteriorated concretes. The depth of the thaumasite deteriorated zone was found to depend on various factors, e.g. w/c-ratio, temperature and sulfate concentration of e.g. soil and aggregates used.

Thaumasite formation has been reported to take place in tunnel structures in Switzerland [60]. It was suggested that thaumasite deterioration is favoured by the interaction of rockwater through leaching since the breakdown of the C-S-H phase is accelerated under these conditions. It was reported that parts of the concrete in the affected tunnel structure were scaling indicating that thaumasite formed at certain depths in the concrete structure according to Romer et al. [85].



Fig. 2.7: Scaling as a result of thaumasite deterioration, BRE (UK) [88]



Fig. 2.8: Soft mash consisting of mainly thaumasite and gypsum, Empa (CH) [60]

Visible destruction due to thaumasite formation has been observed as spalling combined with scaling of the surface of the affected concrete structure (Fig. 2.7). The conversion of C-S-H to thaumasite as described in 2.2.3.2 leads to a significant loss of strength.

Finally, thaumasite formation leads to gradual softening, spalling and significant loss of strength. In its final state thaumasite deterioration converts the concrete into a structureless white or gray mass from which the aggregates can be separated easily (Fig. 2.8).

The more detailed examination of the affected concrete elements [88] indicated the development of a sequence of degradation steps due to thaumasite deterioration during sulfate interaction.

Table 2.2: Idealised degradation sequence for TSA development modified from [40]

| | |
|----------------|--|
| <i>Step 1:</i> | occasional voids, pores lined with thaumasite |
| <i>Step 2:</i> | thin cracks filled in with thaumasite |
| <i>Step 3:</i> | wide cracks filled with thaumasite, thaumasite around aggregates |
| <i>Step 4:</i> | complete transformation of cement paste matrix into thaumasite |

It was concluded that small amounts of thaumasite observed in pores or cracks had no significant impact on strength or elastic modulus. The destructive behaviour of thaumasite might be related to the extent of thaumasite formed in concrete especially at later ages. It was concluded that almost all C-S-H can be transformed into thaumasite as long as sulfate and carbonate sources are available leading to a complete destruction of the concrete [40]. The amount of thaumasite formed during sulfate interaction significantly influences the damage of the structure.

However, no attempt has been made to quantitatively estimate the extent, the limiting factors (sulfate, carbonate, time) and depth of at which thaumasite formation occurs in cementitious materials.

2.2.4 Parameters influencing sulfate attack

The interaction of sulfates from sulfate bearing solutions such as ground water, soil or industry waters with Portland cement concrete can result in different phenomena. Some effects will be looked at in more detail in the following passages.

Influence of the cation on sulfate degradation

Independently from the influence of the sulfate ions (SO_4^{2-}) the accompanying cations can modify the rate and extent of external sulfate attack. As mentioned by Skalny et al. [19] the cations show different deterioration; the extent of destruction was found to be influenced by the type of cations present, in particular $\text{MgSO}_4 > \text{Na}_2\text{SO}_4 > \text{CaSO}_4$.

Sodium and calcium sulfate act similarly on the concrete during sulfate attack. Although in case of calcium sulfate no additional calcium is needed, thus the decalcification of the cement paste is reduced.

Other effects occur if magnesium sulfate solutions interact with the affected concrete structure (Fig. 2.10).

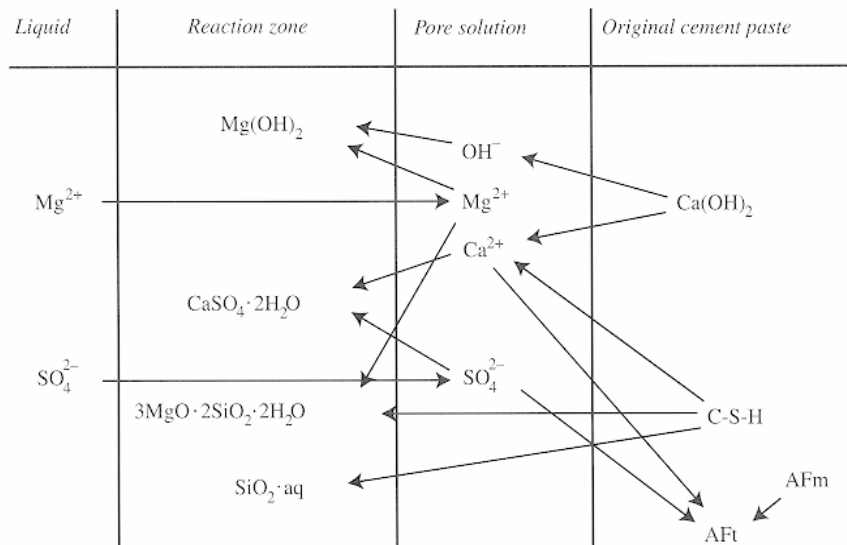


Fig. 2.9: Scheme of sulfate interaction between Portland cement components and magnesium sulfate solution reproduced from [19].

It was found that the decalcification of the cement paste due to decomposition of portlandite and C-S-H phase is accelerated [19], leading to the formation of magnesium hydroxide $\text{Mg}(\text{OH})_2$ (brucite) and amorphous hydrous silica or magnesium silicate hydrate $3\text{MgO} \cdot 2\text{SiO}_2 \cdot 2\text{H}_2\text{O}$ (Fig. 2.9) as reported by Gollop and Taylor [31]. However, the barely soluble brucite can also act as a protective layer which decreases the ingress of further sulfate ions as mentioned by Santhanam et al. [33].

Effect of leaching and sulfate interaction

Generally, leaching and sulfate attack cannot be separated. Physical and chemical changes during leaching have been observed and modeled by various authors [89-93]. It was reported that leaching, the dissolution of portlandite and decalcification of the C-S-H phase affects the pore structure and the stability of the major hydrate phases as mentioned in 2.2.1- 2.2.3. Haga et al. [94, 95] found that leaching leads to an increase in porosity, especially capillary porosity of the affected concrete structures.

Investigations of Planel et al. [91] showed that calcium leaching in sulfate environments shows similar features as leaching in deionised water. However, the presence of sulfate led to the precipitation of ettringite and gypsum and the decomposition of the samples. The failure of the samples was observed to depend on their thickness as thin samples showed faster cracking and scaling.

As sulfate ions migrate into the concrete structure chemical gradients and reactions zones are formed. Calcium ions are necessary for the formation of ettringite, gypsum or thaumasite during sulfate interaction which also leads to a decalcification, especially in the sulfate enriched zones. It was observed that almost all portlandite was transformed into gypsum. After the consumption of the portlandite the C-S-H phase starts to decalcify. The resulting siliceous S-H gel may act as a source of silicate for thaumasite formation as mentioned in section 2.2.3.2.

Gypsum was observed to form as bands parallel to the surface [31] but also intermixed within the C-S-H phase and portlandite. The bands were observed to be 10 to 30 μm thick at intervals of 100 to 200 μm , partly discontinuous [31, 91]. Gypsum formation has also been reported to form protective layers thus decreasing further ingress of sulfate ions with reaction time.

This physical increase in solid volume due to the formation of secondary sulfate phases like ettringite and gypsum, see 2.2.1, was reported to result in a temporary densification of the microstructure [96] which was accompanied by an increase in compressive strength at the early age of sulfate interaction according to Brown and Badger [97].

Sulfate interaction is often related to crack formation, observed to be partly parallel and partly perpendicular to the sample surface. The parallel cracks are often filled with gypsum, whereas the perpendicular cracks are often observed along the aggregates and at greater depth of the affected samples [64]. The regions where crack propagation is observed and expansion is taking place are described as areas where ettringite has formed described by Gollop and Taylor [31]. It appears that expansion is a delayed or possibly an indirect

consequence of ettringite formation and that gypsum recrystallises in cracks formed by other mechanisms.

After the formation of the first micro and macro cracks due to sulfate interaction, the microstructure starts to break down, the compressive strength decreases and gypsum as well as ettringite are observed by Irassar et al. [9]. Furthermore in the presence of cracks the expansion of the samples was found to be accelerated due to an increase in sulfate uptake according to Monteiro and Kurtis [22].

The changes in the microstructure are also influenced by the presence of aggregates in the microstructure. The Interfacial transition zone (ITZ) between aggregates and cement paste is characterised by higher porosities thus influencing the permeability and accelerating the migration of sulphate ions as described by Diamond [98].

Influence of mineral admixtures including limestone

Investigations on the influence of limestone addition on durability of Portland cements during sulfate attack showed that the extent of deterioration varies with the amount of limestone added and the kind of aggregates used.

In particular mortars made of cements with high amounts of limestone (up to 20 wt%) showed high expansion independent of the type of cement used (high or low C_3A content), Irassar et al. [9]. Generally, sulfate attack on the samples containing limestone was found to be more destructive at 5 °C than at 20 °C [59, 99].

Investigation of Higgins, Higgins and Crammond [100, 101] revealed that a replacement of 70% of cement with slag improved the sulfate resistance of the concrete containing carbonate aggregate and cement with both high and low C_3A content. Furthermore it was found that curing in air proved beneficial against conventional sulfate attack. They concluded that air curing leads to the formation of a carbonated surface layer which gives a dense microstructure before sulfate exposure.

Other investigation from Tivillis et al. [6] of limestone cement mortar on different specific mineral replacements, e.g. natural pozzolans, fly ash, slag showed that the use of these mineral additives retards thaumasite formation in limestone cement mortar. They concluded that the incorporation of slag or fly ash substantially improves the resistance against sulfate attack. The effectiveness of pozzolans depends on the rate of reaction and their ability to form additional C-S-H. Pozzolans with high reactivity and high contents of silicon dioxide (SiO_2) are reported to be effective [29, 20, 1, 15].

2.3 Summary

Sulfate attack has been under investigation for many years now. However, a complete understanding of the sulfate induced deterioration processes is still lacking. Especially, the investigations on thaumasite formation are often contradictory. Although, a lot of research has been done recently, it has not been definitively established to what extent sulfate concentration and limestone addition influence the formation of thaumasite. Furthermore, the influence of leaching, which has been observed to have an impact on thaumasite formation in real structures, is not well understood until now.

This study of the literature reveals many questions on sulfate attack and thaumasite formation which this work seeks to address:

- What are the factors favouring thaumasite formation?
- What are the limiting factors for thaumasite formation?
- Is there a correlation between chemical and physical effects during sulfate attack?
- Is it possible to define the mechanisms of thaumasite formation?
- What can we learn about TSA?

Generally, this work attempts to further understand the complex mechanisms of sulfate attack and particularly thaumasite formation and tries to provide a more comprehensive understanding of the sulfate interaction.

2.4 References

1. Taylor, H.F.W., *Cement Chemistry*. 1997 (London: Thomas Telford).
2. Locher, F.W., Richartz, S., and S., S., *Erstarren von Zement: I. Reaktion und Gefügeentwicklung*. Zement-Kalk-Gips, 1976. 29, 435-442.
3. Scrivener, K.L., *The development of microstructure during the hydration of Portland cement*. PhD thesis, 1984, University of London.
4. Damidot, D. and Glasser, F.P., *Thermodynamic Investigation of the $\text{CaO-Al}_2\text{O}_3\text{-CaSO}_4\text{-H}_2\text{O}$ System at 25 °C and the Influence of Na_2O* . Cement Concrete Research, 1993. 23, 221-238.
5. Collepardi, M., Baldini, G., and Pauri, M., *Tricalcium aluminate hydration in the presence of lime, gypsum and sodium sulfate*. Cement Concrete Research, 1978. 5, 571-580.
6. Tsvilis, S., Kakali, G., Skaropoulou, A., Sharp, J.H., and Swamy, R.N., *Use of mineral admixtures to prevent thaumasite formation in limestone cement mortar*. Cement Concrete Composites, 2003. 25 (8), 969-976.
7. Stark, J., *Oprimierte Bindemittelsysteme für die Betonindustrie*. Beton, 2004. 10 486-490.
8. Uchikawa, H., Hanehara, S., and Hirao, H., *Influence of microstructure on the physical properties of concrete prepared by substituting mineral powder for part of fine aggregate*. Cement Concrete Research, 1996. 26, 101-111.
9. Irassar, E.F., Bonavetti, V.L., and Gonzalez, M., *Microstructural study of sulfate attack on ordinary and limestone Portland cements at ambient temperature*. Cement Concrete Research, 2003. 33, 31-41.
10. Torres, S.M., Sharp, J.H., Swamy, R.N., Lynsdale, C.J., and Huntley, S.A., *Long term durability of Portland-limestone cement mortars exposed to magnesium sulfate attack*. Cement Concrete Composites, 2003. 25 (8), 947-954.
11. Kuzel, H. and Pöllmann, H., *Hydration of C_3A in the presence of $\text{Ca}(\text{OH})_2$, $\text{CaSO}_4 \cdot 2\text{H}_2\text{O}$ and CaCO_3* . Cement Concrete Research, 1991. 21, 885-895.
12. Matschei, T., Lothenbach, B., Glasser, F.P., *The role of calcium carbonate in cement hydration*. unpublished, 2006.
13. Lothenbach B., W.F., *Thermodynamic modelling of the hydration of Portland cement*. Cement Concrete Research, 2006. 36 (2), 209-226.
14. Catinaud, S., Beaudoin, J.J., and Marchand, J., *Influence of limestone addition on calcium leaching mechanisms in cement-based materials*. Cement Concrete Research, 2000. 30 (12), 1961-1968.
15. Taylor, H.F.W. and Gollop, R.S., *Some chemical and microstructural aspects of concrete durability*, in *Mechansisms of chemical degradation of cement-based systems*, K.L. Scrivener and J.F. Young, Editors. 1997, E & FN Spon: London. p. 177-184.
16. Scherer, G.W., *Stress from crystalisation of salt*. Cement and Concrete Research, 2004. 34 (9), 1613-1624.
17. Metha, P.K., *Mechansim of expansion associated with ettringite formation*. Cement and Concrete Research, 1973. 3 (1), 1-6.
18. Famy, C. and Taylor, H.F.W., *Ettringite in hydration of portland cement concrete and its occurence in mature concretes*. ACI Materials Journal, 2001. 98, 350-356.
19. Skalny, J., Marchand, J., and Odler, I., *Sulfate attack on concrete*. Modern concrete technology, ed. A. Bentur and S. Mindess. Vol. 10. 2002, London: Spon Press. 217.
20. Stark, J. and Wicht, B., *Dauerhaftigkeit von Beton*. 2001 (Schädigende Ettringitbildung).

21. Kollmann, H., *Untersuchungen über das Ausblühungs- und Treiberscheinungen durch Sulfate, Teil 3*. Betonwerk und Fertigteil-Technik, 1979. 12, 741-746.
22. Monteiro, P.J. and Kurtis, K.E., *Time to failure for concrete exposed to severe sulfate attack*. Cement Concrete Research, 2003. 33 (7), 987-993.
23. Khatari, R.P. and Sirivivatnanon, *Role of permeability in sulphate attack*. Cement Concrete Composites, 1997. 27, 1179-1189.
24. Lothenbach B., Wieland, E., *A thermodynamic approach to the hydration of sulphate-resisting Portland cement*. waste management, 2006. 26 (7), 706-719.
25. Neubauer, J. and Götz-Neunhoeffer, F., *Efficiency of high sensitive heat flow calorimetry in examination of OPC hydration*. Proc 24th Int. Conf. Cement Microscopy, San Diego, Californien, 2002.
26. Möschner, G., Lothenbach, B., Rose, J., Ulrich, A., Figi, R., and Kretschmar, R., *Solid solution between Al-ettringite and Fe-ettringite ($\text{Ca}[\text{Al}_{1-x}\text{Fe}_x(\text{OH})_6]_2(\text{SO}_4)_3 \cdot 26\text{H}_2\text{O}$)*. Geochim Cosmochim Acta, 2007 (submitted).
27. Anderson, M., *Incorporation of aluminium in the C-S-H of hydrated portland cements: a high field ^{27}Al and ^{29}Si MAS NMR investigation*. Inorganic chemistry, 2003. 42, 2280-2287.
28. Richardson, I.G. and Gorves, G.W., *The incorporation of minor and trace elements into calcium silicate hydrate (C-S-H) gel in hardened cement pastes*. Cement Concrete Research, 1993. 23, 131-138.
29. Metha, P.K., *Meachnism of sulfate attack on portland cement concrete-another look*. Cement Concrete Research, 1983. 13, 401-406.
30. Gollop R. and Taylor, H.F.W., *Microstructural and Microanalytical Studies of Sulfate Attack, IV. Reactions of a Slag Cement paste with Sodium and Magnesium Sulfate Solution*. Cement Concrete Research, 1996. 26, 1013-1028.
31. Gollop R. and Taylor H.F.W., *Microstructural and Microanalytical Studies of Sulfate Attack, I. Ordinary Portland Cement Paste*. Cement Concrete Research, 1992. 22, 1027-1038.
32. Marchand, J., Samson, E., Maltais, Y., and Beaudoin, J.J., *Theoretical analysis of the effect of weak sodium sulfate solutions on the durability of concrete*. Cement Concrete Composites, 2002. 24 (3-4), 317-329.
33. Santhanam, M., Cohen, M.D., and Olek, J., *Sulfate attack research -- whither now?* Cement Concrete Research, 2001. 31 (6), 845-851.
34. Kollmann, H., *Untersuchungen über Ausblühungs- und Treiberscheinungen durch Sulfate, Teil 2*. Betonwerk und Fertigteil-Technik, 1979. 11, 671-677.
35. Kollmann H. and Strübel G., *Untersuchungen über Ausblühungs- und Treiberscheinungen durch Sulfate Teil 1*. Betonwerk und Fertigteil-Technik, 1978. 10, 609-613.
36. Koch, A. and Steinegger, H., *Ein Schnellprüfverfahren für Zemente auf ihr Verhalten bei Sulfatangriff*. Zement-Kalk-Gips, 1960. 7, 317-324.
37. Wittekindt, W., *Sulfatbeständige Zemente und ihre Prüfung*. Zement-Kalk-Gips, 1960. 12.
38. Bellmann, F., Moser, B., and Stark, J., *Influence of sulfate solution concentration on the formation of gypsum in sulfate resistance test specimen*. Cement Concrete Research, 2006. 36 (2), 358-363.
39. Erlin, B. and Stark, D.C., *Identification and occurrence of thaumasite in concrete*. Highway Research record, 1965. 113, 108-113.
40. The Thaumasite Expert Group, *The thaumasite form of sulfate attack: risks, diagnosis, remedial works and guidance on new constructions*. 1999: London. p. 180.
41. Nordenskiöld, A.E., *Anmärkningar om thaumasiten*. Geol. Fören. Förhandel., 1880. 62, 270-272.

42. Barnett, S.J., Macphee, D.E., Lachowski, E.E., and Crammond, N.J., *XRD, EDX and IR analysis of solid solutions between thaumasite and ettringite*. Cement Concrete Research, 2002. 32 (5), 719-730.
43. Bensted, J., *Thaumasite -- background and nature in deterioration of cements, mortars and concretes*. Cement Concrete Composites, 1999. 21 (2), 117-121.
44. Crammond, N.J., *Quantitative x-ray diffraction analysis of Ettringite, Thaumasite and gypsum in concretes and mortars*. Cement Concrete Research, 1985. 15 (3), 431-442.
45. Macphee, D. and Diamond, S., *Thaumasite in Cementitious Materials*. Cement Concrete Composites, 2003. 25 (8), 805-807.
46. Sibbick, R.G., Crammond, N.J., and Metcalf, D., *The microscopical characterisation of thaumasite*. Cement Concrete Composites, 2003. 25 (8), 831-837.
47. Skipsted J., Hjorth L., and J., J.H., *Quantification of thaumasite in cementitious materials by $^{29}\text{Si}\{^1\text{H}\}$ cross-polarisation magic-angle spinning NMR spectroscopy*. Advances in cement research, 1995. 7, 69-83.
48. Torres, S.M., Kirk, C.A., Lynsdale, C.J., Swamy, R.N., and Sharp, J.H., *Thaumasite-ettringite solid solutions in degraded mortars*. Cement Concrete Research, 2004. 34 (8), 1297-1305.
49. Bensted, J., *Mechanism of thaumasite sulphate attack in cements, mortars and concretes*. Zement Kalk Gips, 2000. 53, 704-709.
50. Crammond, N.J. and Halliwell, M.A. *The thaumasite form of sulfate attack in concretes containing a source of carbonate ions -- a microstructural Overview*. in *International Symposium for Advances in Concrete Technology*. 1995.
51. Diamond, S., *Thaumasite in Orange County, Southern California: an inquiry into the effect of low temperature*. Cement Concrete Composites, 2003. 25 (8), 1161-1164.
52. Collepardi, M., *Thaumasite formation and deterioration in historic buildings*. Cement Concrete Composites, 1999. 21 (2), 147-154.
53. Hobbs, D.W., *Thaumasite sulfate attack in field and laboratory concretes: implications for specifications*. Cement Concrete Composites, 2003. 25 (8), 1195-1202.
54. Hobbs, D.W. and Taylor, M.G., *Nature of the thaumasite sulfate attack mechanism in field concrete*. Cement Concrete Research, 2000. 30 (4), 529-533.
55. Zhou, Q., Hill, J., Byars, E.A., Cripps, J.C., Lynsdale, C.J., and Sharp, J.H., *The role of pH in thaumasite sulfate attack*. Cement Concrete Research, 2006. 36 (1), 160-170.
56. Gaze, M.E. and Crammond, N.J., *The formation of thaumasite in a cement:lime:sand mortar exposed to cold magnesium and potassium sulfate solutions*. Cement Concrete Composites, 2000. 22 (3), 209-222.
57. Jallad, K.N., Santhanam, M., and Cohen, M.D., *Stability and reactivity of thaumasite at different pH levels*. Cement Concrete Research, 2003. 33 (3), 433-437.
58. M. Kalinowski and Trägårdh, J., *Thaumasite and Gypsum formation in SCC with sulfate resistant cement exposed to a moderate sulfate concentration*. Second North American Conference on the Design and Use of Self-Consolidating Concrete, 2005. Section 3 (durability) 319-325.
59. Hartshorn, S.A., Sharp, J.H., and Swamy, R.N., *The thaumasite form of sulfate attack in Portland-limestone cement mortars stored in magnesium sulfate solution*. Cement Concrete Composites, 2002. 24 (3-4), 351-359.
60. Romer, M., Holzer, L., and Pfiffner, M., *Swiss tunnel structures: concrete damage by formation of thaumasite*. Cement Concrete Composites, 2003. 25 (8), 1111-1117.
61. Collett, G., Crammond, N.J., Swamy, R.N., and Sharp, J.H., *The role of carbon dioxide in the formation of thaumasite*. Cement Concrete Research, 2004. 34, 1599-1612.

62. F. Bellmann, R. Röck, and Stark, J., *Thaumasite damage in a shotcrete tunnel lining*. Cement International, 2005. 3, 103-109.
63. Blanco-Varela, M.T., Aguilera, J., and Martinez-Ramirez, S., *Effect of cement C3A content, temperature and storage medium on thaumasite formation in carbonated mortars*. Cement Concrete Research, 2006. 36 (4), 707-715.
64. Brown, P. and Hooton, R.D., *Ettringite and thaumasite formation in laboratory concretes prepared using sulfate-resisting cements*. Cement Concrete Composites, 2002. 24 (3-4), 361-370.
65. Nobst, P. and Stark, J., *Investigations on the influence of cement type on thaumasite formation*. Cement Concrete Composites, 2003. 25 (8), 899-906.
66. Nobst P. and Stark J., *Untersuchungen zur Thaumasitbildung bei inneren und äusseren Sulfatangriff*. 16. Ibausil 2006, 2006. 2 2-0547-0542-0556.
67. Juel, I., Herfort, D., Gollop, R., Konnerup-Madsen, J., Jakobsen, H.J., and Skibsted, J., *A thermodynamic model for predicting the stability of thaumasite*. Cement Concrete Composites, 2003. 25 (8), 867-872.
68. Barnett, S.J., Adam, C.D., and Jackson, A.R.W., *Solid solutions between ettringite and thaumasite*. Journal of Material Science, 2000. 35, 4109-4114.
69. Macphee, D. and Barnett, S.J., *Solution properties of solids in the ettringite--thaumasite solid solution series*. Cement Concrete Research, 2004. 34, 1591-1598.
70. Barnett, S.J., Macphee, D., and Crammond, N.J., *Extent of immiscibility in the ettringite-thaumasite system*. Cement Concrete Composites, 2003. 25 (8), 851-855.
71. Glasser, F.P., *The stability of ettringite*. Internal sulfate attack and delayed ettringite formation (K.L. Scrivener and J.P. Skalny, eds.), 2002 (RILEM:Villars, Switzerland) 43-63.
72. Pajares, I., Martinez-Ramirez, S., and Blanco-Varela, M.T., *Evolution of ettringite in presence of carbonate, and silicate ions*. Cement Concrete Composites, 2003. 25 (8), 861-865.
73. Bensted, J., *Thaumasite--direct, woodfordite and other possible formation routes*. Cement Concrete Composites, 2003. 25 (8), 873-877.
74. Lukas, W., *Betonzerstörung durch SO₃ - Angriff unter Bildung von Thaumasit und Woodfordit*. Cement Concrete Research, 1975. 5, 503-518.
75. Köhler, S., Heinz, D., Urbonas L., *Effect of ettringite on thaumasite formation*. Cement Concrete Research, 2005.
76. Bellmann, F., *On the formation of thaumasite $\text{CaSiO}_3\text{CaSO}_4\text{CaCO}_3\cdot 15\text{H}_2\text{O}$ Part II*. Advances in cement research, 2004. 16, 89-94.
77. Bellmann, F., *On the formation of thaumasite Part I*. Advances in cement research, 2004. 16 (2) 55-60.
78. Mulenga, D.M., Nobst, P., and Stark, J., *Thaumasitbildung in Beton als Folge des Sulfatangriffs*. Wissenschaftliche Zeitschrift der Bauhaus-Universität Weimar, 2001. 5 51-63.
79. Oberholster, R.E., *Deterioration of mortar, plaster and concrete: South Africa laboratory and field studies*. First International Conference on Thaumasite in Cementitious Materials, 2002. paper 42 (Garston (UK)).
80. Gaze, M.E., *The effects of varying gypsum content on thaumasite formation in a cement:Lime:Sand mortar at 5 °C*. Cement Concrete Research, 1997. 27 (2), 259-265.
81. Bickley, J.A., Hemmings, R.T., Hooton, R.D., and Balinski, J. *Thaumasite related deterioration of concrete structures (V. Mohan Malhotra Symposium)*. in *Concrete technology: past, present, and future*. 1995: ACI.
82. Crammond, N.J., *Thaumasite in Failed cement mortars and renders from exposed brickwork*. Cement Concrete Research, 1985. 15, 1039-1050.

83. Drabik, M., Galikova, L., and Janotka, I., *Determination of the Presence of Thaumasite in Sulphate attacked Concrete by Methods of Thermo Analysis*. Ibautil, 2003, 2-0701-0709.
84. Gouda, G.R., Roy, D.M., and Sarkar, A., *Thaumasite in Deteriorated Soil_Cements*. Cement Concrete Research, 1975. 5, 519-522.
85. Romer, M., *Steam locomotive soot and the formation of thaumasite in shotcrete*. Cement Concrete Composites, 2003. 25 (8), 1173-1176.
86. Crammond, N., *The occurrence of thaumasite in modern construction - a review*. Cement Concrete Composites, 2002. 24 (3-4), 393-402.
87. Crammond, N.J., *The thaumasite form of sulfate attack in the UK*. Cement Concrete Composites, 2003. 25 (8), 809-818.
88. Matthews, S., available at <http://bre.co.uk/service>. BRE, Bucknalls Lane, Watford WD25 9XX, 2007.
89. Andac Muberra and Paul, G.F., *Long-term leaching mechanisms of Portland cement-stabilized municipal solid waste fly ash in carbonated water*. Cement Concrete Research, 1999. 29 (2), 179-186.
90. Galle, C., Peycelon, H., and Bescop, P.L., *Effect of an accelerated chemical degradation on water permeability and pore structure of cement-based materials*. Advances in cement research, 2004. 16, 105-114.
91. Planel D., Sercombe J., Le Besop P., Adenot F., and J.M., T., *Long-term performance of cement paste during combined calcium leaching-sulfate attack: kinetics and size effect*. Cement Concrete Research, 2006. 36, 137-143.
92. Taylor, H.F.W., Famy, C., and Scrivener, K.L., *Delayed ettringite formation*. Cement Concrete Research, 2001. 31, 683-693.
93. Yokozeki, K., Watanabe, K., Sakata, N., and Otsuki, N., *Modeling of leaching from cementitious materials used in underground environment*. Applied Clay Science, 2004. 26 (1-4), 293-308.
94. Haga, K., Shibata, M., Hironaga, M., Tanaka, S., and Nagasaki, S., *Change in pore structure and composition of hardened cement paste during the process of dissolution*. Cement Concrete Research, 2005. 35 (5), 943-950.
95. Haga, K., Sutou, S., Hironaga, M., Tanaka, S., and Nagasaki, S., *Effects of porosity on leaching of Ca from hardened ordinary Portland cement paste*. Cement Concrete Research, 2005. 35 (9), 1764-1775.
96. Mulenga, D.M., *Zum Sulfatangriff auf Beton und Mörtel einschliesslich der Thaumasitbildung*. 2002.
97. Brown, P.W. and Badger, S., *The distribution of bound sulfates and chlorides in concrete subjected to mixed NaCl, MgSO₄, Na₂SO₄ attack*. Cement Concrete Research, 2000. 30, 1535-1542.
98. Diamond, S., *A discussion of paper "Patch microstructure in cement based materials: fact or artefact?"* Cement Concrete Research, 2006. 36, 998-1001.
99. Irassar, E.F., Bonavetti, M.A., Trezza, M.A., and Gonzalez, M., *Thaumasite formation in limestone filler cements exposed to sodium sulphate solution at 20 °C*. Cement Concrete Composites, 2005. 27, 77-84.
100. Higgins, D.D., *Increased sulfate resistance of ggbs concrete in the presence of carbonate*. Cement Concrete Composites, 2003. 25 (8), 913-919.
101. Higgins, D.D. and Crammond, N.J., *Resistance of concrete containing ggbs to the thaumasite form of sulfate attack*. Cement Concrete Composites, 2003. 25 (8), 921-929.

3 Materials and Methods

This chapter describes the strategy of the experimental program, the materials and the analytical techniques used in this study. To understand how and to what extent limestone addition, sulfate concentration, leaching and storage temperature influence thaumasite formation and sulfate interaction, multiple techniques were used. In this project, laboratory cements based on industrial clinkers were produced to cover the compositional variations in C_3A and limestone filler contents comparable to the commercial products used in Switzerland. The experimental program considers two main parts, the cement paste experiments, investigating the conditions of thaumasite formation including thermodynamic modelling. The mortar experiments investigate the consequences of sulfate interaction including frequent measurements, e.g. surface specific measurements, illustrated in Fig. 3.1.

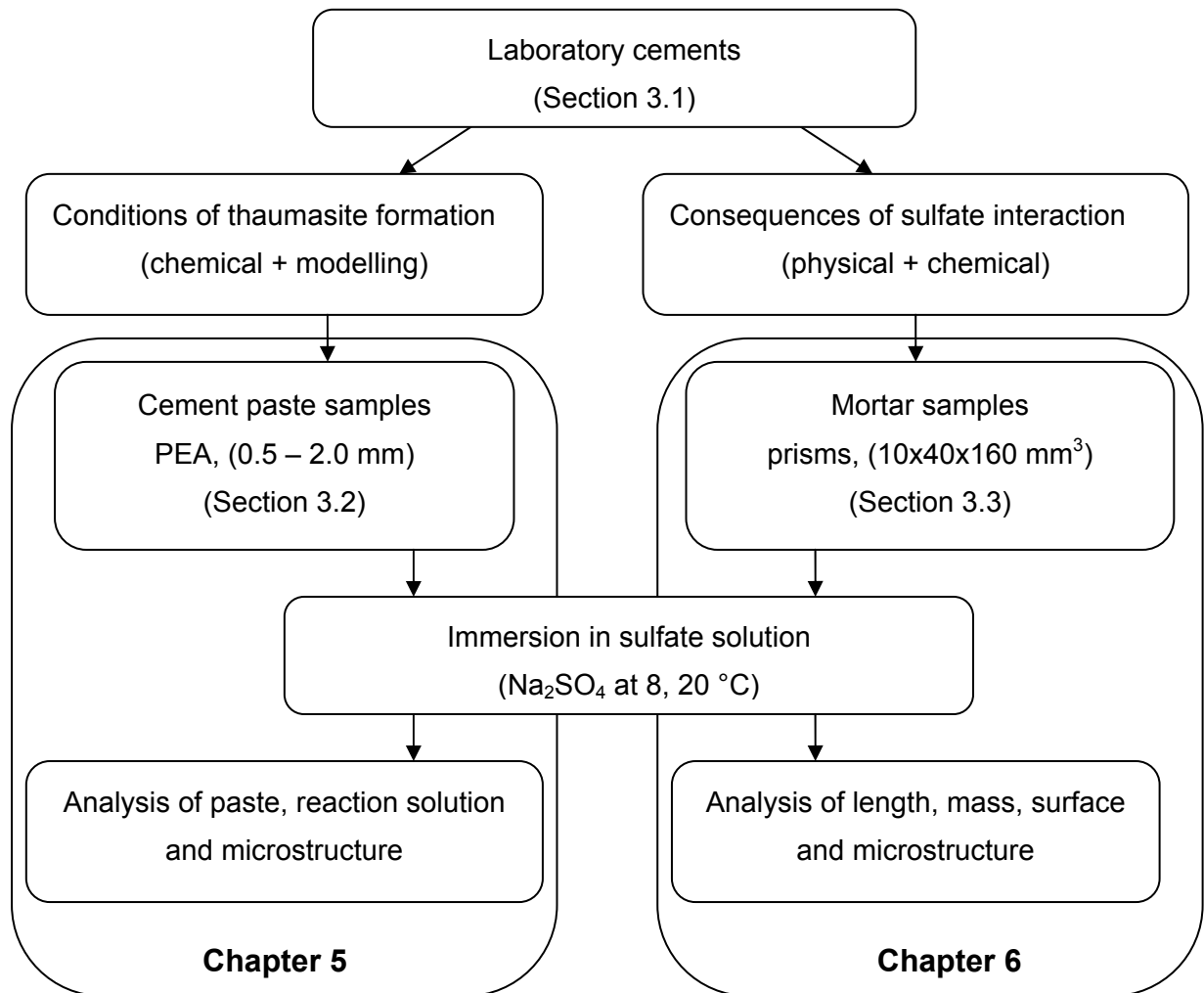


Fig. 3.1: Experimental program and overview of analysis for the study.

3.1 Laboratory cements

The experiments were performed on laboratory cements which were prepared from industrial clinkers representing sulfate resistant Portland cement, HS (low C_3A), and ordinary Portland cement, OPC (high C_3A). The other constituents used for the production of the laboratory cements were synthetic gypsum ($CaSO_4 \cdot 2H_2O$, Fluka Chemie) and fine natural, almost pure calcite powder ($CaCO_3$, Omya, Orgon France) as limestone filler. The limestone filler used has a Blaine specific surface area of $5800 \text{ cm}^2/\text{g}$ – somewhat coarser than the calcite in interground cements.

The chemical composition of the laboratory cements (HS, OPC) without limestone addition, the limestone filler used as well as the mineralogical composition of the cements are given in Table 3.1.

Table 3.1: Composition of the HS and OPC cements including gypsum and limestone filler used

| Chemical composition [wt%] ⁱ | | | | Mineralogical composition [wt%] ⁱⁱ | | |
|---|------|------|-----------|---|-----|-----|
| | HS | OPC | Limestone | | HS | OPC |
| SiO_2 | 19.2 | 20.1 | 0.08 | C_3S | 62 | 66 |
| Al_2O_3 | 4.7 | 4.4 | 0.17 | C_2S | 9 | 10 |
| Fe_2O_3 | 7.2 | 2.7 | 0.03 | C_3A | 0.4 | 7 |
| CaO | 62.2 | 63.7 | 55.6 | C_4AF | 22 | 8 |
| MgO | 1.5 | 1.6 | 0.29 | | | |
| K_2O | 1.1 | 0.9 | 0.01 | | | |
| Na_2O | 0.13 | 0.15 | 0.01 | | | |
| SO_3 | 1.9 | 2.9 | 0.01 | | | |
| CO_2 | 0.1 | 0.2 | 43.7 | | | |
| CaO_{free} | 0.6 | 0.9 | | | | |
| LOI | 0.68 | 1.21 | | | | |
| total | 99.3 | 98.8 | 99.9 | | | |

ⁱobtained from XRF analysis; ⁱⁱaccording to Bogue calculation

For the production of the laboratory cements, the cement clinkers were ground using a laboratory ball mill as described in Appendix A.1. The cement clinkers were ground to Blaine specific surface area of $3500 \text{ cm}^2/\text{g}$.

After grinding of the clinker, pure analytical gypsum was used to adjust the appropriate sulfate content for HS ($SO_3 \text{ tot} = 1.9 \text{ wt\%}$) and OPC ($SO_3 \text{ tot} = 2.9 \text{ wt\%}$) cement using isothermal calorimetry (TAM Air). For this study, about 6g cement were mixed with 2.4g water in glass ampoules to give a water to cement ratio of 0.4 before placing the samples in the calorimeter. The twin configuration of laboratory cement samples and industry cement samples (reference) in the calorimeter channels allows to directly compare the heat flow of

the cement systems (Fig. 3.2). The heat of hydration of the laboratory cements was adjusted compared to the industry cements as shown in Appendix A 1 (Figs. A 1.3, A 1.4).

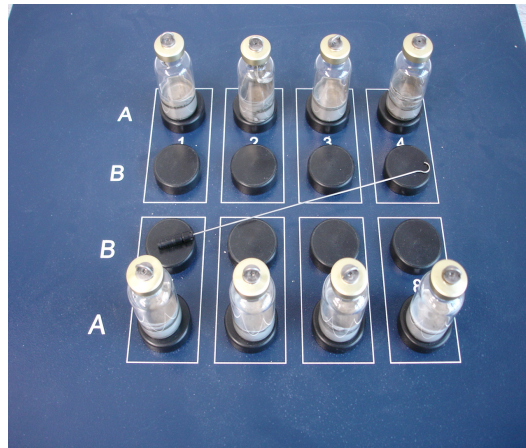


Fig. 3.2: Batch samples on TAM Air calorimeter.

To study the effect of limestone addition during exposure to sulfates some of the cements remained unchanged, without limestone addition (H0, P0) or were blended by replacing 5 wt% (H5, P5) and 25 wt% (P25) cement by calcite as shown in Table 3.2.

Table 3.2: Limestone addition and nomenclature of laboratory cements in wt%

| Cement clinker | Limestone filler addition LF | | |
|---------------------------|------------------------------|--------------|----------------|
| HS (low C_3A) | H0: 0 | H5: 5 | |
| OPC (high C_3A) | P0: 0 | P5: 5 | P25: 25 |

For the final production of the laboratory cements the relevant constituents were mixed and homogenized mechanically as described in the Appendix A 1.1. All laboratory cements were tested according to the standard EN 196 (1-4) [1] and proved to conform with the commercial products as shown in Appendix A 1 (Table A 1.1).

3.2 Cement paste samples

The aim of the cement paste experiments was to investigate the chemical aspects of sulfate interaction. The investigations used a concept - the Progressive Equilibrium Approach (PEA)- to analyse the conditions of thaumasite formation with respect to internal carbonate, sulfate concentration and leaching. To enhance the specific surface and to speed up the chemical interaction the experiments were performed with crushed hydrated cement paste. After interaction with a sulfate solution the compositions of the solid and liquid phase were determined and compared with the calculations from the thermodynamic model (section 3.5). In addition the microstructure of selected samples was investigated.

3.2.1 Experimental set up

The experiments were performed on hydrated cement pastes which were prepared from the laboratory cements. The cement pastes were produced at a water/binder ratio of 0.35 and fabricated as prisms of 40x40x160 mm³ and stored for 24h at 20 °C and 90 % relative humidity. After demoulding, the prisms were cured until 56d in saturated limewater at 20 °C before crushing the hydrated cement paste to particles of the size 0.5 – 2 mm (Fig. 3.4). Particles of smaller or bigger in size (< 30 wt%) were analysed to be chemically identical but not used in the experiments.



Fig. 3.3: Hydrated cement paste prisms, 56d

Fig. 3.4: Crushed, hydrated cement paste

Artificially leached cement paste was obtained from the crushed cement paste by the following procedure. 70 g of crushed cement paste was mixed with 20l of deionised water and stored in sealed in polyethylene containers for four months at 20 °C. After 14, 28, 56 and

112 days the leaching water was exchanged with deionised water and the leachate was agitated frequently. The complete program for the leaching process is given in Table 3.3.

Table 3.3: Entire leaching procedure of the crushed cement paste samples

| leaching process | |
|--------------------|----------------------------------|
| samples | crushed cement paste |
| size | 0.5-2.0 mm |
| mass | 70g |
| liquid | demineralised water, volume: 20l |
| temperature | 20 °C |
| liquid/solid ratio | 286 |
| duration | 4 month |
| storage | polyethylene containers |
| water exchange | after 14, 28, 56 and 112 days |

Before and after leaching the hydrated cement paste particles were dried for 2 days at 40 °C until constant weight was reached. A part of it was ground to $\leq 40 \mu\text{m}$ or left as paste particles and stored in a desiccator at 20 °C until further analysis as described in 3.2.3.

The chemical composition of the laboratory cements before exposure to sulfates and before and after leaching was used as input data for the thermodynamic calculations as described in 3.5.

3.2.2 Progressive equilibrium approach PEA

The PEA aims to simulate the chemical gradient which can be found in real situations on concrete structures undergoing external sulfate attack over durations of several years [2]. The chemical gradient arises due to a diffusive mass exchange involving external sulfate. In the PEA fixed chemical subsystems are defined and subsequently simulated. These subsystems (A-E, sulfate addition only) and (BL-DL, leaching and sulfate addition) are defined by different levels of sulfate addition (Fig. 3.5).

The concentration of sulfate ions varies progressively from 20, 10, 5 to 2.5 wt% SO_4^{2-} in subsystems A to D by weight cement paste. The subsystem E represents the unaffected, sound concrete. For the sulfate interaction after the leaching process the amount of the sulfate addition varies respectively from 10, 5 to 2.5 wt% SO_4^{2-} in subsystem BL, CL and DL by weight of cement paste.

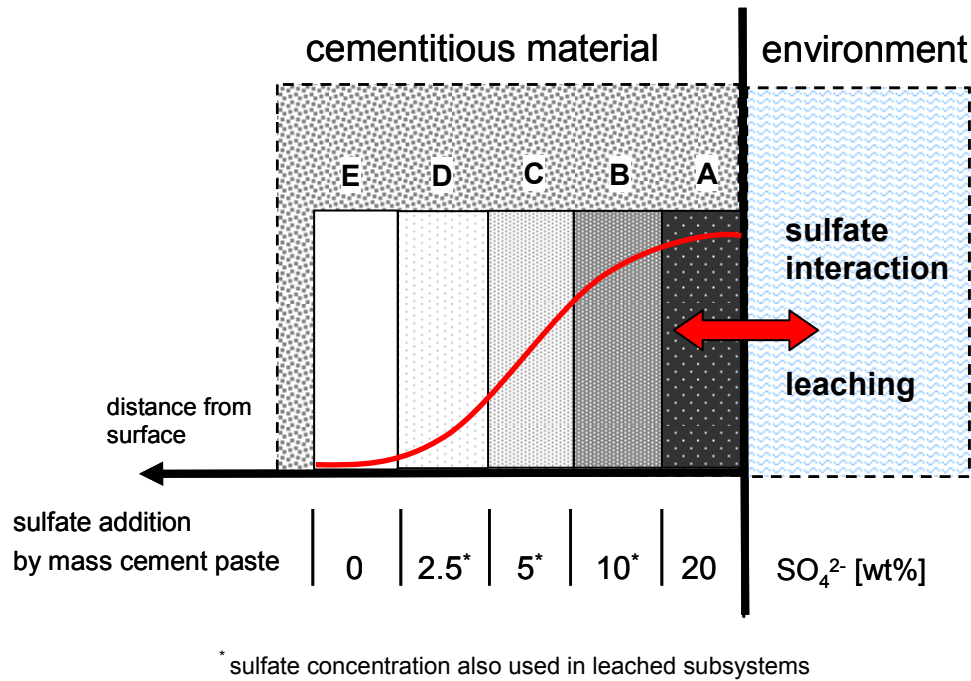


Fig. 3.5: Schematic illustration of the concept for the progressive equilibrium approach (PEA)

For each subsystem the crushed cement paste was immersed in aqueous reaction solution, which was prepared by dissolving adequate amounts of Na₂SO₄ in deionised water as described in more detail, see Appendix A 2. The experiments were then processed as closed subsystems at 8 °C and 20 °C and were shaken periodically (Fig. 3.6).

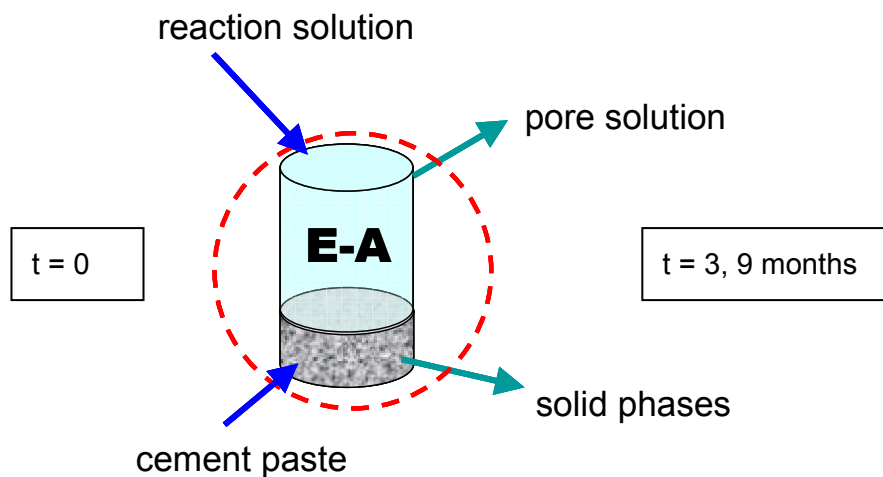


Fig. 3.6: Idealised scheme of subsystems according to the PEA experiments.

Since the time to attain equilibrium was not known, the subsystems were examined after 3 and 9 months. At equilibrium it can be assumed that the solution surrounding the cement paste is identical to the pore solution which itself is in equilibrium with the hydrate phase assemblage.

For the analysis of the PEA experiments the subsystems were filtered dividing the aqueous solution from the solid residue under vacuum using a 45 μm nylon membrane filter. The solid phase was immersed for 30 minutes in isopropanol to remove moisture and dried at 40 °C for 2 days until constant weight was reached. For further analysis the particles were ground to $\leq 40 \mu\text{m}$ and stored in a desiccator at 20 °C.

3.2.3 Analytical methods

For the analysis of the laboratory cements, their constituents and the hydrated cement paste before and during the experiments different analytical methods were applied.

X-ray fluorescence (XRF)

The chemical composition of the laboratory cements and the limestone filler was determined by wavelength dispersive X-ray fluorescence spectroscopy (WD-XRF). Therefore, the cement powders were prepared as homogeneous fused glass beads with dilithiumtetraborate as flux. The WD-XRF spectrometer (PANalytical PW 1404) is equipped with a Cr X-ray tube, 60 kV maximum voltage, 125 mA maximum current. The elemental composition of the powders was calculated as the mass fraction of the corresponding element oxides. The element oxides composition was then used for the calculation of the phase composition of the laboratory cements according to Bogue.

Thermogravimetric analysis (TGA)

The method measures the mass difference of a sample as a function of the temperature level. The loss of weight corresponds to the dehydration of different phases present and the evaporation of gas and water. Thermogravimetric analysis (TGA, Mettler Toledo TGA/SDTA851e) was carried out in nitrogen environment on 10mg of ground cement powder at 20 °C/min over a temperature range of 30 up to 980 °C. The TGA analysis was used on ground cement paste powder to determine the amount of portlandite present in the initial and leached cement pastes. The content of portlandite was calculated from the weight loss between 420-500 °C as shown in Appendix A 2 (Figs. A 2.2, A 2.3).

Mercury intrusion porosimetry

The method uses mercury to penetrate the sample as a non-wetting fluid into various pore diameters d . By increasing the pressure P progressively smaller pores are filled with mercury. The method allows to measure the pore size distribution for particularly capillary pores and air pores of a given sample. The porosity of the initial and leached samples was determined on 3 to 4g cement paste particles by using (MIP, THERMOELECTRON 140/440) up to a pressure of max 400 MPa.

X-ray diffraction (XRD)

X-ray diffraction (XRD) was used as an analytical technique for the identification of crystalline phases. The positions of reflections in the XRD pattern are determined by the spacing d of the crystallographic planes according to the wavelength λ of the radiation used and the angle θ of the diffraction peak.

The ground cement powders were analysed on 27 mm standard sample holders by X-ray diffraction (XRD, PANalytical X'pert PRO X'Celerator) using CuK α radiation, an accelerating voltage of 40 kV, current of 40 mA, angles 5 – 80° 2Theta. Phase identification was achieved by comparing the X-ray pattern obtained with an internationally recognised database of reference patterns (ICDD – International Center for Diffraction Data). The XRD analysis was used for the characterisation of anhydrous, leached cement powder and on ground cement powder from the PEA experiments.

Plasma optical emission spectrometry (ICP-OES, TIC) and pH

The concentration of Al, sulfate, Ca, K and Na of the aqueous solutions were determined using inductively coupled plasma optical emission spectrometry (ICP-OES, Varian, VISTA Pro) and carbonate was determined as total inorganic carbon (TIC, Shimadzu TOC-5000A).

The pH was determined immediately by a pH electrode (Knick pH-Meter 766 with a Knick SE pH7Pt 1000 electrode) which was calibrated against 0.1 to 1.0 molar KOH solutions using a part of the undiluted solution. For further analysis 1ml of pore solution was diluted with 9ml of 6.5% HNO₃ solution stored at 5 °C till further analysis. The analysis of the solutions was done after 3 and 9 months during the PEA experiments.

Nuclear magnetic resonance ²⁹Si-NMR

The NMR experiments were performed on a Bruker Avance 400 NMR spectrometer using a 7mm CP/MAS probe. The ²⁹Si CP/MAS NMR spectra were recorded at 79.49 MHz using the following parameters: 3000 Hz spinning speed, 800 μ s contact time, 6s relaxation delay for cement mixtures and 60s for mineral thaumasite (²⁹Si chemical shifts referenced to an external of tetramethylsilane). The quantities of thaumasite were determined using the method described in detail by Skibsted et al. [3, 4] with RF field strengths of 31.2 kHz during the polarisation transfer and 41.6 kHz for the 90° ¹H excitation pulse and during the decoupling sequence. A sample of natural thaumasite originating from Akschal (Kazakhstan) was found to be almost 100% pure (XRD). The relaxation times T_1^H and $T_{1\rho}^H$ were determined using standard Bruker pulse programs and processing software. For the mineral thaumasite $T_1^H \approx 8$ s was determined, this value decreased to 1s for cement sample containing Fe³⁺. The CP build up rates T_{SiH} were determined from least square two-parameter-fits of the CP build up curves for a) Akschal thaumasite, b) 10 wt-% of Akschal

thaumasite mixed with 90 wt-% of hydrated cement powder and c) thaumasite formed in a mortar sample after 1.5 years sulfate interaction at 8 °C. The following pairs of parameters were determined T_{SiH} [ms] / $T_{1\rho}^H$ [ms]: 0.42/3.83 (Akschal thaumasite); 0.55/3.39 (10% Akschal thaumasite) and 0.33/2.60 (thaumasite in mortar). The latter parameters were applied for the quantification of thaumasite in the PEA cement samples under investigation (accuracy of such results is believed to be within +/- 15%).

For the 10% Akschal sample 9.7% thaumasite was determined and 6.5% was found in the clinker cement. Selected HS samples did not show any ^{29}Si NMR signals at all owing to the increased amounts of iron therein.

3.3 Mortar samples

The aim of the mortar experiments was to investigate the physical consequences of sulfate interaction and thaumasite formation during sulphate exposure. The investigations used traditional test methods, a newly developed and non destructive ultrasound method and microscopy to analyse the microstructural changes during sulfate exposure.

3.3.1 Experimental set up

For the experiments the mortars were fabricated according to EN 196 part 1 [5] with a water/binder ratio of 0.5. The sand used was CEN – Normsand with a maximum grain size of 2mm. Slabs of 40 x 160 x 230 mm³ were cast.

The mortar slabs were cured for 28 days in saturated limewater (Ca(OH)_2 , $\text{pH} \geq 12.5$) at constant temperature (20 °C) to avoid leaching. After curing thin mortar samples were cut and ground to the size of 10 x 40 x 160 mm³. The size of the mortar prisms was comparable to the Wittekindt [6] method, but the exposed surface is sawn not cast (Fig. 3.7).

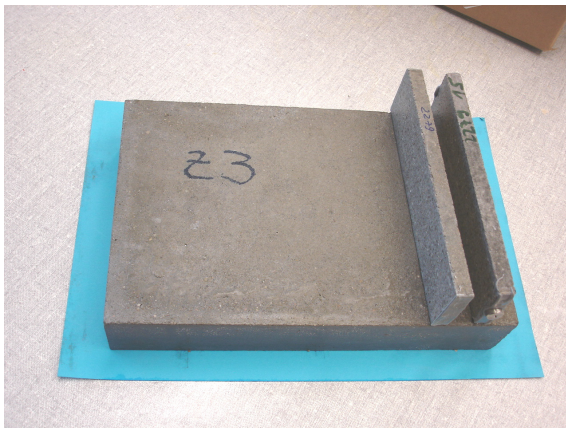


Fig. 3.7: Flat prisms cut from of mortar slab



Fig. 3.8: Mortar prisms sealed with plug gages.

After that the samples were sealed and plug gages were glued, using two components glue (Araldit, AV 138M) with hardener (HV 998) at the ends of the prisms. The samples were stored at 8 °C and 20 °C for 12 h in deionised water before sulfate exposure. For exposure the mortar prisms were stored in Na_2SO_4 solutions at the above mentioned temperatures.

The sulfate concentrations in the solutions were chosen close to common test conditions (30g $\text{SO}_4^{2-}/\text{l}$) as well as closer to real situations in the field (3g $\text{SO}_4^{2-}/\text{l}$). The liquid / solid – volume ratio of the batches was 4 to 1. The sulfate solutions were changed at regular intervals after 7, 14, 28, 56, 91, 180, 270, 365 days to maintain the conditions of constant sulfate concentration at the sample surface.

The reference samples were stored in limewater at the same temperatures. The experimental setup for the mortar experiments is summarized in Table 3.4.

Table 3.4: Experimental setup for mortar experiments

| cement | | H0 | H5 | P0 | P5 | P25 |
|--------------------|----------------------------------|---|----|-----------------------------|----|-----|
| | | HS (low C ₃ A) | | OPC (high C ₃ A) | | |
| limestone addition | [wt%] | 0 | 5 | 0 | 5 | 25 |
| aggregate | | silica sand | | | | |
| w/c – ratio | | 0.50 | | | | |
| compaction | | vibrated | | | | |
| specimen type | | flat prism | | | | |
| sample dimensions | [mm] | 10x40x160 | | | | |
| curing | limewater [Ca(OH) ₂] | 28d, pH ≥ 12.5 | | | | |
| exposure | field conditions | 3g SO ₄ /l (4,4g Na ₂ SO ₄ /l) | | | | |
| | test conditions | 30g SO ₄ /l (44,4g Na ₂ SO ₄ /l) | | | | |
| solution | volume (l/s) ⁱ | 4 to 1 | | | | |
| | exchange [d] | 7, 14, 28, 56, 91, 180, 270, 365 | | | | |
| temperature | ambient [°C] | 20 | | | | |
| | low [°C] | 8 | | | | |

ⁱliquid/solid – volume ratio

3.3.2 Ultrasonic measurements

A non-destructive test method was developed to monitor the physical properties of mortar samples [7]. The method is designed to measure the velocity of the Rayleigh waves. The response is sensitive to the top layer (less than 2 mm) of the samples.

The theory of surface sensitive Rayleigh waves as given by Bertoni and Tamir [8] uses an incident beam near the leaky Rayleigh angle θ_{LR} from the liquid onto the surface of the solid sample. This leads to a direct reflection of the beam (* in Fig. 3.9) and generates a leaky Rayleigh wave which causes a trailing field leaving the sample at the angle θ_{LR} (arrows in Fig. 3.9). The leaky Rayleigh or surface waves have a penetration depth of about one wavelength [9].

For a velocity of the leaky Rayleigh wave of 2 km/s and for a frequency of 1 MHz the wavelength λ corresponds to 2 mm which is suitable to study the top surface layer of a mortar.

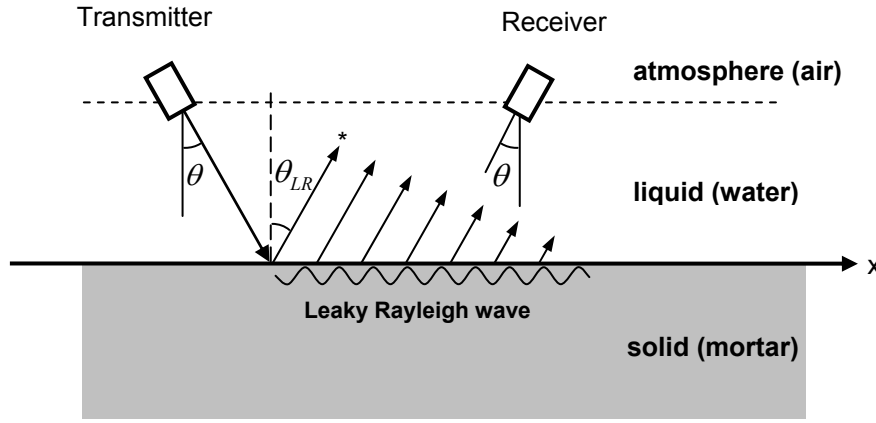


Fig. 3.9: Scheme for the mortar surface immersed in water and arrangement of ultrasonic probes modified from [10].

* direct reflection

The ultrasonic experiments were performed in demineralised water as coupling medium. The probes (1 MHz, 0.75" diameter) were attached to two manual goniometers which could be moved horizontally (parallel to the sample surface). The whole assembly was fixed on a 3-axis computer controlled stage to adjust the probes relative to the samples (Appendix A 5).

After the sample was placed under water the probes (immersed in water) were laterally set to a predefined position. The determination of the leaky Rayleigh wave velocity consisted of several steps. First the goniometers were set at Rayleigh angle and the goniometers angle of both goniometers were then adjusted repetitively with the focus of the probes on the sample surface (z-position) followed by scans with the receiver along the x-axis.

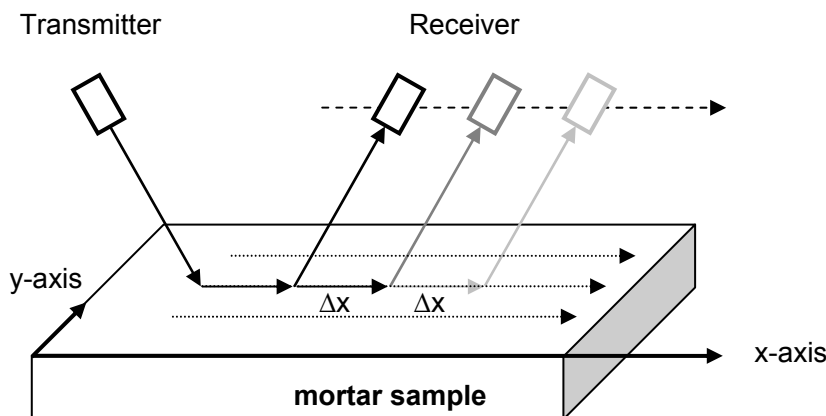


Fig. 3.10: Determination of the velocity of the Rayleigh wave by moving the receiver horizontally.

The probes were then adjusted and moved at intervals of $\Delta x = 5$ mm away from the transmitter to determine the temporal delay of the signal at each position. The whole procedure was repeated for two additional scans with offsets in y-direction of ± 5 mm (Fig. 3.10).

The velocity of the leaky Rayleigh wave with immersion technique can be determined by successively displacing the receiver probe by Δx (Fig 3.10) and measuring the time difference Δt of the signal relative to the preceding position of the receiver to give:

$$c_{LR} = \frac{\Delta x}{\Delta t} \quad (3.1)$$

The result c_{LR} of a sample is given as the average value of the velocities for three separate scans. The corresponding leaky Rayleigh angle θ_{LR} is determined by $\sin\theta_{LR} = c_l/c_{LR}$, with $c_l = 1.48$ km/s being the sound velocity of water.

3.3.3 Analytical methods

For the investigations of the mortar samples and to study the physical effects of the binder system including limestone addition as well as sulfate degradation mechanisms the following test methods were used.

Porosity

For the determination of porosity characteristics and the apparent density of the mortar samples a stepwise drying and wetting procedure was used according to the Swiss standard SIA 162-1 [11]. The porosity data were determined on mortar samples (20 x 40 x 40 mm³). Thereby, the total porosity is measured as the difference in mass of the water saturated sample to the dried (105 °C) sample. The air pores are obtained from the difference of the samples vacuum water saturated to the normal water saturated (7 days) sample. The capillary porosity was similarly obtained as the difference in mass of the water saturated sample (7 days) to the sample dried at 50 °C to constant weight. Finally, the gel porosity was calculated from the mass difference of the sample dried (105 °C) to the sample dried at 50 °C to constant weight.

Mass and length change

The uptake of sulfate from test solution during the exposure was investigated by the mass change of the specimens. The mass of specimen m_t was determined during exposure with a precision of 0.1g. The expansion behaviour of the mortar specimens was determined by measuring the length of the specimen l_t at defined time intervals during exposure. The changes in mass (Δm in %) and length (Δl in mm/m) of the mortar specimens were calculated relative to the initial values determined before sulfate exposure m_0 and l_0 respectively.

For the investigation changes in mass, length and Rayleigh wave velocity were followed up to one year of sulfate exposure according to the monitoring program.

3.4 Microscopy and microanalysis

For the microstructural investigations Scanning Electron Microscopy (SEM, Philips ESEM FEG XL 30) was used to analyse the micro- and nanostructure of selected samples of cement paste and mortar experiments. The chemical analysis was done using Energy Dispersive Spectroscopy (EDS).

The samples for SEM microscopy were prepared from mortar and cement paste by cutting, grinding and polishing to give representative micro sections of the surface and core regions. A detailed description is given in the Appendix A 4.

The samples examined by SEM were investigated using backscattered electron images (BSE) of polished and secondary electron images (SE) of fracture surfaces. Through interaction of the initial electron beam with the atoms of the sample secondary electrons, backscattered electrons and X-rays are generated and emitted (Fig. 3.11). Energy dispersive spectroscopy (EDS) is based on the detection of the characteristic X-rays generated for the elements in the material.

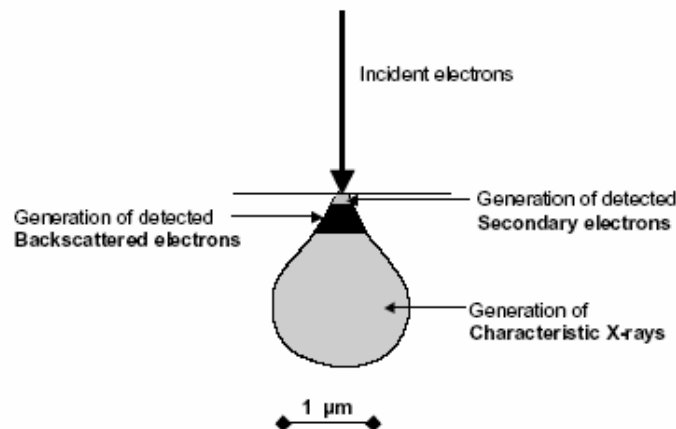


Fig. 3.11: Signal generation in the scanning electron microscope (SEM) reproduced from [12].

The polished samples were examined in high vacuum at a pressure of about $3.5 \cdot 10^{-6}$ mbar. The electron accelerating voltage was 15-20kV. The chemical analysis using EDS was done with a Li/Si crystal detector and an acceleration voltage of 15kV to provide best spatial resolution. The fracture samples were examined in low vacuum at a pressure of 1-2 mbar. The accelerating voltage used was 20kV.

The sulfate uptake was determined on selected, polished samples as the SO_3 content by mass cement paste by window analysis ($100 \times 100 \mu\text{m}$). At defined sample depths from affected surface towards the unaltered core the window analysis was done three times at each depth in order to gain good average values.

At specific sample depths, following the determined sulfate profile, EDS point analysis was done. The elements determined were Na, Mg, Al, Si, S, K, Ca, Fe, Ti and Mn; C and O were excluded to eliminate the effects of the resin and microporosity. The chosen elements were analysed as oxides and the EDS system software was used to automatically correct the analysis using ZAF corrections and suitable phase standard.

The atomic ratios of selected elements were plotted as Si/Ca, Al/Ca and S/Ca to investigate the hydrate phase assemblage of the surface, the transition zone and the unaltered core of selected samples during sulfate interaction. The stoichiometric composition of the pure phases are plotted to indicate the hydrate phases present.

3.5 Thermodynamic modelling approach

Thermodynamic calculations indicate the compositions of the investigated binder systems at equilibrium and can be applied to indicate the chemical reactions occurring during degradation processes. Thus it is possible to calculate the potential evolution of the cement systems under external sulfate attack and especially the conditions for thaumasite formation at equilibrium. However, kinetics will control the speed of chemical reactions at a given time until equilibrium is reached.

As input to the thermodynamic calculations the composition of the laboratory cements (assuming complete hydration) as given in Table 3.1 plus the amount of Na_2SO_4 and H_2O added to the system was used. The hydrate phases which were found to be stable in the investigated systems include C-S-H, portlandite, ettringite, thaumasite, monosulfate, monocarbonate, hemicarbonate, calcite, gypsum and hydrotalcite (M_4AH_{10}).

For iron the precipitation of iron-hydroxide ($\text{Fe}(\text{OH})_3$) or Fe_2O_3 was assumed. As detailed elsewhere [13, 14], C-S-H was calculated as a ideal solid solution between the end-members jennite $\text{C}_{1.67}\text{SH}_{2.1}$ and tobermorite $\text{C}_{0.83}\text{SH}_{1.3}$. The composition and the Ca/Si ratio of the C-S-H can vary from approximately 1.6 to 0. For the modelling it was considered that the alkalis which originate from the cements and from the Na_2SO_4 solution used, partition between the aqueous solution and the precipitating C-S-H. The uptake of Na and K by C-S-H was

calculated using a distribution ratio R_d of 0.42 ml/g [13, 14], where $R_d = \frac{c_s}{c_d} \frac{w}{s} \left[\frac{\text{ml}}{\text{g}} \right]$, c_s alkali

concentration in the solid phase [mol/l], c_d alkali concentration in the solution [mol/l] and w/s is the water/C-S-H ratio in ml/g.

- **Thaumasite solubility as a function of temperature**

Thaumasite $(\text{CaSiO}_3)_2(\text{CaSO}_4)_2(\text{CaCO}_3)_2 \cdot 30\text{H}_2\text{O}$ has a structure similar to ettringite and is reported to form limited solid solutions with ettringite. The solubility of synthetic thaumasite intermixed with ettringite has been measured by Barnett et al. [15]. For thaumasite from a geological source, a significantly lower solubility has been measured by Bellmann [16]. Based on the measured concentrations [15] a tentative solubility product of $10^{-49.4 \pm 1}$ was calculated for the reaction:



at a temperature of 25 °C.

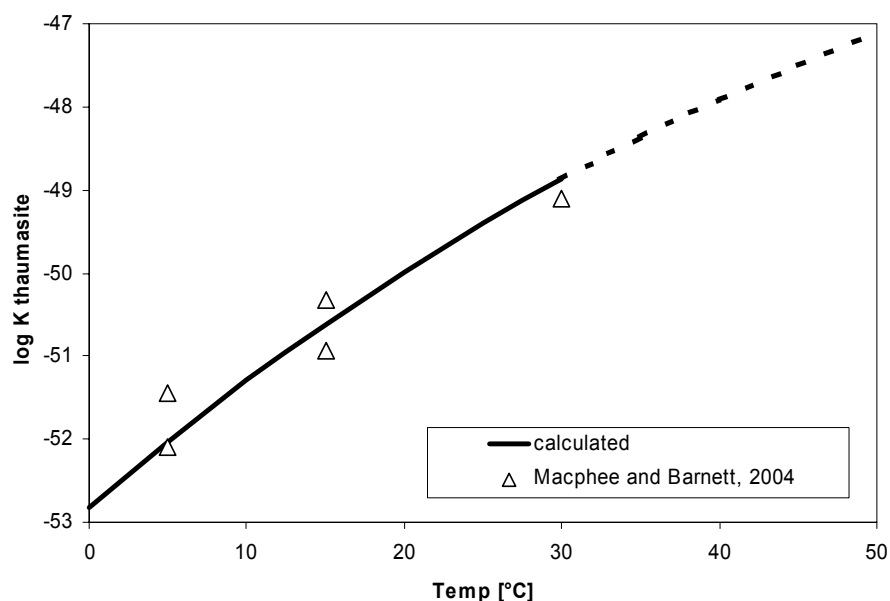


Fig. 3.12:
Calculated and
reported solubility
data for
thaumasite as a
function of
temperature [17]

As only a few solubility measurements in a relatively narrow temperature range are available (Fig. 3.12), the measured solubility data were not used for extrapolating these data to other temperatures. Instead these were estimated from entropy and heat capacity data.

The entropy and heat capacity can be estimated using reference reactions based on structurally similar solids with known S° and C_p° . If such reference reactions involve only solids and no “free” water, the heat capacity and the entropy equals approximately to zero. A more detailed discussion about approaches to estimate the entropy and heat capacities of solids can be found elsewhere [18-20]. Thus, S° and C_p° of thaumasite were estimated from the S° and C_p° values of

$3\text{CaO} \cdot \text{Al}_2\text{O}_3 \cdot 3\text{CaSO}_4 \cdot 32\text{H}_2\text{O}(\text{ettringite}) + 2\text{CaCO}_3(\text{s}) + 2\text{SiO}_2(\text{s}) - \text{CaSO}_4 \cdot 2\text{H}_2\text{O}(\text{gypsum}) - \text{Al}_2\text{O}_3(\text{s}) - \text{CaO}(\text{s}) \rightleftharpoons (\text{CaSiO}_3)_2(\text{CaSO}_4)_2(\text{CaCO}_3)_2 \cdot 30\text{H}_2\text{O}(\text{thaumasite})$ resulting in $S^\circ = 1884$ and $C_p^\circ = 2119 \text{ J/K/mol}$ at 25°C (Appendix A 3, Table A 3.1).

The solubility products calculated for thaumasite based on these estimated data agree well with the measured solubility products as shown in Fig. 3.12.

Further details of the thermodynamic model and data used are given in the Appendix A 3.

3.6 References

1. *DIN EN 196 Prüfverfahren für Zement, Deutsche Fassung EN 196 (1-4):1991.* Europäische Norm EN 196, (Schweizer Norm).
2. Schmidt, T., Lothenbach, B., Romer, M., Scrivener, K.L., Rentsch, D., and Figi, R., *Sulfate interaction and conditions of thaumasite formation.* Cement Concrete Research, 2007 (in preparation).
3. Skibsted, J., Rasmussen, S., Herfort, D., and Jakobsen, H.J., *^{29}Si cross-polarization magic-angle spinning NMR spectroscopy--an efficient tool for quantification of thaumasite in cement-based materials.* Cement Concrete Composites, 2003. 25 (8), 823-829.
4. Skibsted J., Hjorth L., and Jacobsen, J.H., *Quantification of thaumasite in cementitious materials by $^{29}\text{Si}\{^1\text{H}\}$ cross-polarisation magic-angle spinning NMR spectroscopy.* Advances in cement research, 1995. 7, 69-83.
5. *EN 196-1 Prüfverfahren für Zement, Teil 1: Bestimmung der Festigkeit.* 1994.
6. Wittekindt, W., *Sulfatbeständige Zemente und ihre Prüfung.* Zement-Kalk-Gips, 1960. 12.
7. Neuenschwander, J., Schmidt, T., Luthi, T., and Romer, M., *Leaky Rayleigh wave investigation on mortar samples.* Ultrasonics, 2006. 45 (1-4), 50-55.
8. Bertoni, H.L. and Tamir, T., *Unified Theory of Rayleigh-Angle Phenomena for Acoustic Beams at Liquid -Solid Interfaces.* Appl. Phys., 1973. (2), 157-172.
9. Ismail, M.P., Yusof, K.M., and Ibraim, A.M., *Propagation of Rayleigh waves in concrete.* NDT in Civil Engineering, 1996. 38, 338-340.
10. Neuenschwander, J., Schmidt, T., Lüthi, T., and Romer, M., *Leaky Rayleigh wave diagnostics of mortar.* EMPA, Material Science and Technology, 2005. 1.
11. *SN-505-162/1 (1989) Betonbau - Ergänzende Festlegungen.* SIA, Zürich.
12. Scrivener, K.L., *Backscattered electron imaging of cementitious microstructures: understanding and quantification.* Cement Concrete Composites, 2004. 26 (8), 935-945.
13. Lothenbach, B. and Winnefeld, F., *Thermodynamic modelling of the hydration of Portland cement.* Cement Concrete Research, 2006. 36 (2), 209-226.
14. Lothenbach, B., Matschei, T., Möschner, G., Glasser, F.P., *Thermodynamic modelling of the effect of temperature on the hydration and porosity of Portland cement.* Cement Concrete Research, 2007 (submitted).
15. Barnett, S.J., Macphee, D.E., and Crammond, N.J., *Extent of immiscibility in the ettringite-thaumasite system.* Cement Concrete Composites, 2003. 25 (8), 851-855.
16. Bellmann, F., *On the formation of thaumasite Part I.* Advances in cement research, 2004. 16 (2), 55-60.
17. Macphee, D.E. and Barnett, S.J., *Solution properties of solids in the ettringite--thaumasite solid solution series.* Cement Concrete Research, 2004. 34, 1591-1598.
18. Anderson G.M., Crerar, D.A., *Thermodynamics in Geochemistry: the Equilibrium Model.* Oxford University Press, Oxford, 1993.
19. Gu, Y., Gammons, C.H., Bloom M.S., *A one-term extrapolation method for estimating equilibrium constants of aqueous reactions at elevated temperatures.* Geochim Cosmochim Acta, 1994. 58 (17), 3545-3560.
20. Kulik, D., *Minimising uncertainty induced by temperature extrapolations of thermodynamic data: a pragmatic view on the integration of thermodynamic databases into geochemical computer codes.* Proc The use of thermodynamic databases in performance assessment, Barcelona, OECD, 2002, 125-137.

4 Binder systems before sulfate exposure

The following chapter describes the investigation on the initial and leached binder systems before sulfate interaction. With thermodynamic modelling the development of the initial hydrate phase composition are compared with the experimental data.

4.1 Characterisation of the binder systems

The effect of limestone addition and the type of cement clinker was studied. The experimental data are discussed and compared with the thermodynamic modelled data. The results are presented taking into account the physical and chemical aspects of limestone addition and leaching before sulfate interaction.

4.1.1 Influence of limestone addition on physical properties

For the evaluation of the physical influence of the limestone filler and the type of cement clinker the porosity and the development of the compressive strength were investigated on mortar samples as described in section 3.3.3.

The results obtained from the porosity measurements show that limestone addition of 5 wt% led to a decrease in total porosity independent of the type of cement clinker (HS, OPC) used compared to the reference samples without limestone addition (Fig. 4.1, Table 4.1). The results further showed that limestone addition up to 5 wt% lead to a decrease of capillary porosity. Gel porosity increases while the total porosity was observed to slightly decrease.

Table 4.1: Porosity obtained from mortar samples after 28 days of curing in limewater.

| sample | Porosity ⁱ in vol.-% | | | | |
|-----------------|---------------------------------|------|------|------|------|
| | H0 | H5 | P0 | P5 | P25 |
| gel pores | 2.9 | 4.8 | 4.4 | 5.3 | 3.3 |
| capillary pores | 14.5 | 12.1 | 11.5 | 10.0 | 14.5 |
| air pores | 2.2 | 2.4 | 1.0 | 1.2 | 3.0 |
| total | 19.6 | 19.3 | 16.9 | 16.5 | 20.8 |

ⁱaccording to SIA 162-1

These findings indicated that the calcite grains in the cement system could provide additional surface for the nucleation of outer C-S-H during the hydration as described by Stark [1]. This supposition was confirmed by additional microscopic examination as shown in the Appendix

A 6 (Figs. A 6.1, A 6.2). It was found that more C-S-H is formed during hydration in case of limestone addition.

That could explain the observed densification for 5 wt% limestone addition in the cement systems leading to a refinement of the microstructure, as described by Uchikawa et al. [2]. Alternatively, the formation of monocarbonate and stabilisation of ettringite could lower the porosity in the cement system as suggested by Matschei and Glasser [3].

The additional C-S-H could explain the decrease in capillary porosity as described by Thomas and Jennings [4] leading to lower permeability of the cement paste. The limestone filler is also known to act as a filler leading to a physical densification of the microstructure as described by Tsivilis et al. [5].

Higher amounts of limestone in the cement system as in P25 where 25 wt% were added result in an increase in total and capillary porosity for the investigated OPC cement system (Table 4.1, Fig. 4.1). The observations indicated that high amounts of limestone addition will lead to a higher permeability for P25 compared to the reference P0 without limestone addition. This agreed with the observations of Irassar et al. [6] and Torres et al. [7].

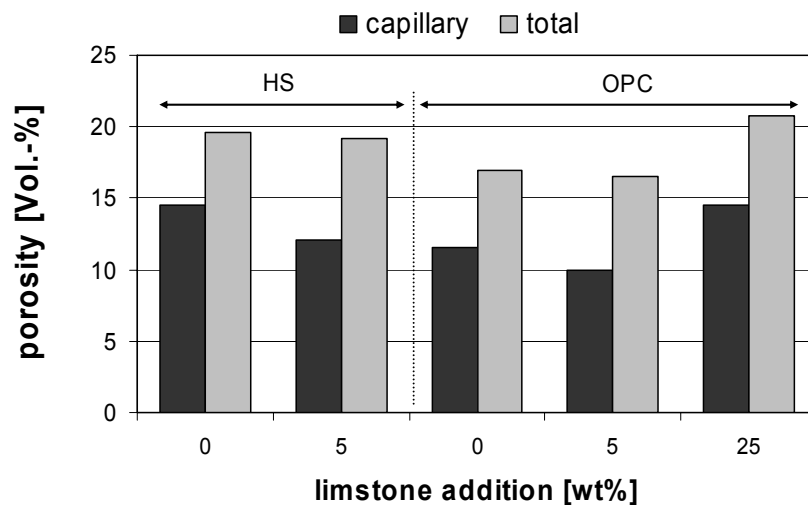


Fig. 4.1: Influence of limestone addition and clinker type on porosity of mortar samples after 28 days of curing.

The type of cement clinker also influenced the porosity. The mortar samples prepared from HS cement with low C_3A showed higher porosities, especially an increased capillary porosity after 28 days of curing (Fig. 4.1). These observations could indicate that cements with low C_3A but high C_4AF contents contributed to slower strength development as mentioned by Kuzel and Pöllmann [8]; Taylor [9], Scrivener [10], Stark and Wicht [11]. As C_4AF in cement systems generally hydrated only very slow and the investigated HS cement systems contain

about 22 wt% C_4AF but almost no C_3A , the expected lower degree of hydration would agree with the increased porosity observed.

Alternatively, the relatively low amount of SO_3 in the H0 and H5 cements, see Table A 1.2 in the Appendix A 1, could be the reason for the increased porosity as more AFm phases than AFt phases are formed during hydration.

The results on the strength development of the investigated mortar samples showed that limestone addition of 5 wt% as in H5 and P5 slightly increased the compressive strength after 28 days of curing compared to the reference samples without limestone addition (Fig. 4.2). However, a slightly negative influence of 5 wt% limestone addition was observed after 2 days of curing. High amounts of limestone addition as in P25 (25 wt%) showed a significant negative effect on the compressive strength after 2 and 28 days of curing (Table 4.2).

Table 4.2: Compressive strength of mortar samples after 2 and 28 days.

| sample | compressive strength ⁱ | | | | |
|--------|-----------------------------------|------|------|------|------|
| | H0 | H5 | P0 | P5 | P25 |
| 2d | 23.1 | 21.7 | 28.3 | 27.5 | 20.7 |
| 28d | 56.1 | 56.8 | 57.6 | 58.8 | 46.5 |

ⁱ according to EN 196-1

The results showed that the compressive strengths were lower at 2 and 28 days. However, the OPC cement systems with 25 wt% limestone addition reached more than 75% of the compressive strength of the reference cement system without limestone addition after 28 days of hydration.

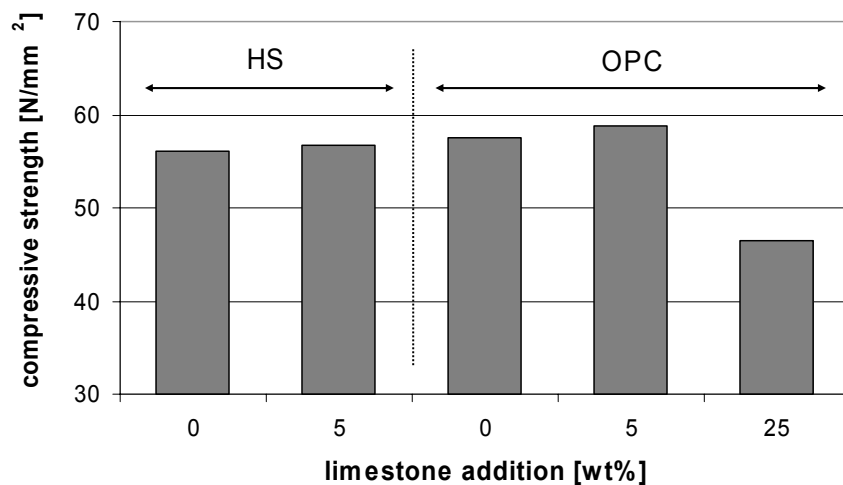


Fig. 4.2: Influence of limestone addition and clinker type on compressive strength of mortar samples after 28 days.

Furthermore, the compressive strengths were observed to correlate inversely with the determined porosities. Limestone addition of 5 wt% led to a decrease in porosity, thus resulted in an increase of compressive strength compared to the cement system without limestone addition (Fig. 4.1, 4.2).

The results further indicated that the HS cement systems (low C_3A) had a lower compressive strength especially after 2 days of hydration than the OPC cement systems (high C_3A) (Table 4.2). It might be indicating that the hydration mechanisms were slower as mentioned previously with ongoing hydration this effect balanced.

4.1.2 Chemical influence of limestone addition

The influence of limestone addition on the resulting hydrate phases was investigated experimentally on cement paste and thermodynamic modelling was used to calculate the development of the solid phases during the hydration of the laboratory cements.

- **Modelled data**

The thermodynamic model of Lothenbach and Winnefeld [12] was applied to calculate the development of the solid phases during the hydration of the laboratory cement systems with or without limestone addition before sulfate exposure.

In this model the composition of the solid and liquid phases was calculated based on (i) the measured composition of the unhydrated cement (ii) the calculated dissolution of the clinkers as a function of time using a set of empirical equations and (iii) a consistent thermodynamic dataset as given in [13]. The hydrate phase assemblage was summarised as volumetric percentages in the cementitious matrix at the given w/c ratio used.

The hydrate phase assemblages of the cement systems without limestone addition (H0, P0) were calculated to be C-S-H, portlandite, ettringite and monosulfate as well as minor amounts of hemicarboxate and hydrotalcite (Fig. 4.3). In the model as described by Lothenbach and Winnefeld [12] the ferrite phase (C_4AF) was assumed to participate and Fe is calculated to precipitate as AFt, AFm and hydrotalcite, respectively.

With additional limestone filler (5 and 25 wt%) in the cement system the thermodynamic model predicted the development of C-S-H, portlandite, ettringite, monocarbonate and hydrotalcite (Figs. 4.4, 4.5).

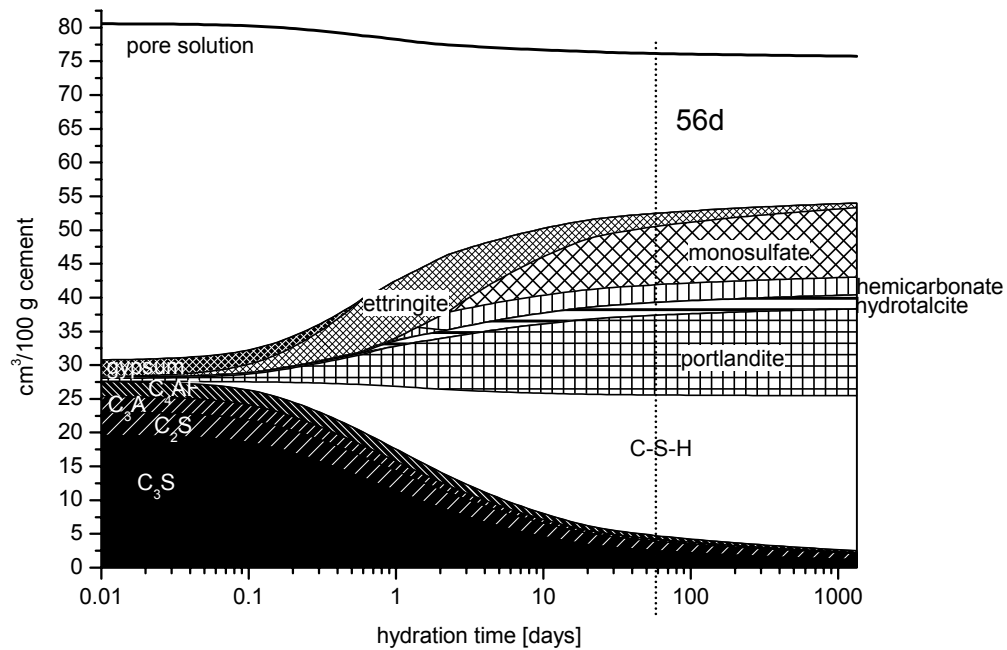


Fig. 4.3: Modelled evolution of the solid phases during the hydration of OPC ($w/c=0.5$) in the absence of additional carbonate.

Furthermore, beside some unhydrated clinker phases also calcite was predicted to be present in hydrated Portland cement indicating that only a part of the calcite is reacting to form hydrate phases as mentioned by Matschei and Glasser [3].

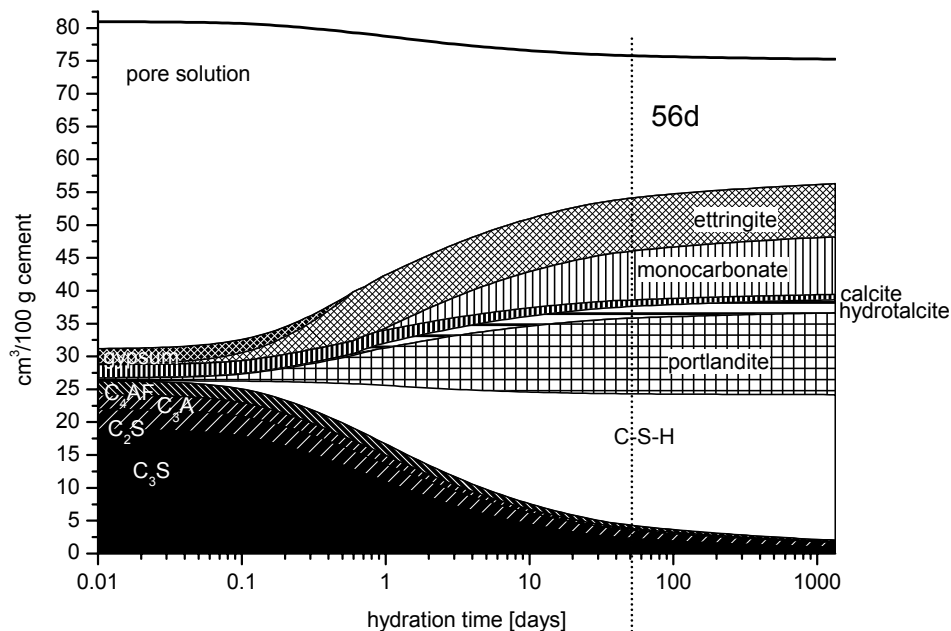


Fig. 4.4: Modelled evolution of the solid phases during the hydration of OPC ($w/c=0.5$) in the presence of 5 wt% additional carbonate.

Another effect of limestone addition was calculated to be the dilution of the cement system leading to the formation of less hydrate phases (Figs. 4.3, 4.5). According to Lothenbach and Winnefeld [12] in the presence of additional carbonate somewhat more aluminium is bound in ettringite in the initial cement paste.

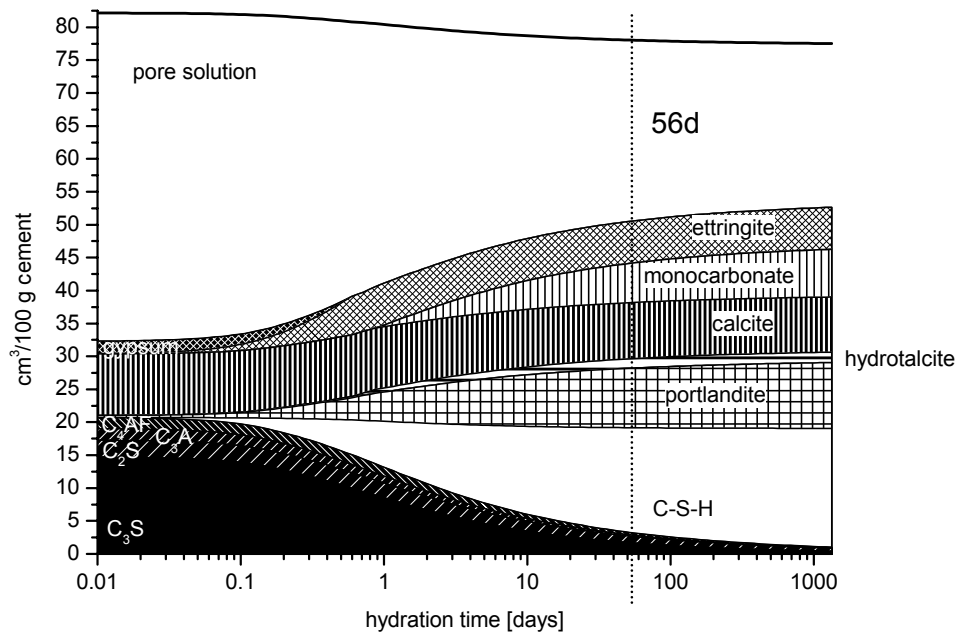


Fig. 4.5: Modelled evolution of the solid phases during the hydration of OPC (w/c=0.5) in the presence of 25 wt% additional carbonate.

• Experimental phase evolution

The phase assemblage of hydrated Portland cement systems were investigated for binder system with and without limestone addition after 56 days of curing in saturated limewater at 20 °C.

The investigations on the hydrated cement paste samples showed that limestone addition influences the formation of AFm phases during hydration.

The XRD results for H5, P5, P25 showed that the presence of additional carbonate led to the formation of monocarbonate as stable AFm phase independent of the type of cement clinker present (Figs. 4.6, 4.7). In cement systems without limestone addition (H0, P0) the experimental results obtained from XRD analysis showed that monosulfate forms as a stable AFm phase.

However, also traces of hemicarboxate and hydrotalcite could be found experimentally indicating that these phases are present but their amounts formed during the hydration was rather small compared to the major hydrates C-S-H (TGA), portlandite, ettringite, monosulfate or monocarbonate (Figs. 4.6, 4.7).

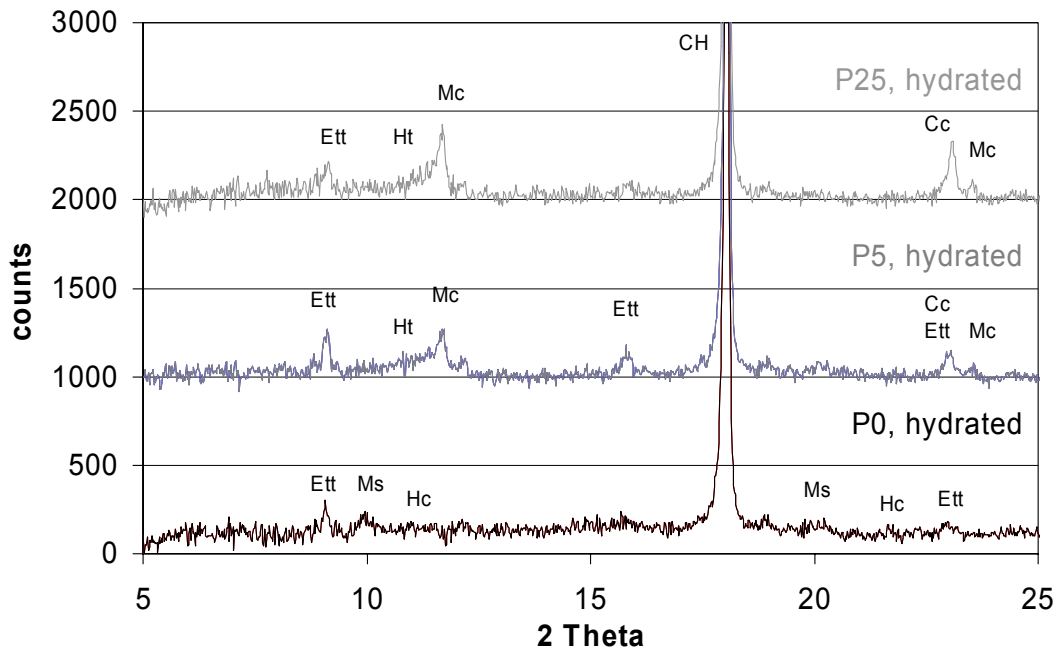


Fig. 4.6: XRD results of OPC cement systems containing 0, 5, 25 wt% limestone filler hydrated for 56 days in limewater. CH = portlandite; Cc = calcite; Ett = ettringite; Hc = hemicarboxate; Ht = hydrotalcite; Mc = monocarbonate; Ms = monosulfate.

Furthermore the XRD investigations showed the presence of a significant ferrite peak for the HS cement systems after 56 days indicating that the hydration kinetics of the ferrite phase (C_4AF) was very slow, especially in the investigated alkaline conditions (Fig. 4.7). These observations agree with the mentioned slow reactions kinetics of the ferrite phase especially in alkaline conditions by Taylor [9], Collepardi et al. [14].

The results also showed that only a small amount of the ferrite (C_4AF), being the major alumina source in the HS cement system, has reacted to form ettringite after 56 days of hydration.

Generally, the experimental observations were in good agreement with the modelled data. Both modelling and experimental data show that in OPC and HS cement systems without limestone addition, monosulfate as well as traces of hemicarboxate and hydrotalcite were stable phases.

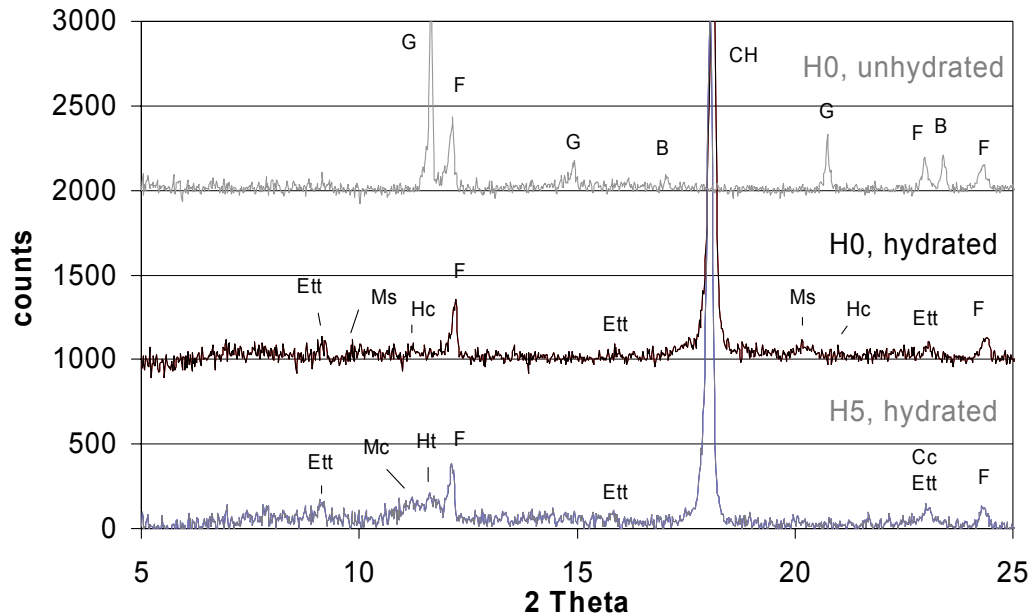


Fig. 4.7: XRD results of HS cement systems containing 0, 5 wt% limestone filler hydrated for 56 days in limewater and unhydrated. B = belite; CH = portlandite; Cc = calcite; Ett = ettringite; F = ferrite; G = gypsum; Hc = hemihydrate; Ht = hydrotalcite; Mc = monocarbonate; Ms = monosulfate.

The modelled and experimental data show that in cement systems with limestone addition the formation of monocarbonate led to the formation of slightly more ettringite during the initial hydration. These findings agreed with the investigations of Kuzel and Pöllmann [15] and Bonavetti et al. [16] who found more ettringite in carbonate containing cement systems. In the limestone containing cement a higher percentage of available aluminium in the cement had reacted to form hydrate phases. This might increase chemically the sulfate resistance since ettringite was assumed to be stable in sulfate environment.

4.1.3 Influence of leaching

Portlandite was reduced by 80 wt% during the leaching process as shown in Table 4.3 and Appendix A 2.2. However, small amounts of portlandite (1-3 wt%) were still present indicating that the leaching process was not complete after 4 months.

The MIP measurements of samples before and after leaching showed that the total porosity almost doubled (Table 4.3). The pore size distribution in the investigated samples showed significantly more small pores ≤ 10 nm and more pores between 10 – 100 nm to be present in leached samples (Fig. 4.8). The increase in pore volume can be attributed to the dissolution of large crystals of portlandite Ca(OH)_2 [17-20].

Table 4.3: Total porosity and portlandite content of the laboratory cements before and after leaching.

| sample | Ca(OH) ₂ content ⁱ [wt%] | | | | | total porosity ⁱⁱ | | | | |
|---------|--|----|----|----|-----|------------------------------|----|----|----|-----|
| | H0 | H5 | P0 | P5 | P25 | H0 | H5 | P0 | P5 | P25 |
| initial | 15 | 14 | 15 | 14 | 12 | 18 | 17 | 15 | 14 | 20 |
| leached | 2 | 2 | 3 | 3 | 1 | 36 | 35 | 28 | 27 | 39 |

ⁱ obtained from thermogravimetric analysis (TGA); ⁱⁱ obtained from mercury intrusion (MIP)

In addition, the dissolution of Ca from C-S-H might also increase the amount of small pores as mentioned by Planel et al. [21] and Galle et al. [22].

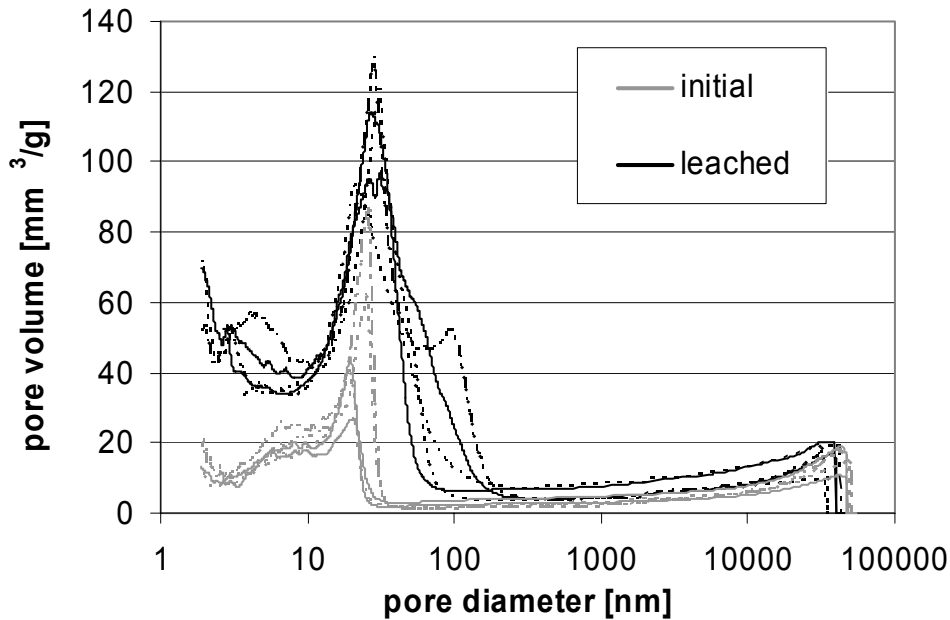


Fig. 4.8: MIP pore size distribution of initial and leached cement pastes.

4.1.4 Microstructural aspects

The microstructural investigations of leached cement paste particles showed that the leaching process also resulted in a layered structure. The leached cement paste particles were composed of a) a strongly leached outer layer close to the surface and b) an unchanged inner layer in the center of the cement paste particles (Fig. 4.9a).

The leached outer layer was characterised by reduced Ca and alkali contents and portlandite was absent. The outer layer appears to be inhomogeneous and was marked by high porosity. This agrees with the observations of Haga et al [20]. Part of the pore space, as

indicated by the darker areas, originated from partial or complete dissolution of portlandite (Fig. 4.9b).

The inner layer of the leached cement paste particles is characterised by a high density of the cement paste matrix. The microstructural investigations showed that the amount of portlandite was decreasing going from the center of the paste particle towards the leached surface which was in good agreement to the findings of Yokozeki et al. [23].

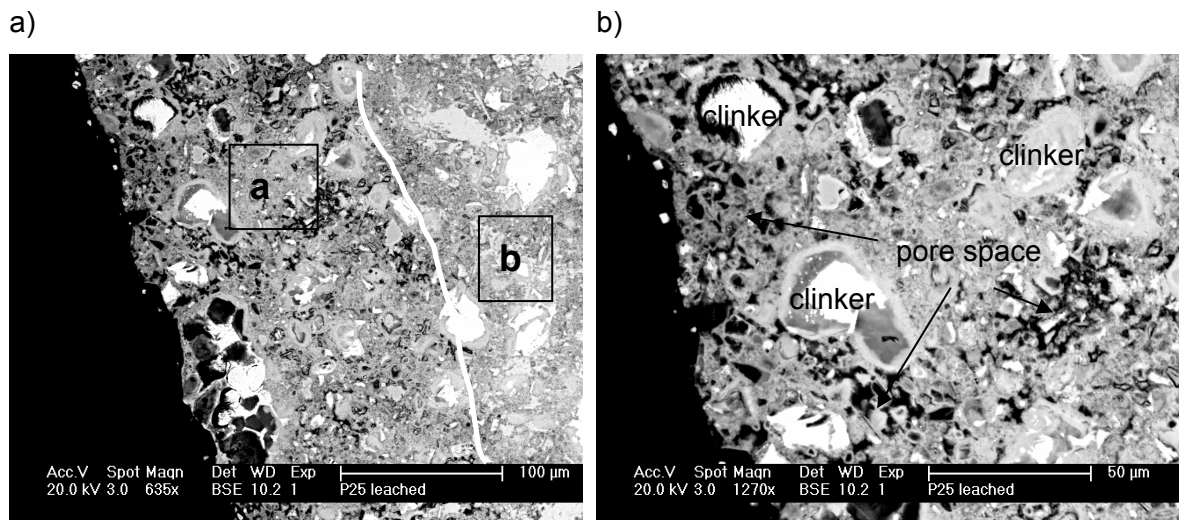


Fig. 4.9: Backscattered electron images of the leached cement paste particles OPC with 25 wt% limestone addition.

However, in the transition zone between the two layers, relicts of portlandite were found around clinker and calcite grains (Fig. 4.10a) whereas in the center of the cement paste particle portlandite was still present in extensive areas in the outer C-S-H phase (Fig. 4.10b).

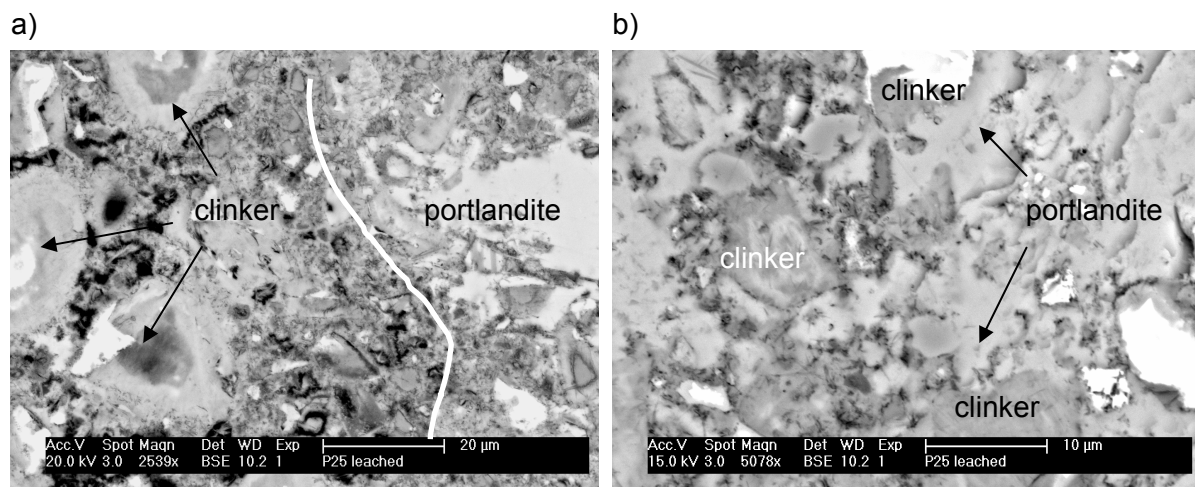


Fig. 4.10: Backscattered electron images of cement paste particles of a) the transition zone between inner - outer layer and b) at the centre of the paste particles (OPC with 25 wt% limestone addition)

The thickness of the leached zone differed from 150 μm for P5 up to 1 mm for P25. The results showed that with lower initial porosity of the cement paste, the extent of leaching was reduced. The influence of leaching, mainly the reduction of portlandite and alkalies was found to increase the porosity which agreed to the findings of Planel et al. [21].

Similarly to cement paste particles exposed to sulfate, leaching of crushed cement paste particles leads to an inhomogeneous, layered structure within the particles. The few percent of portlandite in the leached samples analysed with bulk methods (TGA, XRD) results largely from the contribution of the unchanged cores of the cement paste particles.

4.2 Summary and conclusions

Limestone addition influences the mineralogy of the AFm phases during hydration. Monocarbonate was formed instead of monosulfate, depending on the amount of carbonate available in the cement system. In systems with small amounts of carbonate hemicarbonate may form beside monosulfate.

The presence of monocarbonate also increased the formation of ettringite since more sulfate was available during the hydration process. Thus, a higher fraction of the aluminium was present as ettringite which could chemically increase sulfate resistance.

The addition of 5 wt% limestone in Portland cement systems led to an increase of the compressive strength and reduced the porosity, especially the capillary porosity. The compressive strength was observed to correlate inversely with the porosity. Thus, limestone addition of 5 wt% was resulting in an increase of compressive strength compared to the cement system without limestone addition.

In the case of 25 wt% limestone addition the compressive strength was significantly reduced whereas the porosity, especially the capillary porosity, increases. It can be concluded that high amounts of limestone addition led to an increase of permeability of these cement systems.

It should be mentioned that the thermodynamic model took into account the reaction of both aluminium and iron to form AFt and AFm phases. However, the results showed that significant amounts of C_4AF were still present in the HS-cement systems.

Leaching before sulfate interaction reduced the amount of portlandite and increased the porosity of the investigated cement paste. The thickness of the leached zone differed and a lower initial porosity of the cement paste reduced the extend of leaching.

4.3 References

1. Stark, J., *Optimierte Bindemittelsysteme für die Betonindustrie*. Beton, 2004. 10/2004 486-490.
2. Uchikawa, H., Hanehara, S., and Hirao, H., *Influence of microstructure on the physical properties of concrete prepared by substituting mineral powder for part of fine aggregate*. Cement Concrete Research, 1996. 26, 101-111.
3. Matschei, T., Glasser, F.P., *The influence of limestone on cement hydration*. ZGK International, 2006. 59, 78-86.
4. Thomas, J.J. and Jennings, H.M., *A colloidal interpretation of chemical aging of the C-S-H gel and its effects on the properties of cement paste*. Cement Concrete Research, 2006. 36 (1), 30-38.
5. Tsvilis, S., Kakali, G., Skaropoulou, A., Sharp, J.H., and Swamy, R.N., *Use of mineral admixtures to prevent thaumasite formation in limestone cement mortar*. Cement Concrete Composites, 2003. 25 (8), 969-976.
6. Irassar, E.F., Bonavetti, V.L., and Gonzalez, M., *Microstructural study of sulfate attack on ordinary and limestone Portland cements at ambient temperature*. Cement Concrete Research, 2003. 33, 31-41.
7. Torres, S.M., Sharp, J.H., Swamy, R.N., Lynsdale, C.J., and Huntley, S.A., *Long term durability of Portland-limestone cement mortars exposed to magnesium sulfate attack*. Cement Concrete Composites, 2003. 25 (8), 947-954.
8. Kuzel, H.-J. and Pöllmann, H., *Hydration of C₃A in the presence of Ca(OH)₂, CaSO₄·2H₂O and CaCO₃*. Cement Concrete Research, 1991. 21 (5), 885-895.
9. Taylor, H.F.W., *Cement Chemistry*. 1997 (London: Thomas Telford).
10. Scrivener, K.L., *The development of microstructure during the hydration of Portland cement*. 1984 (University of London).
11. Stark, J. and Wicht, B., *Zement und Kalk*. F.-A.-Finger-Institut für Baustoffkunde der Bauhaus-Universität Weimar; Birkhäuser, 2000.
12. Lothenbach, B. and Winnefeld, F., *Thermodynamic modelling of the hydration of Portland cement*. Cement Concrete Research, 2006. 36 (2), 209-226.
13. Lothenbach, B., Matschei, T., Möschner, G., Glasser, F.P., *Thermodynamic modelling of the effect of temperature on the hydration and porosity of Portland cement*. Cement Concrete Research, 2007 (submitted).
14. Collepardi, M., Baldini, G., and Pauri, M., *Tricalcium aluminate hydration in the presence of lime, gypsum and sodiumsulfate*. Cement Concrete Research, 1978. 5, 571-580.
15. Kuzel, H. and Pöllmann, H., *Hydration of C₃A in the presence of Ca(OH)₂, CaSO₄·2H₂O and CaCO₃*. Cement Concrete Research, 1991. 21, 885-895.
16. Bonavetti, V.L., Rahhal, V.F., and Irassar, E.F., *Studies on the carboaluminate formation in limestone filler-blended cements*. Cement and Concrete Research, 2001. 31, 853-859.
17. Andac Muberra and Paul, G.F., *Long-term leaching mechanisms of Portland cement-stabilized municipal solid waste fly ash in carbonated water*. Cement Concrete Research, 1999. 29 (2), 179-186.
18. Catinaud, S., Beaudoin, J.J., and Marchand, J., *Influence of limestone addition on calcium leaching mechanisms in cement-based materials*. Cement Concrete Research, 2000. 30 (12), 1961-1968.

19. Haga, K., Shibata, M., Hironaga, M., Tanaka, S., and Nagasaki, S., *Change in pore structure and composition of hardened cement paste during the process of dissolution*. Cement Concrete Research, 2005. 35 (5), 943-950.
20. Haga, K., Sutou, S., Hironaga, M., Tanaka, S., and Nagasaki, S., *Effects of porosity on leaching of Ca from hardened ordinary Portland cement paste*. Cement Concrete Research, 2005. 35 (9), 1764-1775.
21. Planel D., Sercombe J., Le Bescop P., Adenot F., and Torrenti, J.M., *Long-term performance of cement paste during combined calcium leaching-sulfate attack: kinetics and size effect*. Cement Concrete Research, 2006. 36, 137-143.
22. Galle, C., Peycelon, H., and Le Bescop, P., *Effect of an accelerated chemical degradation on water permeability and pore structure of cement-based materials*. Advances in cement research, 2004. 16, 105-114.
23. Yokozeki, K., Watanabe, K., Sakata, N., and Otsuki, N., *Modeling of leaching from cementitious materials used in underground environment*. Applied Clay Science, 2004. 26 (1-4), 293-308.

5 Cement paste experiments

The following chapter describes the investigations on the conditions of thaumasite formation with different binder systems and the role of internal carbonate. The results evaluate the effects of sulfate concentration, temperature, time and leaching. The thermodynamically modelled data are discussed and compared with the experimental findings.

5.1 Thermodynamic modelling and thaumasite formation

The formation of thaumasite was investigated with the progressive equilibrium approach (PEA). This approach experimentally simulates the conditions of various levels of sulfate uptake in hardened cement pastes. The results are presented in phase diagrams with the modelled predictions of the hydrate phase composition (upper part) and the hydrate phases identified by XRD (lower part) as a function of the sulfate content in the cement paste.

5.1.1 Model of initial hydrate phases

The thermodynamic modelling approach, developed by Lothenbach and Winnefeld [1], was modified using the Gibbs free energy minimization program GEMS [2] to calculate the hydrate phase assemblages of the cement systems used. As described in section 4.1.2 the initial hydrate phase assemblage before sulfate interaction was calculated for the cement systems with and without limestone addition as shown in subsystems E (Figs. 5.1-5.5).

Basically, the initial hydrate phase assemblage in cement systems without limestone addition was calculated to be C-S-H, portlandite, ettringite, monosulfate, hemicarboxate and hydrotalcite (Figs. 5.1, 5.3). With additional limestone in the cement system the hydrate phase assemblage was calculated to be C-S-H, portlandite, ettringite, monocarbonate and traces of hydrotalcite and calcite (Figs. 5.2, 5.4, 5.5). The iron in the cement systems was assumed to react to iron hydroxide $\text{Fe}(\text{OH})_3$.

The modelled predictions agree well with the experimental observations. In the systems without limestone addition (H0, P0) the presence of C-S-H, portlandite, ettringite, monosulfate and traces of hemicarboxate were observed by XRD (bottom part Figs. 5.1, 5.3). In the samples where limestone has been added, the presence of monocarbonate and ettringite can be observed (bottom Fig. 5.2, 5.4, 5.5).

5.1.2 Effect of sulfate interaction

If sulfate is progressively added to the subsystems moving from E to A the results of thermodynamic modelling show that more ettringite was formed at the expense of the AFm-phases (monosulfate, monocarbonate, hemicarbonate) and hydrotalcite until all available aluminium has been consumed (Figs. 5.1-5.5).

With increasing sulfate content in the subsystems the calculated data show that thaumasite starts to form at sulfate contents between 10 to 20 wt% SO_4^{2-} by weight cement paste. Portlandite was predicted to be consumed by the formation of ettringite and thaumasite. Thaumasite formed at the expenses of portlandite, calcite and C-S-H in the presence of water. In the presence of more than 5 wt% SO_4^{2-} by weight cement paste, ettringite was calculated to be the main Al-containing hydrate phase independently of the original composition of the cement. However, the composition of the cement has a large impact on the amount of thaumasite formed. The thermodynamic calculations indicated that limestone containing cement systems independently of the type of cement clinker (high and low C_3A) used, will be susceptible to thaumasite formation. It was calculated that all calcite in the cements with 5 wt% limestone addition will be consumed by the formation of thaumasite indicating that a limited amount of thaumasite can form within the range of sulfate addition (Figs. 5.2, 5.4, 5.5). The modelled data further show that small amounts of thaumasite are predicted even in the cement systems without limestone addition as the clinkers contain up to 0.2 wt% CO_2 , which was theoretically sufficient to form 3 wt% thaumasite at high sulfate concentrations (Figs. 5.1, 5.3).

In the presence of 25 wt% limestone however, the amount of thaumasite formed was limited by the uptake of sulfate into the system which was theoretically sufficient to form thaumasite until all C-S-H and/or calcite is consumed (Fig. 5.5). Furthermore, the dilution effect mentioned in section 4.1.2, (25 wt% limestone addition) theoretically lead to thaumasite formation at lower sulfate additions according to the molar ratio of $\text{SO}_3/\text{Al}_2\text{O}_3$.

It was interesting to note that thermodynamic modelling indicates that thaumasite becomes stable only above 5 wt% SO_4^{2-} by weight of cement paste. From a thermodynamic point of view, thaumasite is only stable in a cement system if the available Al has been incorporated into ettringite or, in other words, if the molar $\text{SO}_3/\text{Al}_2\text{O}_3$ exceeds 3. These findings agree with the observations reported by Juel et al. [3].

The increase in solid volume with increasing sulfate content in the subsystems (Figs. 5.1-5.5) was due to the formation of the secondary sulfate phases ettringite and thaumasite. However, this increase in solid volume does not necessarily imply expansion of the cement paste as these sulfate phases will partially precipitate in the available pore space.

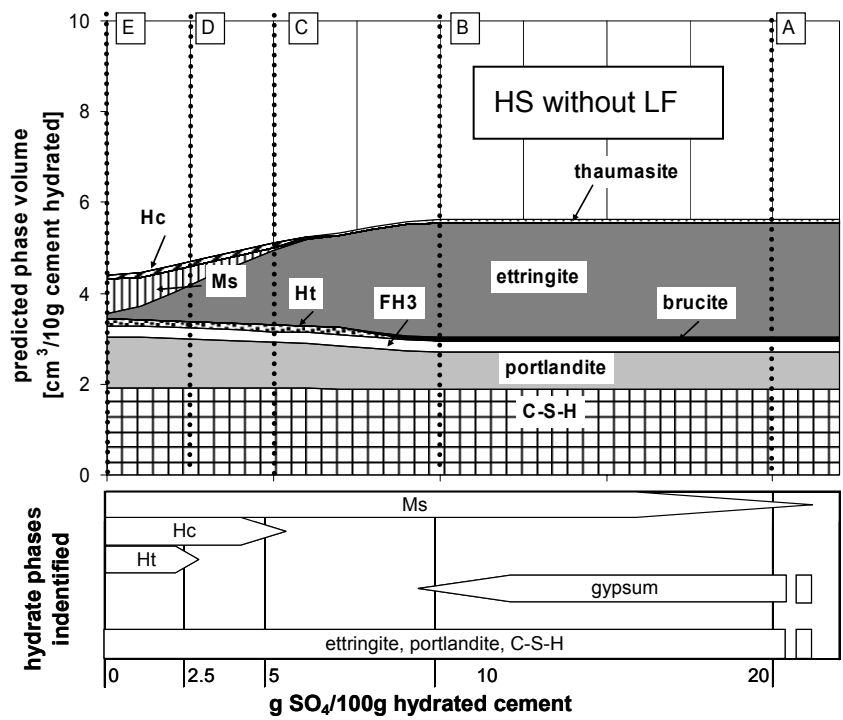


Fig. 5.1: Phase assemblages for HS cement system without limestone addition after 9 months sulfate interaction at 8 °C.

Hc = hemispherical;
Ht = hydrotalcite;
Ms = monosulfate;
FH₃ = iron hydroxide
LF = limestone filler

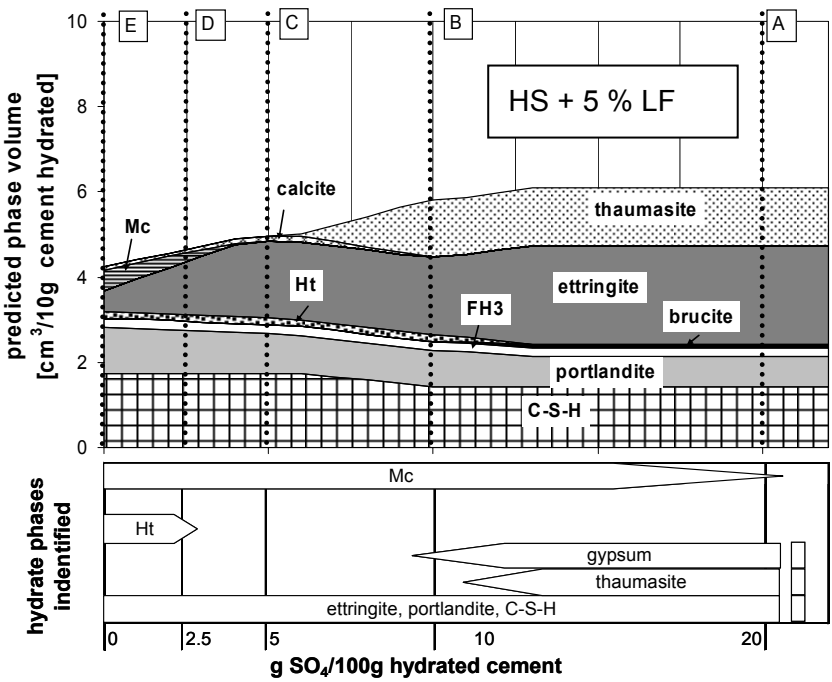


Fig.5.2: Phase assemblages for HS cement system with 5 wt% limestone addition after 9 months sulfate interaction at 8 °C.

Hc = hemispherical;
Ht = hydrotalcite;
Mc = monocarbonate;
FH₃ = iron hydroxide
LF = limestone filler

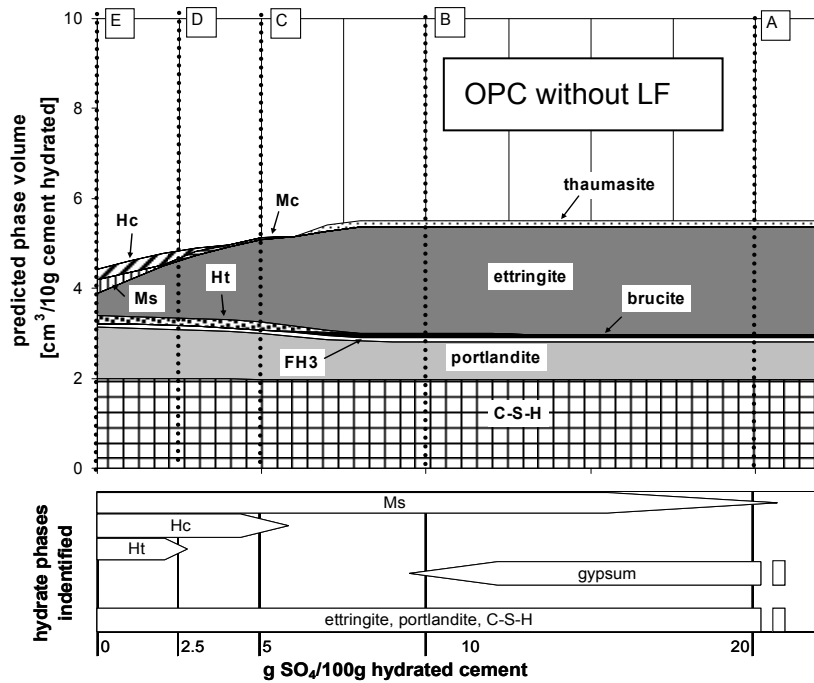


Fig. 5.3: Phase assemblages for OPC cement systems without limestone addition after 9 months sulfate interaction at 8 °C.

Hc = hemisulfate;

Ht = hydrotalcite;

Ms = monosulfate;

FH₃ = iron hydroxide

LF = limestone filler

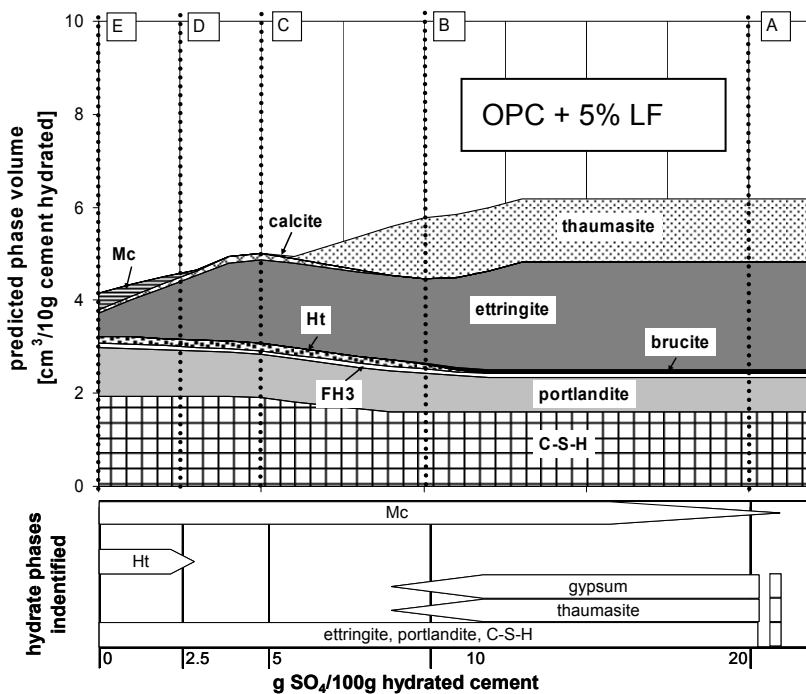


Fig. 5.4: Phase assemblages for OPC cement systems with 5 wt% limestone addition after 9 months sulfate interaction at 8 °C.

Hc = hemisulfate;

Ht = hydrotalcite;

Mc = monocarbonate;

FH₃ = iron hydroxide

LF = limestone filler

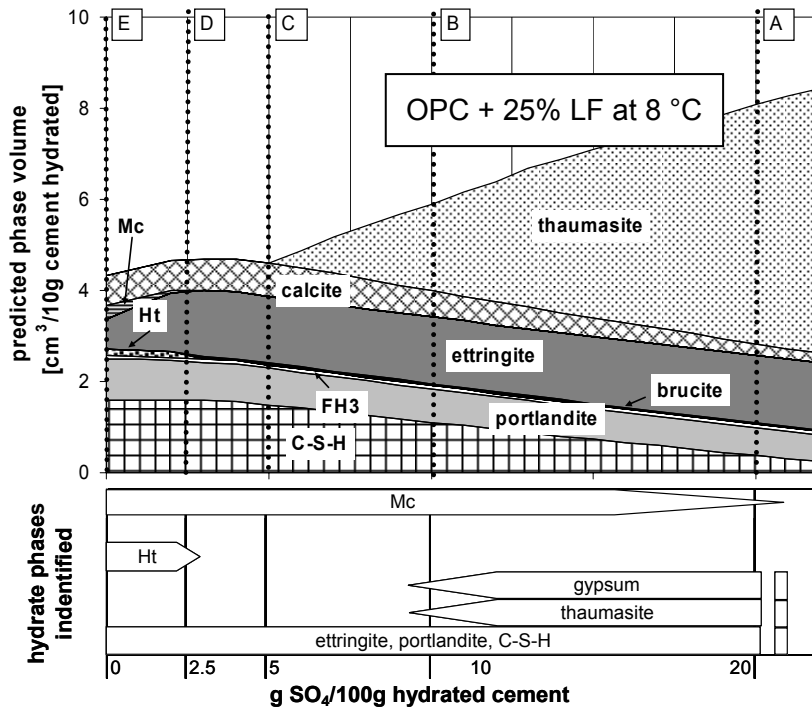


Fig. 5.5: Phase assemblages for OPC cement systems with 25 wt% limestone addition after 9 months sulfate interaction at 8 °C.

Hc = hemicarboxate;

Ht = hydrotalcite;

Mc = monocarbonate;

FH₃ = iron hydroxide

LF = limestone filler

For the experimental evaluation of the development of the hydrate phases during sulfate interaction, the phases were identified using XRD analysis as described in Chapter 3, section 3.2.3.

Experimentally, thaumasite was observed to form only at high sulfate contents in hydrated cement systems containing 5 and 25 wt% limestone and in the presence of 10 or 20 wt% sulfate, see bottom part of Figs 5.1- 5.5. These observations agreed with the results of thermodynamic modelling and with the findings from Juel et al. [3]. Obviously, thaumasite only formed in cement systems where enough sulfate has been added to transform all available aluminium into ettringite. Smaller amounts of sulfate present in the subsystems, e.g. subsystems C, D with < 10 wt% SO₄ by weight cement did not lead to thaumasite formation (Figs. 5.1-5.5).

Thaumasite was identified in samples where limestone has been added to the cement, in both cement systems with low C₃A (H5) and high C₃A (P5, P25) content as shown in Fig. 5.6 and Table 5.1. The results agreed quite well with the findings from Macphee and Diamond [4] and Kalinowski and Trägårdh [5] stating that already minor amounts of carbonate in cements (5 wt%) are sufficient to form thaumasite. Thaumasite could not be identified experimentally in samples without limestone addition as predicted from the thermodynamic data (Table 5.1).

From the results obtained by XRD, it was difficult to identify the relative amounts of thaumasite formed in the cement systems after 9 months of sulfate interaction. So far, the results did not show a significant difference in peak intensities of thaumasite for the investigated cement systems with high (P5, P25) and low (H5) C_3A content after 9 months of sulfate interaction (Fig. 5.6). Thus, it could not be confirmed that low C_3A contents influences or even promotes thaumasite formation as suggested by Nobst and Stark [6-8].

However, in cement systems with low C_3A content thaumasite was identified experimentally at very high sulfate concentrations (20 wt% SO_4 by weight of cement paste) which could indicate that low C_3A contents are not favouring thaumasite formation as suggested by Juel et al. [3].

The experimentally observed phase assemblages show that at higher sulfate contents beside thaumasite and ettringite, gypsum was also identified as sulfate containing phase, see Table 5.1 and lower part of Figs. 5.1-5.5). Between 3 and 9 months of sulfate interaction the amount of gypsum present decreased (Fig. 5.7, Table 5.1). Gypsum seemed to form as an intermediate sulfate phase parallel or instead of thaumasite at high sulfate concentrations and later acts as a source of sulfate applied for thaumasite formation as mentioned by Bellmann [9, 10] and Irassar et al. [11].

In the experiments, thaumasite was observed to be the last sulfate phase forming during sulfate interaction. In subsystems with high sulfate concentrations, i.e. subsystems A, B, where the formation of intermediate gypsum was observed, thermodynamic calculations predict that all sulfate available should be present as ettringite and thaumasite. The model did not predict gypsum as a stable phase but obviously this would eventually occur as the final sulfate phase forming at very high sulfate additions.

In reality, the last sulfate phase which formed during sulfate interaction was thaumasite due to its slow reaction kinetics as mentioned by Köhler et al. [12] and Lachowski et al. [13]. This discrepancy between thermodynamic calculations and experimental results indicates that equilibrium has not been reached in the experiments.

The experimental data further show that some of the AFm phases (monosulfate, monocarbonate) formed during the hydration persist during sulfate interaction, see Figs. 5.1-5.5 and Table 5.1, which is in contrast to the model predictions. This indicates that even though the hydrated cement has been ground to 0.5 – 2.0 mm, equilibrium has not been reached. Obviously, the reactions did not occur throughout the whole cement paste grains but layers have been established within the crushed cement paste.

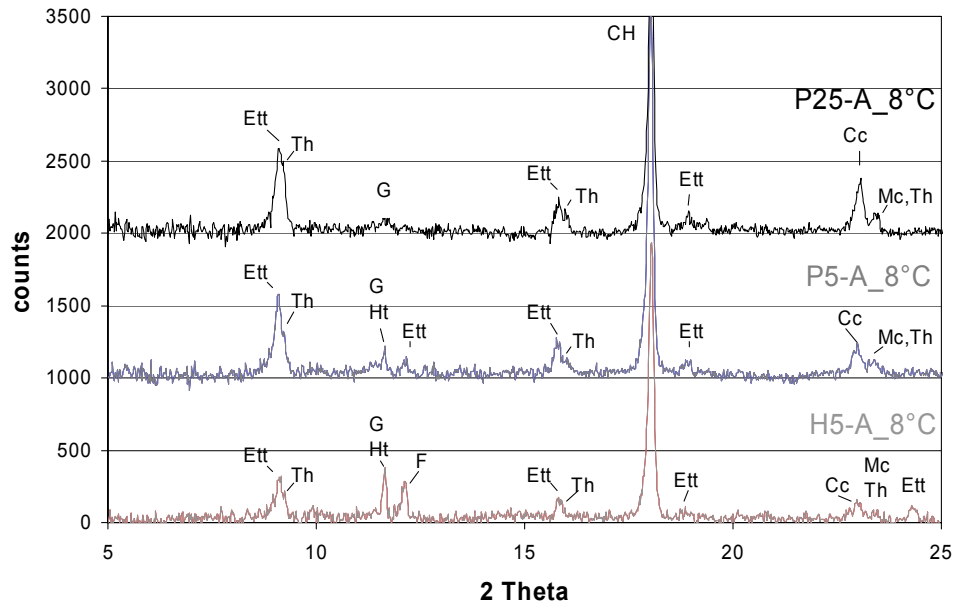


Fig. 5.6: XRD results of selected PEA experiments for HS and OPC cement systems with 5 and 25 wt% limestone additions from subsystem A after 9 months of sulfate interaction at 8 °C. CH = portlandite, Cc = calcite, Ett = ettringite; F = Ferrite, G = gypsum; Ht = hydrotalcite; Mc = monocarbonate, Th = thaumasite.

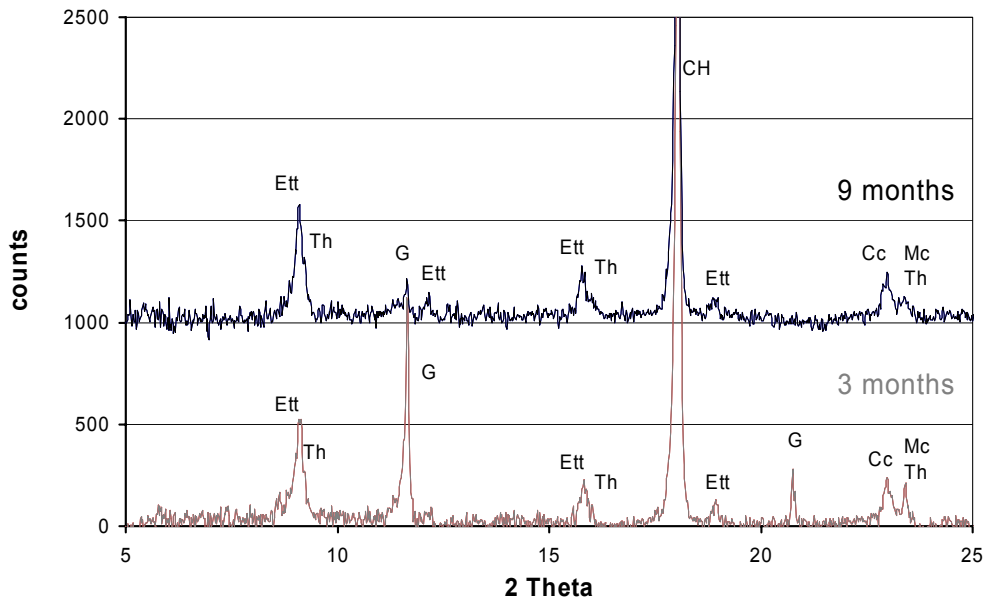
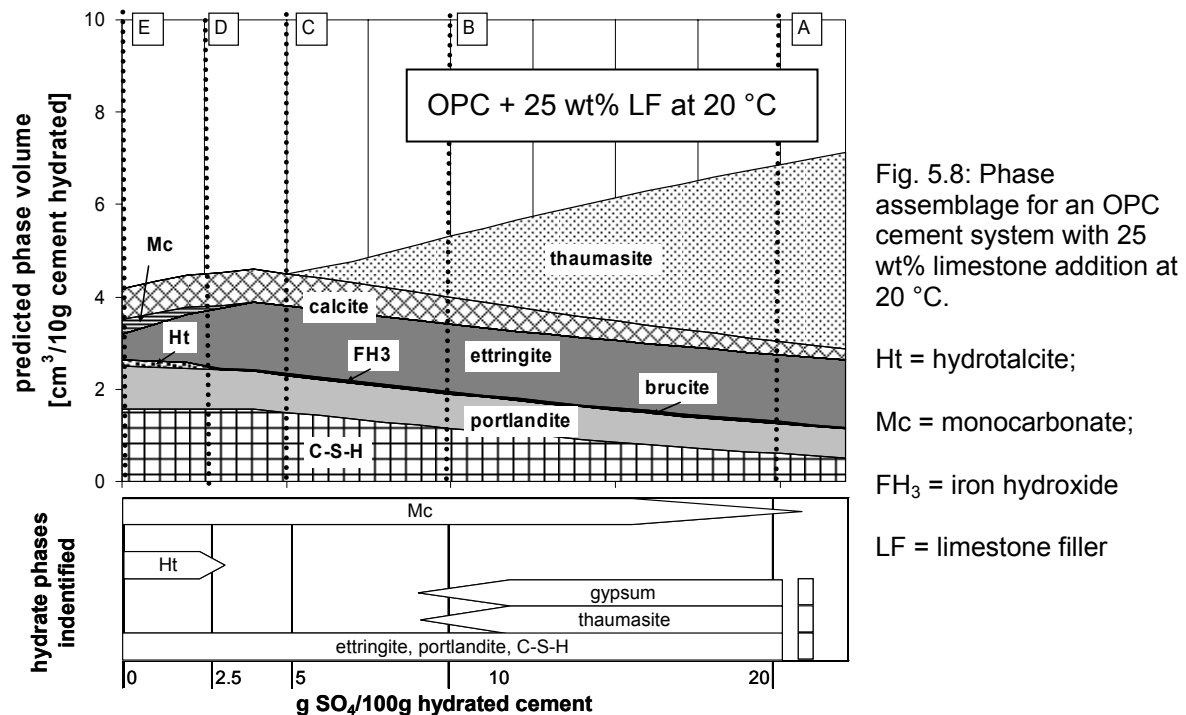


Fig. 5.7: XRD results of selected PEA experiments for OPC cement systems with 5 wt% limestone addition from subsystems A stored at 8 °C for 3 and 9 months. CH = portlandite, Cc = calcite, Ett = ettringite; F = Ferrite, G = gypsum; Ht = hydrotalcite; Mc = monocarbonate, Th = thaumasite.

5.1.3 Effect of temperature

To take into account the temperature aspect, the phase assemblage was modelled for sulfate uptake at 8 °C and 20 °C as shown in Figs. 5.5 and 5.8. In both cases the formation of thaumasite was calculated at higher sulfate concentrations and in the presence of limestone. However, at 20 °C somewhat less thaumasite was calculated to form than at 8 °C. This is due to the relatively strong increase of the solubility of thaumasite with increasing temperature and to the high water/solid ratio used in the experiments.

The thermodynamic calculations indicate that thaumasite is formed at sulfate contents of more than 10 wt% SO_4^{2-} by weight cement paste for both temperatures. Based on the thermodynamic calculations it was found that thaumasite could persist under these conditions up to temperatures of approximately 45 °C.



The quantities of thaumasite determined by Si-NMR for OPC cement systems (Fig. 5.9) showed that thaumasite was detectable after 3 months of sulfate interaction at 8 °C. At 20 °C only very small amounts of thaumasite could be detected even after 9 months of sulfate interaction. Furthermore, at 8 °C, significantly more thaumasite was detected experimentally than in the comparable OPC cement systems with 5 or 25 wt% limestone addition, similar contents of thaumasite were calculated in the thermodynamic modelling. This indicates that thaumasite formation is kinetically faster at 8 °C rather than at 20 °C. The observations of thaumasite formation at 20 °C in the laboratory cements investigated were in good

agreement with the findings of thaumasite formation at 20 °C and above in Italy and Southern California [14, 15]. The results also agreed with findings from other investigations indicating that thaumasite is favoured at lower temperatures [16, 17].

Up to 40 % more thaumasite had formed in the P25 than in the P5 cement system at 8 °C. The difference between subsystem A (10 wt%) and subsystem B (20 wt%) sulfate addition is almost negligible (Fig. 5.9). In contrast to the findings from Hartshorn et al. [18] and Kalinowski and Trägårdh [5] increasing amounts of sulfate concentration (subsystem A, B) did not necessarily increase thaumasite formation, whereas higher amounts of limestone filler from P5 to P25 increased the amount of thaumasite formed during 9 months of sulfate interaction.

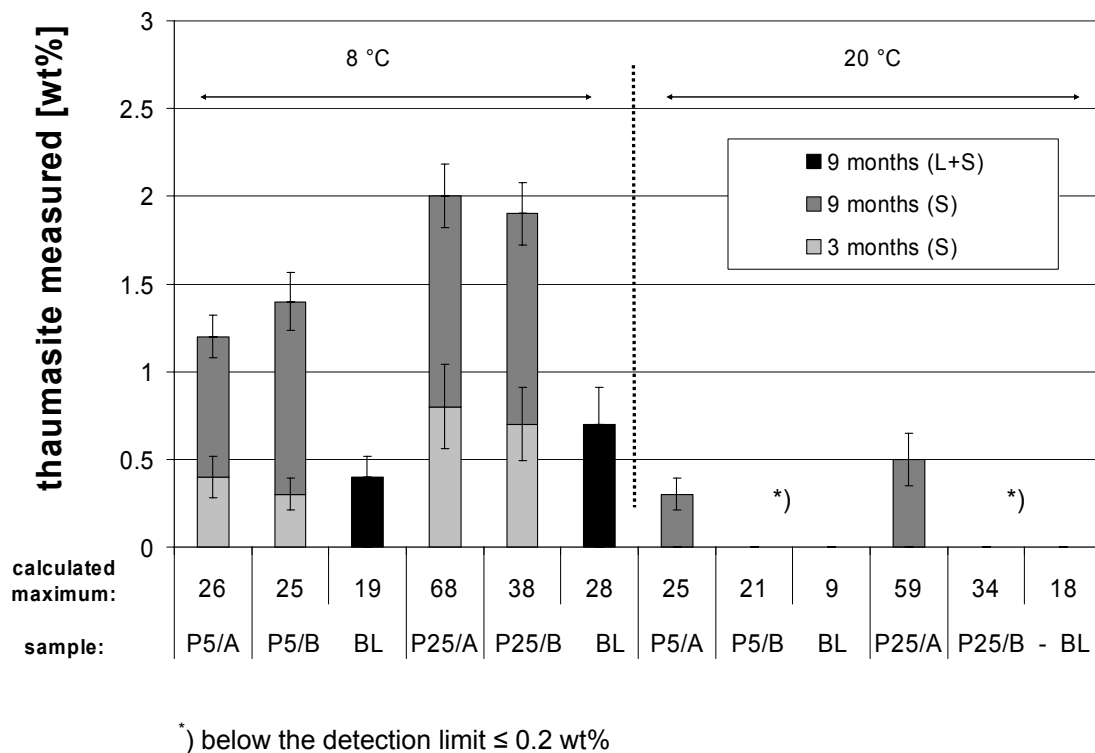


Fig. 5.9: Quantitative concentrations of thaumasite in selected experiments of OPC cement systems with 5 and 25 wt% limestone addition after 3 and 9 months of sulfate interaction (S); leaching and sulfate interaction (L+S) in relation to the calculated maximum amounts.

Generally, the amounts of thaumasite determined by Si-NMR is only a small portion of what is predicted from the thermodynamic data, indicating that thaumasite formation seems to depend strongly on the temperature.

The differences in the phase assemblages between modelled and measured data indicate that equilibrium was not reached after 9 months. However, the assessment of the total risk

potential of the binder systems for thaumasite formation with respect to temperature and sulfate concentration is possible with the help of thermodynamic modelling.

A summary of selected results, e.g. those predicted to contain thaumasite as a consequence of sulfate interaction is given in Table 5.1.

Table 5.1: Pore solution compositions and phase assemblages after 9 months reaction time. Portlandite, C-S-H and clinker phases are present in all samples, Cc = Calcite; C = inorganic carbon; Ett = ettringite; G = gypsum; Mc = monocarbonate; Ms = monosulfate, S = sulfate; Th = thaumasite.

| Sample ⁱ | | Solution composition [mmol/l] ⁱⁱ | | | | | pH | Phase assemblage | | | |
|---------------------|-------|---|------------------|-----|-----|------|------|------------------|-------------------|-------------|----------|
| | | S ⁱⁱⁱ | C ⁱⁱⁱ | Ca | K | Na | | identified | modelled | | |
| 8 °C | H0 | A | 79 | 0.3 | 4.9 | 15.4 | 435 | 13.1 | G Ett (Ms) | Ett (Th) | |
| | | B | 33 | 0.3 | 6.6 | 14.8 | 204 | 13.0 | (G) Ett Ms | Ett (Th) | |
| | H5 | A | 76 | 0.4 | 4.6 | 14.1 | 422 | 13.0 | G↓ Ett Th (Mc) Cc | Ett Th | |
| | | B | 30 | 0.2 | 6.6 | 13.6 | 200 | 12.9 | (G) Ett Mc Cc | Ett Th Cc | |
| | P0 | A | 78 | 0.1 | 4.7 | 11.8 | 435 | 13.1 | G Ett (Ms) | Ett (Th) | |
| | | B | 33 | 0.3 | 5.9 | 11.8 | 200 | 13.0 | (G) Ett Ms | Ett (Th) | |
| | P5 | A | 76 | 0.2 | 4.6 | 10.5 | 426 | 13.0 | G↓ Ett Th (Mc) Cc | Ett Th | |
| | | B | 27 | 0.2 | 5.2 | 10.2 | 183 | 13.0 | (G) Ett Th Mc Cc | Ett Th Cc | |
| | P25 | A | 53 | 0.2 | 3.5 | 6.9 | 335 | 13.0 | G↓ Ett Th (Mc) Cc | Ett Th Cc | |
| | | B | 23 | 0.2 | 4.5 | 7.2 | 152 | 12.9 | (G) Ett Th Mc Cc | Ett Th Cc | |
| | 20 °C | H0 | A | 79 | 0.5 | 4.9 | 14.8 | 435 | 13.0 | G↓ Ett (Ms) | Ett (Th) |
| | | | B | 34 | 0.3 | 5.9 | 15.6 | 209 | 12.9 | (G) Ett Ms | Ett (Th) |
| H5 | | A | 79 | 0.4 | 4.9 | 13.6 | 435 | 13.0 | G↓ Ett (Mc) Cc | Ett Th | |
| | | B | 31 | 0.4 | 5.7 | 13.8 | 191 | 12.9 | (G) Ett Mc Cc | Ett Th Cc | |
| P0 | | A | 79 | 0.3 | 4.6 | 12.3 | 435 | 13.0 | G↓ Ett (Ms) | Ett (Th) | |
| | | B | 31 | 0.4 | 5.1 | 12.3 | 204 | 13.0 | (G) Ett Ms | Ett (Th) | |
| P5 | | A | 78 | 0.3 | 4.3 | 10.5 | 426 | 13.0 | G↓ Ett Th (Mc) Cc | Ett Th | |
| | | B | 28 | 0.2 | 5.1 | 10.5 | 335 | 13.0 | (G) Ett Th Mc Cc | Ett Th Cc | |
| P25 | | A | 56 | 0.2 | 3.9 | 6.9 | 344 | 13.0 | G↓ Ett Th (Mc) Cc | Ett Th Cc | |
| | | B | 25 | 0.2 | 4.5 | 7.2 | 152 | 13.0 | (G) Ett Th Mc Cc | Ett Th Cc | |

↓ = decreasing between 3 and 9 months; () = traces

ⁱ A: 20 wt% SO₄²⁻; B: 10 wt% SO₄²⁻ by mass cement paste

ⁱⁱ measured Si and Al concentration were below the detection limit of 0.1 mmol/l

ⁱⁱⁱ C = inorganic carbon, S = sulfate

5.1.4 Effect of leaching

The formation of thaumasite was calculated for leached and unleached cement systems for the sulfate uptake at 8 °C. The phase assemblage for the leached cement was modelled using the composition of the laboratory cements after the leaching process as given in Table 5.2.

Table 5.2: Composition of selected oxides of the laboratory cements before a) and after b) the leaching process.

| | a) initial ⁱ | | b) leached ⁱⁱ | | | |
|--------------------------------|-------------------------|------|--------------------------|---------|------|---------|
| | HS | OPC | HS | | OPC | |
| SiO ₂ | 19.2 | 20.1 | 19.2 | (± 0) | 20.1 | (± 0) |
| Al ₂ O ₃ | 4.7 | 4.4 | 4.7 | (± 0) | 4.4 | (± 0) |
| Fe ₂ O ₃ | 7.2 | 2.7 | 7.0 | (- 3) | 2.6 | (- 3) |
| CaO | 62.2 | 63.7 | 34.6 | (- 44) | 38.2 | (- 40) |
| MgO | 1.5 | 1.6 | 1.5 | (± 0) | 1.5 | (- 6) |
| K ₂ O | 1.1 | 0.9 | 0.01 | (- 99) | 0.02 | (- 98) |
| Na ₂ O | 0.13 | 0.15 | 0.01 | (- 92) | 0.01 | (- 93) |
| SO ₃ | 1.9 | 2.9 | 1.7 | (- 11) | 2.7 | (- 7) |
| CO ₂ | 0.1 | 0.2 | 0.4 | (+ 300) | 0.5 | (+ 150) |

ⁱ selected oxides from XRF analysis

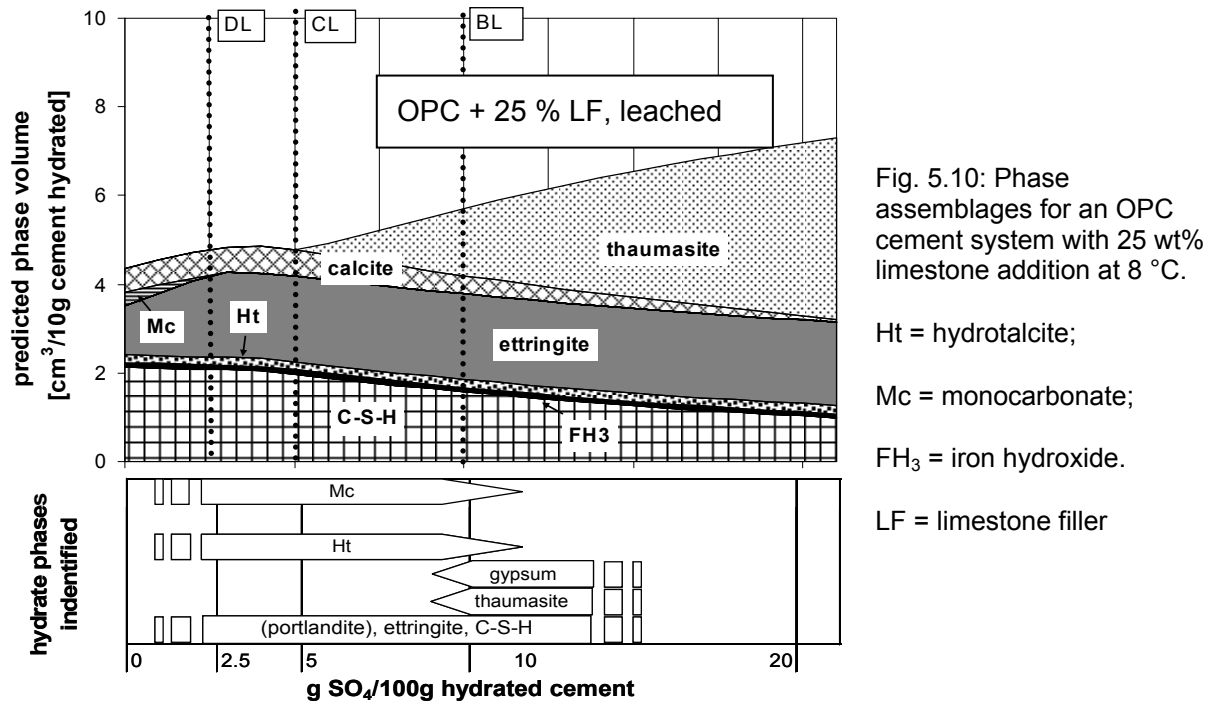
ⁱⁱ normalized on the SiO₂-content (difference in % to initial content)

The calculation indicated that the leached cement system before the addition of sulfate consists of C-S-H, ettringite, AFm (e.g. monocarbonate) and traces of hydrotalcite as stable phases (Fig. 5.10). The main difference to the unleached system is the absence of portlandite as well as a slightly lower Ca/Si ratio of C-S-H.

With progressive addition of sulfate to the cement system, the modelled data indicate that in the leached samples relatively more ettringite is formed (Fig. 5.10) than in the non leached experiments (Fig. 5.5). The calculations further showed that in the presence of sulfate, additional ettringite was formed at the expense of the AFm-phases consuming the available aluminium as shown in Fig 5.10. The modelled hydrate phase assemblages indicated that less thaumasite is formed under leached conditions, in the absence of portlandite, see also Fig. 5.9, samples BL.

The experimental results showed that in leached cement systems the chemical composition and the pore structure changes. After a leaching process of 4 months the amount of calcium (≥ 50 wt%) and alkalies (≥ 90 wt%) was strongly reduced whereas the amounts of silicate,

aluminium and iron remained nearly constant (Table 5.2). In addition, during the leaching a limited uptake of CO_2 into the cement systems is observed.



The experimental results on the leached samples further indicated that with 2.5 wt% sulfate addition ettringite, monocarbonate and traces of hydrotalcite were present, see lower part of Fig. 5.10, subsystem DL. With more sulfate added to the cement systems more ettringite was formed than in the non leached experiments (Figs. 5.12). These observations agree with the calculated data indicating the relative increase of the fraction of aluminium present in leached systems as part of the calcium was removed during leaching. In addition, the increase of porosity in the leached systems may enhance sulfate interaction and thus ettringite formation.

The Si-NMR results showed that significantly less thaumasite was formed in the leached cement systems with high C_3A content (P5, P25) as shown in Fig. 5.9. Thaumasite could not be identified in cement systems with low C_3A content (H0, H5) after 9 months of sulfate interaction following leaching and sulfate interaction which was in contrast to the non leached experiments (Table 5.4) where thaumasite was observed. These findings agreed with the observations of Zhou et al. [19], who found decreasing amounts of thaumasite with decreasing pH, but it is in contrast to the conclusions of Pfiffner and Holzer, Romer et al. [20, 21], who suggested that leaching favours thaumasite formation.

Although, leaching increased the porosity of the cement pastes and therefore accelerated interaction with sulfate, thaumasite formation is not enhanced. Thaumasite formation was found to be even slower in leached samples than in non leached samples at the same sulfate concentrations and exposure times. This could indicate that the precipitation kinetics of thaumasite were not diffusion controlled under these conditions.

The XRD results showed that slightly more gypsum is present in leached subsystems with 10 wt% sulfate addition compared to the unleached subsystems (Fig. 5.11) due to the very slow thaumasite formation.

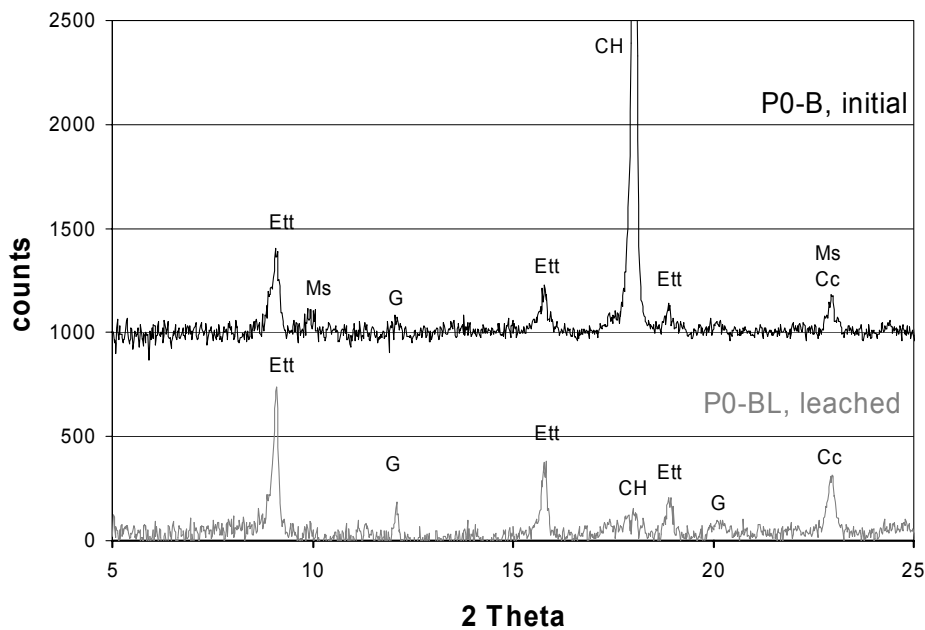


Fig. 5.11: XRD results of selected PEA experiments for OPC cement systems without limestone addition unleached and leached. CH = portlandite, Cc = calcite, Ett = ettringite; F = Ferrite, G = gypsum; Ht = hydrotalcite; Ms = monosulfate, Th = thaumasite.

Low temperatures seemed to favour thaumasite formation also under leached conditions (Fig. 5.9). A possible explanation for the enhanced formation of thaumasite at lower temperatures could be that silicate tends to adopt the octahedral coordination found in thaumasite more easily at lower temperatures as suggested by Bensted [16, 22].

A summary of selected experiments, e.g. those predicted to contain thaumasite under leaching conditions is given in Table 5.3. The differences in the phase assemblages between modelled and measured data indicate that also in the leached experiments equilibrium has not been reached.

Table 5.3: Pore solution compositions and phase assemblages for sulfate interaction (9 months) after leaching. Portlandite and C-S-H present in all samples, Cc = Calcite; Ett = ettringite; G = gypsum; Mc = monocarbonate; Ms = monosulfate, S = sulfate; Th = thaumasite.

| | sample ⁱ | | Solution composition [mmol/l] ⁱⁱ | | | | | pH | Phase assemblage | |
|-------|---------------------|----|---|------------------|-----|-----|-----|------|-------------------|-----------|
| | | | S ⁱⁱⁱ | C ⁱⁱⁱ | Ca | K | Na | | identified | modelled |
| 8 °C | H0 | BL | 33 | 0.8 | 0.9 | 0.2 | 169 | 12.5 | G Ett Ms (Cc) | Ett (Th) |
| | H5 | BL | 33 | 1.2 | 0.5 | 0.2 | 157 | 12.4 | G Ett Mc Cc↑ | Ett Th Cc |
| | P0 | BL | 33 | 1.0 | 0.6 | 0.3 | 169 | 12.7 | G Ett Ms (Cc) | Ett (Th) |
| | P5 | BL | 29 | 1.0 | 0.5 | 0.3 | 157 | 12.7 | G Ett Th Mc Cc↑ | Ett Th Cc |
| | P25 | BL | 29 | 1.4 | 0.4 | 0.1 | 122 | 12.5 | G Ett Th Mc Cc↑ | Ett Th Cc |
| 20 °C | H0 | BL | 31 | 0.8 | 0.7 | 0.2 | 169 | 12.6 | G Ett Ms (Cc) | Ett (Th) |
| | H5 | BL | 33 | 1.0 | 0.4 | 0.3 | 161 | 12.7 | G Ett Ms Cc↑ | Ett Th Cc |
| | P0 | BL | 33 | 0.8 | 0.6 | 0.3 | 174 | 12.7 | G Ett Ms (Cc) | Ett (Th) |
| | P5 | BL | 29 | 0.8 | 0.6 | 0.4 | 165 | 12.8 | G Ett (Th) Cc↑ | Ett Th Cc |
| | P25 | BL | 27 | 1.0 | 0.5 | 0.1 | 122 | 12.6 | G Ett (Th) Mc Cc↑ | Ett Th Cc |

↑ = increasing after leaching; () = traces

ⁱ BL: 10 wt% SO₄²⁻ by mass cement paste

ⁱⁱ measured Si and Al concentration were below the detection limit of 0.1 mmol/l

ⁱⁱⁱ C = inorganic carbon, S = sulfate

5.1.5 Aspects of reaction solution

Beside the solid phases the reaction solutions of the PEA experiments were also investigated. The composition of the solution was calculated for all experiments at 8 and 20 °C. The calculated and measured concentrations of selected ions for an OPC cement system with 25 wt% limestone addition for the non leached and leached experiments are given in Figs. 5.12, 5.13.

In the subsystems where no sulfate has been added, the calculated reaction solutions were dominated by OH^- , Ca, K and Na. The addition of Na_2SO_4 led not only to an increase of calculated Na and sulfate concentration but also to an increase of the hydroxide concentration as part of the sulfate added precipitates as gypsum, thaumasite or other sulfate containing phases. The concentration of Ca decreased according to the increased OH^- concentration in the presence of portlandite (Fig. 5.12).

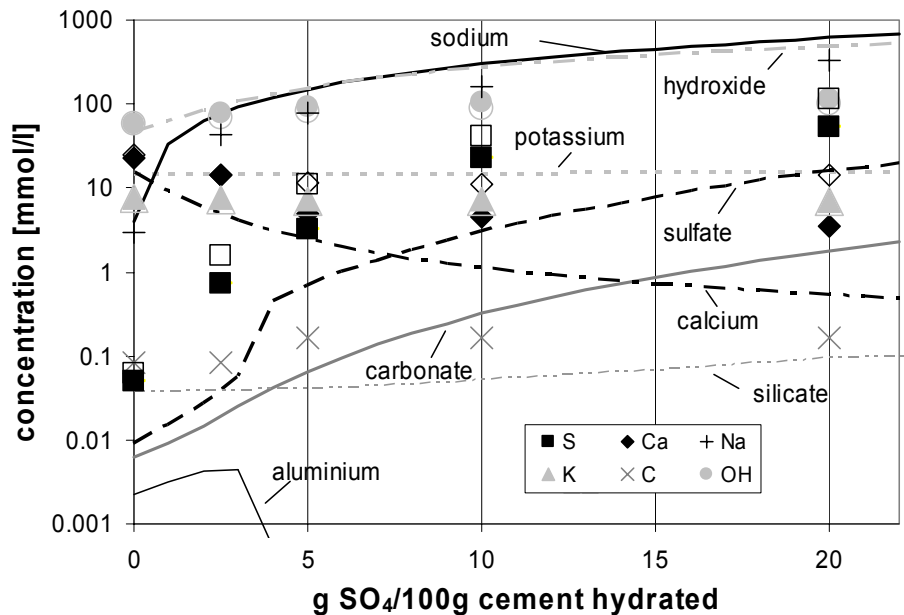


Fig. 5.12: Predicted and experimental composition of the pore solution of an OPC cement system with 25 wt% limestone addition analysed after 3 months (empty symbols) and 9 months (filled symbols) sulfate interaction.

The concentrations of dissolved ions were measured after 3 and 9 months. In Figure 5.12 the data for an OPC with 25 wt% limestone addition were compared to the modelled concentrations assuming equilibrium. The concentrations measured in the subsystems without sulfate addition agree well with the modelled data. The addition of sulfate led to a significant difference between calculated and measured data. The observed trends of the measured ion concentrations over time indicate changes towards the predicted ion concentrations. After 9 months, only a fraction of sulfate added to the subsystem has been

consumed due to the formation of ettringite and thaumasite; gypsum has precipitated instead. At higher sulfate additions, the measured Ca^{2+} and SO_4^{2-} concentrations were buffered by the gypsum present. This indicates that equilibrium has not yet been reached after 9 months of sulfate interaction.

The composition of the reaction solutions for leached cement systems containing 25 wt% limestone is reproduced, see Fig. 5.13. The prediction indicates that leaching reduces the concentration of Ca, Na, and K as well as the OH^- in the solution. The carbonate, aluminium and silicate concentrations in the solution are calculated to be higher in leached than in non leached cement systems (Figs. 5.12, 5.13).

The concentrations of Ca, Na and K as well as OH^- were found to be significantly lower in the systems which had undergone leaching before sulfate interaction (Fig. 5.13). This was due to the fact that portlandite and alkalis are reduced in the leached cement systems as mentioned in 5.1.4 and agrees with the modelling data.

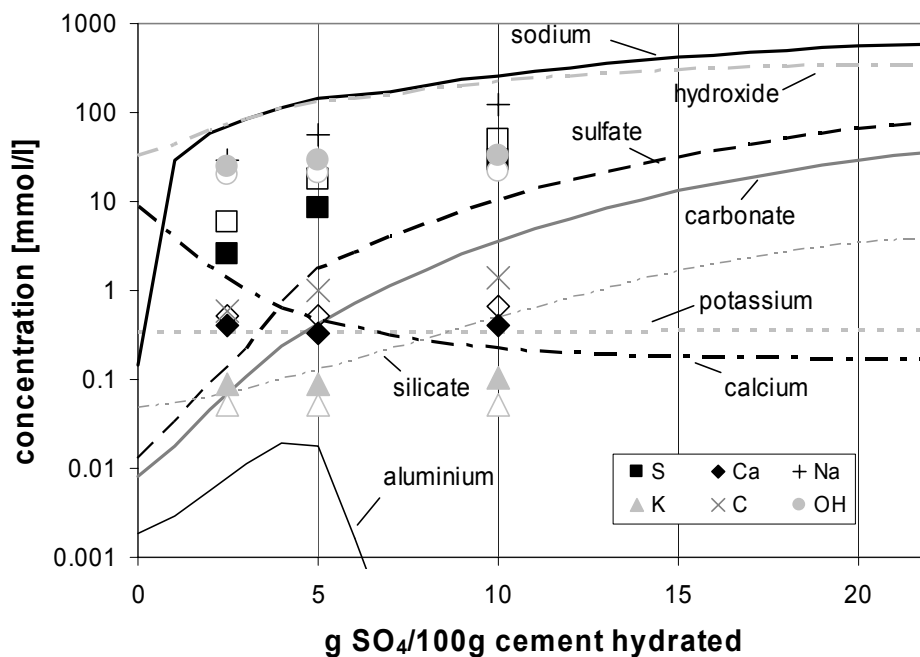


Fig. 5.13: Predicted and experimental composition of the pore solution of an OPC cement system with 25 wt% limestone addition analysed after 3 months (empty symbols) and 9 months (filled symbols) leached before sulfate interaction.

The concentration of carbonate in solution was determined to be slightly increased as indicated by the modelled data. Also for the leached systems the experimental data for the

pore solution composition reproduced the trends which were predicted by the thermodynamic model.

Generally, in the absence of sulfate and at low sulfate concentrations modelled and measured data agreed well. In the subsystem where sulfate has been added, modelled and measured data did not yet agree after 9 months indicating that equilibrium has not been reached.

5.1.6 Microstructural aspects

The microstructure of the cement paste particles was investigated after 9 months of sulfate interaction on samples where 20 wt% SO_4^{2-} (subsystem A) has been added and on samples which have been leached.

- **Sulfate interaction**

The observations on the cement paste particles showed that the samples had a quite inhomogeneous structure after sulfate interaction. After 9 months of sulfate interaction the cement paste exhibited an outer and inner layer (Fig. 5.14). The outer layer was found to be up to 40 μm thick, forming discontinuously at the paste particles. The outer layer was almost completely detached.

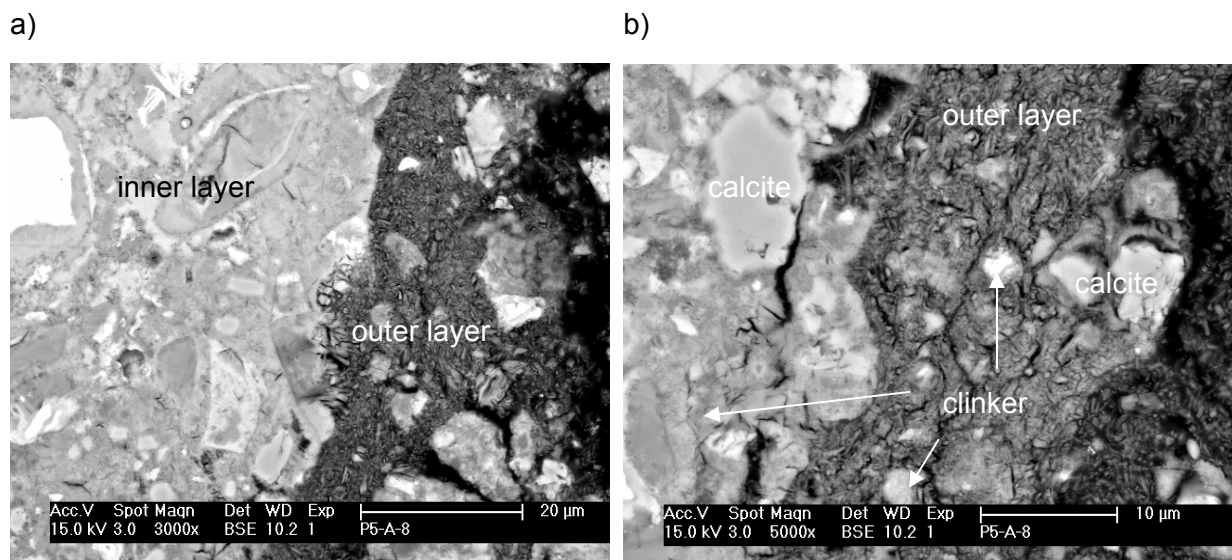


Fig. 5.14: Backscattered electron images of cross section through cement paste particles of subsystem A after 9 months sulfate interaction at 8 °C.

The outer layer was interspersed with microcracks mainly parallel to the surface which indicate the loss of cohesion and binding capacity in the microstructure. The microanalysis of the needle like matrix of the outer layer revealed the presence of mainly Si, Ca and sulfate and only minor amounts of Al, the latter especially around clinker grains (Figs. 5.15, 5.16). A maximum sulfate content of 20 wt% SO_3 by weight cement paste was determined in the outer layer.

The detailed investigation of the outer layer showed that the fine grained matrix consisted of needles with a maximum length of 2 μm as well as some clinker and calcite grains. It was concluded, that the needles were thaumasite which replaced almost completely the hydrated

cement paste. The coexistence of gypsum could not be verified or excluded. Based on microanalytical data there is some evidence for the presence of ettringite around remaining clinker grains (Fig. 5.15).

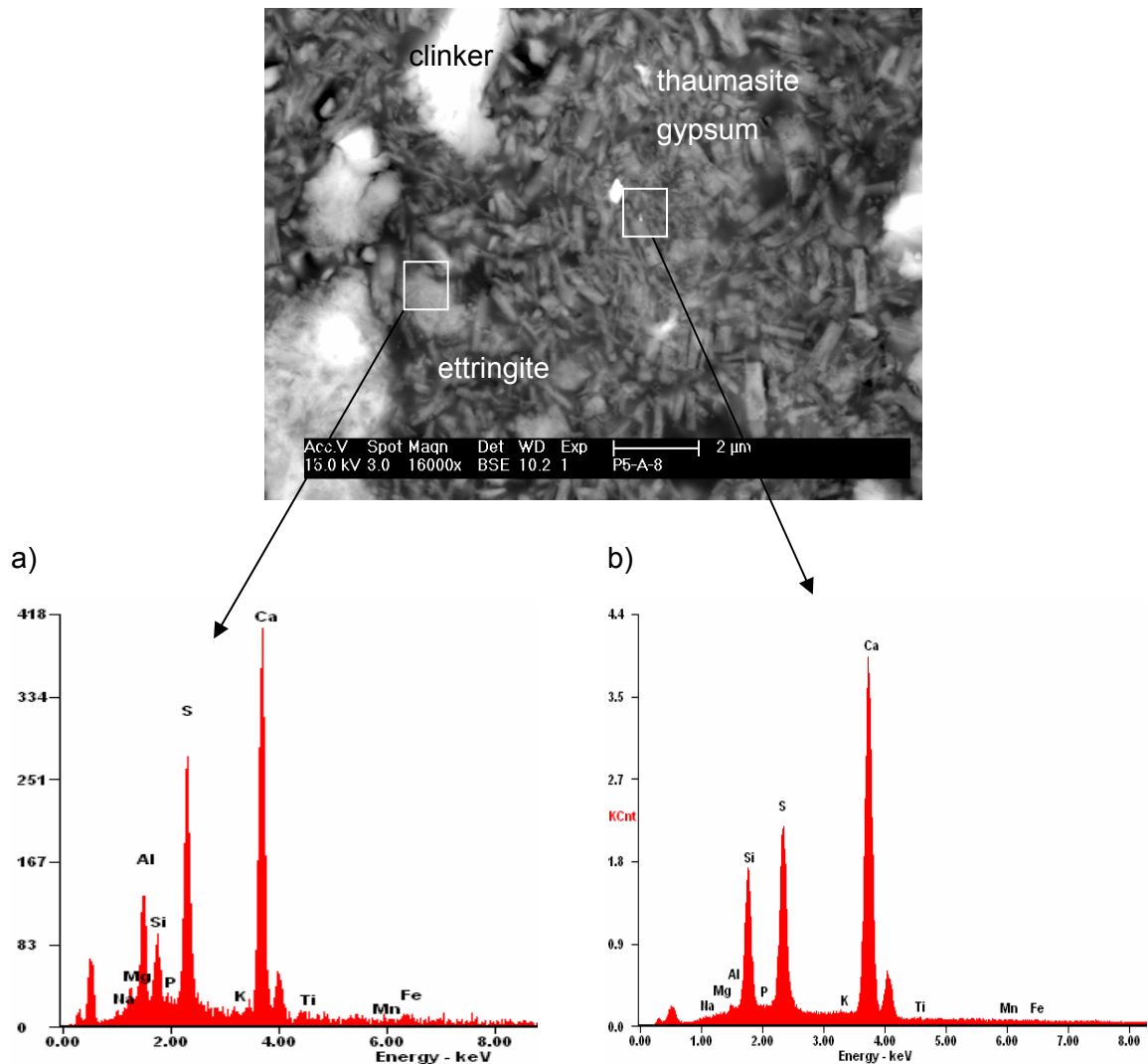


Fig. 5.15: Backscattered electron images of the outer layer from OPC with 5 wt% limestone addition and EDS spectra of a) near clinker grain and b) needle like matrix.

The inner layer was composed of an unchanged region in the center of the cement paste particle and a transition zone between the center and the outer layer characterised by increased sulfate contents and higher density. The microanalysis of the inner part showed that mainly Si, Ca and Al are present; Al mainly near or in the cement clinker grains (Figs. 5.15, 5.16). A maximum sulfate content of 15 wt% SO_3 by weight cement paste was determined at the transition zone between inner and outer layer. Generally, the sulfate uptake was detectable to a depth of 10 μm in P5 and 100 μm in P25 approaching a minimum value of 4 wt% SO_3 in the center of the particles.

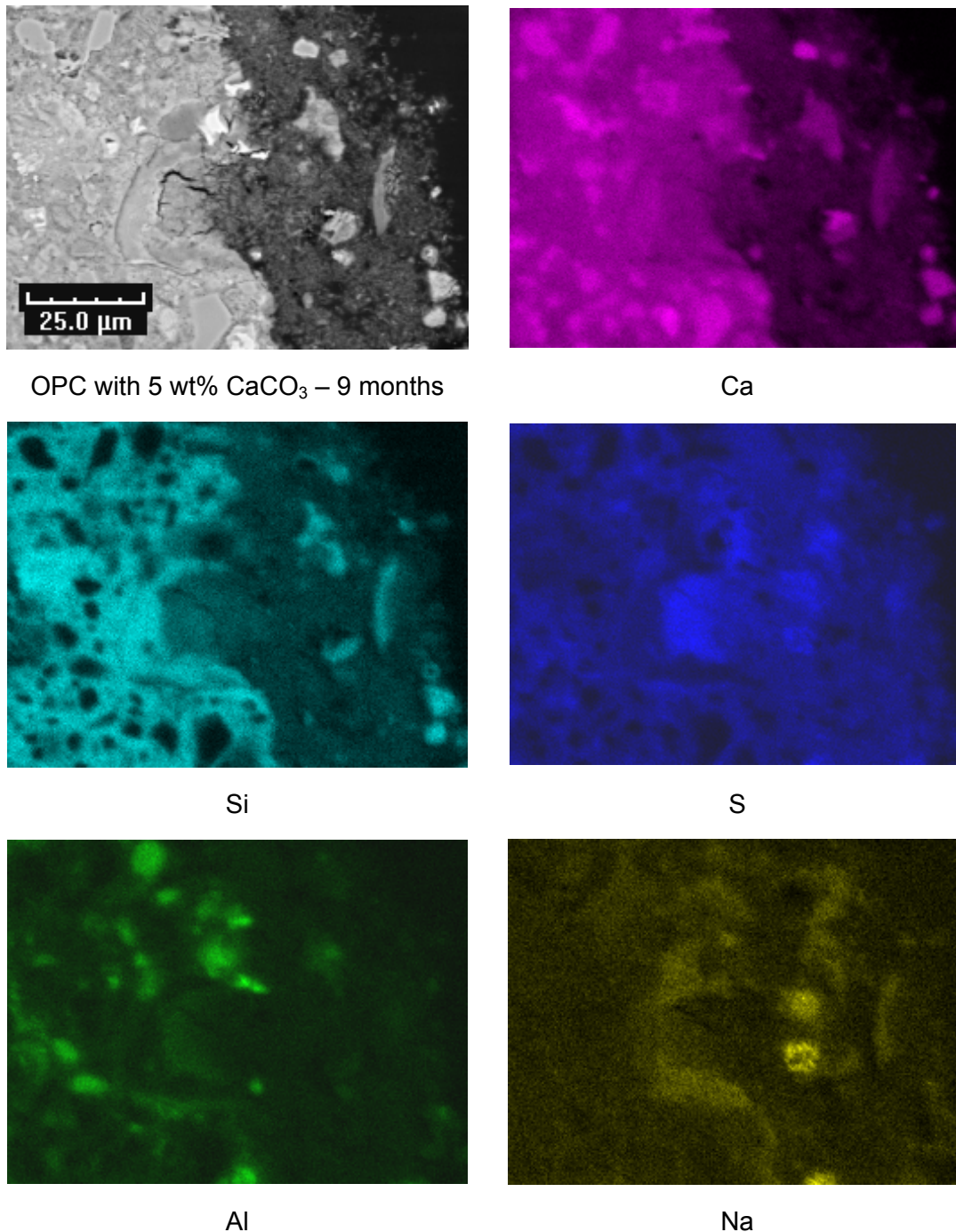
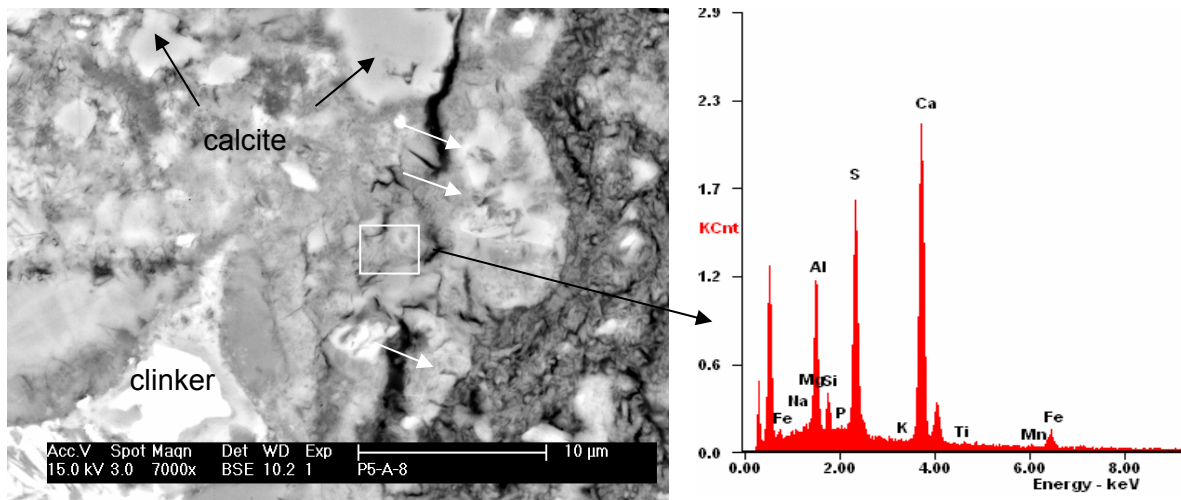


Fig. 5.16: EDS analysis after 9 months sulfate interaction in subsystem A at 8 °C showing the qualitative element distributions of the inner and the outer layer.

A more detailed analysis of parts of the transition zone between the unchanged center and outer layers showed that in many areas mainly Al, S and Ca are present (Fig. 5.17a). Based on microstructural data it was concluded that the topmost part of the transition zone is enriched with secondary ettringite forming preferentially near cement clinker grains (source of aluminium). The observed ettringite formation led to expansion and thus to the separation of parts of the cement paste as indicated by the white arrows (Fig. 5.17a).

a)



b)

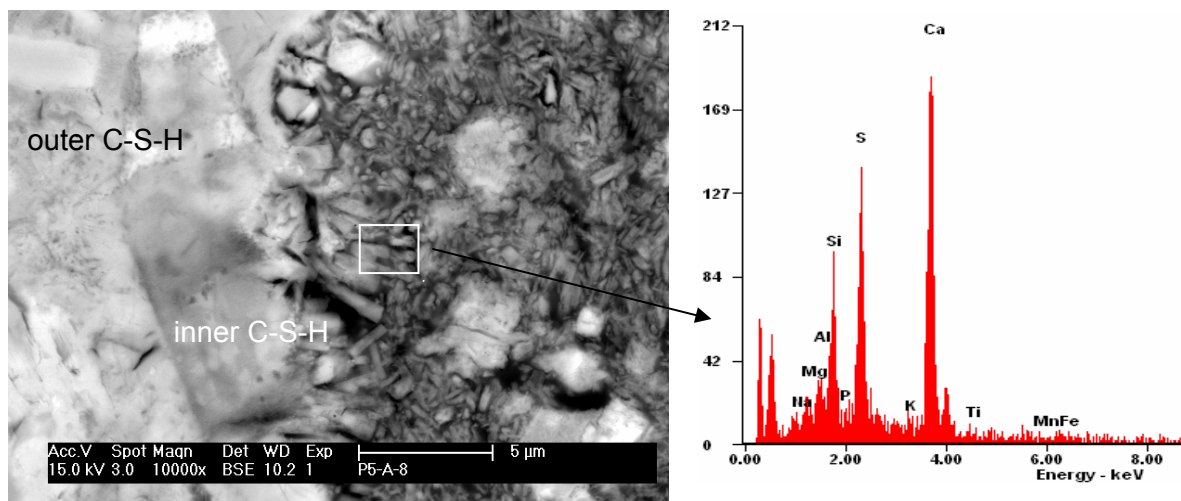


Fig. 5.17: Backscattered electron images of the transition zone of cement paste particles from OPC with 5 wt% limestone addition and EDS spectra of a) ettringite and b) thaumasite enriched areas.

The microanalysis further showed that the contact between transition zone and outer layer is quite sharp leading to ettringite and thaumasite enriched areas in close vicinity and also thaumasite and C-S-H (Fig. 5.17b).

The formation of a sharp boundary between the two layers indicates, that the penetration of sulfate from the reaction solution into the cement paste was slower than the chemical alteration transforming the inner layer of the cement paste into the outer layer of sulfate phases. It was further concluded that the diffusion of sulfate into the cement paste was slowed down by the formation of secondary ettringite. The formation of surface parallel cracks in the transition zone allows further reaction to proceed with the necessary high sulfate concentrations for the formation of gypsum and thaumasite.

Thus, the speed of the reaction front was not controlled by the rather slow formation of thaumasite but by the diffusion of sulfate into the cement paste particles. In the case of a rather dense microstructure (low w/c ratio) it can be assumed, that without the formation of microcracks due to ettringite formation the movement of the reaction front would be even slower. The transformation of cement paste into thaumasite would be faster, if a) microcracks formed earlier due to lower cohesion of the cement paste, or b) the maximum ettringite formation did not block the entire pore space and therefore the sulfate uptake would be faster. In principle ettringite forms first as long as there was a source of aluminium available and when the $\text{SO}_3/\text{Al}_2\text{O}_3$ ratio exceeds 3 thaumasite forms as observed in the outer layer.

The reaction of sulfate with the cement particles was far from complete after 9 months exposure. This explained why the phase composition by using bulk analytical techniques were quite different compared to the modelled phase assemblages. Such that assemblages , e.g. (i) AFm phases have been detected where only AFt phases were predicted and (ii) gypsum was detected in all subsystems, the latter representing the outer layer of the cement paste particles, where the sulfate content was very high. However, since the SEM investigations of the PEA experiments were done after 9 months and not after 3 months of sulfate exposure, no obvious amounts of gypsum could be found. These observations confirmed the assumption that gypsum possibly acts as a source of sulfate during the precipitation of thaumasite as described in section 5.1.2. The observed possible transformation of the C-S-H phase into thaumasite was the reason for the loss of cohesion and the formation of the fine grained, needle like matrix in the outer layer as described by various authors [23, 24, 21, 25].

5.2 Summary and conclusions

On exposure to high sulfate concentrations monosulfate, monocarbonate and hemicarboxate reacted first to form ettringite. Subsequently, thaumasite precipitated at high sulfate contents. Experimental data as well as thermodynamic modelling indicated, that thaumasite can only be formed under conditions where the molar $\text{SO}_3/\text{Al}_2\text{O}_3$ ratio in the cement system exceeds 3. If less SO_3 was added to the cement system, only ettringite was formed.

In Portland cement systems with 5 wt% limestone addition, the amount of calcite limits the extent of thaumasite formation if more than approximately 10 wt% SO_4^{2-} is present. In the case of 25 wt% limestone much more thaumasite can be formed and it was limited by the amount of sulfate added in the range studied.

Gypsum was observed to form in parallel to or instead of thaumasite at high sulfate concentrations. In the experiments gypsum was formed initially since the formation of thaumasite was kinetically very slow. Gypsum acts as a source of sulfate for the precipitation of additional thaumasite. Thaumasite was found to be the last sulfate phase forming during sulfate interaction.

The experimental results further show that limestone containing cement systems with both high and low C_3A content can be affected by thaumasite formation. The C_3A content was not found to have a significant influence on thaumasite formation.

Low temperatures (8 °C) favour thaumasite formation. At lower temperatures thaumasite was formed faster. In addition, somewhat higher amounts of thaumasite were calculated to be stable at lower temperatures.

Leaching reduced the amount of portlandite and increased the porosity of the cement paste systems. Furthermore leaching reduced the amount of alkalis and calcium in the cement systems resulting in lower pH values in the reaction solution. Thaumasite was also formed in leached cement systems. However, experimental and modelling results showed that in leached cement systems the amount of thaumasite formed is smaller than in unleached cement systems, whereas secondary gypsum and ettringite formation are favoured under these conditions.

The progressive equilibrium approach PEA used to investigate the chemical aspects of sulfate attack appeared to be a good tool for simulating various levels of sulfate uptake due to an external sulfate attack. Generally, thaumasite was detected where it has been modelled to be a stable phase in significant amounts. However, the experimental setup, especially the

selection of a w/c ratio of 0.35 in this study did not allow to reach equilibrium after 9 months of sulfate interaction.

5.3 References

1. Lothenbach, B. and Winnefeld, F., *Thermodynamic modelling of the hydration of Portland cement*. Cement Concrete Research, 2006. 36 (2), 209-226.
2. Kulik, D., *GEMS-PSI 2.1*, available at <http://leswebpsi.ch/software/GEMS-PSI>, PSI Villigen, Switzerland. 2006.
3. Juel, I., Herfort, D., Gollop, R., Konnerup-Madsen, J., Jakobsen, H.J., and Skibsted, J., *A thermodynamic model for predicting the stability of thaumasite*. Cement Concrete Composites, 2003. 25 (8), 867-872.
4. Macphee, D. and Diamond, S., *Thaumasite in Cementitious Materials*. Cement Concrete Composites, 2003. 25 (8), 805-807.
5. M. Kalinowski and Trägårdh, J., *Thaumasite and Gypsum formation in SCC with sulfate resistant cement exposed to a moderate sulfate concentration*. Second North American Conference on the Design and Use of Self-Consolidating Concrete, 2005. Section 3 (durability), 319-325.
6. Nobst, P. and Stark, J., *Grundlagenuntersuchungen zur Thaumasitbildung in Zementsteinpasten*. 15. Ibausil, 2003, 2-0685 - 0699.
7. Nobst, P. and Stark, J., *Investigations on the influence of cement type on thaumasite formation*. Cement Concrete Composites, 2003. 25 (8), 899-906.
8. Nobst P. and Stark, J., *Untersuchungen zur Thaumasitbildung bei inneren und äusseren Sulfatangriff*. 16. Ibausil 2006, 2006. 2, 2-0547-0556.
9. Bellmann, F., *On the formation of thaumasite $\text{CaSiO}_3\text{CaSO}_4\text{CaCO}_3\cdot 15\text{H}_2\text{O}$ Part II*. Advances in cement research, 2004. 16, 89-94.
10. Bellmann, F., *On the formation of thaumasite Part I*. Advances in cement research, 2004. 16 (2) 55-60.
11. Irassar, E.F., Bonavetti, M.A., Trezza, M.A., and Gonzalez, M., *Thaumasite formation in limestone filler cements exposed to sodium sulphate solution at 20 °C*. Cement Concrete Composites, 2005. 27, 77-84.
12. Köhler, S., Heinz, D., Urbonas L., *Effect of ettringite on thaumasite formation*. Cement Concrete Research, 2005.
13. Lachowski, E.E., Barnett, S.J., and Macphee, D.E., *Transmission electron optical study of ettringite and thaumasite*. Cement Concrete Composites, 2003. 25 (8), 819-822.
14. Collepardi, M., *Thaumasite formation and deterioration in historic buildings*. Cement Concrete Composites, 1999. 21 (2), 147-154.
15. Diamond, S., *Thaumasite in Orange County, Southern California: an inquiry into the effect of low temperature*. Cement Concrete Composites, 2003. 25 (8), 1161-1164.
16. Bensted, J., *Mechanism of thaumasite sulphate attack in cements, mortars and concretes*. Zement Kalk Gips, 2000. 53, 704-709.
17. Bensted, J., *Thaumasite -- background and nature in deterioration of cements, mortars and concretes*. Cement Concrete Composites, 1999. 21 (2), 117-121.
18. Hartshorn, S.A., Sharp, J.H., and Swamy, R.N., *The thaumasite form of sulfate attack in Portland-limestone cement mortars stored in magnesium sulfate solution*. Cement Concrete Composites, 2002. 24 (3-4), 351-359.
19. Zhou, Q., Hill, J., Byars, E.A., Cripps, J.C., Lynsdale, C.J., and Sharp, J.H., *The role of pH in thaumasite sulfate attack*. Cement Concrete Research, 2006. 36 (1), 160-170.

20. Pfiffner, M. and Holzer, L. *Schädigungsmechanismen der Zementsteinkorrosion: Auslaugung und Sulfatangriff*. in *Symposium Bergwasserproblematik in Tunnelbauwerken*. 2001. Dübendorf: EMPA Akademie.
21. Romer, M., Holzer, L., and Pfiffner, M., *Swiss tunnel structures: concrete damage by formation of thaumasite*. *Cement Concrete Composites*, 2003. 25 (8), 1111-1117.
22. Bensted, J., *Thaumasite--direct, woodfordite and other possible formation routes*. *Cement Concrete Composites*, 2003. 25 (8), 873-877.
23. Crammond, N.J., *The thaumasite form of sulfate attack in the UK*. *Cement Concrete Composites*, 2003. 25 (8), 809-818.
24. Matthews, S., available at <http://bre.co.uk/service>. BRE, Bucknalls Lane, Watford WD25 9XX, 2007.
25. The Thaumasite Expert Group, *The thaumasite form of sulfate attack: risks, diagnosis, remedial works and guidance on new constructions*. *Department of the Environment*. 1999: Transport London. p. 180.

6 Mortar experiments

The following chapter describes the investigations on external sulfate attack on mortar samples with different binder systems. The results evaluate the influence of sulfate concentration, storage temperature, time, limestone addition and clinker type on the performance of the mortar samples.

6.1 Physical and microstructural aspects of sulfate attack

The consequences of external sulfate attack were investigated by traditional test methods, i.e. length and mass change. Furthermore, a newly developed, surface sensitive ultrasonic method was used to determine successive changes in the topmost surface layer of the mortar samples during sulfate attack. The macroscopical changes are discussed and compared with microstructural findings.

6.1.1 Expansion and mass change

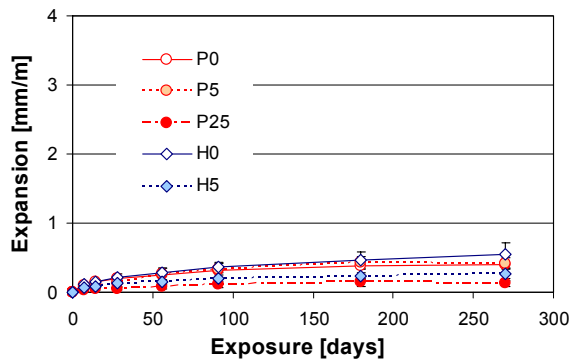
The results of the length change measurements of mortar samples are shown in Fig. 6.1. The measurements indicate that a limestone addition of 5 wt% (H5, P5) reduced expansion at both high (30g $\text{SO}_4^{2-}/\text{l}$) and a low (3g $\text{SO}_4^{2-}/\text{l}$) sulfate concentration. Higher amounts of limestone addition, i.e. 25 wt% in P25 generally led to high expansion during sulfate exposure. The results further showed that up to about 56 days expansion of the samples stored at 3g $\text{SO}_4^{2-}/\text{l}$ days was close to the expansion measured for the reference samples stored in limewater, (Fig. 6.1 a, b).

The measurements showed further that cement systems with low C_3A (H0, H5) generally had a slightly higher expansion at the beginning of sulfate exposure than the cement systems with high C_3A content (P0, P5). The higher initial porosity of the HS cement systems could lead to accelerated sulfate ingress as indicated by the reference samples stored in limewater.

The evolution of expansion had a different behaviour depending on the sulfate concentration in solution (Fig. 6.1). At high sulfate concentration (30g $\text{SO}_4^{2-}/\text{l}$) the mortar samples investigated showed an exponentially accelerating expansion behaviour which started after 28 to 56 days of sulfate exposure (Figs. 6.1 e, f). The samples stored at low sulfate concentration showed a relative moderate and steady expansion during the first 91 days (Figs. 6.1 c, d). Significant differences were observed for samples H0 and H5, P0 and P5 as well as P25 respectively after 91 days of sulfate interaction at 20 °C.

At 8 °C only P25 was different compared to the other samples. The observed expansions were slightly higher at 20 °C than at 8 °C indicating that sulfate interaction, diffusion and reaction of sulfate ions might be accelerated at higher temperatures. However, at low temperatures thaumasite formation may participate in sulfate expansion.

a) limewater at 20 °C



b) limewater at 8 °C

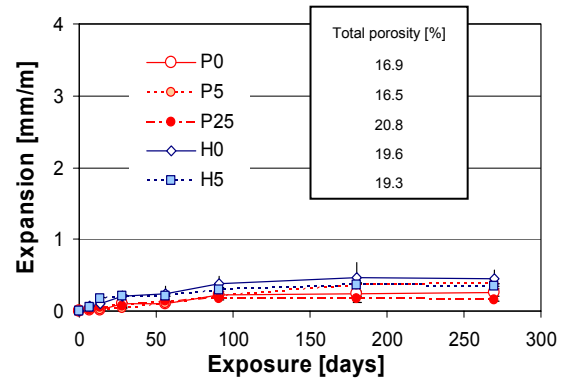
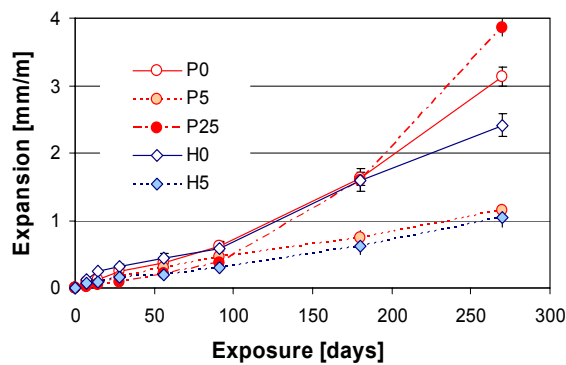
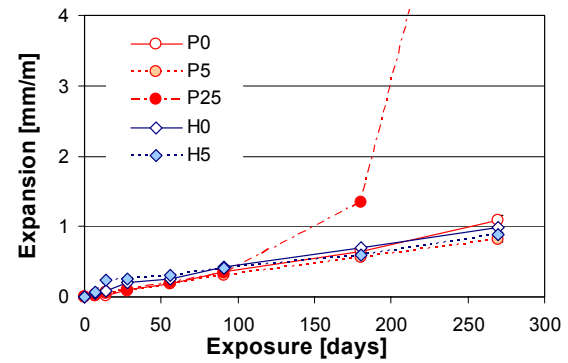
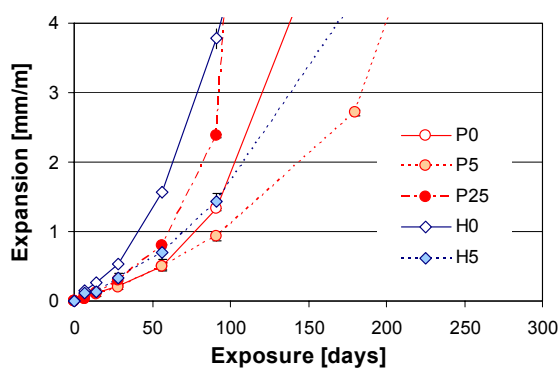
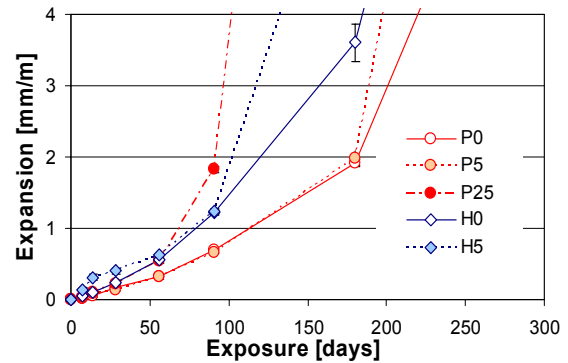
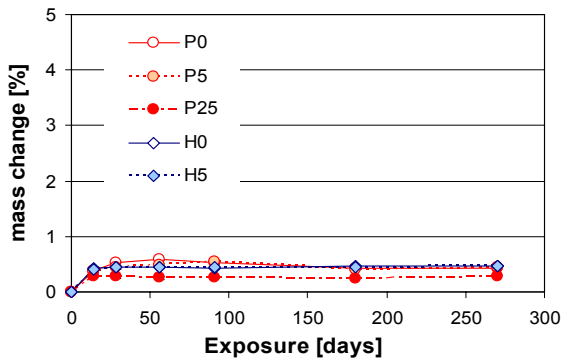
c) 3g SO₄²⁻/l at 20 °Cd) 3g SO₄²⁻/l at 8 °Ce) 30g SO₄²⁻/l at 20 °Cf) 30g SO₄²⁻/l at 8 °C

Fig. 6.1: Expansion of HS and OPC mortar samples immersed in Na₂SO₄ solution at given temperature and sulfate concentration and reference samples stored in saturated limewater.

The corresponding investigations on the mass change of the mortar samples (Fig. 6.2) indicate that at high sulfate concentration and 20 °C in solution, limestone addition of 5 wt% (H5, P5) reduced the sulfate induced increase of mass compared to the reference samples without limestone addition (H0, P0), see Fig. 6.2e. Limestone addition of 25 wt% (P25) led to a significant increase in mass after 91 days of sulfate exposure at 20 °C.

a) limewater at 20 °C



b) limewater at 8 °C

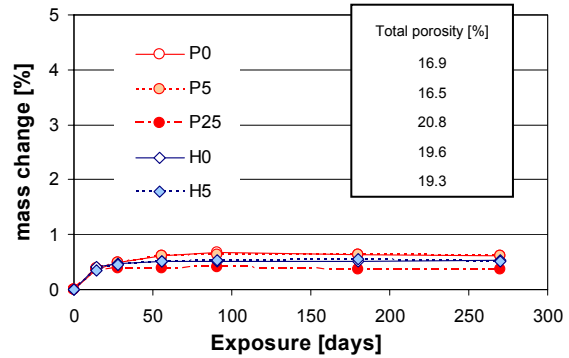
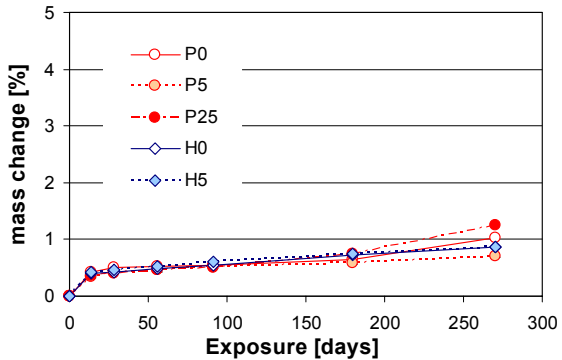
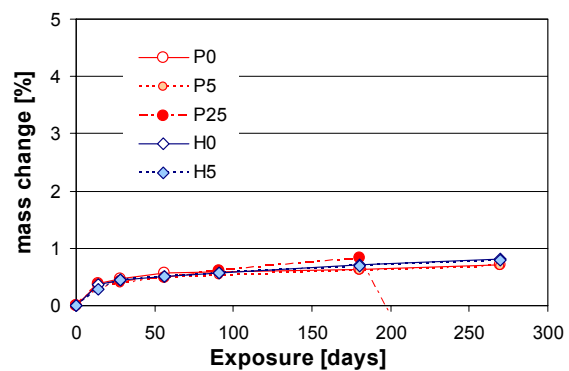
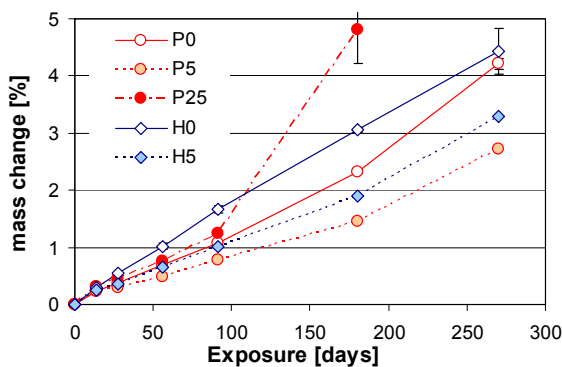
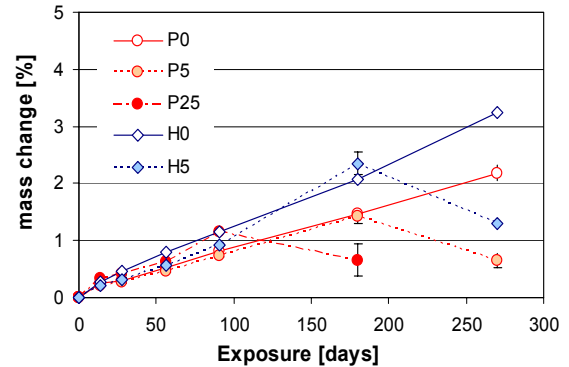
c) 3g SO₄²⁻/l at 20 °Cd) 3g SO₄²⁻/l at 8 °Ce) 30g SO₄²⁻/l at 20 °Cf) 30g SO₄²⁻/l at 8 °C

Fig. 6.2: Mass change of HS and OPC mortar samples immersed in Na₂SO₄ solution at given temperature and sulfate concentration and reference samples immersed in saturated limewater.

The initial higher porosity determined for cement systems without and with high amounts of limestone addition, led to a high sulfate induced mass increase only at high sulfate concentration.

The results further showed that HS cement systems (low C_3A) had constantly higher, almost linear increase in mass than the OPC cement systems at high sulfate concentration. This indicated that the higher initial porosity as determined for the HS cements led to higher sulfate induced mass increases right from the beginning of sulfate exposure. The evolution of the mass change with time showed a significant influence of the sulfate concentration. In comparison to the reference samples stored in limewater, (Figs. 6.2 a, b), the samples stored at low sulfate concentration showed a slight but constant increase in mass with time indicating a constant sulfate induced mass increase during sulfate interaction (Figs. 6.2 c, d). The mortar samples stored at high sulfate concentration had an almost linear increase in mass during sulfate exposure (Fig. 6.2 e, f).

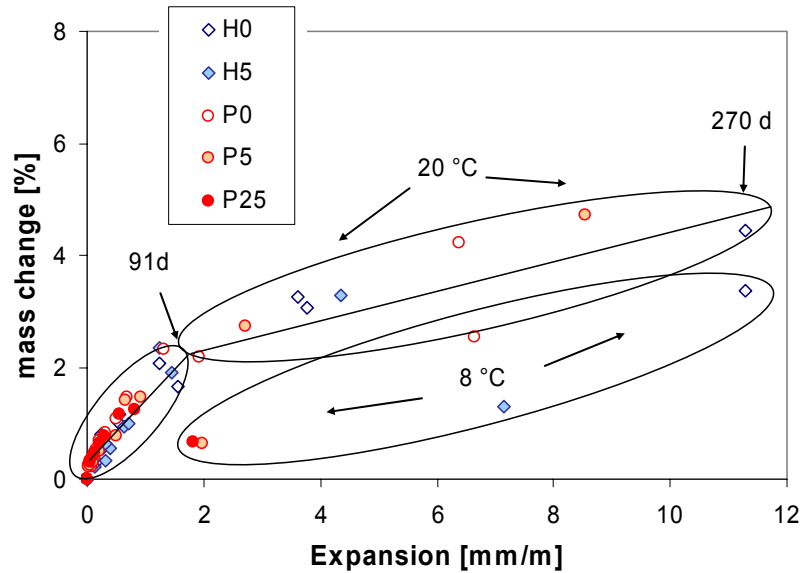
The investigations on the mass change further showed an influence of storage temperature on sulfate interaction (Figs 6.2 e, f). At 8 °C the mortar samples with limestone containing cement systems showed a significant drop in mass between 91 to 180 days (P25) and 180 to 270 days (H5, P5) indicating a significant loss of material. Thereby, increasing amounts of limestone addition (P25) led to an increased sulfate induced mass decrease. This indicated that the observed mass loss could be due to the formation of thaumasite and the successive loss of material due to the loss of cohesion as observed macroscopically, see section 6.1.3.

The comparison of the mass change and the expansion of the mortar samples at both 8 and 20 °C showed that in the beginning of sulfate exposure the weight gain was increased while the expansion was moderate (Fig. 6.3). This suggests that during the first 3 months the uptake of sulfate results mainly in the filling of pores and voids. After approximately 91 days, expansion became more pronounced while the mass gain slowed down indicating the formation of cracks. This effect started approximately after 3 months at high sulfate concentration and after 6 months at low sulfate concentration in solution (Fig. 6.3 a, b). However, mortar samples stored at 30g SO_4^{2-}/l showed a higher mass gain to expansion ratio than the mortar samples stored at 3g SO_4^{2-}/l .

At 8 °C the mortar samples containing carbonate showed a significant drop in mass whereas the expansion level remained similar independent of the storage temperature. These observations indicated progressive mass loss during sulfate exposure possibly due to thaumasite formation as mentioned above (Fig. 6.3 a).

Moreover, at low sulfate concentration in solution the HS mortar samples showed a lower total expansion compared to the OPC mortar samples after 270 days exposure whereas at high sulfate concentration the opposite was observed (Fig. 6.3 a, b).

a) 30g $\text{SO}_4^{2-}/\text{l}$ at 8 and 20 °C



b) 3g $\text{SO}_4^{2-}/\text{l}$ at 8 and 20 °C

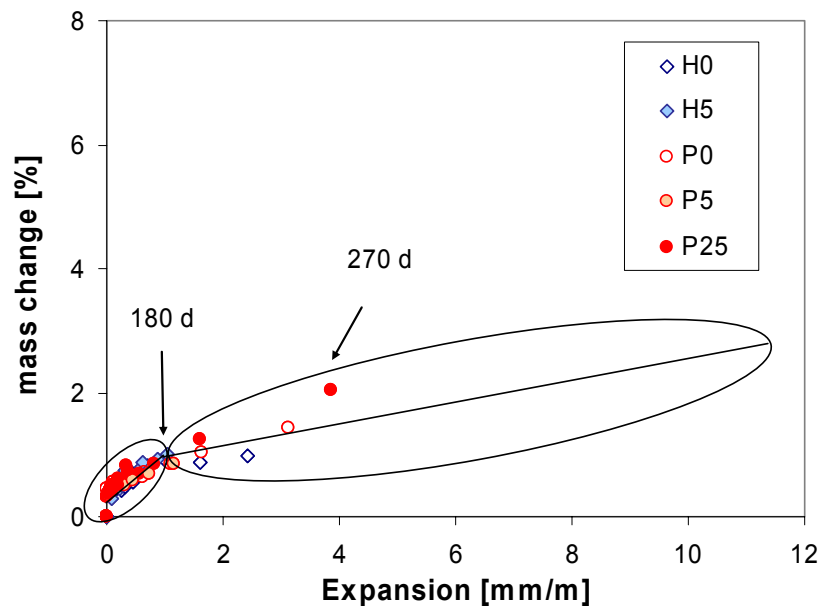


Fig. 6.3: Mass change versus expansion of HS and OPC mortar samples immersed in Na_2SO_4 solution. The lines are intended as eye guides only.

6.1.2 Ultrasonic surface velocity

The ultrasonic measurements were done as described in Chapter 3, section 3.3.2 and the equipment is shown in the Appendix A 5 for both 8 and 20 °C.

The ultrasonic surface velocity of the Leaky Rayleigh wave c_{LR} was measured periodically according to the monitoring program of the mortar samples during sulfate exposure. The results of the ultrasonic measurements are shown in Fig. 6.4. The ultrasonic method allows to follow the degradation processes of the topmost layer of the samples surface (1- 2 mm). The signal is not affected by the unchanged bulk of the samples.

The investigations showed that in the beginning of sulfate exposure the Leaky Rayleigh wave velocity mainly increased indicating an densification of the surface. This effect was also observed for the reference samples stored in limewater, (Figs. 6.4 a, b). As sulfate exposure continued the Leaky Rayleigh wave velocity started to decrease. The observed reduction of the surface density possibly resulted from progressive disintegration and a decrease of the density of the microstructure.

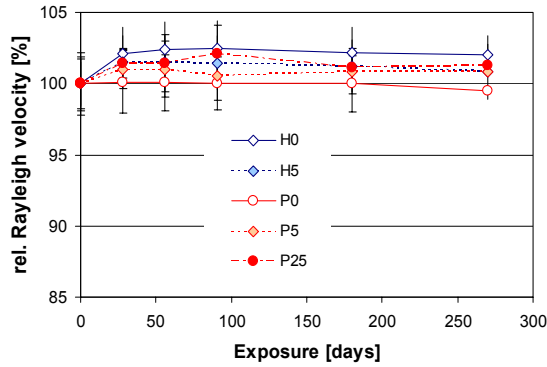
The results further showed that in case of 5 wt% limestone addition in the cement systems (H5, P5) the relative values of Leaky Rayleigh wave velocity are generally high (Figs. 6.4a-d). That indicates a generally dense microstructure compared to the cement systems without limestone addition. The decrease of the density in the surface of the mortar samples was smaller in samples with 5 wt% limestone addition. High amounts of limestone addition as in P25 led to an accelerated decrease in Leaky Rayleigh wave velocity which indicates a deterioration of the surface layer of the sample due to sulfate attack.

The sulfate concentration in solution also influenced the development of the Leaky Rayleigh wave velocity during exposure. Mortar samples stored at high sulfate concentration (30g $\text{SO}_4^{2-}/\text{l}$) showed an accelerated reduction of the surface density after 56 days at 20 °C of sulfate interaction (Figs 6.4e, f). At low sulfate concentration (3g $\text{SO}_4^{2-}/\text{l}$) the measured ultrasound velocity did not show significant differences of the investigated mortar samples up to 180 days (Figs. 6.4 c, d) except the P25 mortar samples with 25 wt% limestone addition.

At low temperature (8 °C) the mortar samples with 5 wt% limestone addition (H5, P5) showed an increased reduction of the surface density after 91 days of sulfate exposure at 30g $\text{SO}_4^{2-}/\text{l}$ (Fig. 6.4f). At 20 °C the mortar samples with 5 wt% limestone addition (H5, P5) had a higher surface density than the mortar samples without limestone addition.

The measurements of the Leaky Rayleigh wave velocity showed a relatively high variation of the measurements especially at the early age of sulfate exposure. The determined ultrasound velocities of the mortar samples did not exhibit significant differences in the beginning of sulfate exposure.

a) limewater at 20 °C



b) limewater at 8 °C

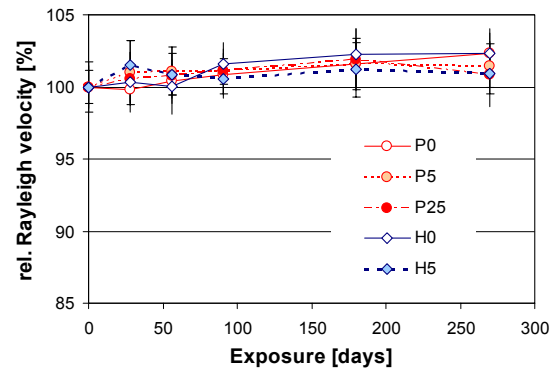
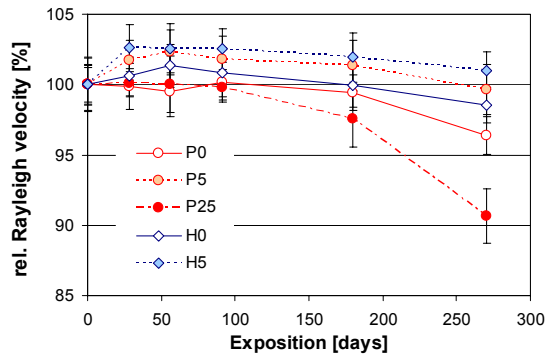
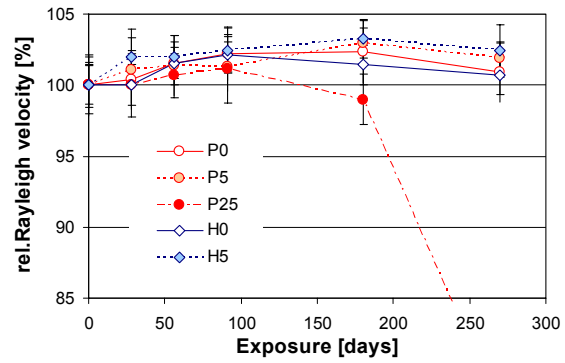
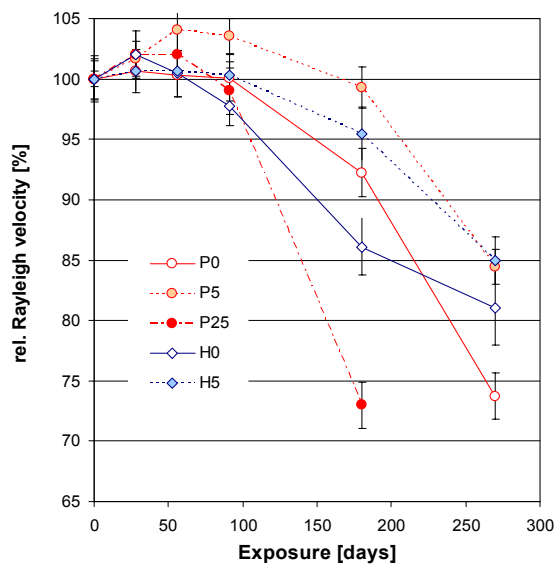
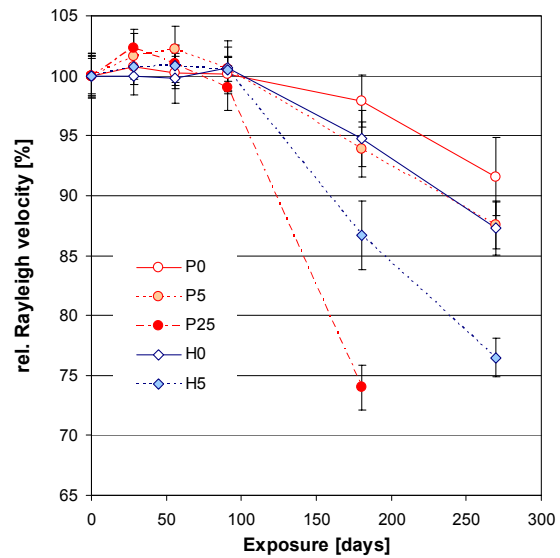
c) 3g SO₄²⁻/l at 20 °Cd) 3g SO₄²⁻/l at 8 °Ce) 30g SO₄²⁻/l at 20 °Cf) 30g SO₄²⁻/l at 8 °C

Fig. 6.4: Relative Rayleigh wave velocity c_{LR} of HS and OPC mortar samples immersed in Na₂SO₄ solution at given temperature and sulfate concentration. Reference samples immersed in saturated limewater.

The comparison of the Leaky Rayleigh velocity and the expansion of mortar samples stored at 8 and 20 °C at high sulfate concentration are given in Fig. 6.5. The results show that in the beginning of sulfate exposure the density of the surface layer in the mortar samples increased accompanied by a first moderate expansion of the whole sample.

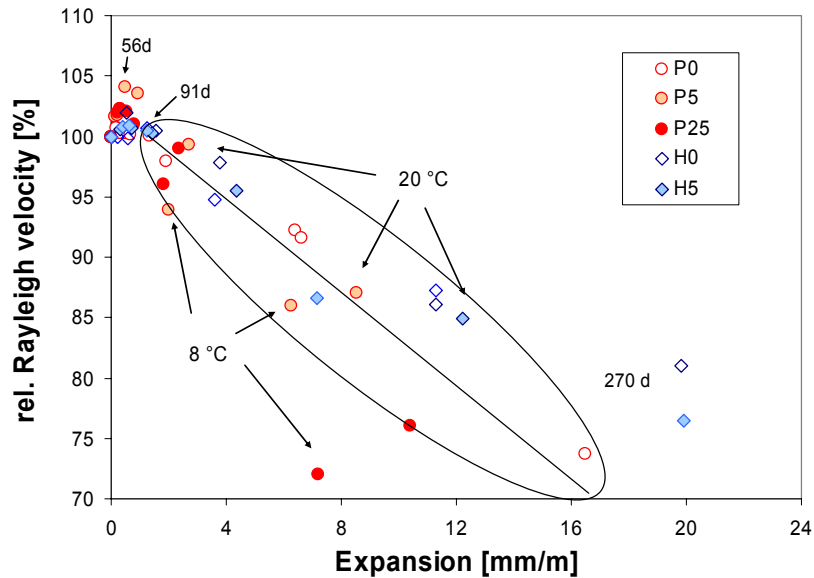


Fig. 6.5: Rayleigh velocity versus expansion of HS and OPC mortar samples immersed in Na_2SO_4 solution ($30\text{g SO}_4^{2-}/\text{l}$) at 8 and 20 °C. The lines are intended as eye guides only.

As sulfate interaction proceeded the density of the surface layer was decreased whereas the expansion of the mortar samples was increased indicating the extended sulfate degradation due to crack formation and disintegration of the sulfate layer, see also Appendix A 5 (Figs. A 5.3-5.8). After 91 days a generally linear dependency between Leaky Rayleigh velocity and expansion of the mortar samples was observed indicating the progress of sulfate interaction with exposure time. Thereby, carbonate containing mortar samples (H5, P5, P25) showed a somewhat higher reduction in the surface densities when stored at low temperatures than the reference mortar samples (H0, P0). These observation indicate that carbonate containing mortar samples stored at low temperatures (8 °C) are characterised by a certain surface softening as observed macroscopically in section 6.1.3 or given in the Appendix A 5 (Figs. A 5.3-5.8).

Generally, this lower surface density of samples stored at low temperatures correlates well with the observed mass loss of these samples (section 6.1.1) due to the formation of thaumasite. The disintegration of the microstructure due to thaumasite formation was confirmed by SEM microscopy as investigated in section 6.1.4.

6.1.3 Visual appearance

The visual inspection of the mortar samples was carried out only for the samples stored in sulfate solution during exposure. The observations are summarised in Table 6.1. Photos of selected samples stored in sulfate solution under different conditions are presented in Fig. 6.6.

The samples stored at high sulfate concentration (III), i.e. $30\text{g SO}_4^{2-}/\text{l}$ showed first signs of deterioration already after 56 days of exposure. The samples stored at low sulfate concentration (II), i.e. $3\text{g SO}_4^{2-}/\text{l}$ did not show any visual signs of sulfate sulfate attack up to 270 days (Fig. 6.6c). Therefore, the observations below concern mainly the samples stored at high sulfate concentration.

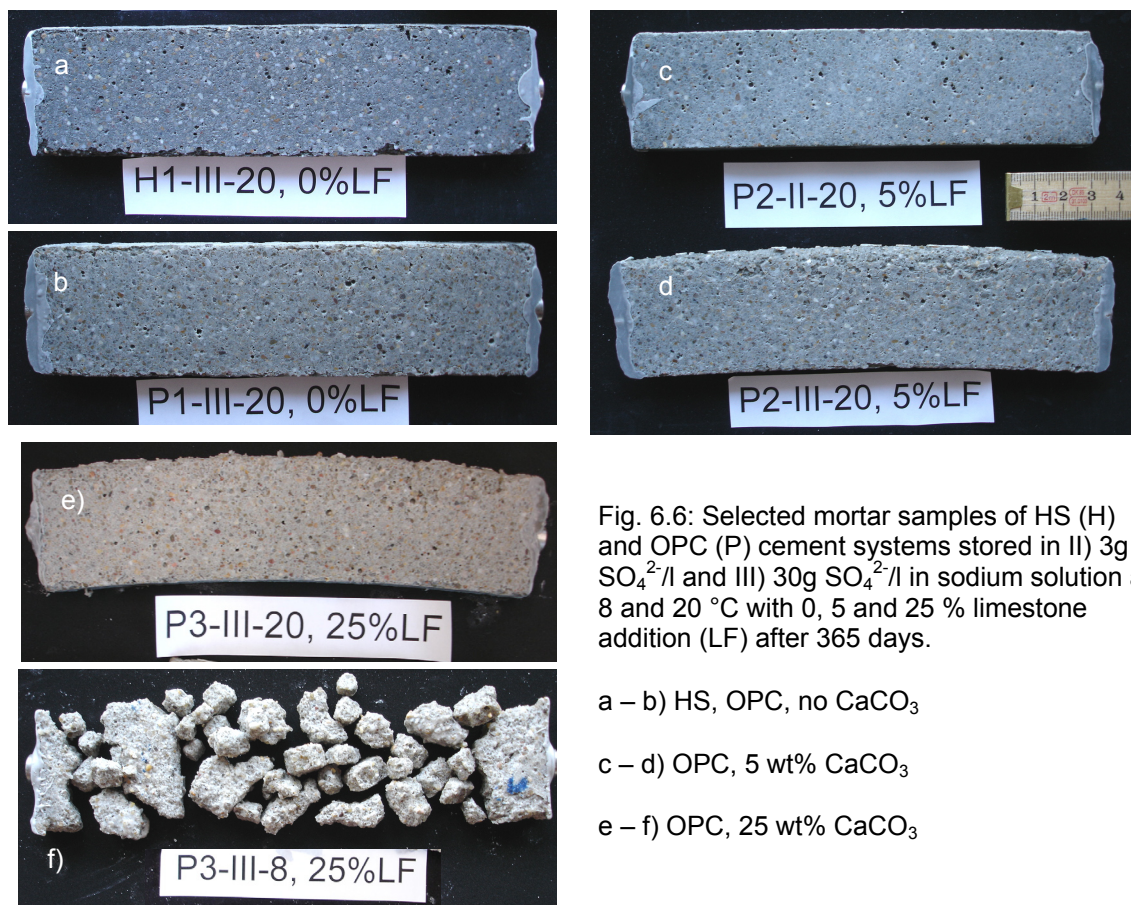


Fig. 6.6: Selected mortar samples of HS (H) and OPC (P) cement systems stored in II) $3\text{g SO}_4^{2-}/\text{l}$ and III) $30\text{g SO}_4^{2-}/\text{l}$ in sodium solution at 8 and 20 °C with 0, 5 and 25 % limestone addition (LF) after 365 days.

a – b) HS, OPC, no CaCO_3

c – d) OPC, 5 wt% CaCO_3

e – f) OPC, 25 wt% CaCO_3

Macroscopically, sulfate deterioration started with spalling and crack formation especially at the edges of the samples (Figs. 6.6 a, b). Sulfate deterioration also led to curvature of the mortar samples (Fig. 6.6 d) indicating imperfections during fabrication of the samples and a non-uniform expansion. A complete catalog of macroscopical observations during sulfate exposure of up to one year is given in Appendix A5 (Figs. A 5.3- 5.8).

The influence of storage temperature was found to be significant for cement systems containing limestone (Figs. 6.6 e, f). It was observed that at 8 °C storage temperatures the mortar samples containing limestone showed a significant softening starting at the sample surface. The damage due to sulfate attack was increased with 25wt% limestone in the cement as shown in (Fig. 6.6f).

Generally, a longer time of sulfate immersion was required for samples containing 5 wt% limestone (H5, P5) until sulfate deterioration was visible.

The two types of cement clinkers used (HS and OPC) did not show any apparent visible difference in the extent of damage of the mortar samples (Figs. 6.6 a, b). In all cases, the deterioration was progressively enhanced starting with crack formation, spalling and finally deformation and finally destruction of the samples. A summary of visual observations is given in Table 6.1.

Table 6.1: Appearance of mortar samples immersed in Na₂SO₄ for up to one year at given temperature and sulfate concentration.

| sample | | sulfate concentration | |
|--------|-----|---|---|
| | | 3 SO ₄ ²⁻ /l | 30 SO ₄ ²⁻ /l |
| 8 °C | H0 | no visible deterioration | microcracks at the edges after 91d |
| | H5 | no visible deterioration | spalling along edges after 180d, softening extensive spalling after 270d |
| | P0 | no visible deterioration | visible cracks along the edges after 91d, signs of curvature after 270 d |
| | P5 | thin coating at the surface | crack formation, spalling along surface after 91d, softening at edges after 270d |
| | P25 | some spalling after 180d, extensive spalling, destruction after 270d | spalling, crack formation after 56d, softening after 180d |
| 20 °C | H0 | no visible deterioration | begin of spalling at the edges after 56d |
| | H5 | no visible deterioration | spalling, crack formation at edges after 180d |
| | P0 | small crack formation along edges after 270d | crack formation, spalling after 91d, signs of curvature after 270d |
| | P5 | thin coating at the surface | visible cracks, small spalling at edges after 180d, sign of curvature after 270d |
| | P25 | crack formation along edges after 270d, spalling at edges | crack formation after 56d, signs of curvature after 91d |

6.1.4 Sulfate uptake and relevant phases

For the characterisation of the mortar samples, SEM and EDS analysis were used to investigate the evolution of the microstructure and the changes in the phase assemblage under sulfate attack.

In the presents study the sulfate uptake was determined by EDS as described in section 3.4 on selected samples according to test conditions after 56 days of sulfate interaction at high sulfate concentration (30g $\text{SO}_4^{2-}/\text{l}$) and field conditions after 270 days at low sulfate concentration (3g $\text{SO}_4^{2-}/\text{l}$) for Portland cement systems with 0, 5 and 25 wt% limestone addition.

The hydrate phases present in the specific regions (core, transition zone and surface region) are indicated qualitatively based on the EDS analysis. The error bars indicate (i) the area (up to 300 μm) covered by the beam during the EDS analysis and (ii) the distribution of the 3 measurements at one specific depth.

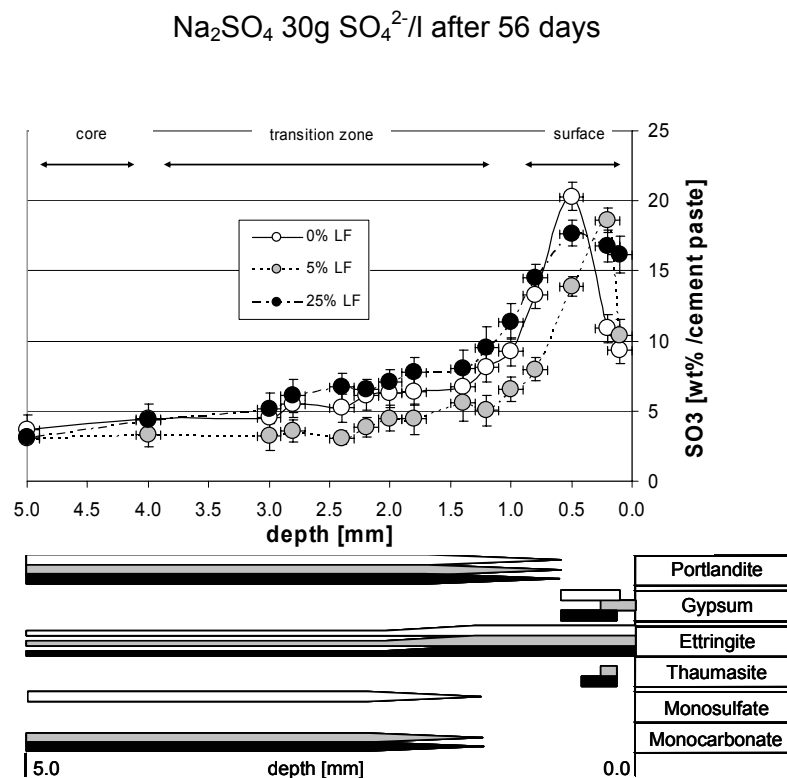


Fig. 6.7: Sulfate profile of mortar samples and phase assemblage (qualitatively) in Portland cement systems containing up to 25 wt% limestone filler.

Sulfate interaction was investigated from the surface towards the core of the mortar samples. The results show that three different zones can be distinguished if mortar was exposed to sulfate solution. These zones are the unaltered core, a sulfate transition zone and the

surface region. Each of these zones was found to be characterised by different phase assemblages and specific microstructural appearance as shown in Fig. 6.9.

At high sulfate concentration in solution the samples with 5 wt% limestone addition showed a sulfate maximum of about 18 wt% SO_3 by weight cement paste which was limited close to the surface (≤ 0.4 mm) indicating dense microstructure. The samples without limestone addition exhibited a sulfate maximum of about 20 wt% SO_3 by weight cement paste which was observed to be at 0.5 mm depth and the sulfate ingress was determined up to 2.5 mm in depth. In case of 25 wt% limestone addition the sulfate uptake led to a distinct sulfate maximum up to 1.0 mm depth and the sulfate ingress was determined up to 3 mm in depth.

The results show that limestone addition of 5 wt% reduced the sulfate uptake in the cross section of the mortar samples compared to the reference sample without limestone, both at low and high sulfate concentration (Figs. 6.7, 6.8).

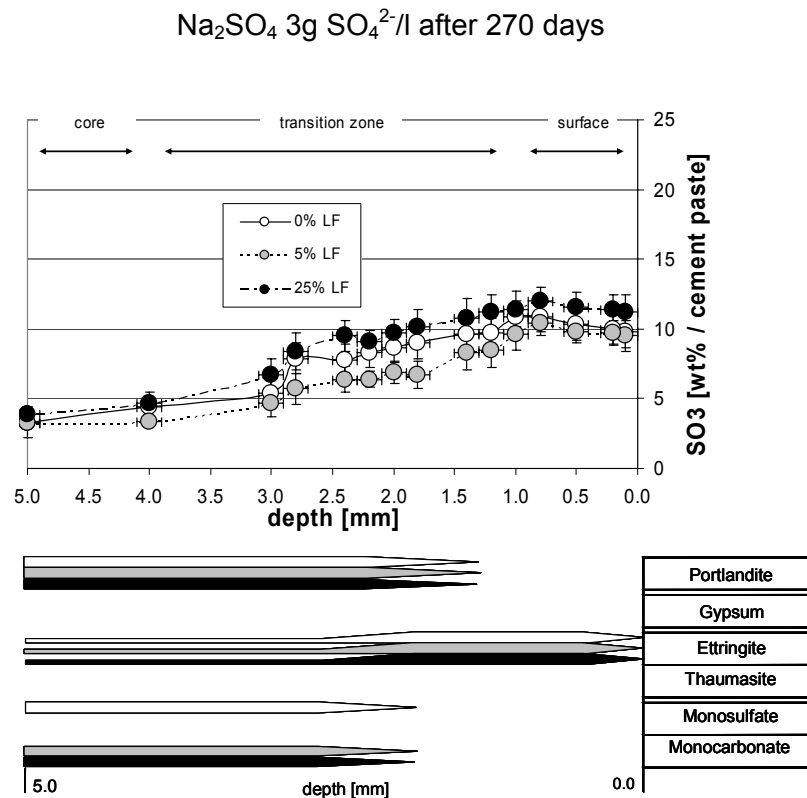


Fig. 6.8: Sulfate profile of mortar samples and phase assemblage (qualitatively) in Portland cement systems containing up to 25 wt% limestone filler.

At low sulfate concentration in solution no distinct sulfate maximum could be determined for the investigated mortar samples (Fig. 6.8). The total sulfate absorption was determined to be higher between 1 – 3 mm depth whereby the samples with 5 wt% limestone showed lower and the samples with 25 wt% limestone showed higher sulfate uptake than the reference without limestone addition. It was observed that after 270 days, portlandite was depleted

within the outer 1.5 mm. Thus, portlandite was reduced to greater depths in the investigated samples than in samples after 56 days (Figs. 6.7, 6.8).

At 56 days in 30g $\text{SO}_4^{2-}/\text{l}$, some indication for the precipitation of thaumasite was found in the carbonate containing cement systems stored at 8 °C (Fig. 6.7). In the whole cross section of the mortar samples, thaumasite could only precipitate in regions with high sulfate contents of $\geq 15 \text{ wt\% SO}_3$ at the sample surface in the presence of gypsum. No indication for the precipitation of thaumasite was found at lower sulfate contents ($\leq 10 \text{ wt\% SO}_3$) by weight cement paste (greater depths), at low sulfate concentration in solution and in samples without limestone addition.

6.1.5 Microstructure and microanalysis

The sequence of changes observed in the microstructure of the different mortar samples was generally similar. This was exemplified for a Portland cement mortar without limestone addition (see below and Fig. 6.9). The microstructure of the other samples is reported in the Appendix A 6 (Figs. A 6.3 and 6.4).

The microstructure of the **unaltered core** (4.0 – 5.0 mm depth from surface) did not show any signs of damage due to sulfate attack. The core region was characterised by a dense and compact microstructure and a good bonding between cement paste and aggregates. Occasional cracks as shown in Fig. 6.9 a might have originated from sample preparation.

The sulfate **transition zone** (1.0 – 3.0 mm depth from surface) showed first signs of changes in the microstructure of the cement paste. In this zone, first signs of transformation reactions were observed indicating increasing sulfate contents (Fig. 6.9 b). The zone appeared to be less compact with visually darker areas in the cement paste indicating some reduction of Ca. The depth of this zone was found to dependent on the permeability or in other words the density of the cement system as shown in the sulfate uptake (Figs. 6.7, 6.8).

In the **surface region** (0 – 1.0 mm depth from surface) of samples, the microstructure was characterised by crack formation forming between or around aggregates. The cracks were either parallel or perpendicular to the sample surface. The mortar samples with 5 wt% limestone addition (H5, P5) showed the smallest crack depths ($\leq 0.5 \text{ mm}$) whereas the samples with 25 wt% limestone addition (P25) showed significantly deeper cracks of up to 1.0 mm during sulfate exposure. The reference samples without limestone addition (H0, P0) showed cracks depths between 0.5 and 0.8 mm. The sulfate concentration in solution also influenced the crack width; widths up to 10 μm were observed at 30g $\text{SO}_4^{2-}/\text{l}$ already after 56 days and widths up to 4 μm were observed at 3g $\text{SO}_4^{2-}/\text{l}$ after 270 days. The surface

region appeared to be strongly influenced by leaching of Ca and disintegration of the microstructure due to sulfate transformation reactions (Fig. 6.9c).

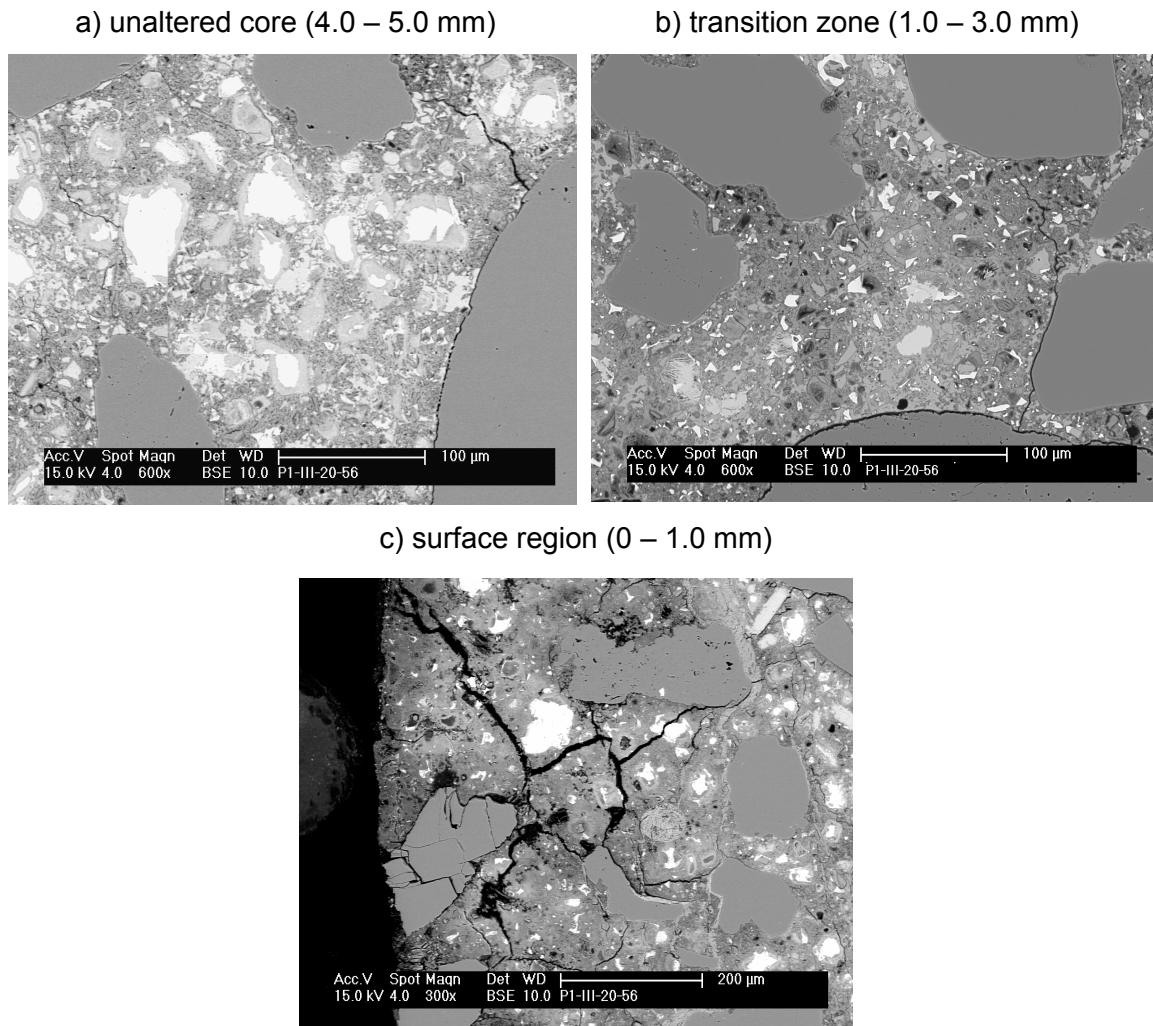


Figure 6.9: Typical microstructure of specific regions in mortar samples immersed in Na_2SO_4 solution as shown for a Portland cement mortar without limestone addition.

A more detailed analysis of the microstructure of selected experiments with element ratios S/Ca, Al/Ca and Si/Ca was carried out by EDS as described in Chapter 3, section 3.4. The stoichiometric composition of the pure phases was used to evaluate the phase assemblages. For the analyses specific regions of the core, the transition zone and the surface region were investigated. Further data are also provided in Appendix A 5 (Figs. 5.9 – 5.13).

- **P0 at 30g SO₄²⁻/l after 56 days (8 °C)**

The results from the microanalysis of the OPC mortar without limestone addition showed that in the core of the sample (5 mm depth), beside portlandite also monosulfate was found to be present as AFm phase (Fig. 6.10c). Ettringite was identified in minor amounts intermixed within the C-S-H phase.

In the transition zone at 1.5 mm depth, increasing amounts of ettringite were detected indicating the progress of sulfate attack into the mortar sample. That indicates that more and more monosulfate was transformed into ettringite. The phase analysis further showed that portlandite was still present in the transition zone after 56 days of sulfate interaction.

In the surface area at 0.5mm depth, the analysis showed that gypsum was present and accompanied by the depletion of portlandite. Gypsum was detected to be partly intermixed within the C-S-H phase. In the surface region no indication for thaumasite was found for the mortar without limestone addition (Fig. 6.10a).

The analysis of C-S-H phase showed that part of the Ca was reduced in the surface region indicating leaching effects and the consumption of portlandite due to the formation of secondary sulfate phases (Fig. 6.11a).

- **P25 at 30g SO₄²⁻/l after 56 days (8 °C)**

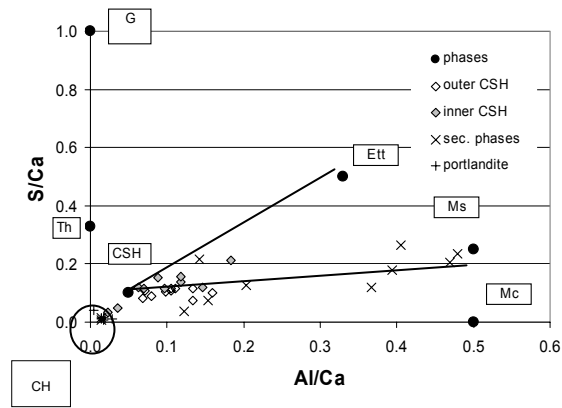
The microanalysis of the mortar sample containing 25 wt% limestone showed that in carbonate containing cement systems, monocarbonate was present in the core region as stable AFm phase beside portlandite, traces of ettringite and C-S-H (Fig. 6.10c).

The analysis further showed that in the transition zone at 1.5 mm depth, more ettringite was detected indicating sulfate uptake and thus, the formation of secondary ettringite from monocarbonate, consuming sulfate and calcium. Portlandite was still detectable, not being completely leached or consumed by the transformation from monocarbonate into ettringite (Fig. 6.10b).

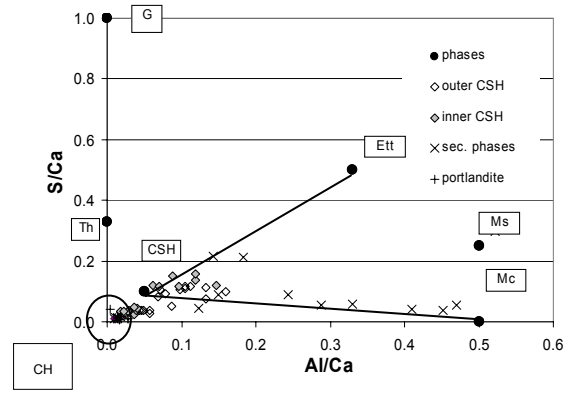
The maximum ettringite formation was present in the surface region partly intermixed with the C-S-H phase. At 0.5 mm depth from the surface no portlandite was found, whereas the maximum gypsum content was detected. Beside that, some indication for the presence of thaumasite was found. At that stage of deterioration (56 days), thaumasite possibly first precipitated together with gypsum intermixed in the C-S-H phase as indicated by SEM microscopy and EDS (Figs. 6.10a, 6.17).

P0 without CaCO_3 P25 with CaCO_3

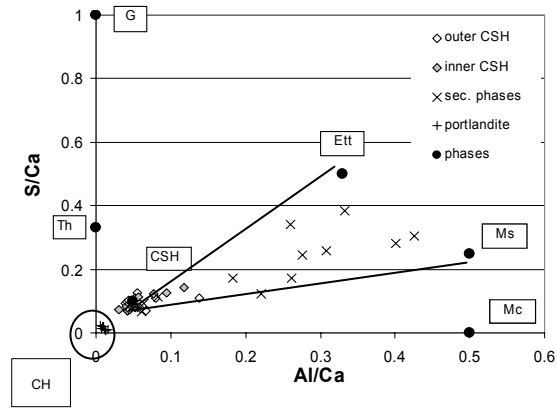
a) unaltered core (5 mm)



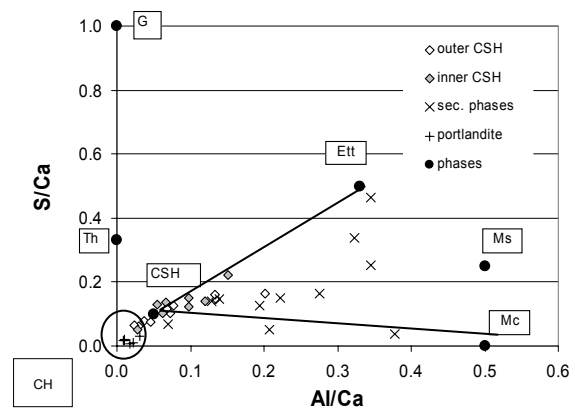
d) unaltered core (5 mm)



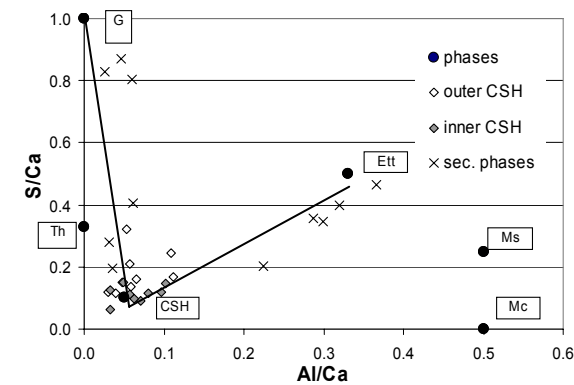
b) transition zone (1.5 mm)



e) transition zone (1.5 mm)



c) surface region (0.5 mm)



f) surface region (0.5 mm)

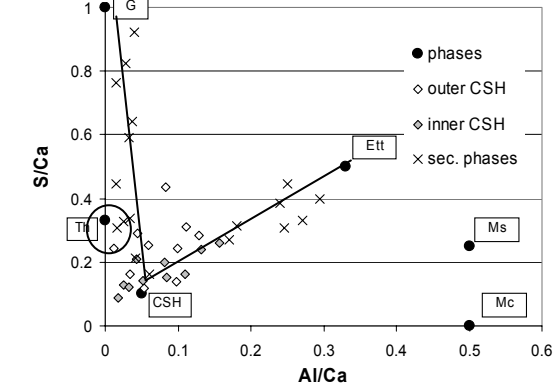


Figure 6.10: Phase assemblages of a Portland cement mortar a-c) without limestone addition and d-f) with 25 wt% limestone addition after 56 days in Na_2SO_4 solution ($30\text{g SO}_4^{2-}/\text{l}$) at 8°C . CH = portlandite; Ett = ettringite; G = gypsum; Mc = monocarbonate; Ms = monosulfate; Th = thaumasite

The analysis of the C-S-H phase showed the depletion of Ca towards the sample surface. This observation seems to indicate the consumption of Ca due to the formation secondary sulfate phases (gypsum, ettringite) and the depletion of Ca due to leaching (Fig. 6.11 b).

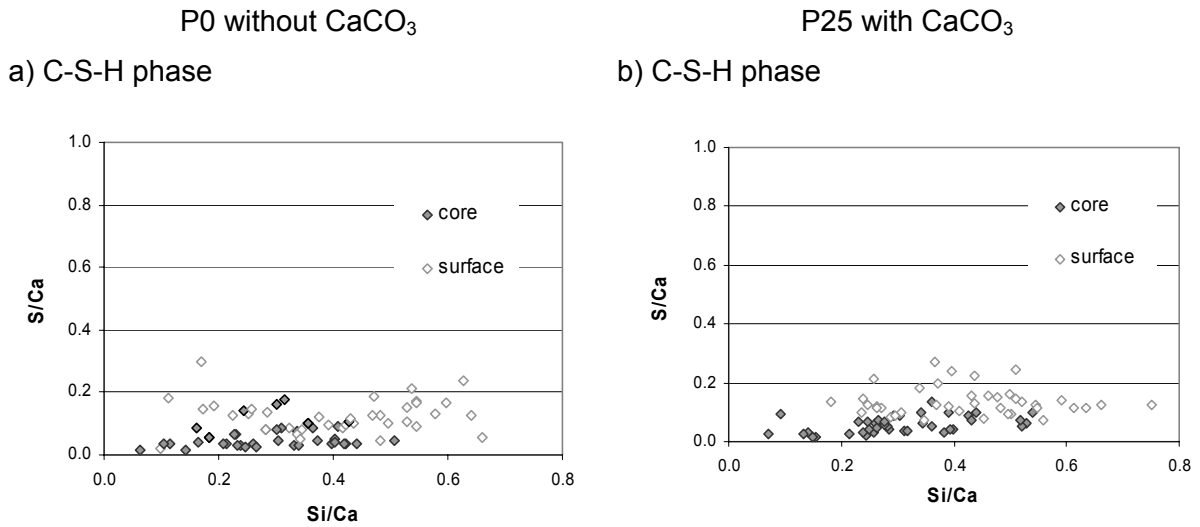


Figure 6.11: Analysis of the C-S-H phase of Portland cement mortars a) without limestone addition and b) with 25 wt% limestone addition after 56 days sulfate exposure (30g $\text{SO}_4^{2-}/\text{l}$) at 8 °C

- **P0 at 3g $\text{SO}_4^{2-}/\text{l}$ after 270 days (20 °C)**

The microanalyses of the mortar sample without limestone addition immersed for 270 days at 3g $\text{SO}_4^{2-}/\text{l}$ in solution are shown in Fig. 6.12. The results show that the core region remained unchanged with monosulfate as the stable AFm phase and portlandite as well as minor amounts of ettringite present. The latter was partly intermixed in the C-S-H phase.

In the transition zone at 1.5 mm depth, somewhat more ettringite than monosulfate was detected indicating the progress of sulfate interaction with time. No portlandite could be detected in this area. It was completely consumed either by phase transformation or by being leached as sulfate exposure proceeded.

In the surface region slightly less ettringite was determined from EDS than in the transition zone. It indicates that ettringite tends to get leached with ongoing sulfate interaction (270 days) in the surface regions. In contrast to the samples immersed at 30g $\text{SO}_4^{2-}/\text{l}$ at low sulfate concentration no gypsum was found in the surface area. The absence of portlandite in the surface area at low sulfate concentration was caused by the formation of ettringite as well as leaching.

At 270 days the analysis of the C-S-H phase showed the influence of leaching between the core and the surface region. The results show that the C-S-H in the surface region was somewhat more affected by leaching after 270 days than after 56 days (Figs. 6.11, 6.12).

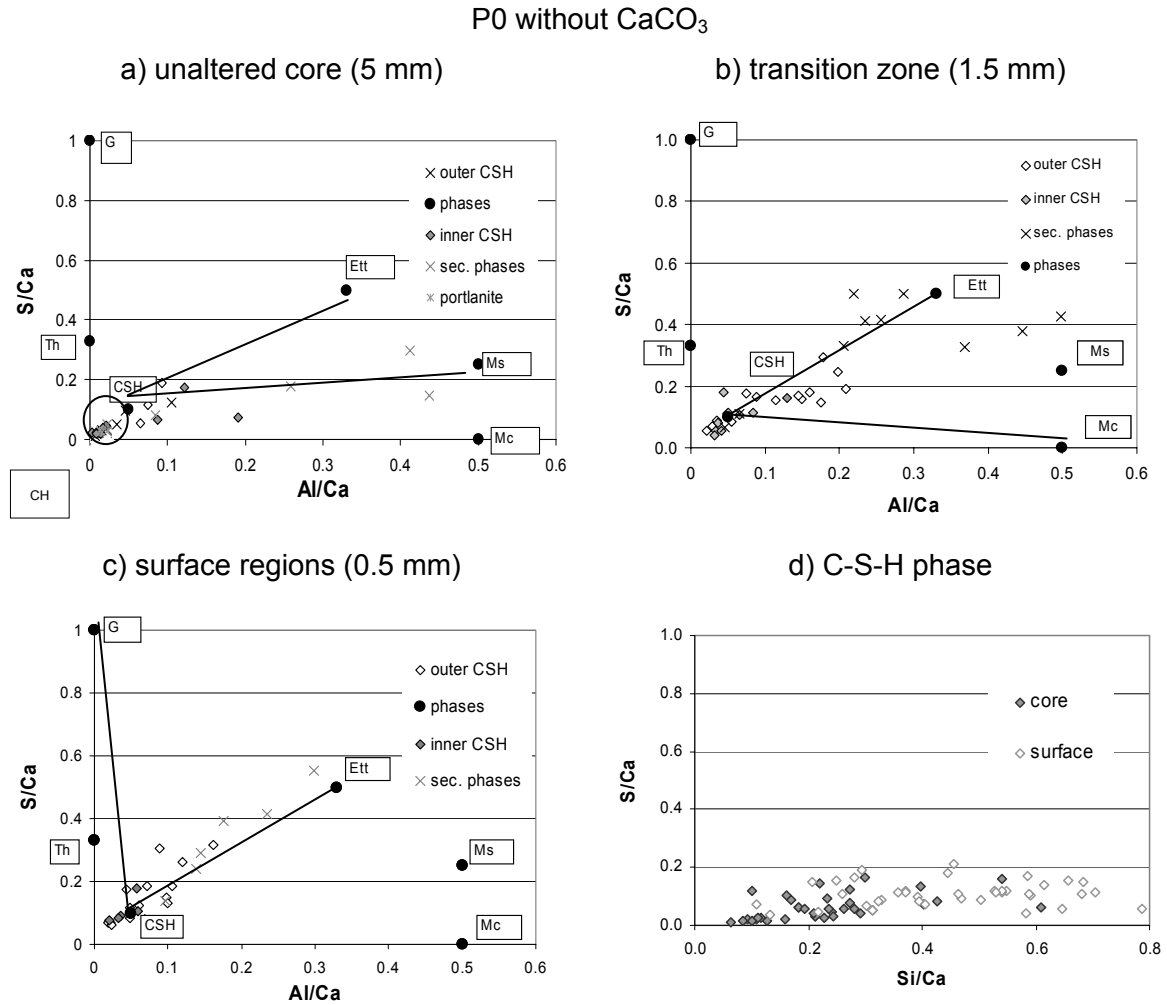


Fig. 6.12: Phase assemblages of a Portland cement mortar without limestone addition after 270 days of sulfate exposure ($3\text{g SO}_4^{2-}/\text{l}$) at 20°C . CH = portlandite; Ett = ettringite; G = gypsum; Mc = monocarbonate; Ms = monosulfate; Th = thaumasite

• Ettringite formation

Secondary ettringite formation was observed in the regions of increased sulfate concentration in the cement paste ($5 - 10\text{ wt\% SO}_3$) which corresponds to the conditions in the transition zone. In this region, secondary ettringite was observed to precipitate close to the cement grain particles intermixed with the C-S-H phase (Fig 6.13). This ettringite, intermixed with the C-S-H phase in the sulfate enriched cement paste of the transition zone (1.2 mm depth) might be expansive as indicated by the small cracks forming in the matrix of the microstructure.

At higher sulfate contents in the cement paste ($10 - 20\text{ wt\% SO}_3$), i.e. at the surface region of the mortar samples, secondary ettringite was increasingly observed filling voids, cracks or space around aggregates (Fig. 6.14). Although, the ettringite formation was extensive in the surface region at about 0.5 mm in depth, the observed ettringite formation might be less

expansive when filling space, voids or already existing cracks during sulfate exposure. The observed ettringite formation at high sulfate contents might expand already existing cracks and thus accelerate sulfate interaction.

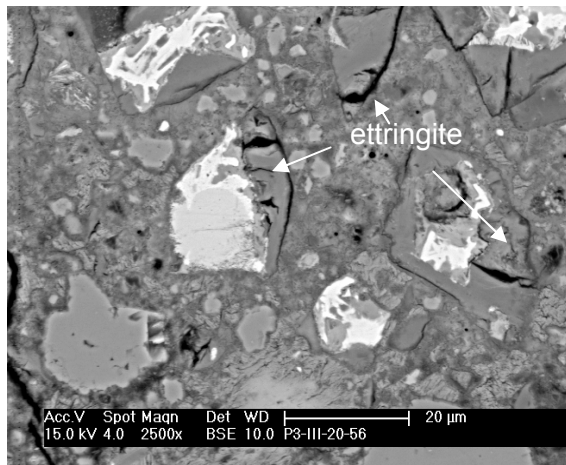


Fig. 6.13: Ettringite formation close to cement clinker grains in P25 mortar after 56 days in 30g $\text{SO}_4^{2-}/\text{l}$ at 1.2 mm depth.

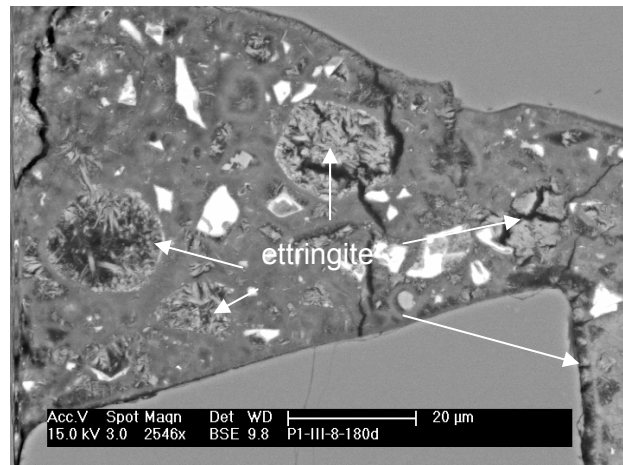
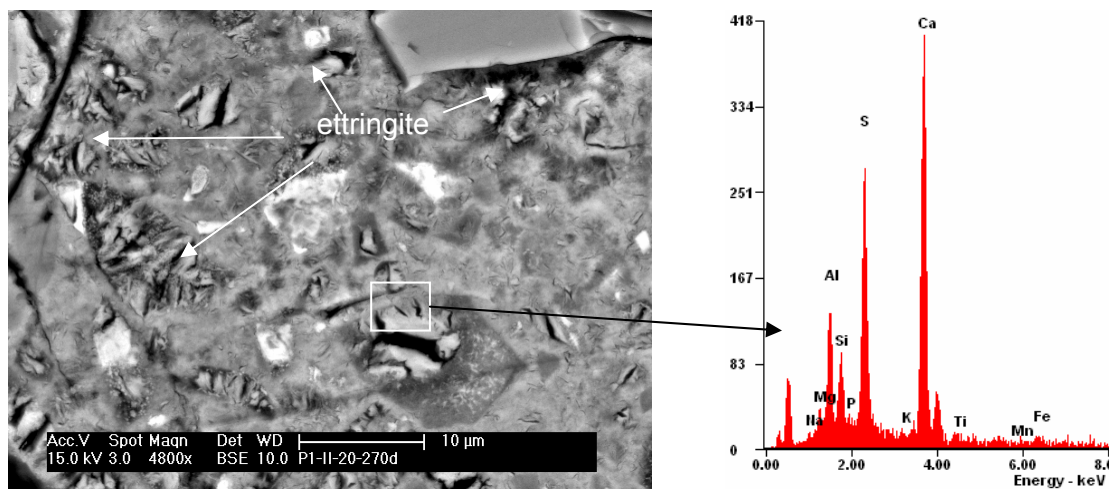


Fig. 6.14: Ettringite formation in pores, voids and cracks in P0 mortar after 180 days in 30g $\text{SO}_4^{2-}/\text{l}$ at 0.5 mm depth.

Substantial depots of secondary ettringite were also observed in the surface region at 0.8 mm depth (10 wt% SO_3) for samples immersed in 3g $\text{SO}_4^{2-}/\text{l}$ after 270 days (Fig. 6.15). The ettringite found intermixed in the C-S-H phase or close to cement clinker grains might be expansive as indicated by the observed cracks observed and the expansion measured as described in section 6.1.1.



6.15: Ettringite formation intermixed in the C-S-H phase and close to former cement clinker grains in P0 mortar after 270 days in 3g $\text{SO}_4^{2-}/\text{l}$ at 20 °C in 0.8 mm depth.

Beside that, some indication of secondary ettringite formation from the C_4AF phase in HS cement systems (low C_3A) was observed at sulfate contents between 10 – 15 wt% SO_3 (Fig.

6.15). Although substantial depots of secondary ettringite were observed in that context in the cement paste, no indication of expansion and crack formation was found in the matrix, see Appendix A 6 (Figs. A 6.5 – 6.6).

• Gypsum formation

Gypsum was observed to precipitate in bands parallel to the surface, around aggregates or pores (Figs. 6.16a, c). In the sections, gypsum was detected on the surface of the samples, in regions where the maximum ettringite formation was observed. Gypsum was present in the areas where high amounts of SO_3 (15-20 wt%) were found and only in samples stored at high sulfate concentration in solution ($30\text{g SO}_4^{2-}/\text{l}$).

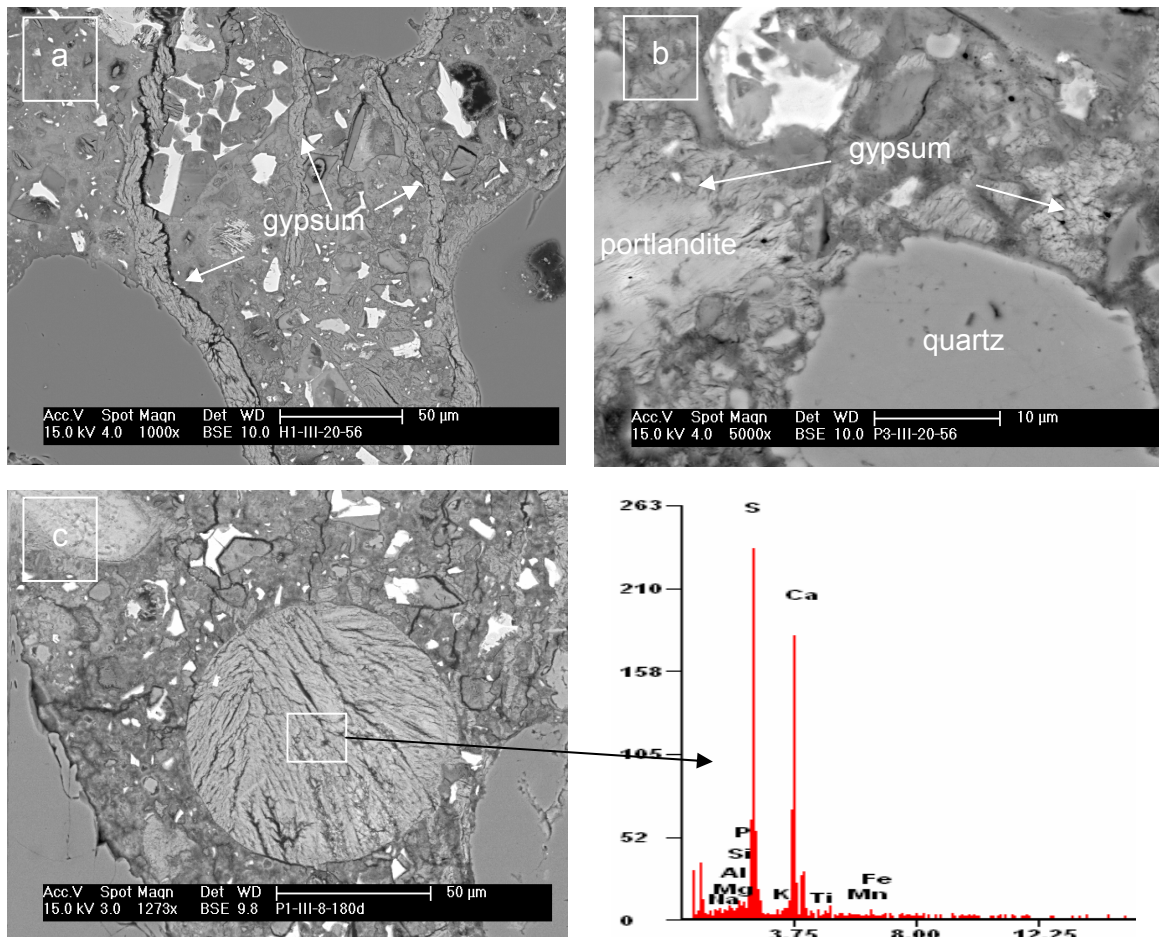


Fig. 6.16: Gypsum formation in a) H0 mortar as surface parallel bands, b) P25 mortar from portlandite in C-S-H both 56 days and c) P0 mortar filling air pore after 180 days.

The formation of gypsum with increasing sulfate contents in the mortar samples was also observed at regions where portlandite is present (Fig. 6.16b). Gypsum also formed intermixed within the C-S-H phase.

The microstructural investigations further showed that massive gypsum formation e.g. in pores led to the formation of some radial cracks indicating that some stress was generated especially at later ages (Fig. 6.16c) during sulfate exposure.

At low sulfate concentrations in solution ($3\text{g SO}_4^{2-}/\text{l}$), no gypsum could be detected in the investigated mortar samples.

• Thaumasite formation

After 56 days of sulfate interaction first indications for the precipitation of thaumasite were found in the regions where high amounts of SO_3 (15 – 20 wt%) were present. At that time rather small amounts of thaumasite were formed intermixed with gypsum, ettringite, calcite and the C-S-H phase in mortar samples stored at 8°C (Fig. 6.17).

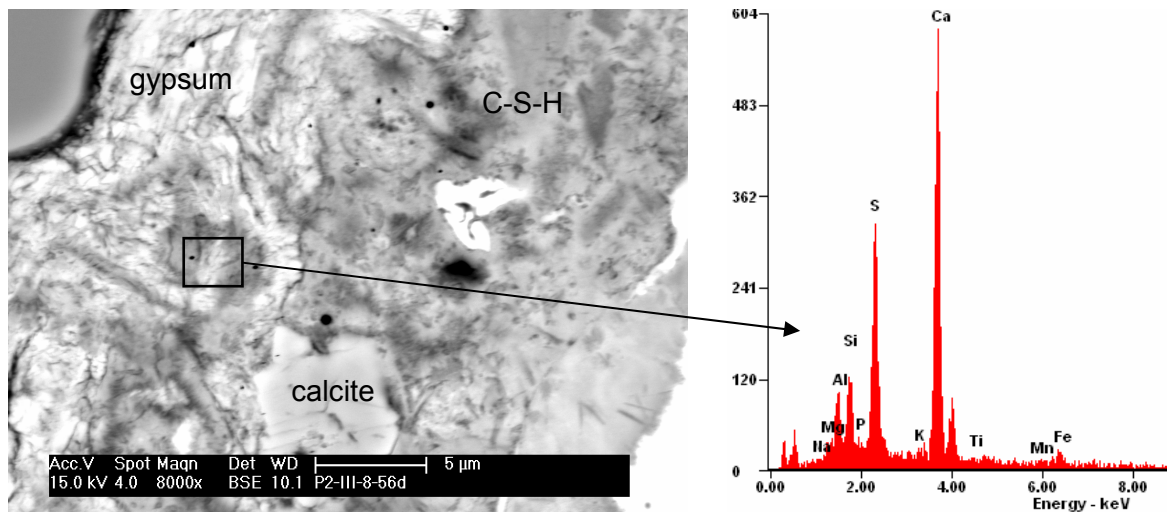


Fig. 6.17: Microstructure of the surface region of an OPC cement with 5 wt% limestone addition after 56 days stored in $30\text{g SO}_4^{2-}/\text{l}$ at 8°C and EDS spectra of ettringite enriched area and first precipitation of thaumasite.

After 180 days of sulfate interaction, the selected mortar samples showed clear signs of thaumasite formation. It was found that the microstructure of carbonate containing mortar samples (H5, P5, P25) was characterised by the formation of a fine, needlelike compound forming within the C-S-H phase (Figs. 6.18a, b). These observations were made in the surface regions of the samples.

The microstructure of the samples was found to be already damaged from previous sulfate deterioration, i.e. ettringite formation as indicated by the crack formation and mentioned earlier (Fig. 6.18a).

The microanalysis of these structures revealed mainly Ca, S and Si to be present beside some minor amounts of Al. The latter, Al was found especially in regions close to former clinker grains.

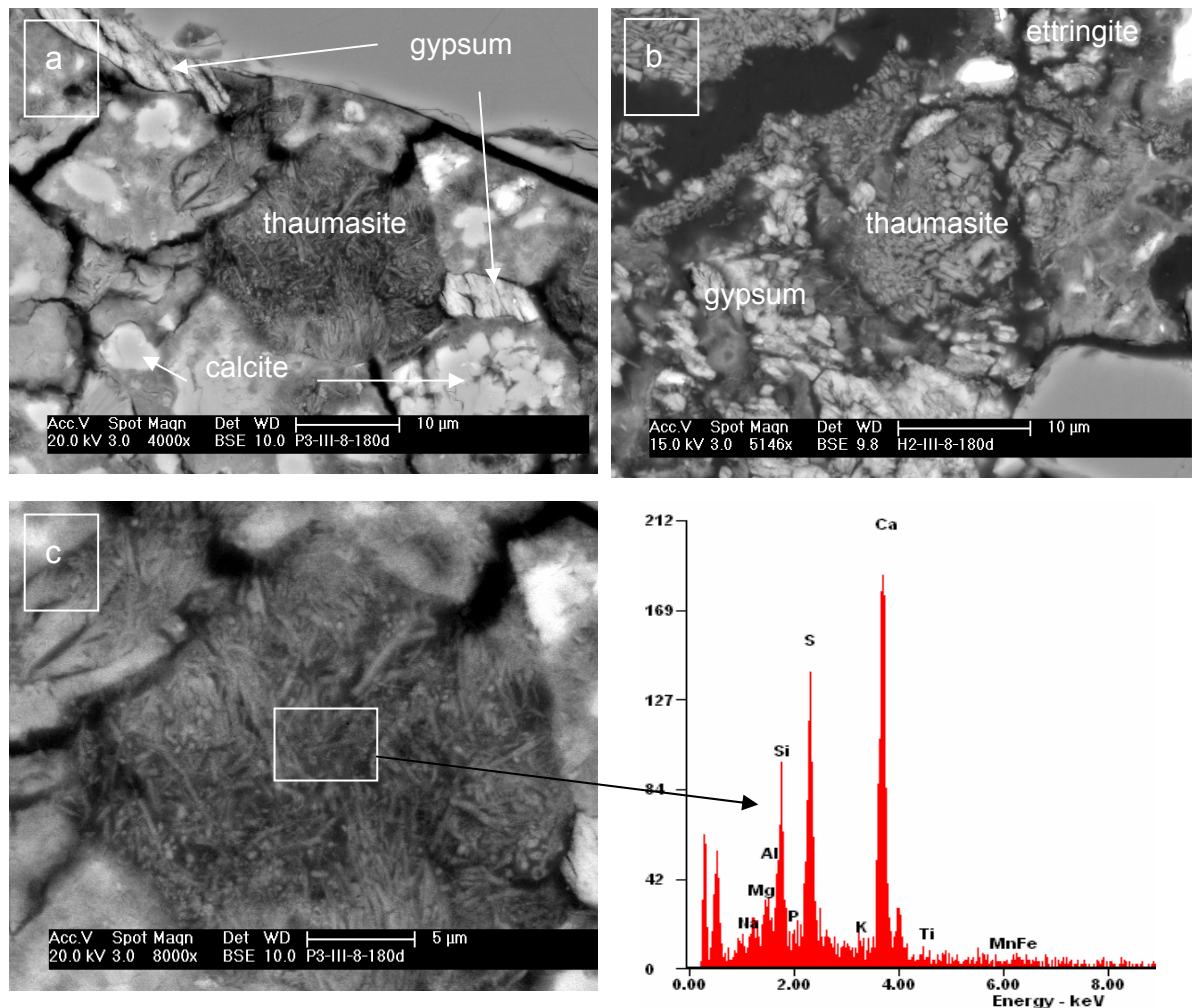


Fig. 6.18: Microstructure of the surface region of a) OPC and b) HS cements with limestone addition after 180 days stored in $30\text{g SO}_4^{2-}/\text{l}$ at 8°C and EDS spectra of thaumasite enriched areas.

It was found that the fine, needle-like structures indicating enrichments of thaumasite preferentially formed within the C-S-H with gypsum depots present (Fig. 6.18a, b). Beside that, parts of the microstructure indicate preferred regions of ettringite formation close to clinker grains (Fig. 6.18b).

Generally, the observed transformation of the C-S-H phase corresponded to a complete loss of cohesion of the cement paste and a structural breakdown of the mortar samples beginning at the surface of the samples as mentioned in section 6.1.3.

The overview of the hydrate phases of the investigated mortar samples of OPC and HS cement systems (Table 6.2) showed that with increasing sulfate content towards the sample surface, the AFm phases (monosulfate, monocarbonate) are transformed into ettringite. At 270 days, these reactions were observed to occur at greater depths in the mortar samples stored in sulfate solution with low sulfate concentration than in mortar samples stored in high sulfate solution after 56 days. At that age, ettringite was still present in the surface regions. At high sulfate concentration in solution, gypsum was detected to be present in all mortar samples between 10 – 20 wt% SO₃ by weight cement paste (surface region) whereas accordingly portlandite was absent from these regions. Gypsum did not precipitate in the mortar samples stored at low sulfate concentration.

Table 6.2: Summary of investigated mortar samples immersed in Na₂SO₄ solution at given temperature and sulfate concentration; C-S-H and calcite assumed to be present in all samples.

| 30g SO ₄ ²⁻ /l after 56 days | | | |
|--|--------|---------------------------------------|---|
| | sample | affected surface | unaltered core |
| 8 °C | (H5) | gypsum, ettringite, <i>thaumasite</i> | portlandite, monocarbonate, <i>ettringite</i> |
| | P0 | gypsum, ettringite | portlandite, monosulfate, <i>ettringite</i> |
| | (P5) | gypsum, ettringite, <i>thaumasite</i> | portlandite, monocarbonate, <i>ettringite</i> |
| | P25 | gypsum, ettringite, <i>thaumasite</i> | portlandite, monocarbonate, <i>ettringite</i> |
| 20 °C | (H0) | gypsum, ettringite | portlandite, monosulfate, <i>ettringite</i> |
| | (P0) | gypsum, ettringite | portlandite, monosulfate, <i>ettringite</i> |
| | (P25) | gypsum, ettringite, <i>thaumasite</i> | portlandite, monocarbonate, <i>ettringite</i> |
| 3g SO ₄ ²⁻ /l after 270 days | | | |
| 20 °C | P0 | ettringite | portlandite, monosulfate, <i>ettringite</i> |
| | (P5) | ettringite | portlandite, monocarbonate, <i>ettringite</i> |
| | (P25) | ettringite | portlandite, monocarbonate, <i>ettringite</i> |

italic = small amounts

() = results refer to Appendix A 5 (Figs. A 5.9 – 5.13)

6.2 Discussion

The results presented here, indicate that sulfate attack on Portland cement mortars is a progressive phenomena starting at the surface of the samples. This agrees with the observations of Taylor and Gollop [1]. Based on the results presented here, physical, chemical and microstructural aspects play an important role.

- **Physical aspects**

The observed increase of the surface velocity of the Leaky Rayleigh wave can be explained by the densification of the microstructure. The densification is caused by the formation of secondary sulfate phases like gypsum and ettringite. With ongoing sulfate exposure the extended influence of secondary sulfate phases, e.g. thaumasite, cracks and leaching, leads to microstructural disintegration and reduces ultrasound surface velocity as discussed in detail by Neuenschwander et al. [2].

The results showed that in the beginning of sulfate attack the uptake of sulfate results mainly in the filling of pores and voids and the increase in mass and length were almost linear. Later during sulfate attack, when all available space was filled by the formation of sulfate phases expansion became more pronounced whereas the mass gain was slowed down.

The monitoring techniques of length, mass change and ultrasound showed that limestone addition of 5 wt% by weight cement with high and low C_3A content, physically improved the resistance against sulfate attack at ambient temperatures (20 °C). However, at low temperatures (8 °C), limestone addition of 5 wt% was disadvantageous and sulfate attack was characterised by a certain softening of the samples surface. These findings agree with the investigation of Irassar et al. [3] and Higgins [4]. High amounts of limestone addition of 25 wt% led to accelerated deterioration during sulfate interaction independent of storage temperature and sulfate concentration in solution.

The intensity of sulfate deterioration processes depended on the initial porosity of the mortar samples. Cement systems with 5 wt% limestone addition had a lower capillary and total porosity. Thus the sulfate uptake was somewhat lower and reduced to the topmost layer of the mortar samples. These findings are supported by the findings from Stark and Wicht [5] and Kalinowski and Trägårdh [6], who found that about 5 wt% limestone addition led to a decreased permeability of the investigated cement systems.

In the case of 25 wt% limestone addition, the higher capillary porosity led to a higher sulfate uptake. Higher amounts of limestone addition (≥ 25 wt%) in cement systems led to higher permeability at equivalent water/cement ratios. These findings agree with the investigations of Irassar et al [3] and Torres et al [7].

- **Chemical aspects**

The investigations on the chemical influence of limestone addition during sulfate interaction in samples with limestone addition showed the conversion of monocarbonate into ettringite. Cement systems without limestone addition showed the conversion of the monosulfate present into ettringite.

The results further showed that chemical composition of the clinker e.g. low C_3A content in the cement systems, did not necessarily protect the mortars from sulfate deterioration. In the present study, HS (low C_3A) and OPC (high C_3A) cement systems partly showed an accelerated sulfate degradation especially at high sulfate concentration. Thus, as also observed by Monteiro et al. [8], the initial porosity (permeability) of the cement system seemed to have a major impact on the failure of the samples during sulfate attack.

The sulfate concentration in solution was found to significantly influence the performance of the mortars during sulfate attack, independently from the type of cement clinker (low and high C_3A) used. At high sulfate concentration ($30\text{g SO}_4^{2-}/\text{l}$), the deterioration processes were found to be accelerated and gypsum is formed. The Wittekindt test [9] conditions, used here do not represent real situations of sulfate exposure under field conditions, where lower sulfate concentrations are present, Maltais et al. [10]. At low sulfate concentration ($3\text{g SO}_4^{2-}/\text{l}$), the deterioration processes were somewhat slower and no gypsum formation was detected. These observations agreed with the investigations from Marchand et al. [11], who reported that at low sulfate concentration gypsum is rarely observed.

- **Microstructure**

At the beginning of sulfate interaction, ettringite precipitated mainly intermixed within the C-S-H phase or close to cement grain particles. The observed precipitation of secondary ettringite might have been the cause for the initial expansion due to the confinement in the microstructure leading to first crack formation as noted by Gollop and Taylor [12].

Later during sulfate interaction, ettringite formation reached the maximum near the surface region. The ettringite crystals forming in cracks or voids do not necessarily generate these cracks as reported by Kollmann et al [13-15] but can lead to a widening of already existing cracks and consequently accelerate sulfate attack. These observations agree with the findings of Bonen and Cohen. [16] and Irassar et al. [3]. However, ettringite started to be dissolved towards the sample surface, where lower pH values are present. This observation agrees with the findings of Damidot and Irassar [17] and Metha [18].

The results also indicate secondary ettringite can also be formed from C_4AF . However the C_4AF dissolves slowly and hardly any crack formation was observed in that region. These findings agree with the investigations of Stark and Wicht [19], Gollop and Taylor [1].

The precipitation of gypsum was only detected at sulfate contents of 15 – 20 wt% SO_3 by weight cement paste in the mortar samples stored at high sulfate concentration in solutions. According to Juel et al. [20] it can be assumed that gypsum precipitates in the cement paste only if all available aluminium present was consumed by the formation of ettringite. Gypsum formation was preferentially observed in the surface regions of the mortar samples. As gypsum was found to form intermixed within the C-S-H phase or in already existing cracks it can possibly expand already existing cracks and thus lead to an acceleration of sulfate interaction. These observations agree with the findings reported by Irassar et al. [3] and Santhanam et al. [21]. Gypsum formation has been reported to decalcify the C-S-H phase [18] which could later form reactive silica and thus support thaumasite formation [22].

Thaumasite formation was found to be generally possible in both cement systems with high and low C_3A contents as long as they contain a source of carbonate. This agrees with the investigations of Brown and Hooton [23] and Macphee and Diamond [24]. This was in contrast to the observations of Nobst and Stark [25], who found that low C_3A contents increased the amount of thaumasite formed since less sulfate is needed to form ettringite from the available aluminium.

Already after 56 days of sulfate interaction at 30g SO_4^{2-}/l the precipitation of rather small amounts of thaumasite was observed in the mortar samples stored at high sulfate concentration in solution. In all cases the precipitation of thaumasite was observed to be enhanced at low temperatures (8 °C) which agrees to the results by Bensted et al. [26].

Thaumasite was found to precipitate only in the surface near regions at high sulfate contents in the cement paste mostly accompanied by gypsum.

Thaumasite formation was found to occur directly from C-S-H reacting with carbonate and sulfate as described by Bensted [27] and Crammond [28]. No indication for thaumasite formation was present in samples stored at low sulfate concentration after 270 days of sulfate interaction. These findings indicate that at low sulfate concentration the formation of thaumasite must be even slower as shown by the investigations of Mulenga et al. [29], who found thaumasite at low sulfate concentration after about 5 years.

6.3 Summary and conclusions

The immersion technique using low frequency (1 MHz) and ultrasonic surface waves was successfully applied for the investigation of degradation processes on mortar samples. The measured Leaky Rayleigh wave velocity indicates surface specific changes which can be related to the formation of secondary sulfate phases and the subsequent disintegration of the cement paste.

The addition of 5 wt% limestone in Portland cement systems led to a decrease in sulfate uptake during sulfate interaction due to a lower porosity. Thus the sulfate induced deterioration was reduced especially at ambient temperatures. In case of 25 wt% limestone addition the porosity was increased and the sulfate induced deterioration was accelerated.

The experiments showed that during sulfate interaction at sulfate contents ≤ 10 wt% SO_3 in the cement paste, ettringite first formed intermixed within the C-S-H phase from AFm phases or near cement clinker grains causing initial expansion and cracking. At higher sulfate contents of 10 – 15 wt% SO_3 in the cement paste close to the sample surface ettringite formation was observed to form in voids, cracks.

In the presence of carbonate, thaumasite was formed preferentially at low temperatures in the regions where gypsum has been detected near the sample surface leading to a specific softening of the sample surface. Thaumasite was determined within the C-S-H phase in the cement paste reacting with the available carbonate and sulfate. Some expansion but a significant weight loss was observed due to thaumasite formation. At low sulfate concentration in solution no gypsum and thaumasite could be detected after 270 days of exposure.

The experiments indicated that the thaumasite form of sulfate attack (TSA) was not a cause but a consequence of sulfate attack and that the initial sulfate induced destruction of the concrete was caused by ettringite and gypsum.

The type of cement clinker did not necessarily protect from sulfate deterioration. Cement systems with high and low C_3A content showed an accelerated sulfate degradation at high sulfate concentration. The observations exhibited that the initial porosity (permeability) of the cement system influences sulfate resistance more strongly. Beside that, the results showed that the ferroaluminate phase (C_4AF) also participated and secondary ettringite was formed.

6.4 References

1. Taylor, H.F.W. and Gollop, R.S., *Some chemical and microstructural aspects of concrete durability*, in *Mechanisms of chemical degradation of cement-based systems*, K.L. Scrivener and J.F. Young, Editors. 1997, E & FN Spon: London. p. 177-184.
2. Neuenschwander, J., Schmidt, T., Lüthi, T., and Romer, M., *Leaky Rayleigh wave diagnostics of mortar*. EMPA, Material Science and Technology, 2005. 1.
3. Irassar, E.F., Bonavetti, V.L., and Gonzalez, M., *Microstructural study of sulfate attack on ordinary and limestone Portland cements at ambient temperature*. Cement Concrete Research, 2003. (33), 31-41.
4. Higgins, D.D., *Increased sulfate resistance of ggbs concrete in the presence of carbonate*. Cement Concrete Composites, 2003. 25 (8), 913-919.
5. Stark, J. and Wicht, B., *Zement und Kalk (Portlandzementklinker)*. 2000.
6. M. Kalinowski and Trägårdh, J., *Thaumasite and Gypsum formation in SCC with sulfate resistant cement exposed to a moderate sulfate concentration*. Second North American Conference on the Design and Use of Self-Consolidating Concrete, 2005. Section 3 (durability), 319-325.
7. Torres, S.M., Sharp, J.H., Swamy, R.N., Lynsdale, C.J., and Huntley, S.A., *Long term durability of Portland-limestone cement mortars exposed to magnesium sulfate attack*. Cement Concrete Composites, 2003. 25 (8), 947-954.
8. Monteiro, P.J. and Kurtis, K.E., *Time to failure for concrete exposed to severe sulfate attack*. Cement Concrete Research, 2003. 33 (7), 987-993.
9. Wittekindt, W., *Sulfatbeständige Zemente und ihre Prüfung*. Zement-Kalk-Gips, 1960. 12.
10. Maltais, Y., Samson, E., and Marchand, J., *Predicting the durability of Portland cement systems in aggressive environments-laboratory validation*. Cement Concrete Research, 2004.
11. Marchand, J., Samson, E., Maltais, Y., and Beaudoin, J.J., *Theoretical analysis of the effect of weak sodium sulfate solutions on the durability of concrete*. Cement Concrete Composites, 2002. 24 (3-4), 317-329.
12. Gollop R. and Taylor H.F.W., *Microstructural and Microanalytical Studies of Sulfate Attack, I. Ordinary Portland Cement Paste*. Cement Concrete Research, 1992. 22, 1027-1038.
13. Kollmann, H., *Untersuchungen über Ausblühungs- und Treiberscheinungen durch Sulfate, Teil 2*. Betonwerk und Fertigteil-Technik, 1979. (11), 671-677.
14. Kollmann, H., *Untersuchungen über das Ausblühungs- und Treiberscheinungen durch Sulfate, Teil 3*. Betonwerk und Fertigteil-Technik, 1979. (12), 741-746.
15. Kollmann H. and Strübel G., *Untersuchungen über Ausblühungs- und Treiberscheinungen durch Sulfate Teil 1*. Betonwerk und Fertigteil-Technik, 1978. (10), 609-613.
16. Bonen, D. and Cohen, M.D., *Magnesium sulfate attack on portland cement paste - I Microstructural analysis*. Cement and Concrete Research, 1992. (22), 169-180.
17. Damidot, D. and Glasser, F.P., *Thermodynamic Investigation of the CaO-Al₂O₃-CaSO₄-H₂O System at 25 °C and the Influence of Na₂O*. Cement Concrete Research, 1993. (23), 221-238.
18. Metha, P.K., *Meachnism of sulfate attack on portland cement concrete-another look*. Cement Concrete Research, 1983. (13), 401-406.

19. Stark, J. and Wicht, B., *Dauerhaftigkeit von Beton*. (Schädigende Ettringitbildung). F.A. Fingerinstitut für Baustoffkunde der Bauhaus-Universität Weimar, Birkhäuser, 2001
20. Juel, I., Herfort, D., Gollop, R., Konnerup-Madsen, J., Jakobsen, H.J., and Skibsted, J., *A thermodynamic model for predicting the stability of thaumasite*. Cement Concrete Composites, 2003. 25 (8), 867-872.
21. Santhanam, M., Cohen, M.D., and Olek, J., *Sulfate attack research -- whither now?* Cement Concrete Research, 2001. 31 (6), 845-851.
22. Gaze, M.E., *The effects of varying gypsum content on thaumasite formation in a cement:Lime:Sand mortar at 5 °C*. Cement Concrete Research, 1997. 27 (2), 259-265.
23. Brown, P. and Hooton, R.D., *Ettringite and thaumasite formation in laboratory concretes prepared using sulfate-resisting cements*. Cement Concrete Composites, 2002. 24 (3-4), 361-370.
24. Macphee, D. and Diamond, S., *Thaumasite in Cementitious Materials*. Cement Concrete Composites, 2003. 25 (8), 805-807.
25. Nobst, P. and Stark, J., *Investigations on the influence of cement type on thaumasite formation*. Cement Concrete Composites, 2003. 25 (8), 899-906.
26. Bensted, S.A., Sharp, J.H., and Swamy, R.N., *Thaumasite formation in Portland-limestone cement pastes*. Cement Concrete Research, 2001. (31), 511-512.
27. Bensted, J., *Thaumasite--direct, woodfordite and other possible formation routes*. Cement Concrete Composites, 2003. 25 (8), 873-877.
28. Crammond, N.J., *The thaumasite form of sulfate attack in the UK*. Cement Concrete Composites, 2003. 25 (8), 809-818.
29. Mulenga, D.M., Nobst, P., and Stark, J., *Thaumasitbildung in Beton als Folge des Sulfatangriffs*. Wissenschaftliche Zeitschrift der Bauhaus-Universität Weimar, 2001. (5), 51-63.

7 General discussion and conclusions

The focus of this study was on the conditions of thaumasite formation. The study involved modelling, experimental and microstructural investigations. The influence of limestone addition, sulfate concentration, C_3A content, temperature and leaching were studied systematically. The study is based on two different industrial clinkers which were used to produce 5 laboratory cements.

A good agreement was achieved between the different techniques of thermodynamic modelling, bulk analytical methods, microscopy, and ultrasound measurements. The potential risk of external sulfate attack and, especially, the conditions for thaumasite formation can be described by combining experimental and calculated data.

- **Thermodynamic modelling approach**

The modelling approach indicated that during sulfate uptake first all aluminium available in the cement paste is consumed to form secondary ettringite before thaumasite forms. It was shown that thaumasite is stable only at high sulfate contents in the cement paste; more than 10 wt% SO_4^{2-} by weight cement paste or in other words if the molar SO_3/Al_2O_3 ratio in the cement paste exceeds 3.

Thermodynamic modelling predictions further indicated that when only small amounts of limestone are present in Portland cement systems it is this, which limits the amount of thaumasite formed whereas high amounts of limestone in Portland cement systems increase the potential amount of thaumasite which can be formed. It was further shown, that cement clinker systems with both high and low C_3A content can be affected by thaumasite formation as long as they contain a source of carbonate.

The experiments on pastes and mortars confirmed, that carbonate is needed in the cement systems to form thaumasite but that the amount of thaumasite formed during 9 months of sulfate exposure is not directly related to the amount of limestone addition.

The thermodynamic predictions indicated that thaumasite is only stable when all reactive aluminium is transformed into ettringite and that gypsum should be stable only at even higher levels of sulfate addition. In fact, the cement paste experiments revealed that gypsum formed in parallel to or before thaumasite during sulfate ingress due to the very slow formation of thaumasite. Furthermore, the mortar experiments confirmed that gypsum only forms with immersion in solutions of high sulfate concentration and there are only few signs of rather

small amounts of thaumasite in the samples surface regions of the samples after 56 days of exposure.

The thermodynamic modelling showed that thaumasite is also stable at ambient temperatures (20 °C). However, it was confirmed experimentally that the formation of thaumasite was much more significant at low temperatures (8 °C) after 9 months.

The thermodynamic modelling indicated that thaumasite is stable, both in the presence and in the absence of portlandite indicating that prior leaching of cement paste (reduced pH level, portlandite and alkalies content) does not significantly influence the stability of thaumasite. However, the experimental investigations showed that in pre-leached cement pastes thaumasite precipitated more slowly than in the unleached pastes.

The slow formation of thaumasite as confirmed by microstructural and microanalytical investigations is the reason for the difference between modelling and experimental observations. Generally, thaumasite was detected where it has been modelled to be stable in significant amounts. It was found that thaumasite is the last sulfate phase forming during sulfate attack.

The progressive equilibrium approach (PEA) used to investigate the chemical aspects of sulfate attack turned out to be a good tool for simulating external sulfate attack. However, in this study, the predicted equilibrium conditions have not been reached after 9 months exposure.

- **Physical effects of sulfate attack**

During sulfate attack, the progress of sulfate deterioration and crack formation was somewhat different between the cement paste and mortar samples. In the case of paste samples, the sulfate ingress was limited to a few micrometer at the sample surface and crack formation was observed after 9 months of sulfate exposure mainly parallel to the sample's surface. The mortar samples revealed a distinct zonation of sulfate ingress up to some millimetres and the cracks were forming already after 2 – 3 months either parallel or perpendicular to the sample surface. These difference may be attributed either to the difference in w/c ratio (paste: 0.35; mortar: 0.50) used or the influence of inhomogeneities in the microstructure (aggregates) giving additional pathways for sulfate interaction.

In the paste and in the mortar samples, the crack formation originated from the precipitation of ettringite within the cement paste matrix. This caused the initial expansion due to a confinement in the microstructure. After some months of sulfate attack, the storage temperature and the ongoing leaching processes influenced sulfate degradation. The

formation of thaumasite, which occurred in the sample containing limestone especially at low temperatures (8 °C) also show a dramatic softening and disintegration starting at the sample surface.

The investigations showed that at the early stages of sulfate interaction, after 1-3 months the AFm phases (monosulfate, monocarbonate) present are transformed into secondary ettringite leading to a densification of the microstructure and the above mentioned initial crack formation. As sulfate deterioration continues, after 3 to 9 months the formation of thaumasite was observed as long as sulfate (from solution or as gypsum) and carbonate (limestone filler) are available leading to a successive disintegration and finally to the complete destruction of the microstructure.

- **Effects of limestone addition**

The addition of limestone (5, 25 wt%) influenced chemically the mineralogy of the AFm phases formed during hydration; monocarbonate was formed instead of monosulfate. The presence of monocarbonate in the carbonate containing cement systems also stabilized ettringite. These findings agree well with other experimental findings reported in the literature [1, 2]. The stabilisation of ettringite in the presence of calcite might have increased the chemical resistance against sulfate attack, as a significant part of the aluminium was already bound in ettringite.

The experimental results showed that limestone addition of 5 wt% in Portland cement systems improved the physical properties leading to a lower porosity and higher compressive strength compared to the corresponding cements without limestone addition. Thus, the reduced permeability decreased the sulfate uptake and the sulfate resistance was improved independent of the type of cement clinker used. With 25 wt% limestone addition in Portland cement the compressive strength was decreased, whereas the porosity of these cement systems increased which led to an accelerated sulfate degradation. These findings agree well with the investigation in the literature [3, 4].

In this study, both chemical and physical effects in cement with 5 wt% limestone addition have been observed. Somewhat more ettringite was found in the initial cement paste and a lower porosity and decreased expansion indicating an increased sulfate resistance. However, it is difficult to distinguish between pure chemical and physical aspects since both depend and influence each other.

- **Summary and conclusions**

In summary, it can be concluded that:

- (1) Only carbonate containing cement systems were affected by thaumasite formation independently of the type of cement clinker (high and low C_3A content) used
- (2) High sulfate contents of more than 10 wt% by weight cement paste ($SO_3/Al_2O_3 > 3$) are necessary to form thaumasite
- (3) Leaching, i.e. the reduction of alkalies and portlandite, has no significant influence on the stability of thaumasite, it slightly reduced the amounts of thaumasite formed
- (4) Low temperatures (8 °C) accelerate thaumasite formation but thaumasite is also formed and stable at ambient temperatures (20 °C)
- (5) Thaumasite formation is not the first stage of sulfate attack. The disintegration known as thaumasite form of sulfate attack (TSA), occurs only in the later (last) stages of sulfate attack
- (6) The initial sulfate induced deterioration is caused by ettringite and partly gypsum formation
- (7) The addition of a few percent limestone increase the resistance of Portland cement systems against sulfate attack

- **Outlook and implications for sulfate testing**

The PEA approach used to investigate sulfate attack could be further improved by using a higher water to cement ratio (≥ 0.35) in the cement paste and smaller particle fractions (≤ 0.5 mm) in order to shorten the reaction time for the experiments. Additionally, the batch experiments could be shaken permanently to accelerate sulfate interaction.

However, the PEA experiments used to investigate the chemical aspects of an external sulfate attack, revealed a good handling in the laboratory and turned out to be a very promising approach for systematic investigations.

The test conditions of sulfate tests should use lower sulfate concentrations ($<< 30\text{g SO}_4^{2-}/\text{l}$) in order to better match real conditions. Tests, such as Wittekindt [5] often use a criteria at 56 days and high sulfate concentrations ($30\text{g SO}_4^{2-}/\text{l}$) in order to accelerate sulfate degradation.

The sulfate concentration (3 or 30g $\text{SO}_4^{2-}/\text{l}$) in solution significantly influenced the progress of degradation and the formation of sulfate phases, e.g. gypsum being absent or present.

The test criteria of 56 days according to Wittekindt [5] should be further extended, e.g. ≥ 91 days in order to reach the relevant level of expansion due to secondary ettringite formation as observed experimentally. Due to the very slow formation of thaumasite, a thaumasite test would have to have a long duration and low temperatures.

Further studies should investigate the reactivity of C_4AF in relation to sulfate attack. The reactivity of C_4AF during sulfate attack will determine the availability of further aluminium. In addition, the fate of iron which is released during C_4AF hydration is also an open question, either it precipitates as iron ettringite or as amorphous iron hydroxide will have a significant influence on the expansion.

References

1. Bonavetti, V.L., Rahhal, V.F., and Irassar, E.F., *Studies on the carboaluminate formation in limestone filler-blended cements*. Cement and Concrete Research, 2001. 31, 853-859.
2. Kuzel, H. and Pöllmann, H., *Hydration of C_3A in the presence of $Ca(OH)_2$, $CaSO_4 \cdot 2H_2O$ and $CaCO_3$* . Cement Concrete Research, 1991. 21, 885-895.
3. Irassar, E.F., Bonavetti, V.L., and Gonzalez, M., *Microstructural study of sulfate attack on ordinary and limestone Portland cements at ambient temperature*. Cement Concrete Research, 2003. 33, 31-41.
4. Stark, J., *Optimierte Bindemittelsysteme für die Betonindustrie*. Beton, 2004. 10/2004, 486-490.
5. Wittekindt, W., *Sulfatbeständige Zemente und ihre Prüfung*. Zement-Kalk-Gips, 1960. 12.

Appendix

A.1 Laboratory cements

- **Grinding and production**

The cement clinkers were ground using a laboratory ball mill as shown in Figure A.1.1. The grinding was done in several steps with different sets of balls (70/40 mm, 17/17 mm).



Fig. A.1.1: Ball mill used for the grinding of the cement clinker

The constituents of the laboratory cements were mixed mechanically in batches using plastic bottles of 2 liters volume. For the preparation of the laboratory cements batches of 6 plastic bottles a 1.5 kg filled with rubber cubes were placed in a barrel and homogenized for 2 hours under constant axial rotation (Fig. A.1.2).



Fig. A.1.2: Barrel arranged with plastic bottles for homogenisation

• Testing and performance

The laboratory cements were tested according to the standard EN 196 (1-4) and proved to fulfil the technical requirements for the given commercial Portland cements as shown in Table A 1.1.

Table A 1.1: Characterisation of laboratory and industrial cements according to EN 196 (1-4)

| cement | | CEM I | H0 | H5 | CEM I | P0 | P5 | P25 |
|------------------------------|----------------------|-------|------|------|-------|------|------|------|
| | | 42.5 | | | 42.5 | | | |
| type: | | HS | HS | HS | OPC | OPC | OPC | OPC |
| limestone addition LF: | | | 0 | 5 | | 0 | 5 | 25 |
| | [wt%] | | | | | | | |
| Strength | fc 2d | 23.4 | 23.1 | 21.7 | 26.6 | 28.3 | 27.5 | 20.7 |
| | [N/mm ²] | | | | | | | |
| | fc 28d | 52.9 | 56.1 | 56.8 | 54.2 | 58.2 | 58.8 | 46.5 |
| | ft 2d | 5.4 | 5.2 | 5.0 | 5.7 | 6.1 | 5.1 | 4.8 |
| Blaine [m ² /kg] | | 311 | 331 | 348 | 302 | 356 | 363 | 408 |
| Density [g/cm ³] | | 3.18 | 3.19 | 3.17 | 3.10 | 3.12 | 3.10 | 3.01 |
| setting | begin | 235 | 220 | 200 | 200 | 160 | 155 | 145 |
| [min] | end | 270 | 270 | 245 | 235 | 195 | 190 | 170 |
| Le Chatelier [mm] | | 1.5 | 2.0 | 2.0 | 2.5 | 2.0 | 2.0 | 2.0 |
| water demand [%] | | 24.5 | 25.3 | 25.5 | 25.8 | 26.0 | 26.3 | 26.8 |

• Isothermal calorimetry

The analysis of the heat of hydration was performed on laboratory and industry cements using isothermal calorimetry (TAM Air). The given SO_3 contents are relative to the cement clinker used.

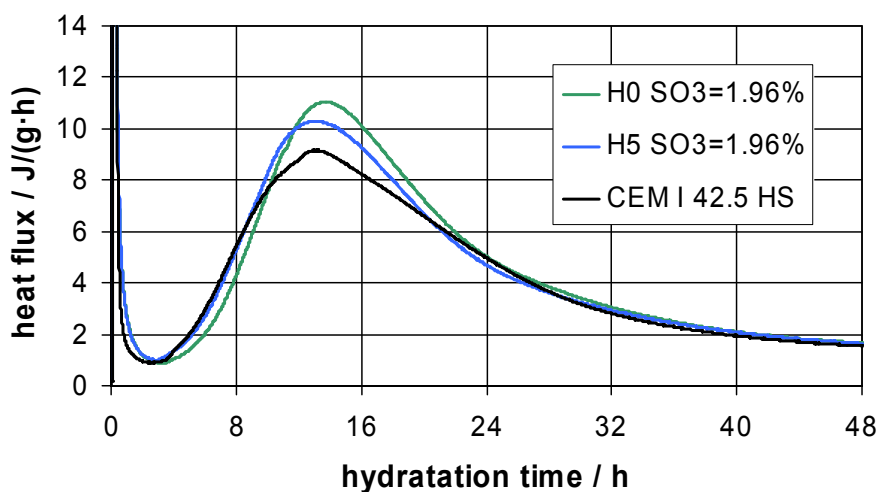


Fig. A 1.3: Heat of hydration of HS cement systems

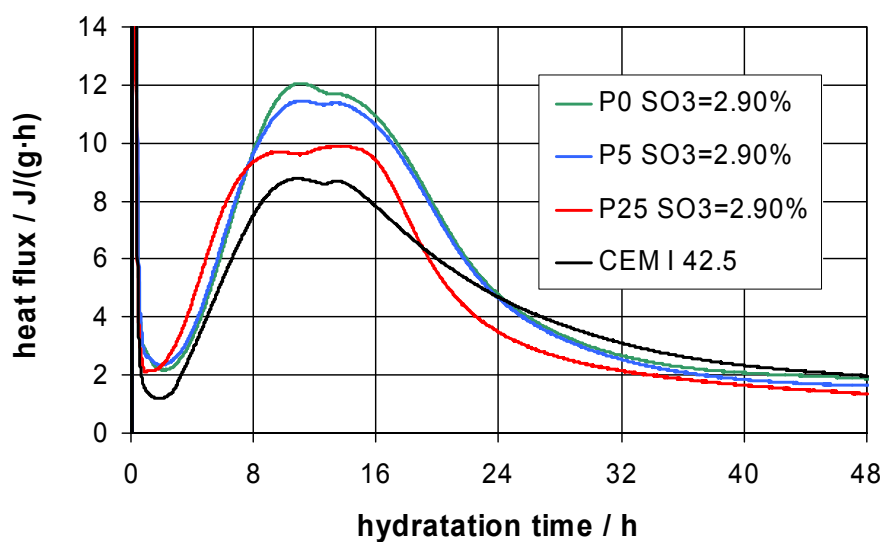


Fig. A 1.4: Heat of hydration of OPC cement systems

• Chemical and mineralogical analysis

Table A 1.2: Chemical analysis of the laboratory and industry cements and mineral composition according to Bogue in wt%

| cement | CEM I 42.5 | H0 | H5 | CEM I 42.5 | P0 | P5 | P25 |
|--------------------------------|---------------|------|------|---------------|------|------|------|
| type | HS | HS | HS | OPC | OPC | OPC | OPC |
| limestone addition LF | | +0% | +5% | | +0% | +5% | +25% |
| <u>Chemical Analysis:</u> | | | | | | | |
| SiO ₂ | 18.7 | 19.2 | 18.1 | 20.0 | 20.1 | 19.6 | 15.2 |
| Al ₂ O ₃ | 4.3 | 4.7 | 4.4 | 4.8 | 4.4 | 4.3 | 3.4 |
| Fe ₂ O ₃ | 6.2 | 7.2 | 6.7 | 2.5 | 2.7 | 2.6 | 2.0 |
| CaO | 61.2 | 62.2 | 61.2 | 63.4 | 63.7 | 63.7 | 61.4 |
| MgO | 1.8 | 1.5 | 1.5 | 1.8 | 1.6 | 1.5 | 1.3 |
| K ₂ O | 1.0 | 1.1 | 1.1 | 0.9 | 0.86 | 0.78 | 0.61 |
| Na ₂ O | 0.13 | 0.13 | 0.12 | 0.1 | 0.15 | 0.15 | 0.11 |
| SO ₃ | 2.3 | 1.9 | 1.7 | 2.8 | 2.9 | 2.7 | 2.2 |
| CaO _{free} | 0.47 | 0.55 | 0.55 | 0.76 | 0.85 | 0.77 | 0.66 |
| CO ₂ | 2.56 | 0.15 | 2.39 | 1.85 | 0.25 | 2.37 | 10.5 |
| LOI | 2.74 | 0.68 | 2.79 | 2.29 | 1.21 | 3.30 | 11.4 |
| <u>Minerals by Bogue:</u> | | | | | | | |
| C ₃ S | 53 | 62 | 57 | 56 | 66 | 60 | 50 |
| C ₂ S | 14 | 9 | 9 | 15 | 10 | 11 | 7 |
| C ₃ A | 0.9 | 0.4 | 0.4 | 9 | 7 | 7 | 6 |
| C ₄ AF | 19 | 22 | 20 | 8 | 8 | 8 | 6 |
| gypsum | 4.9 | 4.2 | 4.2 | 6.0 | 6.2 | 6.2 | 6.2 |

A.2 Cement paste experiments

- **Experimental setup**

For the experiments of the PEA approach the subsystems were processed with 10g of the hydrated and crushed cement paste and 70 ml of aqueous reaction solution which was prepared by dissolving the respective amounts of Na_2SO_4 in deionised water. The experiments were processed as sealed plastic containers at 8 °C and 20 °C.

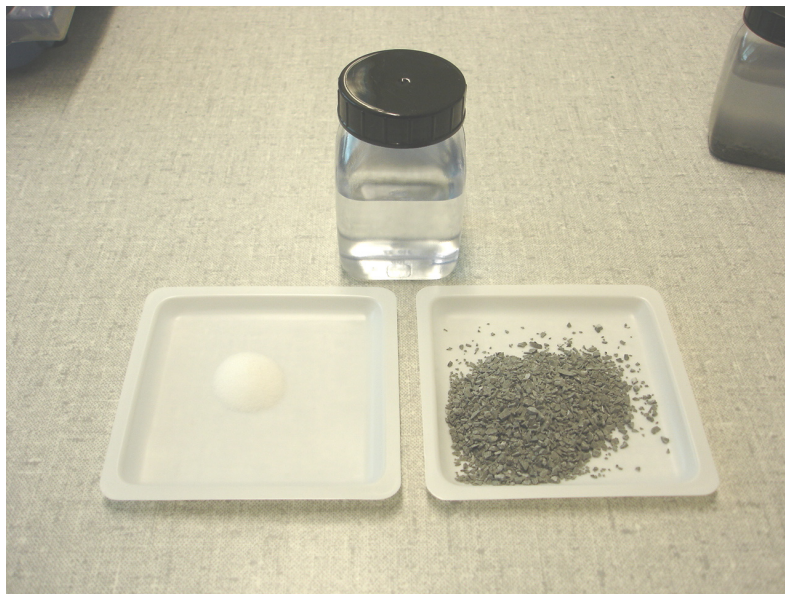


Fig. A 2.1: Constituents of a subsystem according to the PEA experiments

• Thermogravimetric measurements

The thermogravimetric analysis was used to determine the amount of portlandite present in the hydrated, initial and successive leached cement paste samples for the HS and OPC cement systems.

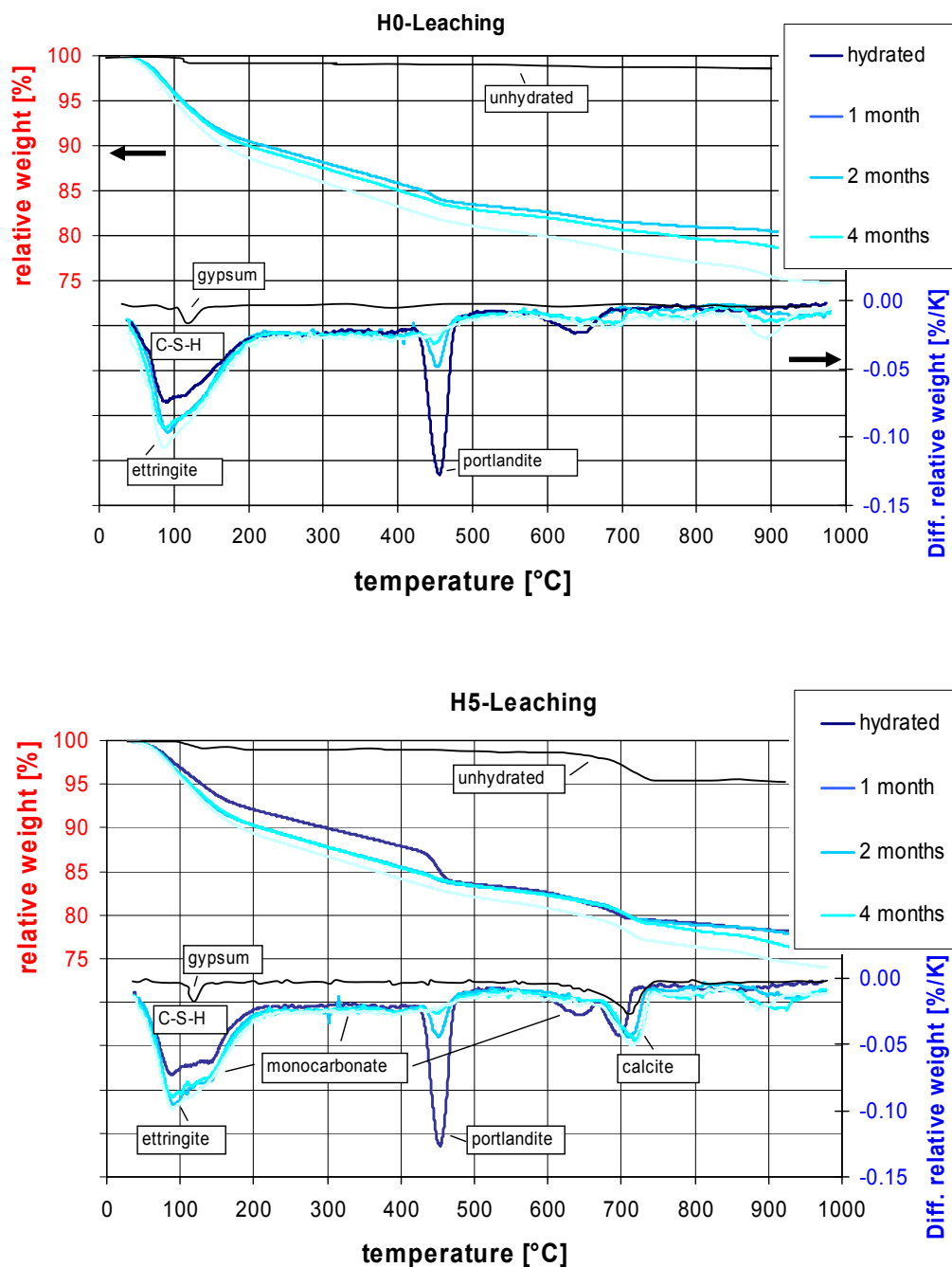


Fig. A 2.2: Leaching of HS cement systems after 4 months

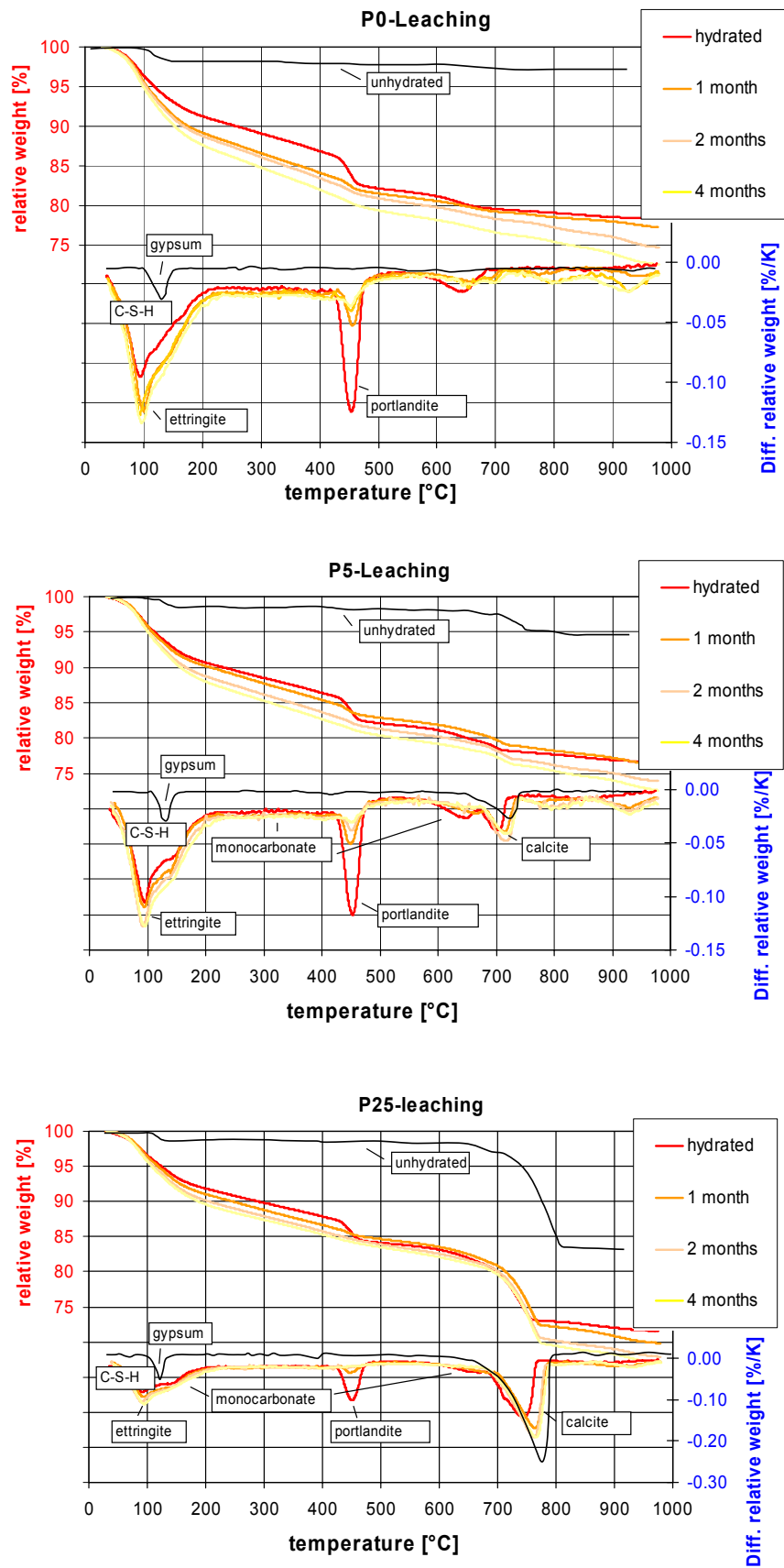


Fig. A 2.3: Leaching of OPC cement systems after 4 months

A.3 Thermodynamic software and data

The Gibbs free energy minimization program GEMS [1] is a broad- purpose geochemical modelling code which uses Gibbs energy minimization and computes equilibrium phase assemblage and speciation in a complex chemical system from its total bulk elemental composition. Chemical interactions involving solids, solid solutions and aqueous electrolyte are considered simultaneously. Thermodynamic data for aqueous species as well as for many solids were taken from PSI thermodynamic dataset [2], which has been adapted for the use in GEMS [3]. Solubility products for cement minerals at 25 °C were taken from the compilation of Lothenbach et al. [4], who prepared a consistent thermodynamic dataset for cement minerals (data relevant for the investigated system are reproduced in Table A.3.1).

The Gibbs free energy of formation $\Delta_f G^\circ$ at 25 °C as given in Table A 3.1 is related to the

Gibbs free energy of reaction $\Delta_r G^\circ = \sum_i \nu_i \Delta_f G^\circ$ and to the solubility product $K_{s0} = e^{\frac{-\Delta_r G^\circ}{RT}}$,

where ν_i are the stoichiometric reaction coefficients, $R = 8.31451$ J/mol/K and T the temperature in K. The apparent Gibbs free energy of formation $\Delta_a G^\circ$ at 8 and 20 °C is calculated by GEMS from the data at 25 °C according to [5]:

$$\begin{aligned} \Delta_a G_T^\circ &= \Delta_f G_{T_0}^\circ - S_{T_0}^\circ (T - T_0) - \int_{T_0}^T \int_{T_0}^T \frac{C_p^\circ}{T} dT dT \\ &= \Delta_f G_{T_0}^\circ - S_{T_0}^\circ (T - T_0) - a_0 \left(T \ln \frac{T}{T_0} - T + T_0 \right) - 0.5a_1 (T - T_0)^2 - a_2 \frac{(T - T_0)^2}{2T \cdot T_0^2} - a_3 \frac{2(\sqrt{T} - \sqrt{T_0})^2}{\sqrt{T_0}} \end{aligned} \quad (1)$$

where a_0 , a_1 , a_2 , and a_3 are the empirical coefficients of the heat capacity equation $C_p^\circ = a_0 + a_1 T + a_2 T^{-2} + a_3 T^{-0.5}$, T_0 the reference temperature (298.15 K) and S° the entropy. The apparent Gibbs free energy of formation $\Delta_a G^\circ_\tau$ refers to the free energies of the elements at 298 K. A more detailed description of the temperature corrections used in GEMS is given in Kulik et al. [6] and in the online documentation of GEMS [1].

Table A 3.1: Standard thermodynamic properties of solids at 25 °C. All data with exception of thaumasite are taken from Lothenbach et al. [4].

| | Log K_{S0} ^a | $\Delta_f G^\circ$ [kJ/mol] | $\Delta_f H^\circ$ [kJ/mol] | S° J/K/mol] | a_0 [J/K/mol] | a_1 | a_2 | a_3 | V° ^b [cm ³ /mol] |
|---------------------------|---------------------------|--------------------------------|--------------------------------|-----------------------|--------------------|--------|---------|------------------|--|
| ettringite | -44.90 | - | -17535 | 1900 | 1939 | 0.789 | | | 707 |
| | | 15205.94 | | | | | | | |
| thaumasite ^c | -49.40 | - | -17373 | 1883 | 1860 | 0.703 | -3.94e6 | 1600 | 663 |
| | | 15128.46 | | | | | | | |
| C_3AH_6 | -20.84 | -5010.09 | -5540 | 419 | 292 | 0.561 | | | 150 |
| C_4AH_{13} | -25.40 | -7326.55 | -8302 | 700 | 711 | 1.047 | | -1600 | 274 |
| C_2AH_8 | -13.56 | -4812.75 | -5432 | 440 | 392 | 0.714 | | -800 | 184 |
| $C_4A\bar{S}H_{12}$ | -29.26 | -7778.50 | -8750 | 821 | 594 | 1.168 | | | 309 |
| $C_4A\bar{C}H_{11}$ | -31.47 | -7337.46 | -8250 | 657 | 618 | 0.982 | -2.59e6 | | 262 |
| $C_4A\bar{C}_{0.5}H_{12}$ | 29.13 | -7335.97 | -8270 | 713 | 664 | 1.168 | -1.30e6 | -800 | 285 |
| C_2ASH_8 | -19.70 | -5705.15 | -6360 | 546 | 438 | 0.749 | -1.13e6 | -800 | 216 |
| M_4AH_{10} | -56.02 | -6394.56 | -7196 | 549 | -364 | 4.21 | 3.75e6 | 629 ^d | 220 |
| brucite | -11.16 | -832.23 | -923 | 63 | 101 | 0.017 | -2.56e6 | | 25 |
| $C_{1.67}SH_{2.1}$ | -13.17 | -2480.81 | -2723 | 140 | 210 | 0.120 | -3.07e6 | | 78 |
| $C_{0.83}SH_{1.3}$ | -8.00 | -1744.36 | -1916 | 80 | 85 | 0.160 | | | 59 |
| portlandite | -5.20 | -897.01 | -985 | 83 | 187 | -0.022 | 0 | -1600 | 33 |
| $SiO_{2, am}$ | 1.476 | -848.90 | -903 | 41 | 47 | 0.034 | -1.13e6 | | 29 |
| gypsum | -4.58 | -1797.76 | -2023 | 194 | 91 | 0.318 | | | 75 |
| anhydrite | -4.36 | -1322.12 | -1435 | 107 | 70 | 0.099 | | | 46 |
| calcite | -1.85 | -1129.18 | -1207 | 93 | 105 | 0.022 | -2.59e6 | | 37 |
| $Fe(OH)_3$ | -4.60 | -711.61 | -844 | 88 | 28 | 0.052 | | | 34 |
| Al_2O_3 | 1.64 | -1586.26 | -1662 | 51 | 115 | 0.012 | -3.51e6 | | 26 |

a_0, a_1, a_2, a_3 are the empirical coefficients of the heat capacity equation: $C_p^\circ = a_0 + a_1T + a_2T^2 + a_3T^{0.5}$, ^a All solubility products refer to the solubility with respect to the species $Al(OH)_4^-$, $Fe(OH)_4^-$, $SiO(OH)_3^-$, OH^- , H_2O , Ca^{2+} , Mg^{2+} or SO_4^{2-} , ^b Molar volumes V° at standard conditions were calculated from densities derived from crystallographic data; ^c this work; V° calculated from unit cell given in Jacobsen et al. [7]; ^d $C_p^\circ = a_0 + a_1T + a_2T^2 + a_3T^{0.5} - 0.00424T^2 + 2.11E-6T^3$

A.4 SEM sample preparation

The mortar samples were prepared from sections cut from the flat prism to give a cross sections perpendicular to the surface representative for the microstructure of surface and core regions (Fig. A 4.1). The cement paste samples of the crushed particles from the PEA experiments were prepared to give microsections (Fig. A 4.2). Before impregnation the samples were immersed for 30 min in isopropanol and then dried for 2 days at 40 °C.

The samples preparation included pressure impregnation with two components epoxy resin (Araldit BY 158, Aradur 21), cutting, grinding and polishing. The polishing was done in several steps by using diamond suspensions from 9 to 0.25 μm (BUEHLER, Beta-vector) as described elsewhere [8, 9]. The polished samples were then coated with carbon to get an electrically conductive surface. For the fracture surfaces selected parts of the sample were carefully broken off and prepared directly used for the investigation in the microscope.

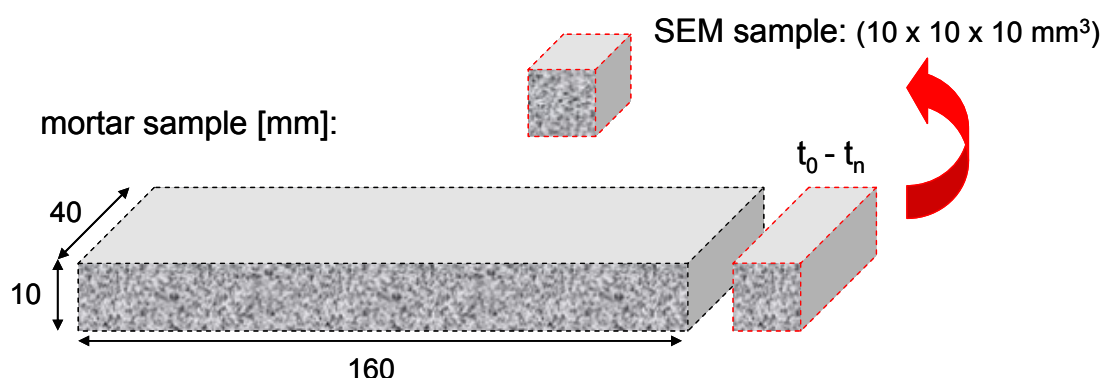


Fig. A 4.1: SEM sample preparation for mortar samples.

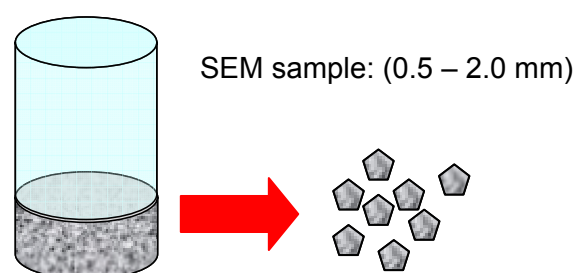


Fig. A 4.2: SEM sample preparation for paste samples.

A.5 Mortar experiments

- **Ultrasonic measurements**

For the ultrasonic measurements a 3-axis computer manipulator was used with adjusted probes of transmitter and receiver. The probes were set relative to the samples surface immersed in demineralised water. To achieve nearly isothermal conditions, the measurements at 8 °C were done in a thermal insulated basin.

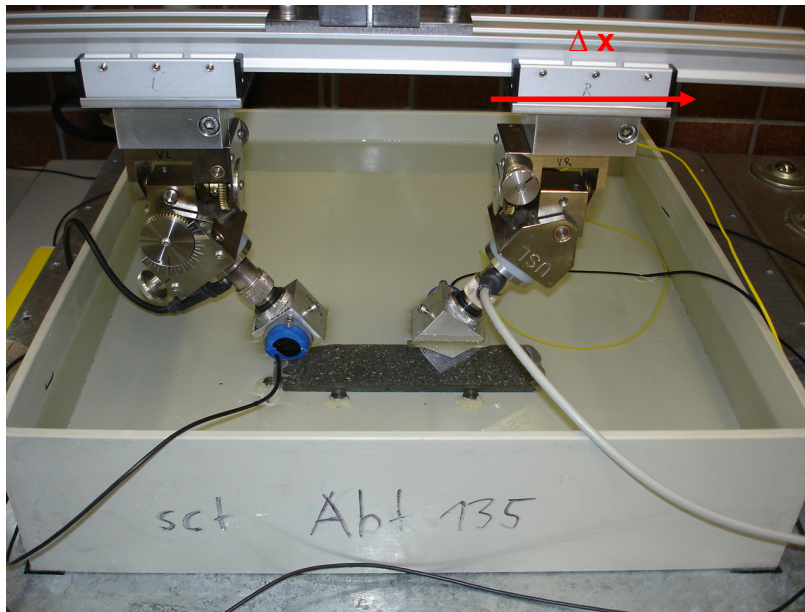


Fig. A 5.1: Situation for measurements at 20 °C in demineralised water at the same temperature

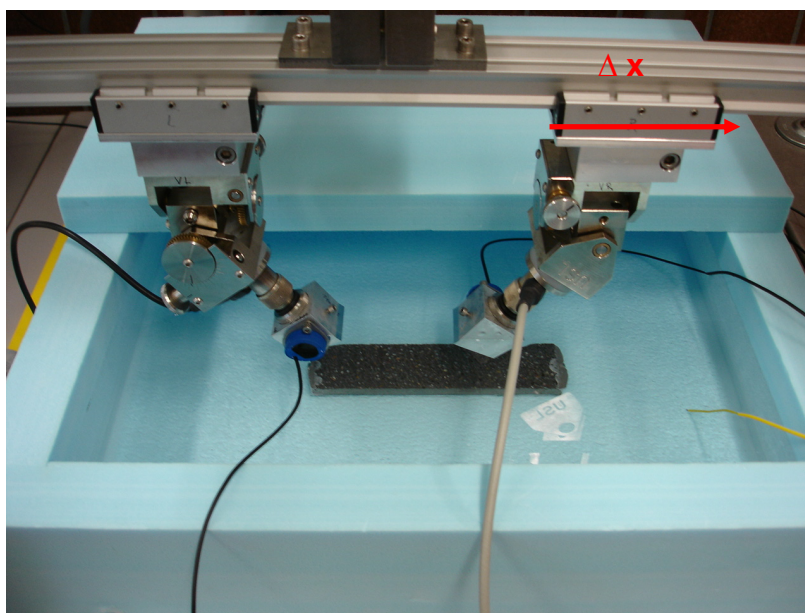


Fig. A 5.2: Situation for measurements at 8 °C with thermal insulated basin and demineralised water at the same temperature

• Additional results from monitoring

The following Table shows the measurements of the expansion and mass change of the mortar samples stored Na_2SO_4 with high and low sulfate concentration at 8 and 20 °C.

Table A 5.1: Expansion and mass change of mortar samples at given sulfate concentration and temperature.

| Sample | | | 30g SO ₄ ²⁻ /l | | | | 3g SO ₄ ²⁻ /l | | | |
|------------------|-----|-------|--------------------------------------|-------|-------|-------|-------------------------------------|------|------|------|
| | | | 91d | 180d | 270d | 365d | 91d | 180d | 270d | 365d |
| Expansion [mm/m] | H0 | 8 °C | 1.23 | 3.60 | 11.28 | 20.02 | 0.43 | 0.70 | 0.98 | 1.44 |
| | | 20 °C | 3.78 | 11.28 | 20.84 | 27.51 | 0.58 | 1.59 | 2.41 | 2.75 |
| | H5 | 8 °C | 1.24 | 7.15 | 25.92 | - | 0.41 | 0.59 | 0.88 | 1.23 |
| | | 20 °C | 1.44 | 4.35 | 12.21 | 21.67 | 0.30 | 0.62 | 1.04 | 1.51 |
| | P0 | 8 °C | 0.69 | 1.92 | 6.64 | 17.22 | 0.35 | 0.65 | 1.09 | 1.66 |
| | | 20 °C | 1.33 | 6.39 | 16.49 | 30.97 | 0.62 | 1.62 | 3.13 | 6.46 |
| | P5 | 8 °C | 0.67 | 1.99 | 12.29 | - | 0.31 | 0.56 | 0.83 | 1.29 |
| | | 20 °C | 0.93 | 2.71 | 8.54 | 33.73 | 0.46 | 0.75 | 1.16 | 1.72 |
| | P25 | 8 °C | 1.82 | 19.20 | - | - | 0.35 | 1.34 | 9.05 | - |
| | | 20 °C | 2.38 | 32.40 | - | - | 0.38 | 1.59 | 3.86 | 6.74 |
| Mass change [%] | H0 | 8 °C | 1.15 | 2.08 | 3.25 | 3.37 | 0.58 | 0.71 | 0.82 | 0.93 |
| | | 20 °C | 1.66 | 3.06 | 4.44 | 5.23 | 0.55 | 0.72 | 0.87 | 0.98 |
| | H5 | 8 °C | 0.93 | 2.35 | 1.30 | - | 0.57 | 0.69 | 0.79 | 0.93 |
| | | 20 °C | 1.01 | 1.91 | 3.29 | 4.56 | 0.60 | 0.74 | 0.87 | 1.01 |
| | P0 | 8 °C | 0.82 | 1.46 | 2.18 | 2.55 | 0.59 | 0.63 | 0.72 | 0.86 |
| | | 20 °C | 1.07 | 2.32 | 4.21 | 5.65 | 0.55 | 0.64 | 1.03 | 1.43 |
| | P5 | 8 °C | 0.74 | 1.42 | 0.64 | - | 0.52 | 0.61 | 0.70 | 0.85 |
| | | 20 °C | 0.77 | 1.45 | 2.72 | 4.71 | 0.52 | 0.59 | 0.70 | 0.84 |
| | P25 | 8 °C | 1.15 | 0.66 | - | - | 0.61 | 0.83 | - | - |
| | | 20 °C | 1.24 | 4.82 | - | - | 0.51 | 0.75 | 1.25 | 2.03 |

(-) samples destroyed

- **Macroscopical investigations (180 days)**

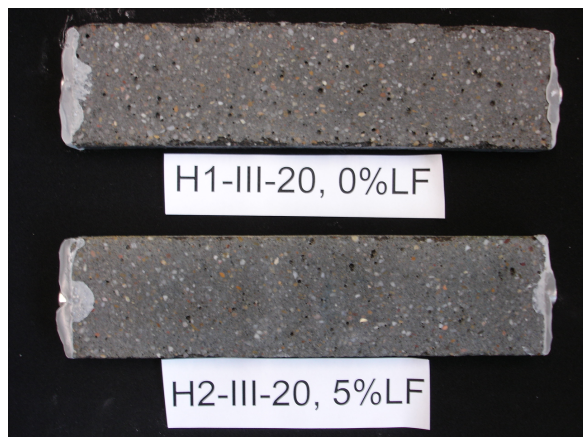
The visual appearance of the mortar samples was investigated during sulfate exposure for up to one year. The photo documentation of the samples is carried out after 180, 270 and 365 days of storage in sulfate solution.



HS + 0% limestone addition at 20 °C



HS + 0% limestone addition at 8 °C

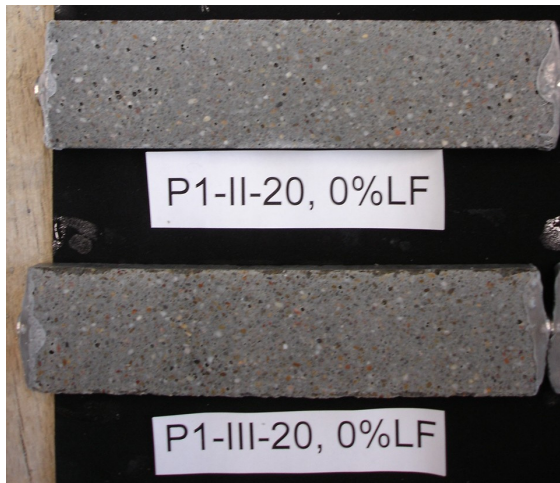


HS + 5% limestone addition at 20 °C



HS + 5% limestone addition at 8 °C

Fig. A 5.3: HS cement systems after 180 days of exposure, II = 3g $\text{SO}_4^{2-}/\text{l}$, III = 30g $\text{SO}_4^{2-}/\text{l}$



OPC + 0% limestone addition at 20 °C



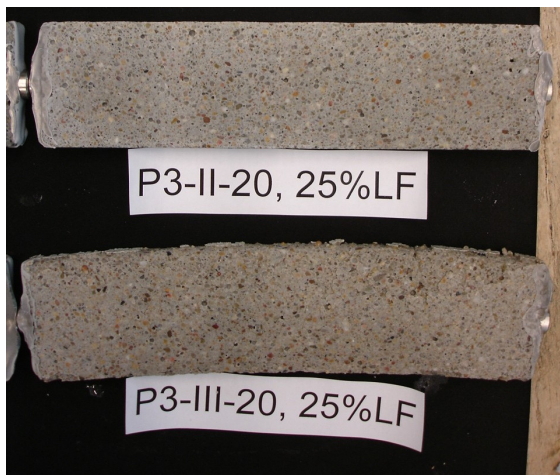
OPC + 0% limestone addition at 8 °C



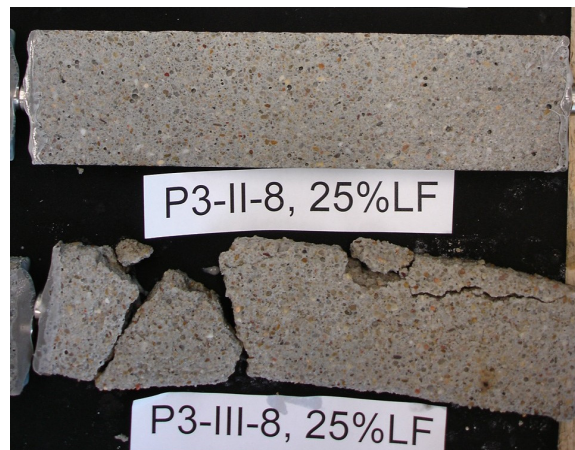
OPC + 5% limestone addition at 20 °C



OPC + 5% limestone addition at 8 °C



OPC + 25% limestone addition at 20 °C



OPC + 25% limestone addition at 8 °C

Fig. A 5.4: OPC cement systems after 180 days of exposure, II = 3g SO₄²⁻/l, III = 30g SO₄²⁻/l

- Macroscopical investigations (270 days)

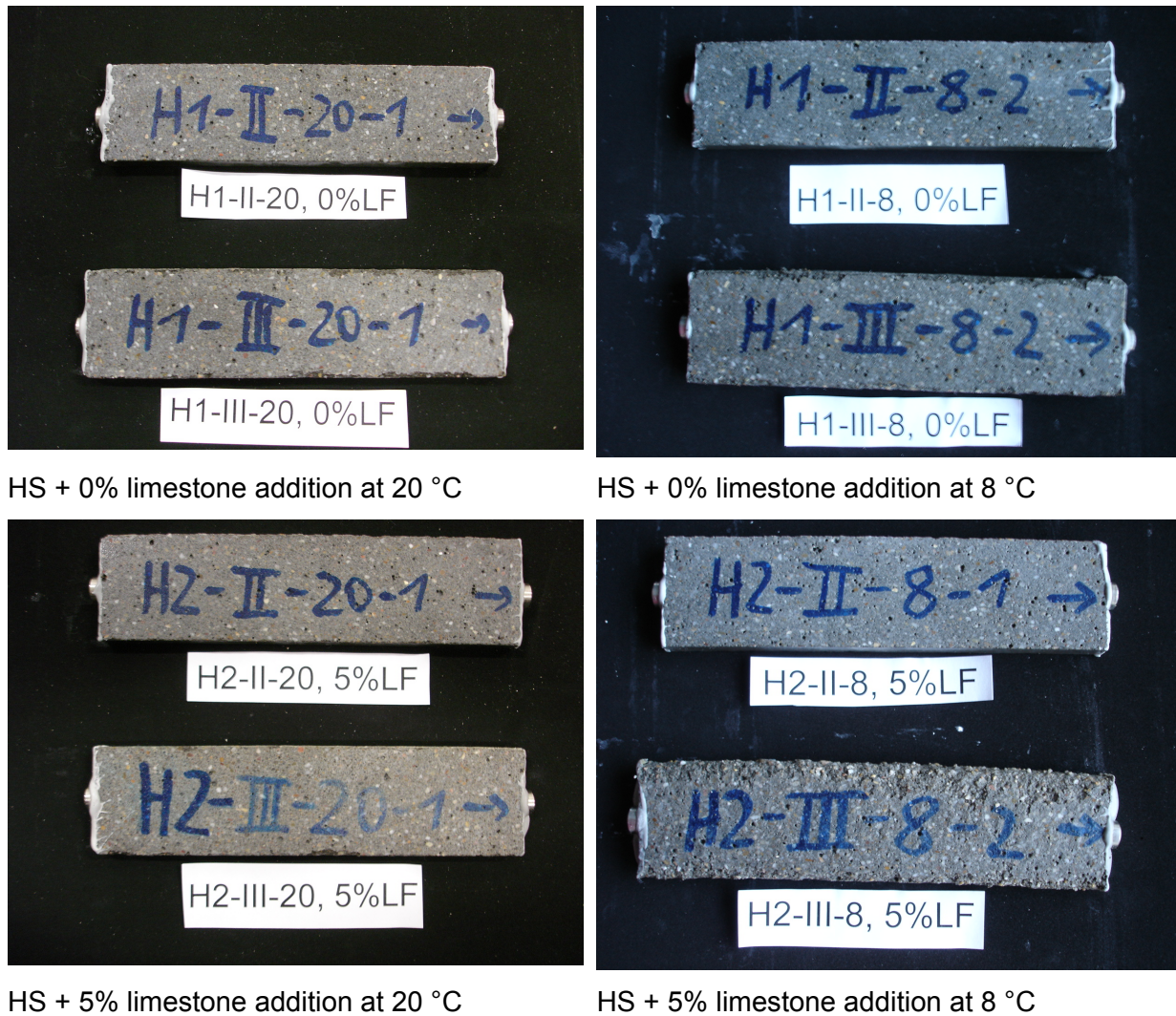
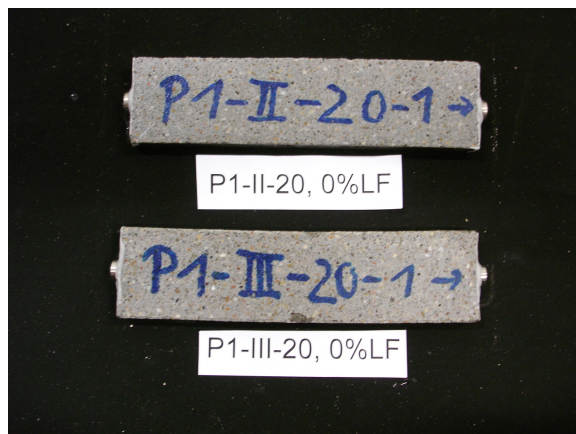


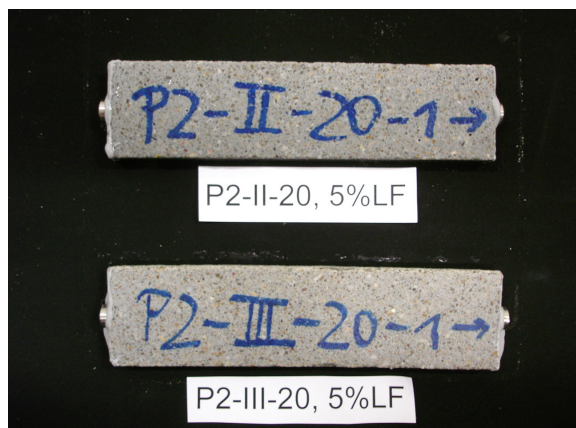
Fig. A 5.5: HS cement systems after 270 days of exposure, II = 3g $\text{SO}_4^{2-}/\text{l}$, III = 30g $\text{SO}_4^{2-}/\text{l}$



OPC + 0% limestone addition at 20 °C



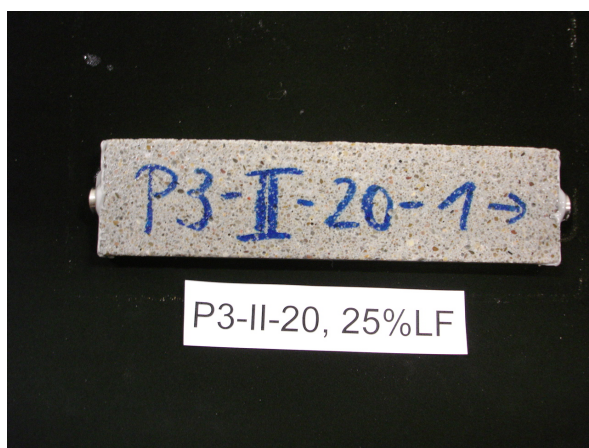
OPC + 0% limestone addition at 8 °C



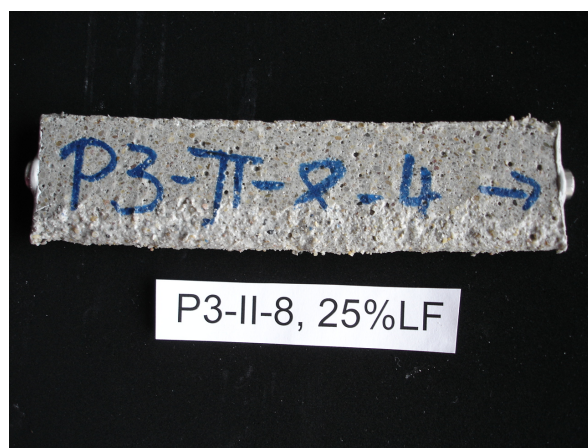
OPC + 5% limestone addition at 20 °C



OPC + 5% limestone addition at 8 °C



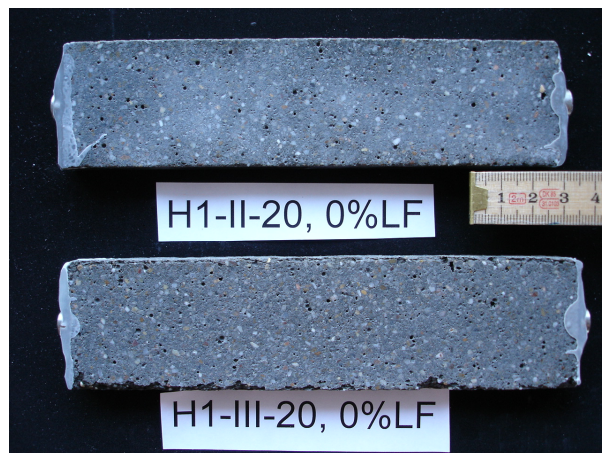
OPC + 25% limestone addition at 20 °C



OPC + 25% limestone addition at 8 °C

Fig. A 5.6: OPC cement systems after 270 days of exposure, II = 3g SO₄²⁻/l, III = 30g SO₄²⁻/l

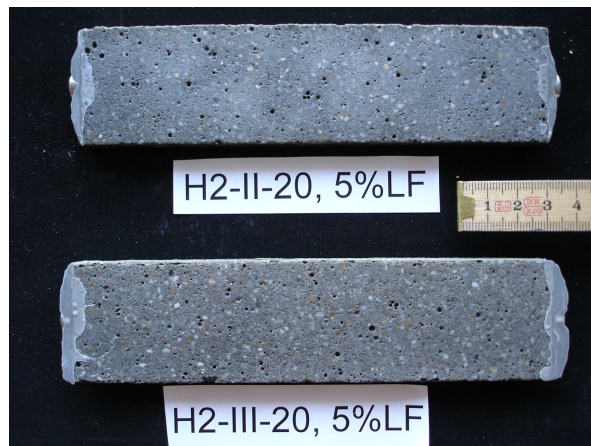
- Macroscopical investigations (365 days)



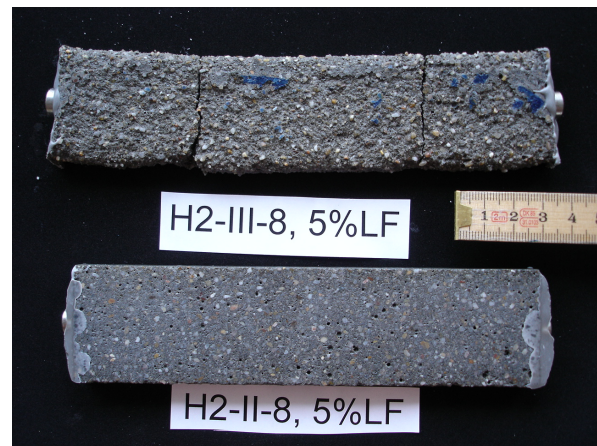
HS + 0% limestone addition at 20 °C



HS + 0% limestone addition at 8 °C



HS + 5% limestone addition at 20 °C



HS + 5% limestone addition at 8 °C

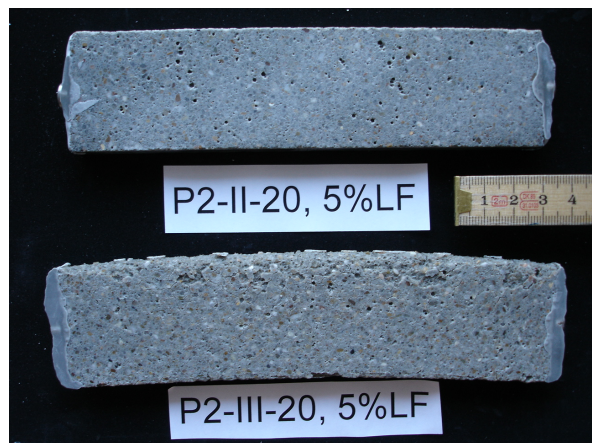
Fig. A 5.7: HS cement systems after 365 days of exposure, II = 3g $\text{SO}_4^{2-}/\text{l}$, III = 30g $\text{SO}_4^{2-}/\text{l}$



OPC + 0% limestone addition at 20 °C



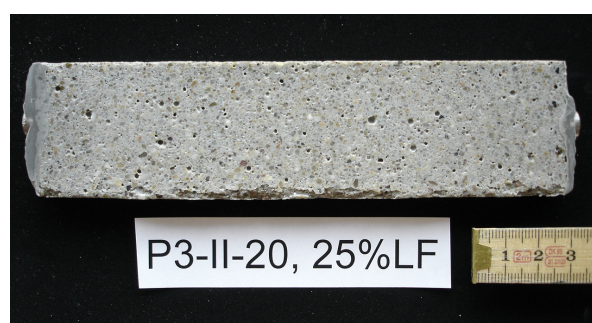
OPC + 0% limestone addition at 8 °C



OPC + 5% limestone addition at 20 °C



OPC + 5% limestone addition at 8 °C



OPC + 25% limestone addition at 20 °C

Fig. A 5.8: OPC cement systems after 365 days of exposure, II = 3g $\text{SO}_4^{2-}/\text{l}$, III = 30g $\text{SO}_4^{2-}/\text{l}$

• Microstructural investigations (56 days)

The following pages show the atomic ratio plots from additional EDS-analysis representing S/Ca versus Al/Ca ratios of selected samples.

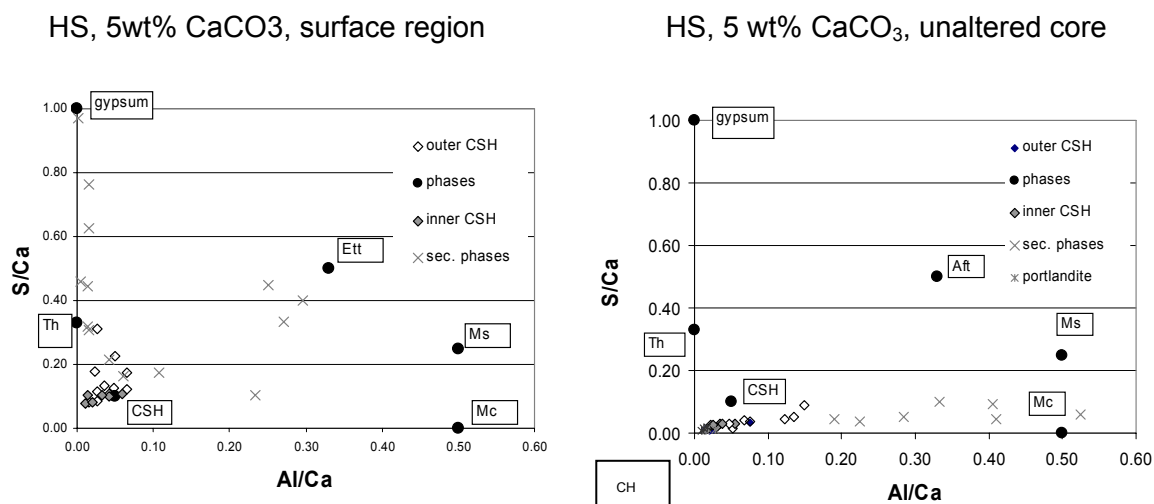


Fig. A 5.9: Phase assemblages of Portland cement mortars after 56 days sulfate exposure in 30g SO₄²⁻/l at 8 °C. CH = portlandite; Ett = ettringite; G = gypsum; Ms = monosulfate; Th = thaumasite

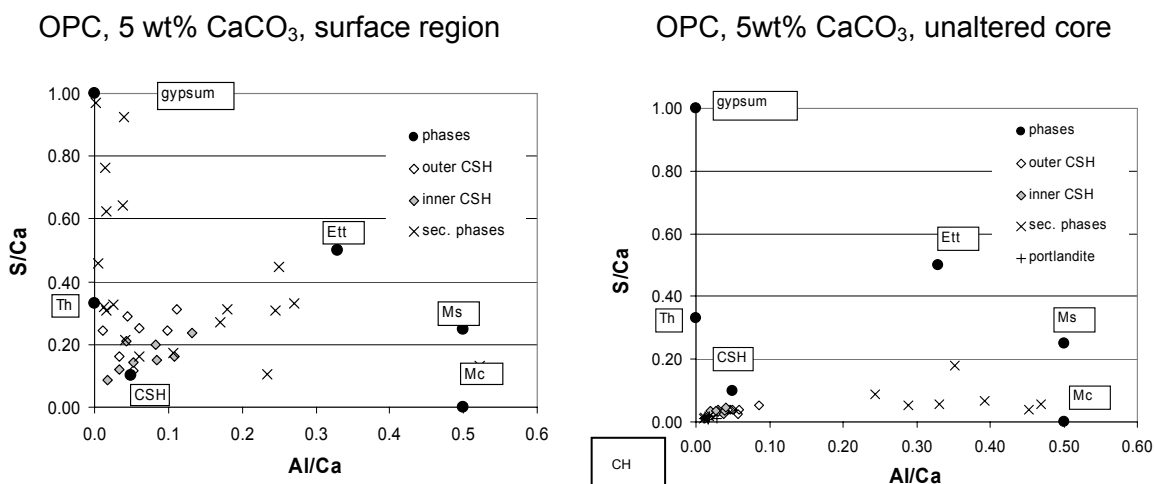
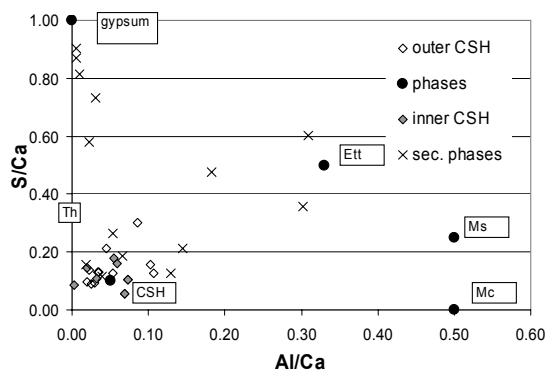


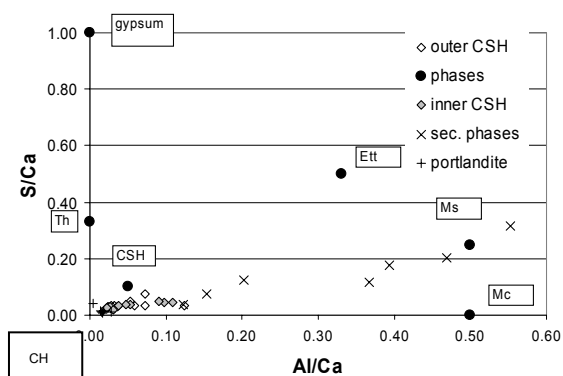
Fig. A 5.10: Phase assemblages of Portland cement mortars after 56 days sulfate exposure in 30g SO₄²⁻/l at 8 °C. CH = portlandite; Ett = ettringite; G = gypsum; Mc = monocarbonate; Th = thaumasite

• Microstructural investigations (56 days)

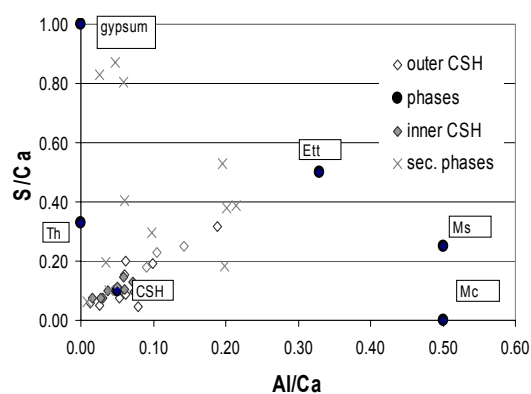
HS, no CaCO_3 , surface region



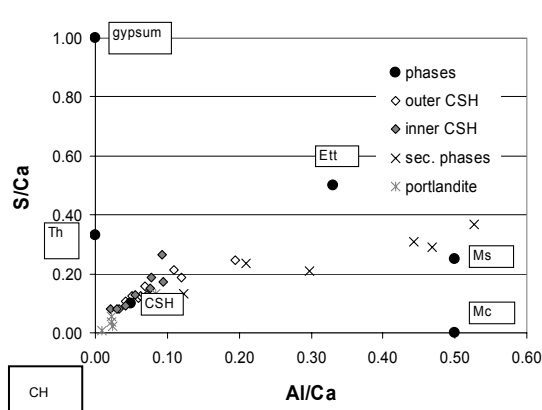
HS, no CaCO_3 , unaltered core



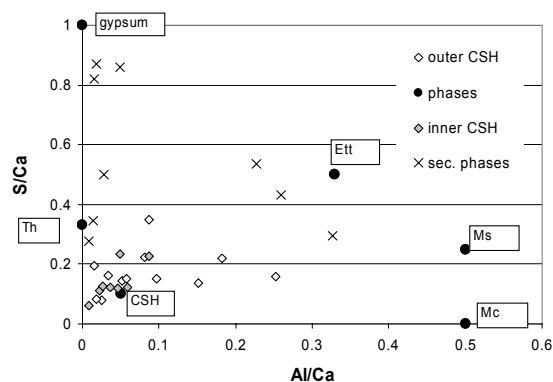
OPC, no CaCO_3 , surface region



OPC, no CaCO_3 , unaltered core



OPC, 25 wt% CaCO_3 , surface region



OPC, 25 wt% CaCO_3 , unaltered core

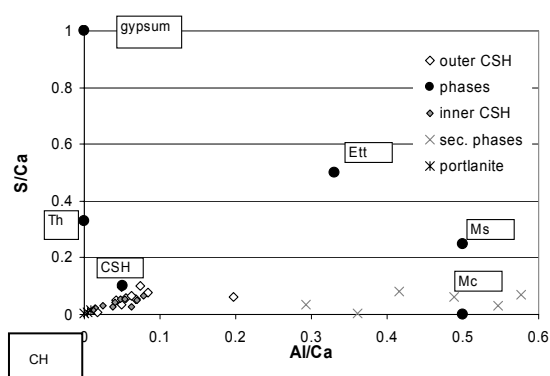


Fig. A 5.11: Phase assemblages of Portland cement mortars after 56 days sulfate exposure in 30g $\text{SO}_4^{2-}/\text{l}$ at 20 °C. CH = portlandite; Ett = ettringite; G = gypsum; Mc = monocarbonate; Ms = monosulfate; Th = thaumasite

• Microstructural investigations (270 days)

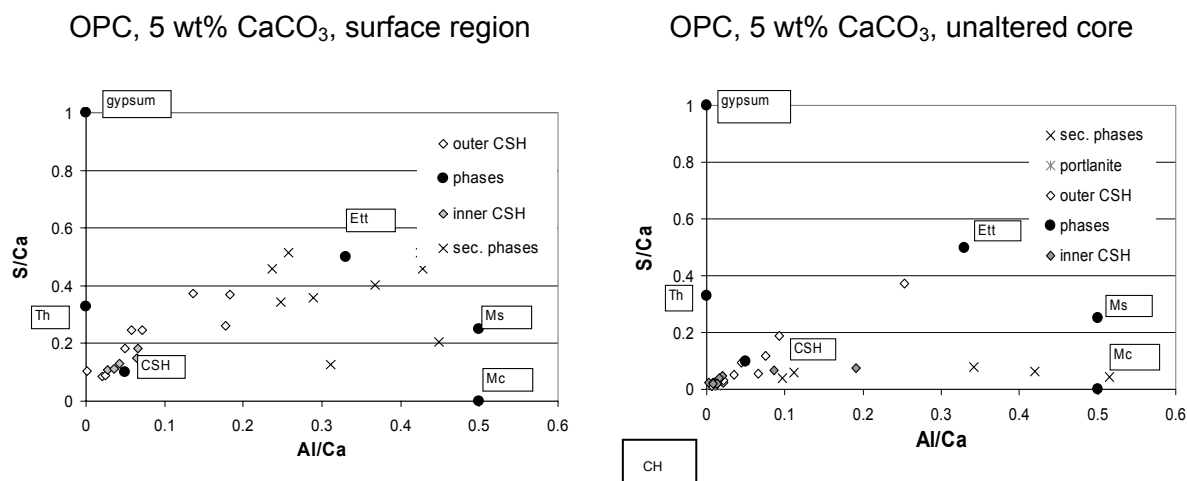


Fig. A 5.12: Phase assemblages of Portland cement mortars after 270 days sulfate exposure in $3\text{g SO}_4^{2-}/\text{l}$ at 20°C . CH = portlandite; Ett = ettringite; G = gypsum; Mc = monocarbonate; Ms = monosulfate; Th = thaumasite

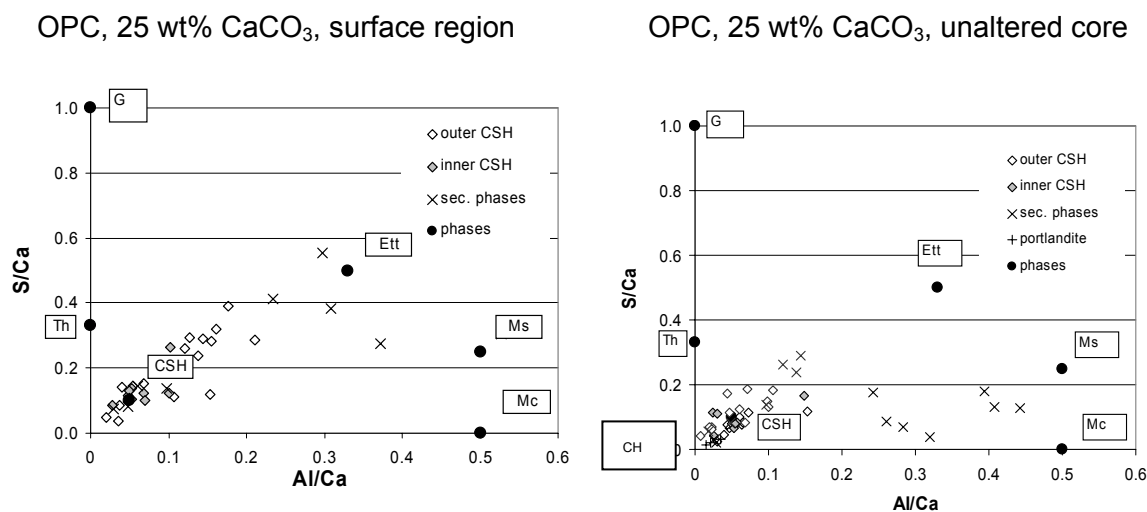


Fig. A 5.13: Phase assemblages of Portland cement mortars after 270 days sulfate exposure in $3\text{g SO}_4^{2-}/\text{l}$ at 20°C . CH = portlandite; Ett = ettringite; G = gypsum; Mc = monocarbonate; Ms = monosulfate; Th = thaumasite

A.6 Additional microstructural aspects

Figures A 6.1 and A 6.2 show the C-S-H forms a 1 μm thick rim around the calcite grains of the limestone filler in the cement paste matrix. Cc = calcite

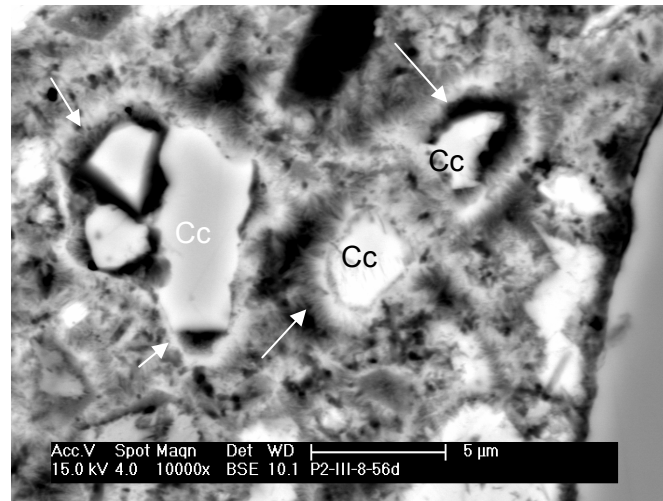


Fig. A 6.1: C-S-H rims formed around calcite grains in the cement paste of P5

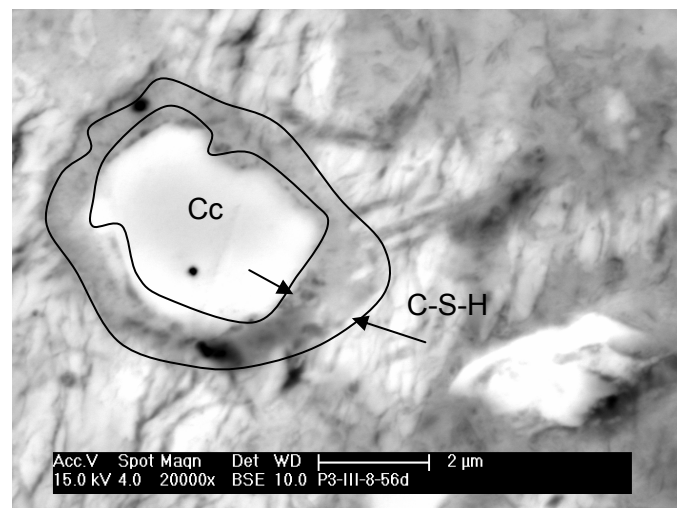


Fig. A 6.2: C-S-H boundary on the surface of a calcite grain in cement paste of P25

Figures A 6.3 and A 6.4 show the sulfate deteriorated microstructure at the surface region of mortar samples after 91 and 180 days of sulfate exposure ($30\text{g SO}_4^{2-}/\text{l}$) at 8°C .

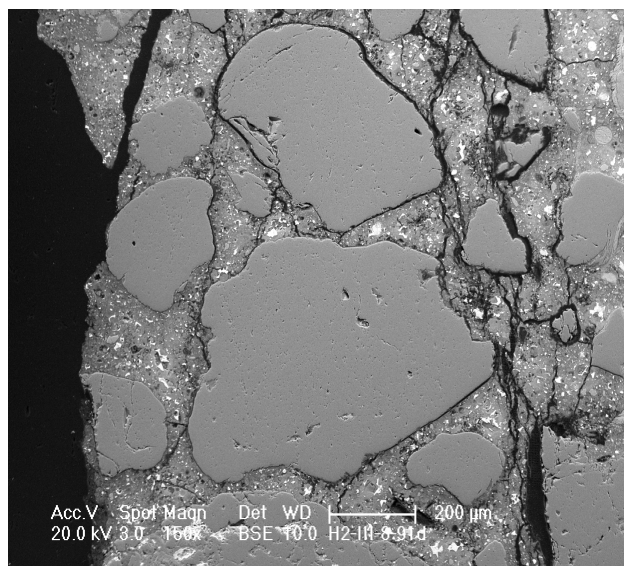


Fig. A 6.3: Surface region of H5 mortar sample after 91 days in Na_2SO_4 solution.

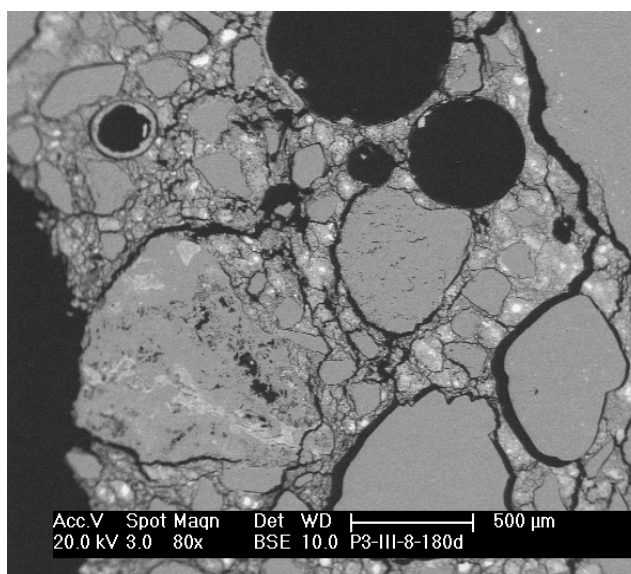


Fig. A 6.4: Surface region of P25 mortar sample after 180 days in Na_2SO_4 solution.

Figures A 6.5 and A 6.6 show ettringite formation in the surface region at between 0.5 and 0.8 mm depth after sulfate exposure at the given time and temperature.

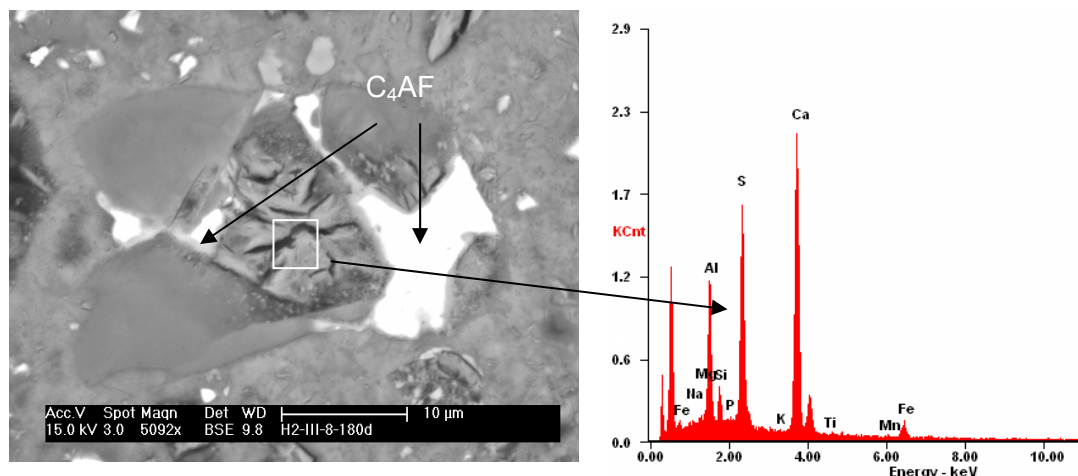


Fig. A 6.5: Ettringite formation from C_4AF phase in H5 mortar after 180 days at 8 °C.

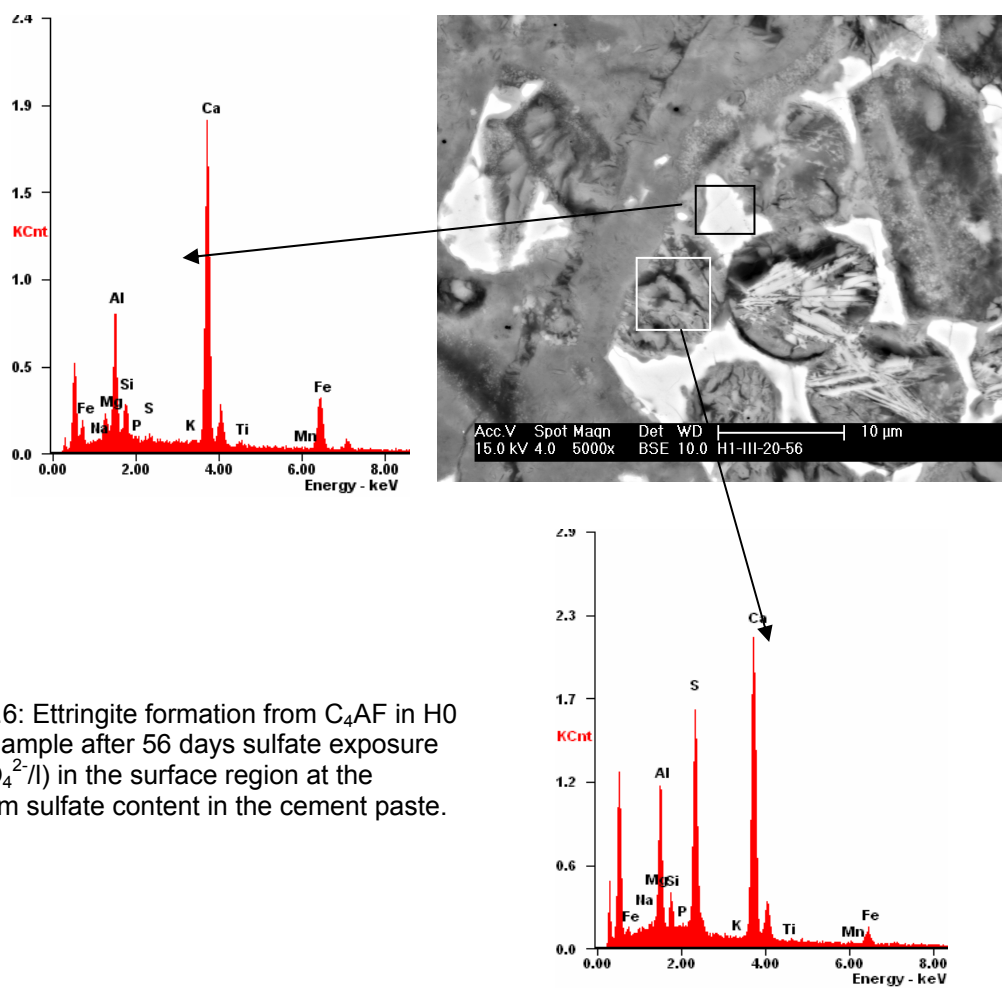


Fig. A 6.6: Ettringite formation from C_4AF in H0 mortar sample after 56 days sulfate exposure ($30\text{g SO}_4^{2-}/\text{l}$) in the surface region at the maximum sulfate content in the cement paste.

Figure A 6.7 and A 6.8 show gypsum formation in mortar samples after 56 days of sulfate exposure in Na_2SO_4 solution. Cc = calcite; G = gypsum

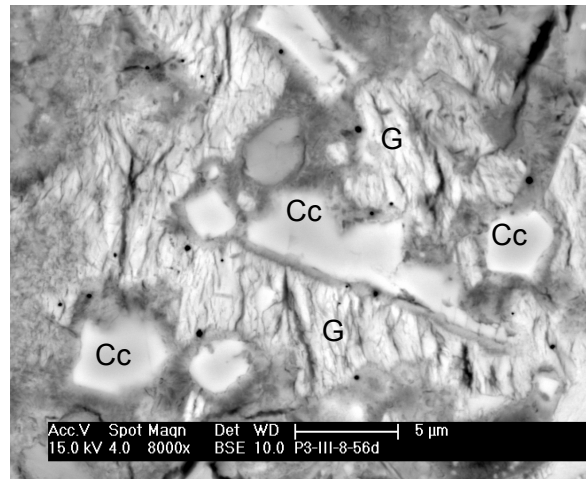


Fig. A 6.7: gypsum formation in P25 mortar sample stored at 8 °C.

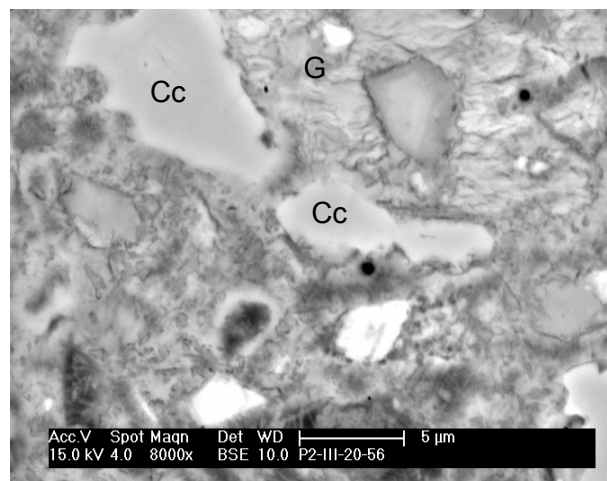


Fig. A 6.8: gypsum depot in P5 mortar sample stored at 20 °C

Figures A 6.9 A-D show the deteriorated microstructure of the surface region of mortar samples after 180 days of sulfate exposure in Na_2SO_4 solution at 8 °C. Cc = calcite; Ett = ettringite; G = gypsum; Th = thaumasite

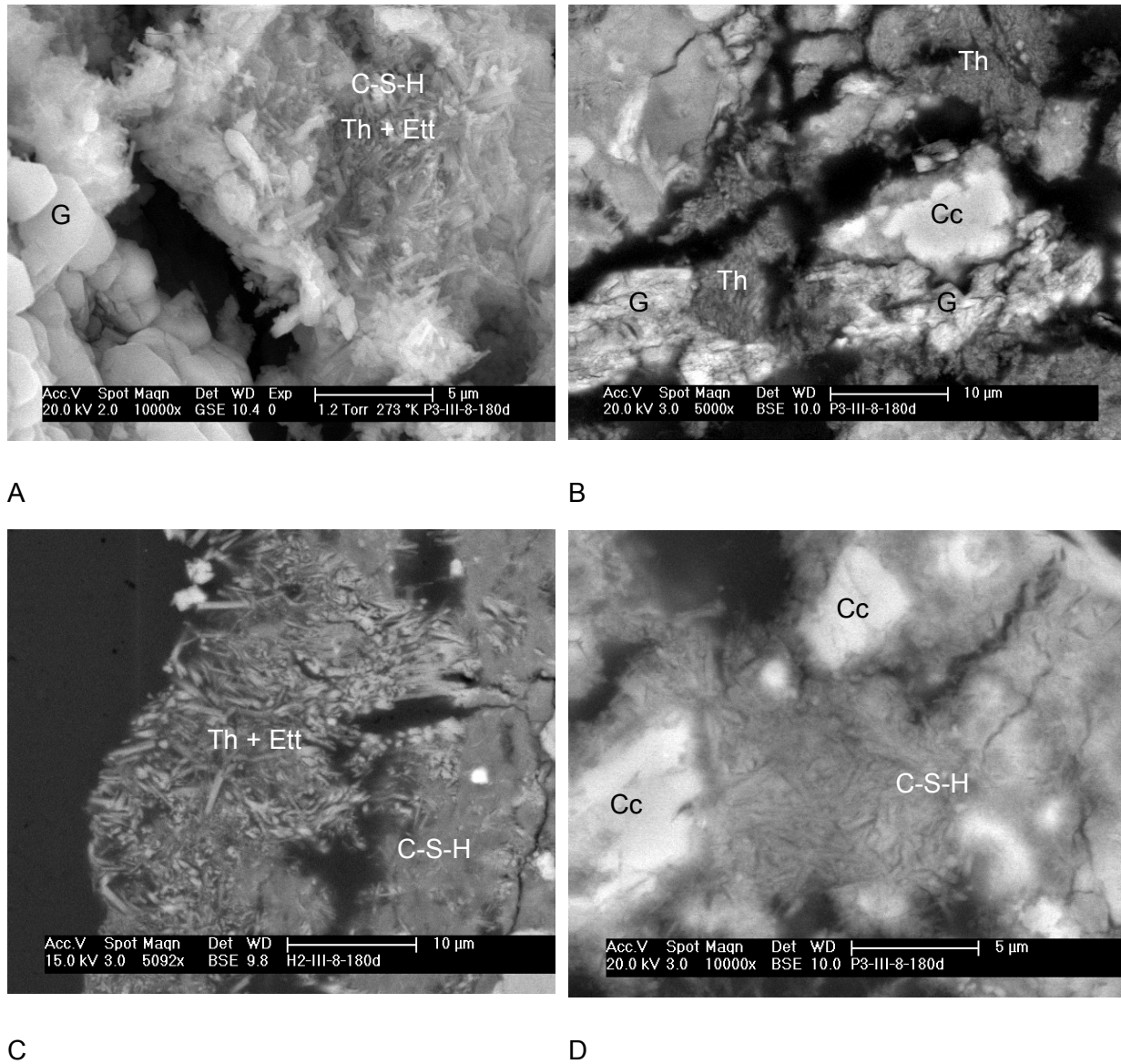


Fig. A 6.9: Microstructure of A) P25 mortar fracture sample and polished samples of B,C) P25 mortar samples and D) H5 mortar samples stored at 30g $\text{SO}_4^{2-}/\text{l}$.

Figures A 6.9 A-D show the deteriorated microstructure of the surface region of cement paste samples after 9 months of sulfate exposure in Na_2SO_4 solution at 8 °C. Cc = calcite; Ett = ettringite; Th = thaumasite

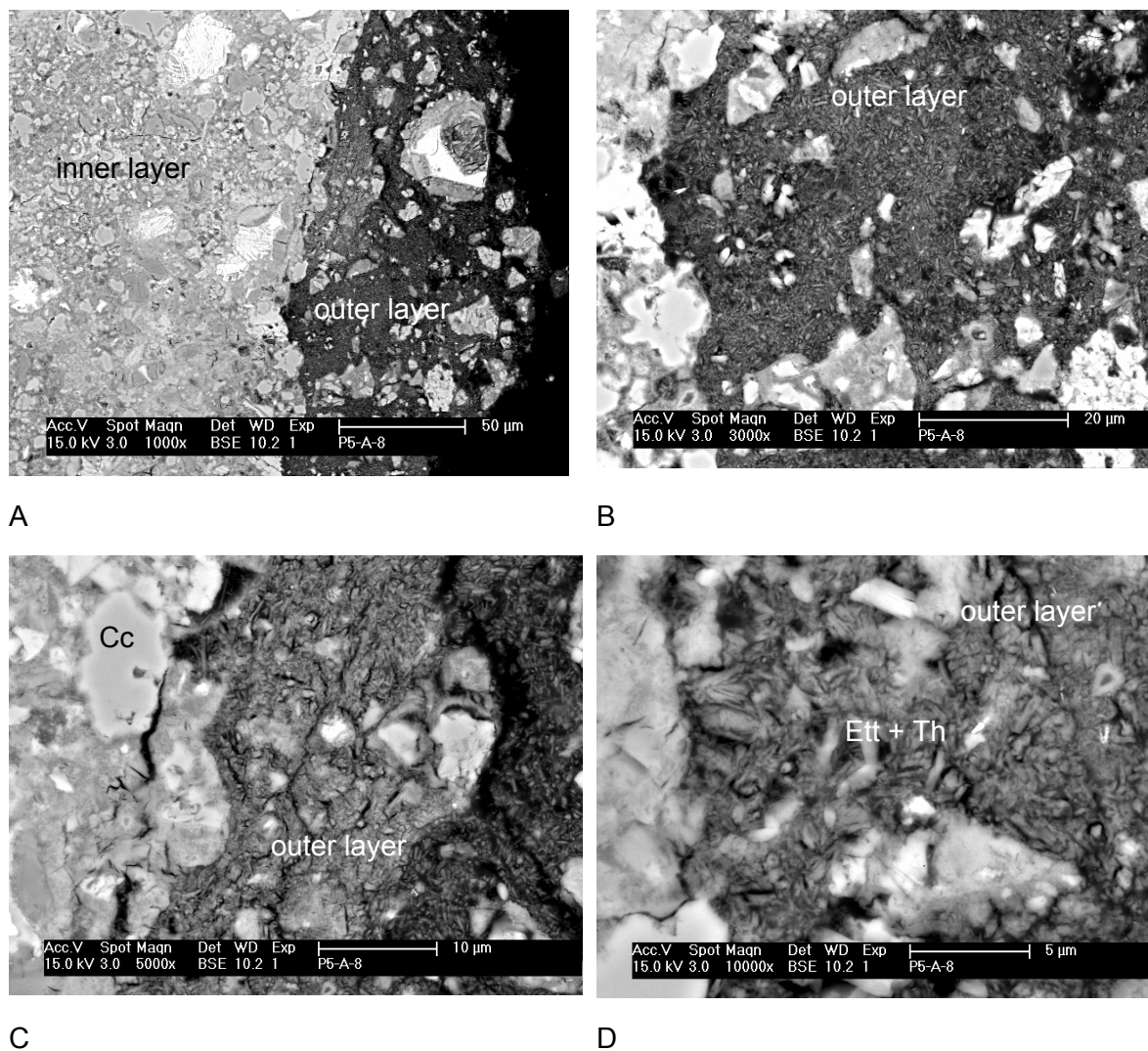


Fig. A 6.10: Microstructure of cross section through cement paste particles of A-D) P5 in subsystems A with 20g SO_4^{2-} by weight cement paste.

References

1. Kulik, D., *GEMS-PSI 2.1*, available at <http://leswebpsi.ch/software/GEMS-PSI>, PSI Villigen, Switzerland. 2006.
2. Hummel W., B.U., Curti E., Pearson F.J., Thoenen T., *Nagra/PSI Chemical Thermodynamic Data Base 01/01*, University Publishers/uPUBLISH.com, USA, also published as *Nagra Technical Report NTB 02-16*, Wettingen, Switzerland. 2002.
3. Thoenen, T. and Kulik, D., *Nagra/PSI chemical thermodynamic database 01/01 for the GEM-Selektor (V.2-PSI) geochemical modeling code*, PSI, Villigen; available at <http://les.web.psi.ch/software/GEMS-PSI/doc/pdf/TM-44-03-04-web.pdf>. 2003.
4. Lothenbach, B., Matschei, T., Möschner, G., and Glasser, F.P., *Thermodynamic modelling of the effect of temperature on the hydration and porosity of Portland cement*. Cement Concrete Research, 2007 (submitted).
5. Anderson, G.M. and Crerar, D.A., *Thermodynamics in Geochemistry: the Equilibrium Model*. Oxford University Press, Oxford, 1993.
6. Kulik, D., Berner, U., and Curti, E., *Modeling chemical equilibrium partitioning with the GEMS-PSI code*. PSI Scientific Report 2003, 2004. IV, 109-122.
7. Jacobsen, S.D., Smyth, J.R., and Swope, R.J., *Thermal expansion of hydrated six-coordinate silicon in thaumasite, $\text{Ca}_3\text{Si}(\text{OH})_6(\text{CO}_3)(\text{SO}_4)12\text{H}_2\text{O}$* . Physics and Chemistry of Minerals, 2003. 30 (6), 321-329.
8. Kjellsen, K.O., Monsoy, A., Isachsen, K., and Detwiler, R.J., *Preparation of flat-polished specimens for SEM-backscattered electron imaging and X-ray microanalysis--importance of epoxy impregnation*. Cement Concrete Research, 2003. 33 (4), 611-616.
9. Stutzmann, P.E. and Clifton, J.R., *Soecimens preparation for SEM*. 21st Conference on Cement Microscopy, 1999. Las Vegas.

Curriculum Vitae

Thomas SCHMIDT

Personal data

Date of Birth: July 7, 1976

Place of Birth: Hohenmölsen (D)

Nationality: German

Family status: single

Education

| | |
|-------------|--|
| 2004 – 2007 | EPFL, Swiss Federal Institute of Technology (EPFL), PhD student (CH) |
| 2002 – 2003 | Webstar Graduate Studies Center, London (UK) and FAW Business English Academy for continuing Training, Zwickau (D) |
| 1996 – 2002 | Bauhaus University, Weimar (D), Studies of civil engineering, Diploma |

Work experience

| | |
|-------------|---|
| 2004 – 2007 | Empa, Swiss Federal Institute for Materials Testing and Research (CH) PhD project in coordination with EPFL and cemsuisse |
| 2003 – 2004 | Michael Hadi Associates, London (UK), consulting structural engineer NBU Naumburger Bauunion, Görschen (D), project engineer |
| 2001 – 2002 | HOLCIM (Switzerland) AG, Siggenthal (CH), internship as assistant |
| 1999 – 2000 | Fingerinstitut für Baustoffkunde, Weimar (D), research assistant |